AN INVESTIGATION OF THIN FILM MAGNETIC RECORDING MEDIA

MICHAEL STEPHEN HEMPSTOCK

Doctor of Philosophy

THE UNIVERSITY OF ASTON IN BIRMINGHAM

September 1997

AN INVESTIGATION OF THIN FILM MAGNETIC RECORDING MEDIA

MICHAEL STEPHEN HEMPSTOCK

Doctor of Philosophy

September 1997

SUMMARY

Mechanical, physical and chemical changes in the surface of commercial thin film metal evaporated magnetic recording media have been correlated to recording error and signal degradation measurements. Modified and adapted commercial Hi-8 video recorders have been used for sample generation whilst analytical techniques such as XPS, SIMS and SEM have been employed in the surface characterisation.

The durability of the media was assessed through stop motion (still frame) and cycling tests, where error growth and signal degradation were measured as a function of running time. The tests were performed under ambient (22 °C, 40% RH) and high humidity (22 °C, 80% RH) conditions.

Characterisation of the lubricant layer on each tape was performed through models based on XPS and angle resolved XPS. The lubricant thickness can significantly affect the durability and signal output level of a thin film tape and thus it is important that reliable quantification can be achieved. Various models were considered for determining the lubricant thickness although ultimately, the most suitable technique was deemed to be a model that assumed a uniform layer structure.

In addition to thin film metal evaporated media, equivalent durability tests and surface analysis experiments were performed using a commercial metal particle tape in order that comparisons could be made between the two types of recording media. The signal performance of the thin film metal evaporated media was found to be quite different from that for the metal particle tape since dropout errors and signal degradation increased at a much earlier stage.

Extensive surface analyses enabled the mechanisms responsible for media failure and error growth to be identified in the ME and MP tapes and these were found to result from cyclic stressing and fatigue on the immediate substrate of the media.

Dedicated to my parents and to the memory

of my Grandad, Dr. T. A. Hempstock

Acknowledgements

Contents

List of Figures

13

List of Tables

Glossary of Symbols

VCR = Video cassette recorder

ME = Metal evaporated tape

MP = Metal particle tape

ME#1 = Commercial metal evaporated tape, Number 1

ME#2 = Commercial metal evaporated tape, Number 2

ME#3 = Commercial metal evaporated tape, Number 3

PFPE = perfluoropolyether

DLC = Diamond-like carbon

MIG - Metal-in-gap

MR = Magneto-resistive

XPS = X-ray photoelectron spectroscopy

SIMS = Secondary ion mass spectrometry

TOF-SIMS = Time of flight secondary ion mass spectrometry

SEM = Scanning electron microscopy

TEM = Transmission electron microscopy

AFM = Atomic force microscopy

AES = Auger electron spectroscopy

FTIR = Fourier-transform infrared spectroscopy

RF = Radio frequency

NTSC = National television system committee

PW_{50} = Width of output pulse at half the maximum amplitude

d = Head-media spacing

δ = Media thickness

λ = Signal wavelength

H = Magnetic field strength

B = Magnetic flux density

B_{int} = Internal magnetic flux density

B_{sat} = Saturation magnetic flux density

B_r = Remanent magnetic flux density

H_c = Coercivity

SFD = Switching field distribution

FM = Frequency modulation

AM = Amplitude modulation

F = Frictional force

F_A = Frictional force due to adhesion

W = Normal load

μ = Coefficient of friction

A_a = Apparent area of contact

A_r = Real area of contact

ψ = Plasticity index

ψ_p = Plasticity index for polymers

H = Hardness of softer material

σ_p = Standard deviation of peak height distribution

R_p = Effective radius of curvature of contact asperity

Y = Tensile yield strength of polymer

E_c = Effective elastic modulus of interacting surfaces

E_1 = Young's modulus of elasticity for interfacing surface

ν_1 = Poisson's ratio for interfacing surface

ω = Wear rate.

k = Constant of proportionality (wear coefficient)

p_m = Flow pressure (hardness)

p_0 = Yield pressure for plastic flow

τ_a = Interfacial shear stress of dry contact

τ_l = Interfacial shear stress of lubricant

α = Fractional areal coverage of lubricant

ϕ = Work function

24

E_k = Kinetic energy

E_b = Binding energy

$h\upsilon$ = Photon energy

λ = Inelastic mean free path / attenuation length

IMFP = Inelastic mean free path

AL = attenuation length

θ = Analyser take-off angle, normal to the analyser

d = Vertical sampling depth

t = Overlayer thickness

I'_s = Intensity of signal from substrate

I'_o = Intensity of signal from overlayer

I^0_B = Signal from an element in the substrate, in the absence of a contamination layer

I^0_M = Signal from an element in the magnetic film, in the absence of the lubricant

d_A = Thickness of contamination layer

d_L = Lubricant thickness

$\lambda_L(E_M)$ = Inelastic mean free path of photoelectrons from the magnetic film

$S(E_i, \theta)$ = spectrometer detection efficiency

E_L = kinetic energy of the photoelectrons from an element in the lubricant

E_M = kinetic energy of the photoelectrons from an element in the magnetic layer

σ_L = photo-ionisation cross section for the core level of an atom in the lubricant

σ_M = photo-ionisation cross section for the core level of an atom in the magnetic layer

n_L = atomic density of an element in the lubricant

n_M = atomic density of an element in the magnetic layer

λ_L = inelastic mean free path of photoelectrons from the lubricant

λ_M = inelastic mean free path of photoelectrons from the magnetic layer

a = Ratio of the carbon atom density in the resin and γ-Fe$_2$O$_3$ to that in the fluorocarbon layer, when analysing the constituents separately

R = Ratio of the carbon atom density in the resin and γ-Fe$_2$O$_3$ to that in the fluorocarbon layer, when analysing the complete disk

R_1 = C-F peak area of the C 1s XPS spectrum

R_2 = C-C + contamination peak area of the C 1s XPS spectrum for the carbon

protective layer only.

R_3 = C-F peak area of the C 1s XPS spectrum when analysing just the lubricant.

R_4 = C-C + contamination peak area of the C 1s XPS spectrum for the carbon

protective layer only.

$\varphi(x,\theta)$ = Depth distribution function

$c_j(x)$ = Concentration depth profile

x = Depth from sample surface

$n_{j,i}$ = the proportion of element j at a depth i

$m_{j,i}$ = the initial estimate for the proportion of the element j at a depth I

$I_j(\theta)$ = Angular distribution

λ_t = Total mean free path of the photoelectrons

λ_{tr} = Transport mean free path, calculated using a quasi classical formula

A = Atomic weight of matrix atoms

N_A = Avogadro's Number (6.023 x 10^{23} per gram mole)

ρ = Bulk density (Kgm^{-3})

27

CHAPTER 1

LITERATURE SURVEY

1.1 Introduction

Tape storage technology has always been driven by the demands of the market. The need for reliable cost-effective storage systems, coupled with the increasing competition from the optical and solid state recording technologies, has compelled the magnetic media industry to develop products with ever increasing recording densities and improved performance characteristics. Previously, these improvements have been achieved by using narrower track widths, smaller read/write head dimensions and a narrower spacing on thinner magnetic coatings. However, a combination of these factors is now beginning to lead to tribological contact problems that need to be addressed in order for further improvements to be realised.

Additional impetus for improvement is provided by the fast developing market for digital camcorders, the migration path of Hewlett Packard's Digital Data Storage (DDS) format (currently DDS-3) and the imminent arrival of digital video cassette recorders for High Definition Television, HDTV. Consumers have already experienced the benefits of digital technology through other forms of consumer electronics products, such as compact disc players, but to date, the use of digital technology in the television industry has mainly been restricted to the areas of programme production and post production. This will change with the advent of digital transmission since it will be possible to use digital compression techniques to transmit wide screen high definition television pictures [1]. HDTV pictures are to be viewed on a screen with an aspect ratio of 16:9, as opposed to the conventional screen size of 4:3. In Europe, the Eureka 95 program has proposed that a HDTV picture will consist of 1250 horizontal lines with each picture being updated 25 times per second. Slightly different specifications have been proposed in Japan with each picture consisting of 1125 horizontal lines and an update rate of 30 pictures per second.

The amount of information needed to record HDTV pictures is approximately four times that for a corresponding conventional television picture. Prototype digital video recorders have illustrated that conventional television pictures can be reproduced to a quality that is comparable to the original broadcast. However, if HDTV pictures are to be recorded digitally on magnetic media, the industry must produce higher performance media with greater areal recording densities.

Digital video recorders achieve large areal densities by using high density media in conjunction with fast head-to-tape speeds. Clearly the tape and heads are integral to the performance of the overall system. The signal-to-noise ratio should be high which accordingly requires a high output signal, especially at the small wavelengths used in high density recording. Also, the tape and heads must have a low noise level and the tape should be smooth in order for a good head-to-tape contact to be obtained.

The tape must satisfy stringent performance criteria if it is to be viable as media for commercial digital video recording. Mechanically, the tape must be thin to help achieve high cassette capacities but it must also be relatively stiff in order to ensure good tape handling properties. The tape must also perform consistently over a wide range of environmental conditions and be reliable over the media lifetime.

At present, the two forms of flexible magnetic media capable of realising the required specifications are metal particle (MP) and metal evaporated (ME) tape. However, the tribology of flexible magnetic media is now becoming a limiting factor as the industry strives for higher recording densities. Lubrication is essential if catastrophic failure of a system is to be avoided, particularly in applications such as video and other helical scan recorders where the heads and media are in intimate contact. The lubricant can be applied to the media as a topical or internal lubricant although the most effective method depends on the specific nature of the media. In the case of particulate media, such lubricants as complex fatty acid esters are incorporated into the binder formulation,

providing adequate lubrication for the expected life-time of the media. However, unlike particulate media, flexible thin film metal evaporated media have no binder system for incorporating such internal lubrication and thus the media has to be protected through the application of a topical lubricant. The task of achieving and maintaining suitable lubrication is far more critical than that for MP media since the level of protection afforded by the lubricant film must at the very least be equivalent to that of particulate media over a wide range of environmental conditions.

The research reported in this thesis was undertaken to investigate the effects of lubrication on the mechanical properties of thin film metal evaporated media, to study the effects on signal performance and to identify the specific wear mechanism of various commercial thin film ME tapes. The lubricant layer on the ME tapes was characterised in terms of end-group, backbone and thickness. The study was extended to include an analysis of a commercial MP tape since it was important to have comparative data for the two types of tape.

In this first chapter, a general introduction to the theories of magnetic recording is given, together with an account of the development of ME and MP magnetic media. The general principles of friction and wear are then described, with particular attention given to tape wear and the effects of humidity.

Commercial Hi-8 video recorders were adapted to enable error growth mechanisms to be investigated. This was achieved by performing various mechanical measurements and then analysing any changes to the surface of the tape samples. The modifications included the addition of a bridging amplifier to each of the recorders and the provision of indefinite stop motion times through adapted pause mode control. The mechanical measurements consisted of tape cycling and stop motion durability tests, as described in Chapter 2.

Surface analysis techniques including X-ray photoelectron spectroscopy, secondary ion mass spectrometry and scanning electron microscopy were used to study the physical and chemical characteristics of the tape surface before and after durability tests.   A description of each of these techniques is given in Chapter 2.

Various models based on XPS data for determining the thickness of the lubricant layer on ME tapes are described in Chapter 3.

The results of cycling and stop motion durability tests are reported in Chapter 4, together with the findings from the surface analytical experiments.   In addition, the models described earlier in Chapter 3 for calculating the thickness of the lubricant layer were assessed using XPS data reported in Chapter 4.

In Chapter 5, the information reported in the literature survey and the experimental results are discussed to enable a wear mechanism for ME tape to be postulated. Finally, in Chapter 6, a number of conclusions are drawn from the investigation as a whole and suggestions for future research are made.

1.2 General Magnetic Recording Theory

In order to record an electrical signal using magnetic media, it is first necessary to convert the signal via a suitable transducer into a representative magnetic pattern. The transducer, known as the magnetic head, is commonly a ring core electromagnet, designed with a narrow gap in order to create two pole pieces, as shown in Figure 1.1.
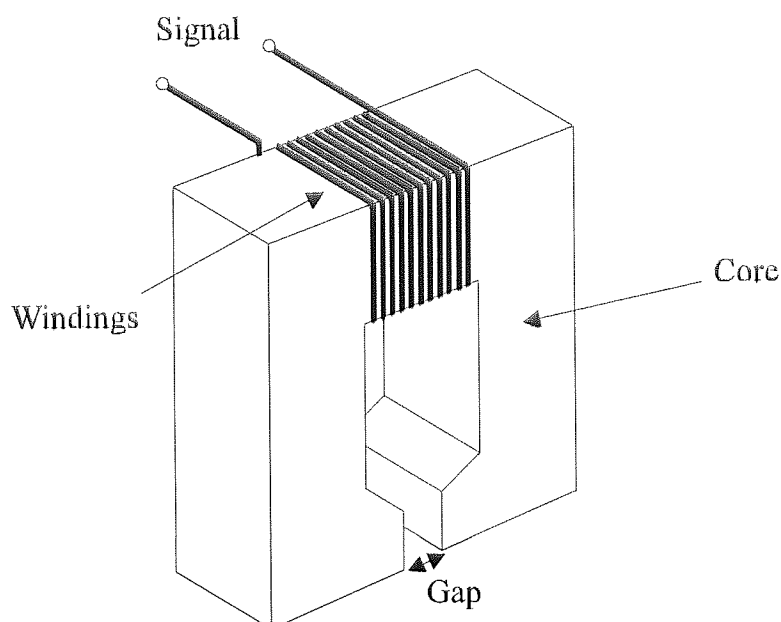
Figure 1.1 Ring Core Magnetic Head

The materials used in the construction of magnetic heads are commonly referred to as soft magnetic materials and usually comprise of either a metallic alloy such as permalloy (e.g. Ni-Fe), or a composition of a magnetic oxide such as nickel-zinc ferrite. These materials are suitable for use in the design of magnetic heads because they exhibit a low remanence and coercivity, where the remanence is defined as the magnetisation that remains after the field has been removed and the coercivity is the field that would have to be applied in order to reduce the magnetisation to zero.

The soft magnetic materials used in the design of heads must have a high permeability in order to guide the flux with minimal losses and to ensure the ring core will saturate when in close proximity to a small magnetic flux. In addition, the core must be able to switch magnetisation quickly so any changes in the signal field can be readily followed. A high saturation magnetisation is essential in order to ensure that a sufficiently high field can be generated without the head material becoming saturated. Also, the remanence and coercivity of the heads should be relatively small since high values can result in the existence of a remanent magnetic field, ultimately leading to the erasure of the media flux and hence data corruption.

In the recording process, the signal current induces a magnetic field within the core of the head which gives rise to a characteristic fringing field that emanates from the gap and creates a recording field to magnetise the media. The media passes over the gap at a constant velocity and is left with a representation of the original signal in the form of a remanent magnetic flux. The fringing field from the gap is dependent upon the physical size of the gap although the magnitude of the field is limited by the saturation flux density of the core head.

In the playback process, the recorded magnetic media is passed over the magnetic head at the same velocity as before so that the remanent magnetic flux of the media will protrude into the head and induce a voltage in the copper windings. This voltage (or pulse) is proportional to the rate of change of flux and hence is representative of the original electrical signal. The shape of the pulse is described by the PW_{50} and is defined as the width of the output pulse at half the maximum amplitude, as illustrated in Figure 1.2.

The pulse shape is proportional to the magnitude of the fringing field, as illustrated in Figure 1.3 [2], since the depth to which the field penetrates the media effects the height and width of the pulse. The field spreads out as it emanates from the gap in the head and this results in a broader and lower pulse.

Output
Voltage

Zero-peak
Voltage

PW_{50}

time
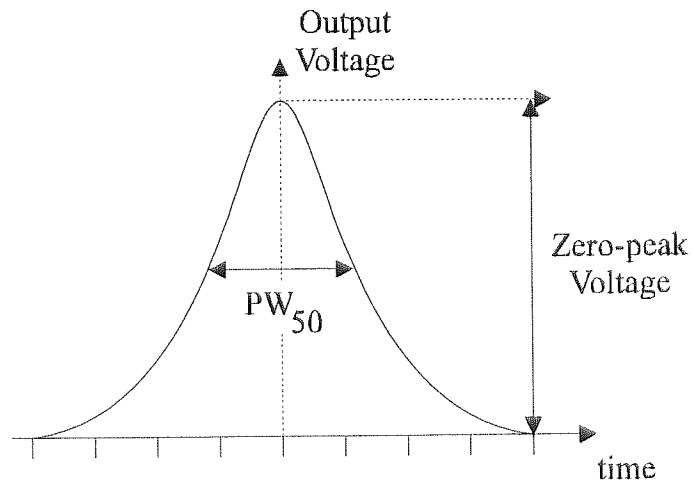
Figure 1.2 *Output Pulse Illustrating* PW_{50} *Definition*

Ring Core
Magnetic Head

Gap

d

1
2
3

Magnetic
Medium

Fringing
Field

y

x

z

1

2

3

x
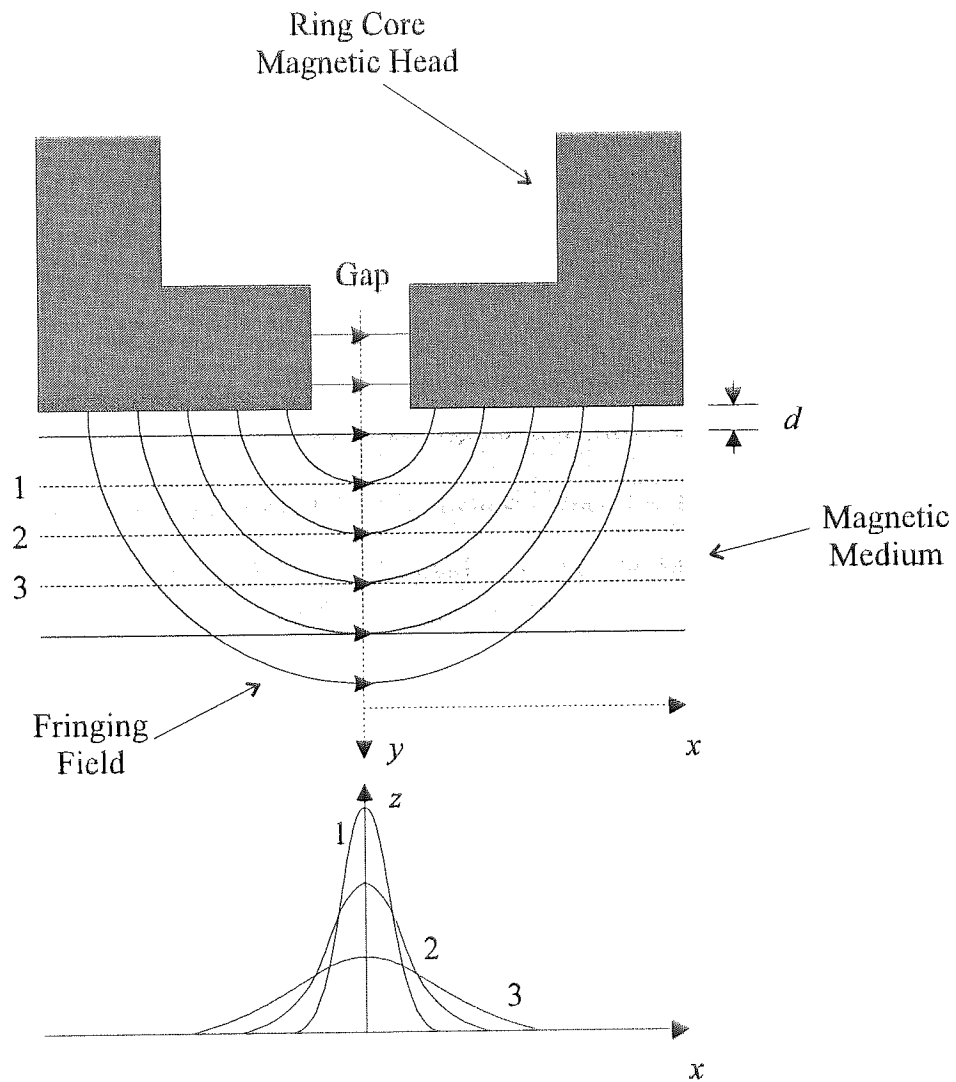
Figure 1.3 *Proportionality of Output Pulse Shape to the Magnitude of the Fringing Field [2]*

The parameters associated with a recording system such as the geometry of the heads, together with the magnitude of the signal current used in the reading and writing of a transition, place restrictions on the overall recording density of the system. If a transition previously recorded on the media is initially some distance away from the gap of a head, none of the flux associated with that transition will enter the gap region and thus the output voltage will be zero. Then, as the transition approaches the gap, flux will emanate into the leading part of the head and will be guided through the coils and onto the trailing part of the head. As a result, the output voltage will increase because of the change of flux with time. Then, as the transition moves even nearer to the gap, the trailing part of the head will begin to encounter flux directly and accordingly, the flux through the head coils will begin to decrease until eventually, the direction of the flux through the coils will have reversed completely, giving a pulse shape similar to that illustrated in Figure 1.2.

A system which generates a large output voltage during playback is advantageous since this makes it easier to recognise each individual transition. Indeed, a narrow PW_{50} value enables greater recording densities to be realised since the transitions can be positioned closer together without being subjected to the problems of interference from neighbouring transitions. In the case of an inductive ring head, the PW_{50} is given by Equation 1.1.

$$PW_{50} = 2\sqrt{d(d+\delta)}\qquad\qquad(1.1)$$

where $d =$ Head-media spacing

$\delta =$ Media thickness

Clearly, a greater head-media spacing and/or media thickness will lead to a larger PW_{50} value. In order to optimise a system, the properties of the materials used in the construction of the heads and media must satisfy several specifications. The properties

for the head materials have already been discussed but in the case of the media, hard magnetic materials should be used since these exhibit a high coercivity. This will help minimise self-demagnetisation as bits get shorter whilst still not being too high for state of art record and erase heads to do their job. Another characteristic which magnetic media must possess is that of a high remanent magnetisation since this is essential if a large output voltage is to be observed on play-back.

A further compromise in the design of a video recording system has to be made in relation to the distance between the head and media. In terms of recording performance, the best quality will be achieved when the head and magnetic part of the media are in intimate contact since the field strength diminishes in size with distance from the head. However, tribological problems become more pronounced when the media is in contact with the head and a greater spacing between the two would ease these problems. The demand for higher recording densities has tilted the balance towards finding a solution to the tribological problems since very high recording densities will only be achieved in conjunction with the use of shorter wavelength signals. Losses are most significant when short wavelength signals are to be recorded since according to Wallace [3], the wavelength is related to the spacing loss in dB by Equation 1.2, where d is the head to tape separation.

$$\text{spacing loss} = 54.6\left(\frac{d}{\lambda}\right) \text{ dB} \tag{1.2}$$

Clearly, the problems which occur through the existence of a spacing loss are greatest at large head to tape separations and are exacerbated further when short wavelength signals are recorded. The primary reason for this phenomenon is that the flux associated with a short wavelength signal does not extend the same distance as it does with a longer wavelength signal and hence a gap between the head and media will be even more detrimental to the overall recording. Indeed, a 6 dB loss in the output signal (equivalent

to losing half the original signal) approximately corresponds to an additional head/media spacing of 0.1 μm when recording at a wavelength of 1 μm.

A high coercivity media is essential because once magnetised, the remanent magnetic flux must be retained for the projected lifetime of the media. Materials such as these which exhibit a high coercivity and remanence are classed as hard magnets. All magnetic materials can be characterised in terms of a B-H hysteresis loop, irrespective of whether they are soft, hard or intermediate magnetic materials.

For a ferromagnetic material, individual magnetic moments of the domains may not necessarily be aligned in any one given direction but the net magnetic moment for the whole magnet will have a directional bias. A hard magnetic material, such as those used in magnetic media, will when subjected to an external magnetic field of strength H, have a B-H hysteresis loop similar to that illustrated in Figure 1.4.
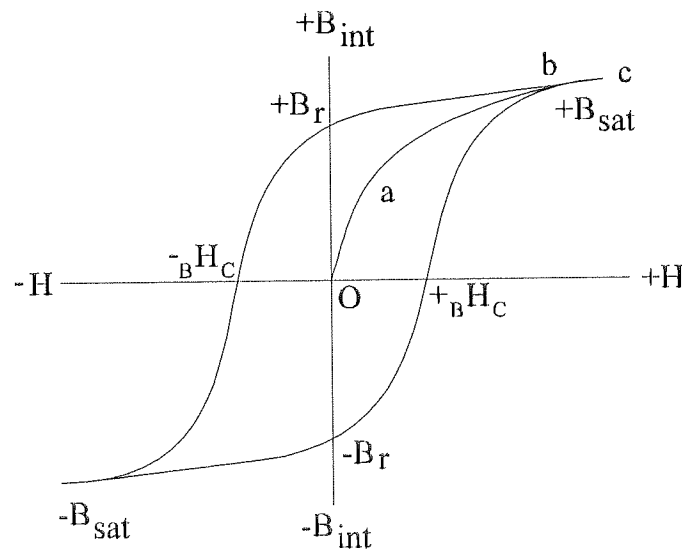
Figure 1.4 B-H Loop for a Hard Magnetic Material

If the sample is initially unmagnetised, the flux density within the sample, B_{int}, will increase along the magnetisation curve with the applied magnetic field, H, depicted by

the path Oa. At position b, when the magnetic field is high, the increase in flux levels off as the material reaches saturation, B_{sat} (The slope between points b and c on the magnetisation curve is equal to the permeability of free space). When the magnetising field is removed, the flux density will not return to zero since a remanent flux, B_r, will remain within the material and hence in order to reduce the flux density to zero, the direction of the applied magnetic field, H, must be reversed. The field strength needed to remove the flux density is known as the coercive force, $_BH_C$ and if the applied field is maintained in the reverse direction, the flux density will eventually saturate to give $-B_{sat}$.

Soft magnetic materials such as those used in the construction of magnetic heads are highly permeable since they must be able to respond quickly to any changes in the magnetisation. It is not necessary for the head to retain the magnetic flux density but it must saturate readily, even when just a small magnetic flux is induced within the core. The B-H curve for such a material is illustrated in Figure 1.5, with the low coercivity and remanence a typical feature.
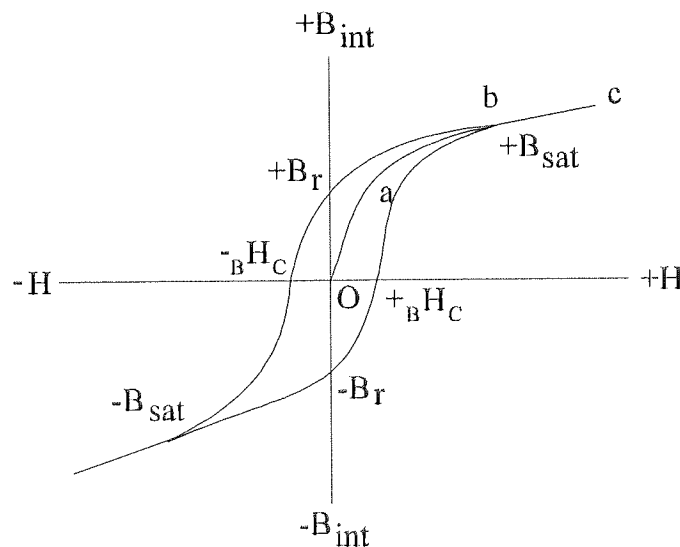
Figure 1.5 B-H Loop for a Soft Magnetic Material

The hysteresis loop associated with the magnetic particles of an ideal material will be square shaped because the remanence must be equivalent to the maximum magnetic flux density. The squareness of a hysteresis loop, which is simply the ratio of the remanent flux to the saturation flux density, is often used to assess the properties of magnetic media and whether the particles would be suitable for use in the recording and playback processes.

The recorded signal may be removed from the magnetic media by exposing the remanent magnetic flux to a field greater in strength to that used in the recording process. Some instruments use the same head to read, write and erase a signal, although systems such as a Hi-8 VCR, in which the recorded signals are high frequency, use a completely separate erase head.

1.3 Flexible Magnetic Media

The tribological performance and magnetic recording characteristics of magnetic media have evolved considerably since their inception in the 1930's. Indeed, since these early days when the media only consisted of a simple carbonyl iron magnetic coating on a layer of paper, magnetic tape technology has continued to advance each year, particularly through the use of better recording materials such as magnetic particles, lubricants, dispersants, substrates, superior recording heads and improved recording mechanics.

The simplest method of obtaining higher capacities for any given magnetic recording system is to reduce the thickness of the substrate in the media. This is only a short term solution because there is a stage beyond which reduction of the thickness of the substrate will significantly affect the mechanical performance of the tape. In order to achieve long term increases in data density, new recording systems in conjunction with improved media have to be developed. However, the important consideration of backwards compatibility in applications such as video cassette recorders has to be retained which then places the emphasis of improvement with the development of the media.

The magnetic particles used in media have been developed extensively over the decades from γ-Fe_2O_3 particles to CrO_2 and Co-modified γ-Fe_2O_3 whilst today, the market for high density magnetic media is dominated by metal particle (MP) and metal evaporated (ME) tape.

Metal particulate tape was originally developed for use in Hi-8 video systems because the conventional particulate media could not deliver the required improvement in the electromagnetic recording characteristics. The advances in tape performance which have arisen from using metal particles have included the realisation of much higher coercivity values and a higher saturation magnetisation. This has been supplemented by an

improvement in the archival stability of the tapes which had previously been a major problem with metal particulate media.

When ME tape was first launched onto the commercial market, the recording performance was significantly better than that of the equivalent metal particle tapes [4]. However, the implementation of very thin MP coatings, first led to MP media which had comparable recording properties to that of ME tape but now the latest development MP tape has been shown to have recording characteristics which surpass the rival ME tapes [5,6]. MP^{++} media use very small metal particles in conjunction with double coating technology and this has been shown to produce tapes which have very high coercivity value and high magnetisation [7].

Thin film metal evaporated media may yet play an increasing role in the high density magnetic media market but it is unclear which, if either, type of media will become the standard for use in new and developmental memory intensive applications such as digital data tapes. Commercial rather than technical issues are likely in the end to be decisive. Meanwhile, many international and major company format standards are being written on the basis of covering each option.

1.4 Development of Particulate Media

For many years, the three basic constituents of particulate media were the magnetic particles, the substrate and the binder system, although more recently, the application of a back-coating has become a regular feature. In general, the principles of construction of particulate media are universal, with the basic structure illustrated in Figure 1.6.

Magnetic Coating
within Binder
(2 - 5 μm)

Substrate
(12 - 30 μm)

Back Coat
(1 μm)
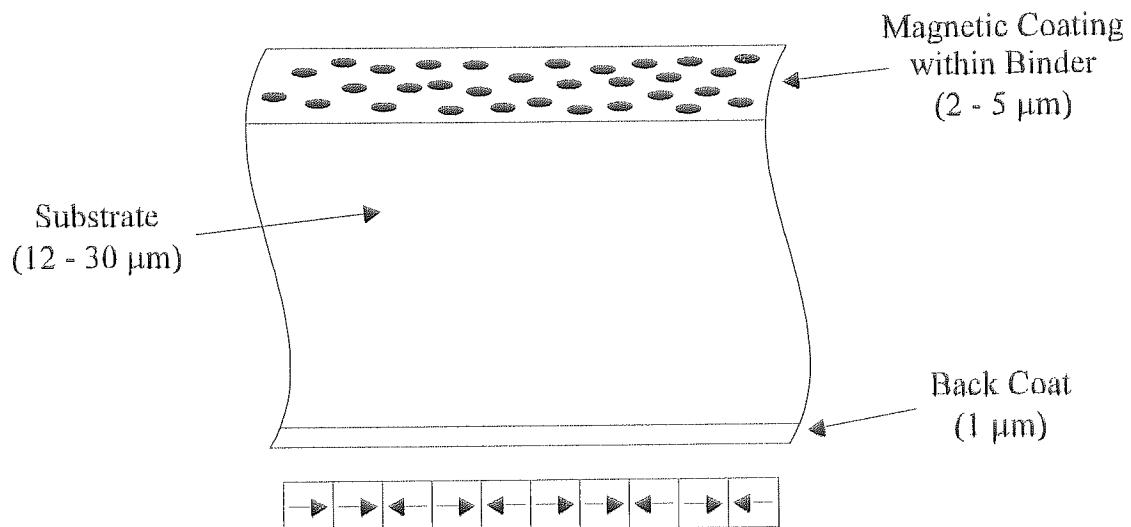
Figure 1.6 *Sectional View of a Particulate Magnetic Tape*

In terms of the electromagnetic recording characteristics of particulate media, the magnetic particles are the most important constituent since in order to obtain a substantial output at high linear densities, the particles must possess a high coercivity and remanence. The basic signal-to-noise ratio (that in the replay of an erased tape) depends on the particle size because S/N is inverse to a function of the particle size distribution. Noise depends on the number of reporting elements per second and on the adequacy of the dispersion to minimise the interaction fields. Hence, small particles are advantageous since they are easier to disperse than larger particles and they will naturally help to produce a smoother exterior tape surface, ensuring the recording head will be closer to the magnetic part of the media. In addition, smaller bit dimensions will also allow smaller transition widths to be achieved which at present are of the order of 0.2 μm.

Magnetic particles are commonly accicular and essentially behave as miniature bar magnets. The coercivity of particles is determined by both crystal and shape anisotropy (material species and accicularity). Gamma-ferric oxide particles, γ-Fe_2O_3, have been the principle magnetic particle used in the manufacture of commercial flexible magnetic media since the original development of magnetic recording. Thus, it has been possible to confirm that these particles possess long term stability without having to rely on the results of accelerated environmental tests. Particle lengths range from 0.15 to 0.5 μm, have an aspect ratio typically of 10:1 and a coercivity of approximately 350 Oe.

An alternative particle to pure γ-Fe_2O_3 is chromium dioxide, CrO_2, and these particles have the advantage of offering a higher coercivity than basic ferric oxide. The resultant tape possesses a larger remanent magnetisation, partly since the saturation magnetisation is higher but also because the particles are easier to orientate. The particles are needle shaped and have extremely parallel sides. Indeed, due to the near perfect structure of the particles, they are relatively easy to align during the tape production process and as such, squareness ratios of 0.9 can be achieved. However, the tape can be chemically unstable when exposed to the atmosphere and as a result, it is necessary to include a protective layer for the particles. This has the detrimental effect of reducing the relative performance advantage of the CrO_2 media although even when this layer is included, the overall magnetic performance is still better than that of basic ferric oxide. The CrO_2 media has an additional advantage of possessing some head cleaning properties due to the CrO_2 particles being harder than ferric oxide particles. However, the head wear which results from the abrasive CrO_2 media particles is too high for sustained operation and as such, alternative less abrasive particles have been developed. Also, γ-Fe_2O_3 media may be better suited to certain applications because chromium dioxide is grown at high temperatures and pressures which accordingly incurs higher production costs in comparison with ferric oxide media. Thus, if an application only requires low recording densities, γ-Fe_2O_3 tape may be able to meet the required specifications but at a lower cost. As a consequence, many CrO_2 tapes today contain only a minority of CrO_2 to

keep costs to a minimum in order to be able to compete with alternative tape formulations.

The improved recording characteristics delivered by chromium dioxide media was the catalyst for further modifications to be instigated to the γ-Fe_2O_3 particles through the introduction of cobalt into the gamma iron oxide lattice. Epitaxial surface cobalt was diffused into the gamma iron oxide lattice by heat treatment which helped give the media a much higher coercivity of up to 1000 Oersteds and hence a higher areal recording density. The increased coercivity was due to the additional resistance to the switching of the magnetisation direction provided by the interaction between the cobalt ions and the iron oxide. i.e. The presence of cobalt increased the crystal anisotropy of the magnetic particles.

The cobalt modified γ-Fe_2O_3 particles are relatively independent of temperature in ambient operating conditions, fluctuating by just 2 Oe per degree Celsius. However, if the surface modified particles are heated to a temperature of above 300° C, the cobalt atoms will diffuse to deeply into the γ-Fe_2O_3 particles and although the increased coercivity will be retained, the media will become highly dependent on temperature change (10 Oe per degree Celsius) [8].

Metal particles may play a vital role in the future of high density magnetic recording since they exhibit substantially higher coercivity than rival forms of particulate media [9]. The elongated metal particles, usually iron, are each protected by a passivation layer which is carefully introduced during a controlled oxidation process of the particle surface. On completion of the passivation process, a core of (iron) metal remains which forms approximately 50% of the particle volume. One of the challenges for the magnetic media industry is to increase the proportion of absolute metal relative to the oxide passivation layer since the passivation layer reduces the effective magnetisation of the media although the remanence is still orders of magnitude greater than that of a fully

oxidised metal particle. Indeed, metal particle tapes have a coercivity of up to 2200 Oersteds and are increasingly used for high quality video tapes.

Barium ferrite particles have proved to be of interest to the magnetic media industry since they possess unique properties which distinguish them from the particles used in all other forms of particulate media. Firstly, they are hexagonal in shape rather than the conventional accicular form and due to the strong magneto crystalline anisotropy associated with the hexagonal platelets, coercivity values of between 2000 and 3000 Oersteds can be readily obtained. For practical applications such as those found in the magnetic recording industry, such high coercivity values are too high and thus their magnitude has to be reduced. This is performed by doping the barium ferrite particles with cobalt and titanium which when administered in the correct proportions, will reduce the coercivity to the order of 1000 Oe, without having a significant effect on the saturation magnetisation. However, the magnetisation associated with barium ferrite particles is relatively low and they must be heavily doped even to reach the magnetisation levels of γ-Fe_2O_3 particles. The production of high quality barium ferrite media on a commercial scale, where web lengths are typically 7000 m, has also proved to be a difficult process to repeat on a regular basis, and this has hindered the progress of barium ferrite media to the commercial market. However, the very high coercivity associated with these particles makes barium ferrite ideal for lower technology applications such as phone cards and car park passes since the magnetic strips used in these applications are more prone to come in to contact with large stray magnetic fields than is the case with magnetic media recording technologies and hence the high coercivity will help protect the cards and passes from data corruption.

The high anisotropy associated with the hexagonal platelets of barium ferrite results in such media having very square remanent loops and very narrow switching field distributions. Stacking of the platelets also occurs when the platelets form long chains in the direction of an applied field. Fujiwara [10] showed that the aspect ratio of the

barium ferrite particles affects several properties of the media. For instance, the saturation magnetisation, coercivity, packing density, wavelength response and signal to noise ratio are all affected by the magnitude of the particle aspect ratio. Barium ferrite tape is very stable because it does not suffer from oxidation or corrosion problems and since the particles are also very small, the associated media has excellent signal to noise characteristics. However, this inherent advantage is reduced with the introduction of digitalisation techniques since the signal to noise ratio is not as critical as with analogue recording.

Many tape manufacturers have ceased research and development into barium ferrite media due to the difficulties of low magnetisation and high volume production. However, the media may still have a future as the trend of recording at higher frequencies continues and particularly in comparison to ME media where the costs of production are less since existing particulate production techniques can be used.

1.4.1 Production of Particulate Recording Media

The production of particulate media comprises of 2 distinct stages in which firstly, a dispersion of all the relevant particles is produced followed by a second stage in which the dispersion is coated onto a flexible substrate and treated until the final media has been produced. The dispersion usually consists of the pigment (magnetic particles) contained within a mixture of solvents, binders, lubricants, anti-static agents and anti-wear agents. After the dispersion has been coated onto the substrate, a series of treatments are performed which ultimately leave the tape with a very smooth shiny top coating and a minimal amount of voids. During this second stage, whilst the coating is still wet, the tape is exposed to a magnetic field in order to give the magnetic particles a common easy axis. This results in the finished tape having a larger coercivity and remanence than would have been the case without such an alignment process.

The method by which the magnetic particles are dispersed during the first stage is usually through a milling process. The particles are dispersed in a mixture of solvents and milled until the viscosity of the dispersion is at an acceptable level. This level will vary depending on the tape specifications and manufacturers research but in general, several hours of milling may have to be performed before the correct level of viscosity is obtained. However, once a satisfactory viscosity level has been reached, binders and lubricants are added to the dispersion, together with anti-static agents and other anti-wear agents. The dispersion is then diluted by adding precise amounts of solvent until a characteristic laquer is produced. At this point in the process, the first stage has been completed and the second stage of coating the flexible substrate can commence.

Coating of the substrate takes place under carefully controlled conditions since temperature changes and roller speeds can considerably affect the final properties of the media. During coating, the substrate is commonly referred to as a "web" and can typically have a width of 0.5 m. The web is passed through a series of precision rollers and is eventually directed to a region where the web is either passed through a bath of dispersion or to an area where the dispersion is poured onto the top surface, whilst ensuring that the complete width of the web is covered. The web is then fed towards a knife edge, which it then passes underneath, leaving a smooth uniform coating of dispersion on the substrate. At this point, the web is directed though a series of permanent magnets in order for the magnetic particles to be aligned in a common direction. The uniform layer of dispersion on the web is then dried by feeding it through several heated rollers in a carefully controlled environment. Finally, the tape is split into widths, using a series of knife blades placed at equidistant positions, giving multiple lengths of identical tape which can then be used in commercial products. The outer strips of tape are discarded rather than being wound onto spools like the rest of the strips because they are more susceptible to blemishes from the coating and/or cutting processes.

1.4.2 Substrate

The most commonly used substrate or base film for particulate magnetic media is polyethylene terephthalate (PET). The thickness of the film used in magnetic media applications usually falls within the range 6 μm to 25 μm with smaller thicknesses yielding greater recording capacity. The thickness and mechanical properties of such a film can be altered by subjecting it to stretching during processing. The substrates are characterised as "balanced" or "tensilised" base films depending upon the ratio of stretching in the longitudinal direction compared to that in the transverse direction. Typically, for balanced films, the ratio is equal to unity whereas for tensilised films, the ratio usually falls within the range 2 to 3.

The thinner films (<10μm) have to be tensilised in order to maintain the yield strength and hence minimise any damage that might occur through general tape handling. However, tensilised films possess anisotropic properties which are detrimental to the overall tape performance and which can lead to off-track errors especially when the media is recorded and played back in different environmental conditions. The need for an alternative substrate which is both thinner and possesses improved mechanical properties is imperative if higher recording densities are to be realised through the modification of the substrate alone. In practice, other important factors will be improved in combination with advancements to the substrate film which will then result in substantial increases in the areal recording densities of flexible magnetic media. Polyethylene Napthalete (PEN) is a material which possess a higher strength and better mechanical stability than the conventional PET films. Thus, it is a good candidate for use as a thin substrate, even though its increased cost over PET films places it at a commercial disadvantage.

1.4.3 Binder System

The binder system holds the magnetic particles to the substrate and must possess good tribological properties such as low head wear and a low coefficient of friction. Furthermore, it must be chemically stable under different environmental conditions and exhibit minimal degradation for archival storage applications. It must also be sufficiently rigid to provide support when necessary but flexible in order to ensure the tape is able to keep close contact with the tape transport system and recording heads. The contradictory requirements of flexibility and rigidity led to the binder being manufactured from a polymeric material, usually consisting of two or more phases.

For several years, the binder system was typically a polyester polyurethane in which the polyester section of the copolymer gave the binder a soft phase for flexibility whereas the strong hydrogen bonds present in the polyurethane gave the binder an improved rigidity and greater thermal stability [11]. The ratio of the soft phase polymer to hard phase polymer was crucial since incorrect proportions could significantly affect the characteristics of the final tape. For instance, a higher percentage of hard phase polymer would lead to greater head wear and hence the percentage ratio of soft to hard phase was usually restricted to the range 50:50 to 30:70.

The polyurethane section of the binder was a hydrophobic polymer chain with a small number of hydrophilic functional groups added to interact with the water molecules, as illustrated in Figure 1.7. The hydrophilic functional groups anchored the binder to the magnetic particles whereas the hydrophobic segments formed a flexible chain, allowing the magnetic particles some movement within the binder.
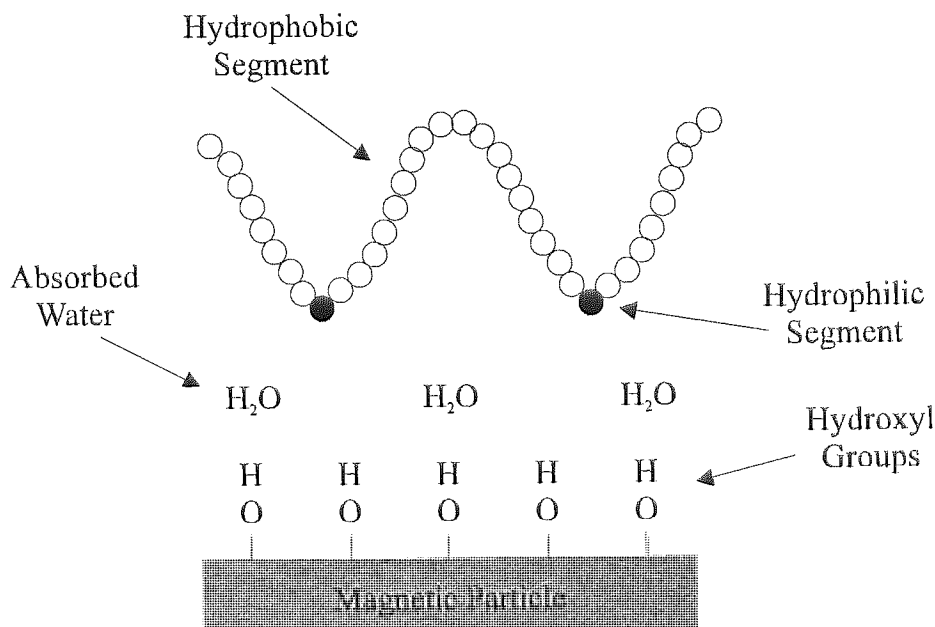
Figure 1.7 Anchoring of Binder System to Magnetic Pigment

The binders in use today are known as wetting binders and combine the functionality of both a dispersant and a binder. Most wetting binders are typically based on copolymers of vinyl chloride-vinyl acetate and contain carboxyl and hydroxyl functional groups which act to anchor the binder to the surface of the magnetic particles. The magnetic particles are dispersed by initially breaking up any existing aggregates through a milling process followed by the adsorption of the wetting binder on the pigment. The binder forms a steric barrier which physically blocks the close approach of neighbouring magnetic particles by lowering the magnetic interactions between the particles and forming a potential energy barrier which cannot be surmounted by the attractive forces of the pigments. An effective wetting binder, such as MR-110 (Nippon Zeon), will provide the magnetic coating film with excellent dispersion and orientation properties, together with a smooth outer surface.

Weingart et al. [12] reported that the use of AB-block copolymers as dispersants in magnetic coatings was advantageous since compared to wetting binders made from vinyl chloride-vinyl acetate, a higher rate of dispersion can be achieved. This is essential as the trend towards using ultra fine metal particles with large saturation magnetisations

continues. The two main functions of the dispersant (stabilisation and wetting of the pigment) can be divided into two different chemical blocks, A and B. Thus, block A provides the excellent wetting properties through interaction with the pigment surface whereas block B ensures good stabilising properties. However, one of the main advantages of using AB-block copolymers is the rapid dispersion process which allows shorter milling times without the need to add low molecular weight dispersing aids.

1.4.4 Head Cleaning Agent (HCA)

The high head-to-tape speeds associated with helical scan video recording results in wear of both the head and media. Thus, a head cleaning agent is often incorporated into the magnetic coating in order to help maintain the performance of the heads. The abrasive particles which act as the head cleaning agent are typically alumina or chromium dioxide and they help to ensure a good contact between the heads and media for the lifetime of the system by preventing a build up of debris on the heads. However, the abrasivity of the particles has to be carefully controlled because the agent must be effective in cleaning the heads but cannot be too aggressive since this would result in a high level of head wear and ultimately reduce the lifetime of the head to an unacceptable level.

1.4.5 Lubricant

A lubricant is included in the binder system to increase the lifetime of the media by reducing the friction between the media and the heads since without a suitable lubricant, the condition of the media would deteriorate rapidly due to the large coefficient of friction at the head/media interface. However, it is also important not to produce media with excess lubricant since this would lead to stick-slip behaviour (causing seizure of the system), raise the probability of generating more debris particles and increase the head-

to-tape separation [13]. A major advantage of incorporating the lubricant within the binder system is that a reservoir of lubricant will exist which can be continuously drawn upon as the media wears. The lubricant will migrate towards the extremity of the media, filling troughs and covering any asperities that might exist on the tape surface and thus providing the necessary lubrication [14, 15]. In addition to top surface migration, the lubricant may also move towards the substrate/binder interface leading to bonding problems between the magnetic coating and the substrate. Thus, the amount of lubricant within a binder system must be carefully controlled in order to ensure there is sufficient lubricant to afford the media excellent protection against wear whilst minimising the risk of media instability through excess lubricant at the binder substrate boundary.

The lubricants used in particulate media are generally fatty acid esters since these compounds possess the stringent characteristics needed for use in particulate magnetic media. Inertness is essential because lubricant interaction with the binder system, recording heads or any part of the tape guide system could result in catastrophic failure. The lubricant must also have a low surface tension in order to facilitate migration of the lubricant to the tape surface, be non-flammable, have a low surface energy to avoid adherence to debris and exhibit thermal and oxidative stability.

Static charges are generated when the media is in continuous sliding contact with the heads and tape guides of a recording system and since the polymer substrates in flexible magnetic media are good insulators, they will tend to attract the static charges. An accumulation of these charges must be avoided since it can lead to tape transport problems from high frictional forces and ultimately to data errors. The magnitude of any charge accumulation and hence the severity of the related problems can be significantly reduced by incorporating a conductive back coat to the reverse side of the media. The back coat is often produced using the same formulation as that used for the top coat with the important exception that carbon black replaces the magnetic pigment. Typically, the thickness of the back coat is 1.0 μm and it should be kept to a minimum since the

inclusion of a back coat reduces the overall cassette capacity. Additional functions of the back coat are to protect the substrate from being scratched and to act as a cushion between contacting layers of the tape, when wound on a cassette spool.

1.5 Development of Metal Evaporated Media

ME tape was first launched onto the world market by Matsushita in the late 1960's as "Angrom". It was essentially a metal evaporated thin film over a gamma double layer but it failed because at the time, the tape was incompatible with the world's recorder settings [16].

In the spring of 1989, Sony Corporation introduced thin film metal evaporated video tapes for use with Hi-8 video recorders because of the tapes high areal recording densities [17]. The Hi-8 video format uses a larger frequency bandwidth than conventional VHS recorders in order to obtain increased resolution and picture quality. It is essential that the media used with the Hi-8 system has excellent recording characteristics, especially at high frequencies in order to take full advantage of the extended band width. When metal evaporated tape was launched, the recording performance was better than that of metal particle tape [1] and hence it was considered to be the better tape for making high quality recordings. However, each tape has been developed extensively since 1989 and both formats now offer exceptional performance when used in conjunction with Hi-8 VCR systems. Further evidence of ME tapes development was provided by Exabyte when they announced that advanced metal evaporated media would be used with their "Mammoth 8 mm Tape Drive" in order to achieve a recording capacity of 20 GB without any need for data compression [18].

The magnetic particles of a particulate tape only make up about 35% to 45% by volume of the magnetic layer due to the necessity of including other constituents such as lubricants, solvents and wetting agents. These additional components have no magnetic properties and thus do not contribute to the remanence flux density of the tape. In contrast to particulate media, metal evaporated thin film tape does not incorporate a binder system since the magnetic layer is applied directly to the substrate through a vacuum evaporation technique. Thus, the proportion of magnetic material within the

magnetic layer is substantially greater with approximately 80% of the magnetic layer contributing towards the remanence flux density of the tape. The remainder consists of a non-magnetic cobalt oxide layer and a series of small voids which exist within the structure of the layer. Figure 1.8 shows a schematic cross section of a metal evaporated thin film tape.
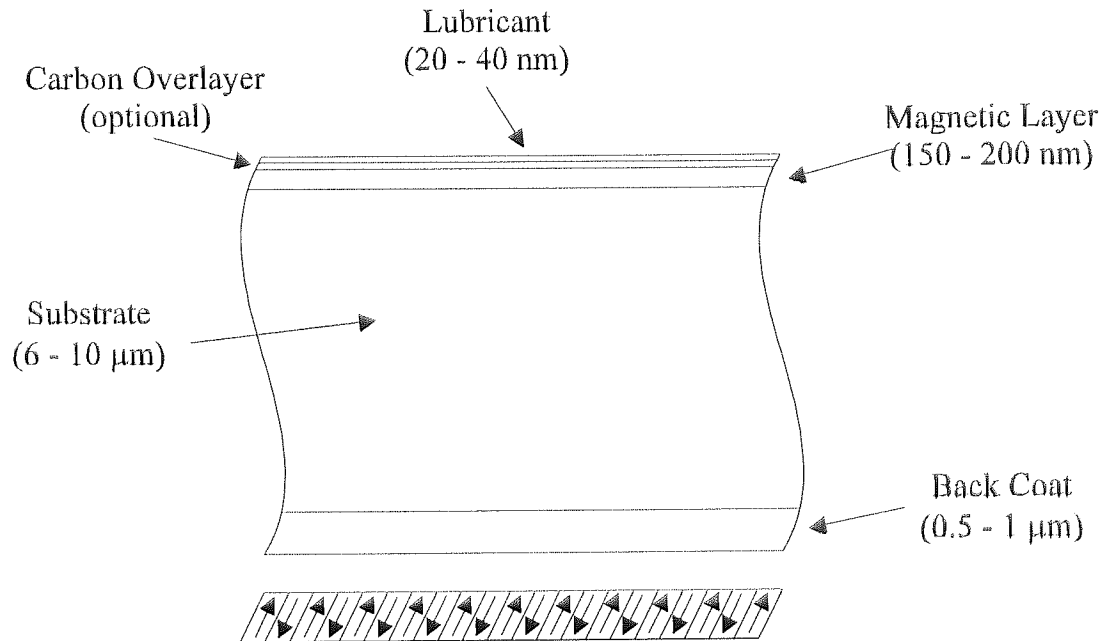
Figure 1.8 Schematic Cross Section of a Metal Evaporated Tape

1.5.1 Substrate

The materials used for the substrate of ME media must be flexible, adhere well to the magnetic layer and backcoat, be mechanically strong for good tape handling and be very thin in order to facilitate high tape capacities. These properties are also common to the substrates used in the production of particulate media and hence either polyethylene terephthalate (PET) or polyethylene napthalates (PEN) films are commonly used. A further characteristic which the substrates for ME media must possess is that of being able to withstand the higher temperatures associated with the vacuum coating technique.

The development of ME media has lead to the utilisation of thinner base films and this has tended to make PET a minority substrate. PET films are more susceptible to the effects of temperature and have slightly poorer mechanical properties than PEN films. Polyaramids such as "TX" are also used in the latest generation of ME tapes since like PEN films, they have good temperature resistance properties and can afford the tape sufficient stiffness for use in helical scan formats.

The surface roughness and texture of the substrate films are of paramount importance for ME media because it is the surface characteristics of the substrate which dictates the surface roughness of the metal layer. Indeed, the surface of the substrate is far more crucial for thin film ME media than for particulate media because no calendering of the tape is possible with ME media. Calendering is a common process in the manufacture of particulate media in which the tape is passed through a set of rollers which exert pressure on the tape in order to remove any air bubbles. Ultimately, this helps give the tape a smoother outer surface.

In order to give the finished ME film the correct surface properties, the pure PET substrate film is pre-treated to give it a textured surface. The precise construction of the substrate film various with each manufacturer but generally, the surface which is to be metalised is given a smoother texture to that of the backcoat surface, as illustrated in Figure 1.9. This construction consists of a base layer of pure PET without any slip agent particles with a second thinner layer of PET on the back side containing a slip agent. The ME side of the substrate is coated with a binder which contains smaller slip agent particles than on the backside. In the configuration shown in Figure 1.9, the backside of the substrate is left uncoated but some manufacturers prefer to use a substrate in which both surfaces are coated with a binder containing slip agent particles.

Surface Treated

Pure PET

No Surface Treatment
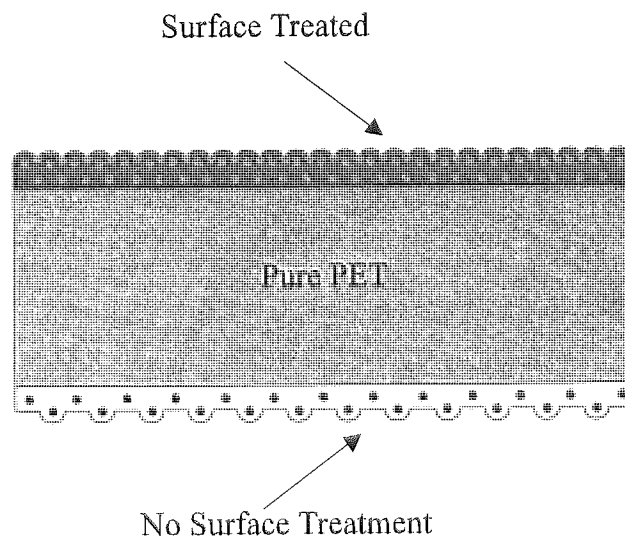
Figure 1.9 Sectional View of a Typical Substrate with Textured Surfaces

The difference in roughness results from the necessity of keeping the recording heads and magnetic layer in close proximity with a smooth clean contact whereas the backcoat must be relatively rough in order to ensure good tape handling properties. Typical values for the average roughness (R_a) of the top surface and backcoat are 2.5 nm and 5.0 nm respectively.

1.5.2 The Magnetic Layer

The magnetic layer of a metal evaporated tape is produced by the evaporation of a magnetic alloy such as $Co_{80}Ni_{20}$ onto a polymer substrate as shown in Figure 1.10 [19]. The magnetic layer on the first commercial ME tapes had an approximate thickness of 200 nm but with the latest tapes, this has been reduced to nearer 150 nm as technology has advanced to keep apace with the market demands for increased data storage.
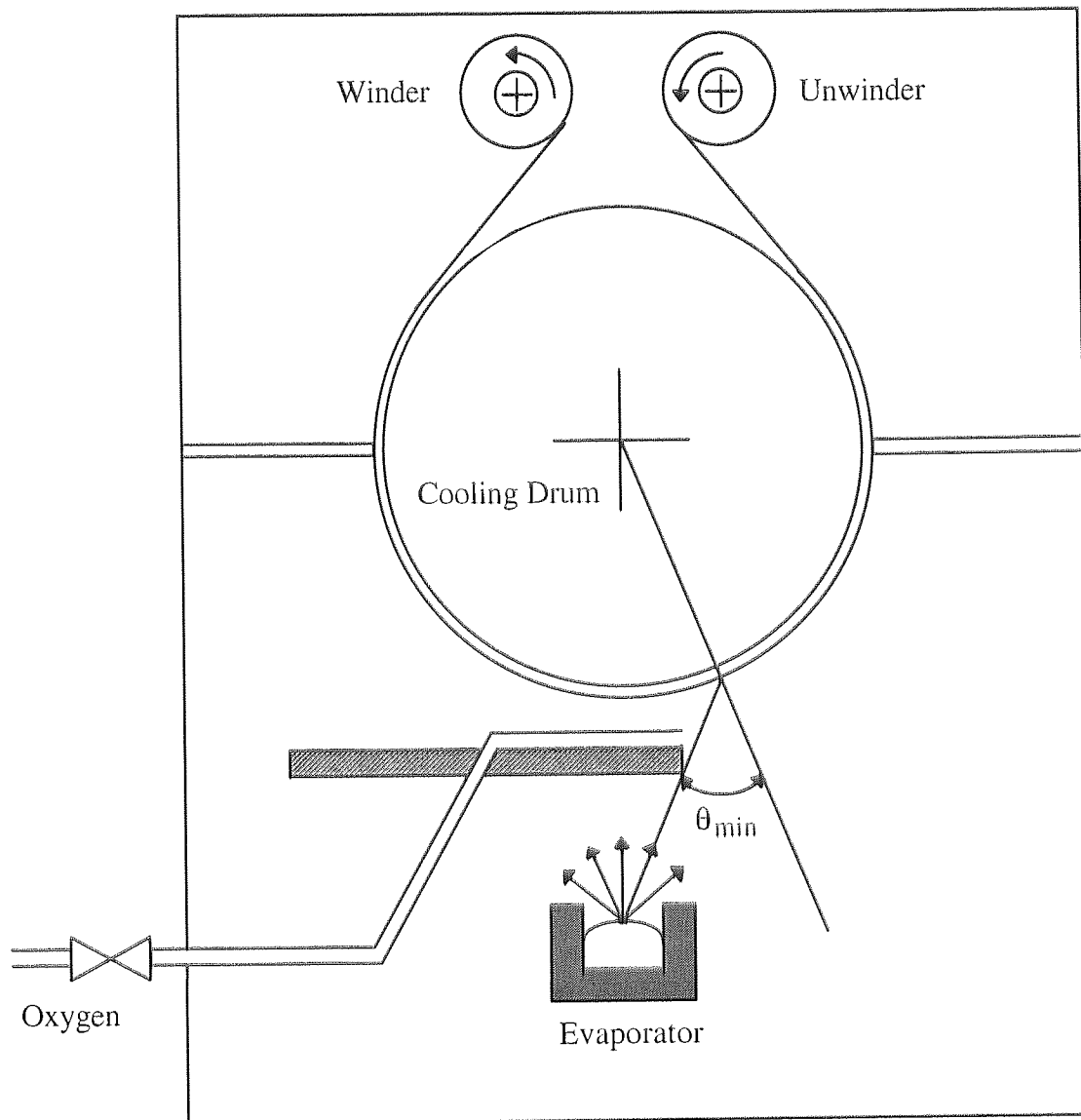
Figure 1.10 *Schematic Diagram of the Basic Equipment for Deposition of a Magnetic Layer*

The magnetic alloy is liquefied by an electron beam under vacuum conditions and the resultant metal vapour is directed towards the substrate. The pre-treated substrate is in contact with a rotating drum such that the substrate is cooled to a temperature of -25°C. This ensures that when the vapour comes into contact with the substrate, the vapour will immediately condense, forming of a thin metal layer. It is also necessary to introduce a carefully controlled amount of oxygen during the evaporation process in order to partially oxidise the cobalt and nickel metals. The magnetic layer consists of very small ferromagnetic cobalt and cobalt-nickel crystallites intermixed with antiferromagnetic

oxides of cobalt and nickel, inclined in a columnar structure parallel to the plane of deposition as shown in Figure 1.11. The existence of the metal oxides and voids within the layer are essential since they contribute towards the stability of the film and influence the magnetic characteristics of the tape [20].

0.1 μm
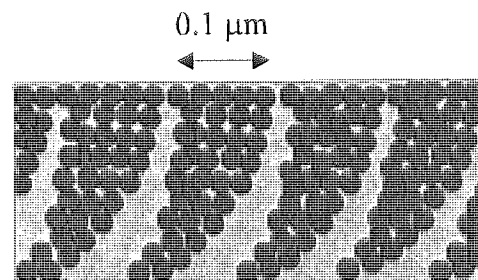
Figure 1.11   Characteristic Curved Columnar Structure of a ME Thin Film

The susceptibility of cobalt and nickel to corrode is significantly reduced by the presence of the metal oxides since they form a protective layer over the nickel and cobalt crystallites. The stability of the magnetic layer is improved further by the addition of a topical lubricant layer and sometimes by a thin intermediate carbon layer [21].

The magnetic properties of the metal film are dependent on the amount of oxygen flow and the oblique incidence angle of deposition, θ_{min}. The incidence angle, θ_{min} controls the evaporation efficiency and the magnetic characteristics of the thin metal film. Chiba et al. [4] show how the coercivity of the thin film media is dependent upon the flow of oxygen and the oblique incidence angle of deposition. For instance, higher coercivity values can be achieved if the initial deposition of the film is performed at large angles, with the subsequent growth occurring at smaller angles. In a production system, the angles are controlled by a mask which prevents the deposition angle from moving outside a designated range. Typically, the initial angle of deposition is 90° which is then reduced to 60° in order to obtain the correct curved profile for optimum magnetic properties. Feuerstein and Mayr [22] showed how the columnar structure varies in shape depending upon the range of angles used in the deposition of the film, as illustrated in Figure 1.12.
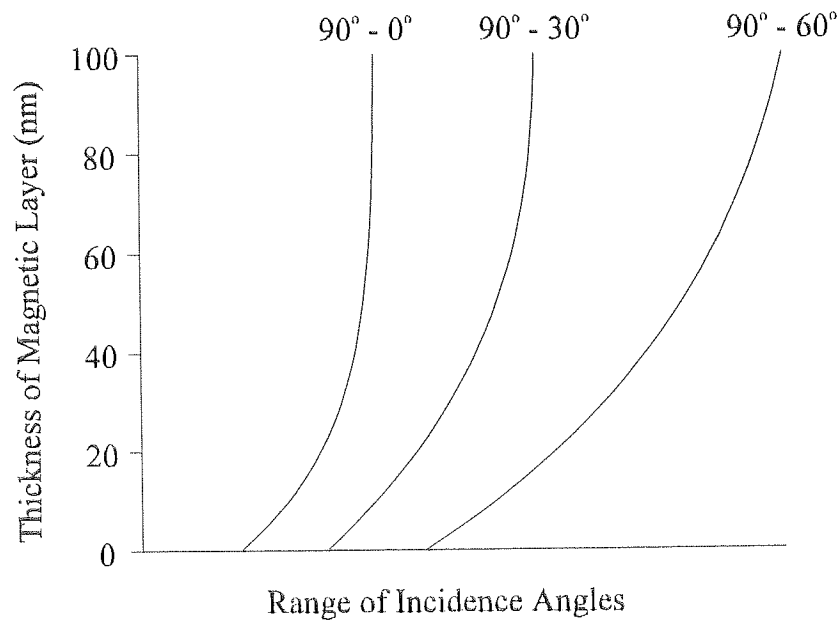
Figure 1.12 Profiles of Columns Deposited within Different Ranges of Incidence Angle

In addition to the angle of incidence for deposition of the thin film, the magnetic and mechanical characteristics of the magnetic layer are affected by the oxygen content within the layer [23] and hence the amount of oxygen introduced during the evaporation process has to be carefully controlled. The construction of the magnetic layer is further complicated by the relationship between the angle at which the oxygen is introduced and the properties of the film since the microstructure of the magnetic layer varies depending on the geometry of the oxygen injection. When the oxygen is introduced, it reacts with the surface of the columns which ultimately yields an improvement in the isolation between neighbouring columns and hence a reduction in the amount of noise. Indeed, the magnetic layer can be considered to have a pseudo-particle microstructure as a result of the decoupling effects of the oxygen. However, the amount of oxygen introduced during evaporation has to be limited since its presence reduces the magnetisation of the magnetic layer. Thus, a compromise has to be found in which the improved noise and stability characteristics of the layer are balanced with maintaining good magnetisation properties.

1.5.3 Multilayer Films

The recording characteristics of ME tape are highly dependent on the relative direction of travel between the head and the tape. A higher output voltage is obtained when a signal is recorded and played back in the same direction as the grain tilt compared to when the signal is recorded and played back in the opposite direction to the grain tilt. Indeed, the output pulses exhibit a strong asymmetry where the height and width are significantly different for each direction of tape travel. Applications such as video recording, in which the recording and playback processes are uni-directional, are not significantly affected by the dependence on direction of tape travel. However, the same cannot be said for linear applications such as data cartridge systems where the tape is played in both directions. In these cases, there cannot be any significant difference in the shape or magnitude of the output pulses since this will lead to data errors. Thus, if ME tape is to have a future in such applications, the directional dependency problem must be overcome. One possible solution is to use a multilayer configuration, such as that shown in Figure 1.13, in which the needle shaped columns of each layer are oriented in opposite directions, relative to the film normal. The pulse asymmetry problem can be alleviated by ensuring the lower layer has a larger thickness than that of the upper layer since this will compensate for the effects of spacing loss.

Non-Magnetic
Isolation Layer

Double Magnetic Layer

Substrate
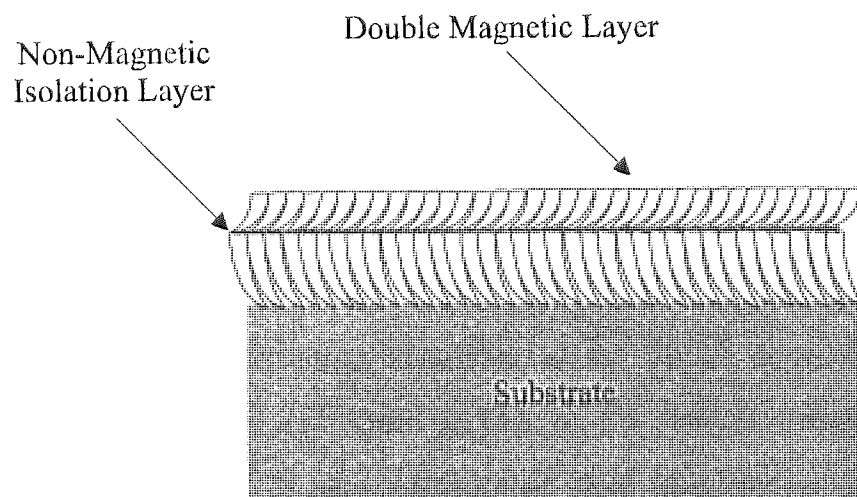
Figure 1.13 Columnar Structure of a Double Magnetic Layer

Media noise is one of the major sources of noise within a recording system and is greatly influenced by the structure of the film. Indeed, multilayer magnetic films with thin non-magnetic isolation layers between each magnetic layer exhibit lower media noise than single layer media of the same total thickness. Duan et al. [24] studied the magnetic and recording properties of single and multilayer magnetic media and found there was a significant increase in the signal-to-noise ratio for double and triple magnetic layer media, when comparing media with a similar coercivity. They also observed that the increase in the signal-to-noise ratio was highly dependent on the total magnetic layer thickness and on the number of magnetic layers.

The improved performance through the reduction of media noise in laminated thin film media arises from two mechanisms. Hata et al. [25] initially proposed that the noise reduction was due to magnetic decoupling between magnetic layers. This was then extended by Lambert et al. [26] who proposed that an additional mechanism existed because very thin films inherently exhibit an improved noise performance due to the nature of the grain structure within the layers. The grains in the initial part of the layer are smaller and less tightly packed than those in thicker layers and hence voids exist which help to decrease the exchange coupling between neighbouring grains. The characteristic low density grain structure in the initial part of the layer is then repeated every time a magnetic layer is deposited on a non magnetic interlayer. Thus, the low noise properties of a single thin film are maintained for a multilayer film even though the total thickness of the multilayer film is equivalent to that of a conventional single layer thin film.

The two noise reducing mechanisms contribute to the overall improved recording performance but the dominant mechanism depends on the number of magnetic layers. For instance, the decoupling of adjacent layers is more likely to be the significant mechanism when several layers exist although the improved noise properties of a very thin film will contribute to some of the improvement. However, a limit exists, beyond

which no advantage will be achieved through merely increasing the number of layers within a tape structure. Sanders et al. [27] have shown that very thin films with a thickness of approximately 10 nm exhibit no improvement in the signal to noise ratio.

1.5.4 Carbon Overlayer

A continuous overlayer must be incorporated into the structure of thin film ME media in order to protect the tape from the effects of wear and corrosion, and to increase the lifetime of the tape. The protective overcoat on ME tape always includes a topical lubricant but sometimes also incorporates a hard carbon overlayer between the magnetic layer and lubricant. The carbon layer improves the tribological performance of magnetic media, as has been proved by the thin film rigid disk industry [28], since it is tough, durable and acts as a primer for the mandatory lubricant. The overcoat must also be dense and be non-permeable to oxygen and water vapour. Deposition of the carbon layer has to be a low temperature process since high production temperatures may adversely affect the properties and structure of the magnetic layer. The coating must also be extremely thin in order to ensure that any decrease in the output signal caused by the introduction of spacing losses will be kept to a minimum.

The thin film rigid disk industry has successfully incorporated Carbon and Diamond-Like Carbon (DLC) layers as protective overcoat films and thus both have been considered as possible materials for inclusion within ME media [29-30]. Diamond is synonymous for possessing the unique properties of extreme hardness and excellent chemical inertness. It also has a high electrical resistivity and thermal conductivity which are all essential requirements for a good protective overcoat.

The most effective method of depositing the DLC film is a two phase method in which a chemical vapour deposition (CVD) technique is used to form a stable graphite film at a

low pressure by activating compounds which contain carbon. Atomic hydrogen is then introduced to remove the graphite in order to leave a diamond-like structure. Conventionally, a hydrocarbon gas is used as the source for both the carbon and hydrogen, with high process temperatures or high frequency plasmas introduced to supply the activation energy. However, high process temperatures are unacceptable for depositing the carbon layer on thin film media and hence chemical vapour deposition is not a suitable technique if it involves hot filament or high frequency plasma generators.

A low temperature (<150 $^{\circ}$C) plasma CVD technique has been developed in which amorphous diamond films can be deposited onto polyester substrates. A high frequency (13.56 MHz) discharge is generated within a mixture of hydrocarbon and hydrogen. A negative potential is generated on the substrate which is then bombarded with ionised gas species, giving rise to the formation of a plasma. The exact form of the DLC film is highly dependent on the process environment but this can be controlled by varying the deposition and plasma conditions. Several plasma-enhanced CVD techniques are currently under development, using a combination of RF and DC potentials to generate high density plasmas at large growth rates.

The microstructure and tribological properties of the DLC films are greatly affected by the method of deposition and if incorrect, can lead to a poor protective film. Factors identified were the RF-power, pressure and film composition used during deposition [31]. A further problem associated with DLC is the low adhesion between itself and the magnetic layer although Suzuki et al. [30] reported that high wear durability could be obtained if the magnetic layer was cleaned before deposition of the carbon. The oxide present at the interface between the DLC and the media was found to have a detrimental effect on the adhesion of the film but this could be removed by pre-cleaning the magnetic layer with hydrogen plasma.

1.5.5 Lubricants

The inclusion of a lubricant on the top surface of ME media is imperative in order to give the tape good durability and low wear characteristics. Video systems place high tribological demands on media, particularly when the recorder is operated in still frame mode. Thus, the lubricant must protect the media from continuous head contact without significantly impairing the magnetic properties of the tape. Spacing losses become more appreciable at higher frequencies and thus the lubricant layer should be made to be as thin as possible, whilst still affording the tape good protection. Lubricant thicknesses of 2 - 4 nm can provide complete areal coverage whilst not significantly detracting from the magnetic characteristics of the ME film.

The rigid disk industry commonly use lubricants with a perfluoropolyether (PFPE) backbone due to the good chemical inertness, low surface tension, good lubricity, excellent thermal stability and low viscosity. These properties are also highly desirable for ME media although the exact characteristics are dependent on the structure and molecular weight of the PFPE backbone. Table 1.1 shows the chemical structure of a group of commercial PFPE's, each of which possesses high adhesion energy and low vapour pressure. These are essential properties if the lubricant is to have a useful lifetime on the surface of thin film ME media.

Trade Name	Chemical Structure
Fomblin Y	$CF_3 - O - [(CF_2 - O)_m - (CF_2 - CF - O)_n] - CF_3$ with pendant CF_3
Fomblin Z	$CF_3O - [(CF_2 - O)_m - (CF_2 - CF_2 - O)_n] - CF_3$
Demnum	$F - [CF_2 - CF_2 - CF_2 - O]_n - CF_2 - CF_3$
Krytox	$F - [CF_2 - CF - O]_n - CF_2 - CF_3$ with pendant CF_3

Table 1.1 Chemical Structure of Commercial PFPEs

PFPE's are non-reactive with plastics, polymers and most metals. However, thin film ME media require a strong chemical bond between the PFPE lubricant and the magnetic layer in order to improve overall durability. Adhesion of the lubricant to metal or metal oxide is enhanced through the introduction of a reactive end group to the extremities of the molecular chain. These end groups are known as 'functional derivatives' and are essential if good bonding of the lubricant to the tape surface is to be achieved. Table 1.2 shows the chemical structure of commercial functional PFPE's.
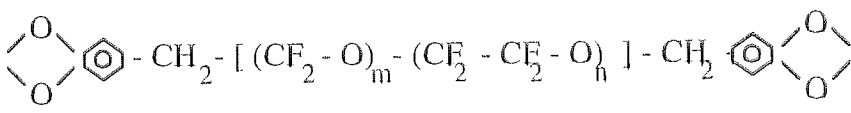
Trade Name	Chemical Structure
Fomblin Z-Dol	$HO - CH_2 - [(CF_2 - O)_m - (CF_2 - CF_2 - O)_n] - CH_2 - OH$
Fomblin Z-Deal	$\begin{matrix} & O & & & O \\ & \parallel & & & \parallel \\ CH_3 O - C - & [(CF_2 - O)_m - (CF_2 - CF_2 - O)_n] & - C - O - CH_3 \end{matrix}$
Fomblin AM2001	
Krytox 157 FSM	$CF_3 - CF_2 - O - \left[\begin{matrix} CF_2 - CF - O \\ | \\ CF_3 \end{matrix} \right]_n - CF_2 - \underset{\underset{O}{\parallel}}{C} - OH$

Table 1.2 Chemical Structure of Commercial Functional PFPEs

The exact nature of the lubricant to be applied to the media depends on whether a protective carbon layer has already been deposited onto the magnetic film. For instance, PFPE lubricants with neutral terminal groups are usually applied when a carbon surface is the recipient layer since PFPE lubricants with neutral terminal groups can interact strongly with carbon. Such lubricants also possess greater hydrophobic properties than those with functional derivatives and hence exhibit lower water permeability, increasing the protection afforded to the magnetic layer from the effects of corrosion. If a carbon overlayer has not been deposited onto the metal film, a PFPE lubricant terminated with functional end groups must be used in order to ensure strong bonding between the

67

lubricant and metal or metal oxide surfaces. A choice has to be made between accepting the higher spacing losses associated with including a dual carbon and PFPE protective layer, or giving the magnetic film maximum protection. The necessity of having the smallest possible spacing losses for the greatest signal output may dictate that thin film media of the future can only afford to have a single protective layer.

A variety of bonds exist between the molecules of the lubricant and surface of the tape. However, the interaction between the backbone of the PFPE lubricant and the tape surface is primarily through van der Waals forces. Takeuchi et al. [32] measured the energy of such an interaction and found the energy associated with each CF_2 unit of the polymer chain to be 6 KJ/mol. Furthermore, Perry et al. [33] estimated the van der Waals energy associated with the interaction between the backbone of a 2000 amu PFPE lubricant and a recipient carbon surface to be approximately 200 KJ/mol. These energies are sufficiently strong to ensure the molecules of the lubricant lie flat on the tape surface.

The stronger energy bonds associated with hydrogen and covalent bonding occur at the interactions between the functional end group of the lubricant and the recipient surface of the tape. However, the strength of the interaction is dependent on the type of adsorption site that exists on the tape surface but if the lubricant has an alcohol end group (-OH), the molecules would be expected to interact with an unpaired pair of electrons in the recipient surface through hydrogen bonding whereas if the lubricant had a carboxyl end group (-COOH), the lubricant would be expected to interact with the recipient surface through covalent bonding.

The improvement and optimisation of PFPE lubricants was the breakthrough which originally enabled ME media to be introduced to the commercial market. However, manufacturers of ME tape still invest large resources on improving the performance of lubricants, particularly the functionalisation of the PFPE's, since significant improvements in the durability of the media can only be achieved in conjunction with improvements to

the lubricant [34]. Such improvements include the mechanical behaviour and surface chemistry between the heads and media during tribological interactions.

It has been shown that bonding can be enhanced by subjecting the PFPE lubricant to different forms of radiation [35-37]. Saperstein and Lin [35] treated the lubricant with ultraviolet radiation which improved the anchoring of the PFPE to the metal film. Heidemann and Wirth [36] used low energy X-rays whilst Homola, et al. [37] experimented with nitrogen plasma radiation. A further study by Lee [38] compared the effects on tape durability when the PFPE lubricant was exposed to X-rays, electron beams and ion beams. Dissociation of the PFPE occurred with each type of irradiation resulting in the formation of metal fluoride bonds and an improvement in the durability of the media.

In addition to the strong chemical bonds between the lubricant-metal interface, a lubricant may also include a mobile component. A combination of the flexible molecular structure of the CF_2 - CF_2 - O ether bonds and the weak van der Waals cohesive forces between each chain give the PFPE polymers the essential low viscosity and surface tension which help ensure that if any lubricant is removed locally by strong contact between the head and media, it can flow back, cover the damaged area and extend the lifetime of the tape.

The lubricant can be applied to the magnetic film or carbon layer, using a gravure roller technique, as shown in Figure 1.14, or by spray coating methods.

Thin Film Media
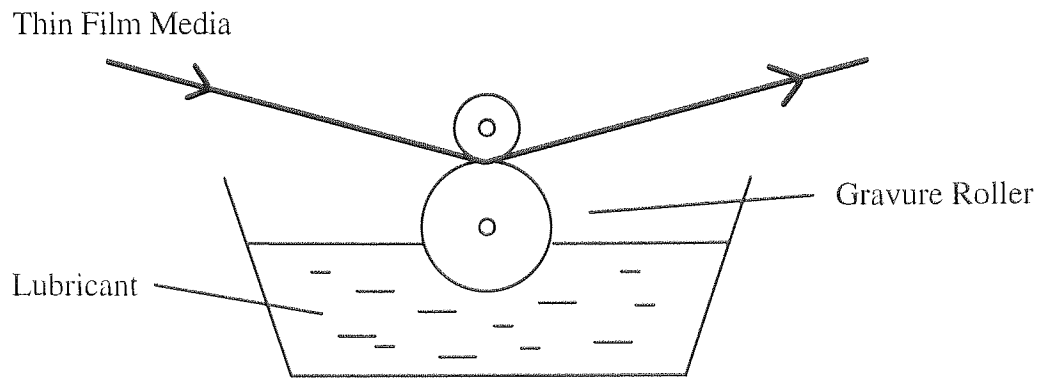
Figure 1.14 Deposition of the Lubricant Layer by Gravure Roller Techniques

Both techniques must apply a thin evenly distributed lubricant coating at a very low web tension since high tensions can lead to cracking of the metal film. When the spray coating technique is used, a dilute solution of the lubricant solvent in trichloro-trifluoro-ethane is sprayed onto the metalised substrate or carbon film. The solvent is then evaporated, leaving a lubricant coating with a thickness of just one or two monolayers. If the thickness of the lubricant layer is lower than the peak-to-peak height of the surface onto which it was deposited, boundary lubrication will occur. If however the thickness of the lubricant is comparable with, or larger than, the surface roughness, elasto-hydrodynamic lubrication will take place, which may lead to an increase in the coefficient of friction between the head and media, due to the effects of stiction.

1.5.6 Backcoat

The substrate, magnetic layer and lubricant coating have all been developed extensively since the original conception of flexible thin film media. However, the back coat is also a key constituent since the absence of a good backcoat can significantly affect the overall runnability and performance of the tape. Backcoats are incorporated within ME media, primarily for the same reasons as for particulate media. Namely, to enhance tape transport and to aid static dissipation. However, the formulation is slightly different to

that used on particulate media since the backcoat must exhibit greater adhesion and durability. This is achieved by using a pigment which has slightly better dispersive properties although the backcoat formulation still includes polymers, solvents, abrasives, lubricants, anti-static agents, plasticizers and wetting agents. Without any improvement, the pigment would tend to stick to the magnetic layer, ultimately leading to an increase in the number of dropouts and eventually to head clogging [39]. The pigment must be conductive, usually carbon black, and can be applied using the conventional techniques such as gravure methods. If the backcoat is applied prior to deposition of the thin metal film, it can be calended in a similar manner to that performed to the dispersion coating on particulate media. However, if the backcoat is applied after the metal film has already been deposited onto the substrate, calendering is not feasible due to the incompressible character of the thin metal film.

1.6 Future Trends of Magnetic Media

Recording densities are expected to continue to increase at a high rate of expansion as new memory intensive applications evolve. It is anticipated that the vast majority of information will be stored digitally, recorded at short wavelengths in order to facilitate high areal recording densities.

Thin film metal evaporated media is at an immediate disadvantage to particulate media because of the higher manufacturing costs associated with the complex production of ME media. Indeed, there are several discrete stages involved from applying a textured undercoat to the substrate, evaporating a metal layer under vacuum conditions, and finally the application of a topical lubricant. Additional stages are necessary if, for example, a double layer metal thin film is to be included within the tape or a protective diamond like carbon film is applied between the metal film and the lubricant layer.

The cost of production of any particular type of media is irrelevant if the media cannot meet the specifications demanded by high density recording applications. Thus, excellent electromagnetic characteristics for recording at short wavelengths are essential if the media is to be viable for use in the latest memory intensive applications.

Media with a high coercivity is imperative in order to help reduce demagnetisation effects, especially at short wavelengths. However, it is not necessary to produce a tape with an indefinitely large coercivity because the magnitude of the coercivity is limited by the need to be able to write a field on the media using state of the art recording heads. Currently, Ferrite/Metal-in-Gap (MIG) heads and thin film heads can be used to write fields on media with a coercivity of approximately 2000 Oe. It is expected that film materials with a magnetisation saturation of 3000 Oe will soon be developed [40] and hence this will enable the coercivity of media to be extended beyond the current maximum value and still be used in high density recording systems.

Producing media with high coercivity values depends upon the nature of the media. For instance, barium ferrite media can be readily produced with a coercivity of 5000 Oe whereas for conventional particulate tape, coercivity values approaching 2500 Oe are relatively difficult to produce. In the case of thin film media, it is very difficult to produce media with a coercivity beyond 2000 Oe so not only does thin film media have higher associated production costs but at the present time, it is not possible to produce media with very high coercivity values.

Thin film media has, since its conception, had at least one advantage over particulate tape in that it has very high magnetisation. However, particulate technology has advanced on several fronts in the past few years, especially through the introduction of double coating techniques and the utilisation of smaller particles. Indeed, the latest MP^{++} media has been improved to such an extent that it not only rivals thin film media in terms of magnetisation but experimental results have been published which show the magnetisation of MP^{++} to exceed that of thin film media. Table 1.3 lists typical values for properties of different types of particulate and thin film media.

	MP	MP^{++}	$BaFe^{++}$	ME
Particle Shape	Accicular	Accicular	Platelet	Cubic
B_r (G)	2500	3500	1350	3700
H_c (Oe)	1550	1900	2000	1100
B_r/H_c	1.6	1.8	0.7	3.4
Squareness	0.82	0.82	0.75	0.80
SFD	0.35	0.33	0.10	0.10

Table 1.3 Summary of Properties of Particulate and Thin Film Media

1.7 Video Heads and Hi-8 Recording System

The heads used in consumer and professional video recorders are conventional inductive thin film heads consisting of a ferrite or metallic alloy ring, divided by a gap of nominal width, where the width of the gap determines the width of the track recorded on the tape. The main formulations of ferrite used in the construction of video heads are Ni-Zn and Mn-Zn, or in the case of a permalloy, Ni-Fe. Each of these materials possess the essential features required for efficient and reliable magnetic heads, namely mechanical hardness, chemical stability and excellent magnetic properties (See Section 1.2).

The use of such non-conducting head materials significantly reduces eddy current losses, particularly at high frequencies and this has eliminated the need to manufacture heads with a laminated structure. The main technique for producing video heads is by cutting the head material from a single crystal in the crystal plane which exhibits the greatest hardness. This ensures the head will have the optimum wear characteristics for a particular crystal structure and this plane is then orientated with its surface parallel to the direction of the tape motion. The surface of the head also curves away from the gap in parallel and perpendicular directions to the tape motion in order to ensure that the maximum head-tape contact will occur at the gap and hence help minimise the wear characteristics of the overall system.

In a Hi-8 video recording system, there are two read/write metal-in-gap (MIG) heads positioned diametrically opposite to each other on a drum (or scanner). Each of these heads is constructed from single crystal Mn-Zn ferrite with a crystalline Sendust metal alloy (Fe-Si-Al) in the gap, as shown in Figure 1.15. MIG read/write heads are used in Hi-8 recording systems since they possess a high magnetic field strength which enables then to write onto high coercivity magnetic media. In addition to the two read/write heads, a flying erase head is also included on the drum and sometimes a fourth head for automatic track finding.
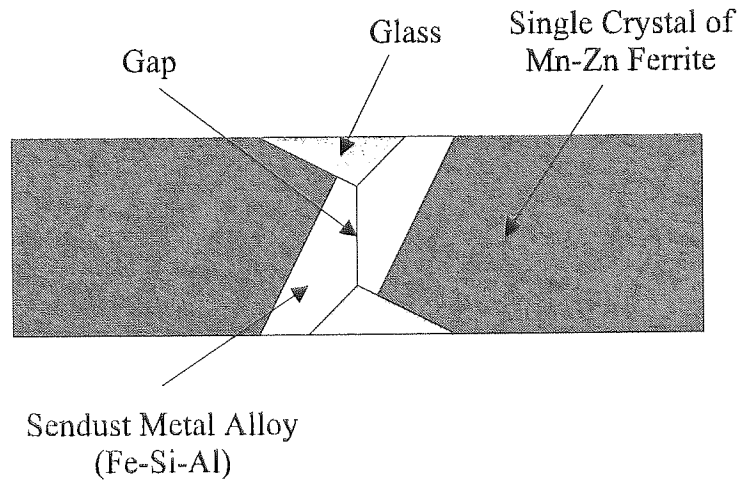
Figure 1.15 Read/write MIG Head, as used in Hi-8 Video System

All video signals consist of a luminance signal, Y, and a chrominance signal, C, as illustrated for a Hi-8 video system in Figure 1.16. The luminance signal contains all the monochrome information and gives the image its shape whereas the chrominance signal contains all the colour information. The high upper frequency limit of 7.7 MHz for the luminance signal necessitates frequency modulation (FM) recording of video signals in combination with the use of rotary head technology.
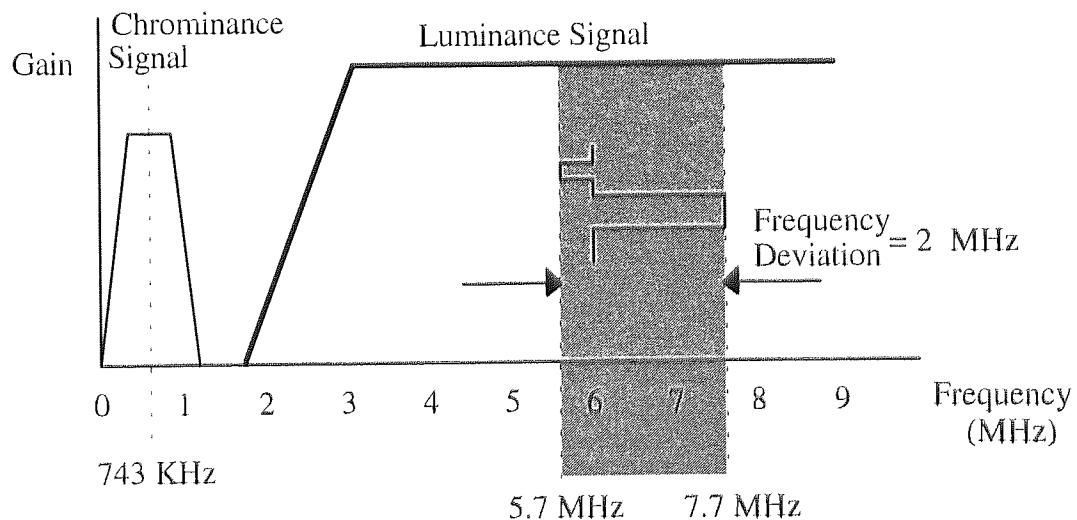
Figure 1.16 Frequency Spectrum of a Hi-8 Video Signal

In FM recording, the initial input waveform signal is passed through a frequency modulator prior to the signal being recorded in order to produce a frequency dependent signal which exactly corresponds to the initial input signal. The frequency modulated signal is dependent on the timing of zero crossing points rather than on the shape or amplitude of the waveform itself. This effectively makes the system insensitive to the effects of amplitude instability, the effects of which are responsible for AM radio broadcasts being of a poorer quality than FM radio broadcasts. When the initial signal waveform is to be retrieved, the frequency modulated signal is passed through a demodulator in order to convert the signal back to its initial state.

Another reason for using FM to record signals in video recorders is the need to reduce the ratio of the upper to lower signal frequency. For instance, the upper frequency signal in a Hi-8 video system is 7.7 MHz and this prevents the signal being recorded directly using amplitude modulation since the maximum upper to lower frequency ratio for practical video heads is approximately 5000:1. This ratio figure is limited by the physical length of the head and also by the size of the gap within the head since each of these determine the longest and shortest wavelengths it is possible to record and thus ultimately, the minimum and maximum recorded frequencies.

In order to be able to record at high frequencies, FM must be used in conjunction with very high relative head-tape speeds (3.81 ms^{-1} for Hi-8 video recorders). Such speeds are not sustainable for normal operation with a fixed head configuration since the media would not be able to survive such a harsh local environment. In order to overcome this problem, rotary head technology is used whereby the heads are fixed on a rotating drum (scanner) which then rotates at 1800 rpm (Hi-8 system) whilst the tape moves at a much slower rate of 0.0143 ms^{-1}. The relative motion between the heads and tape is sufficient to enable the high frequencies to be recorded. In the Hi-8 video system, the tape is wrapped around the drum in a helical scan format such that heads on the drum scan diagonally across the tape, as shown in Figure 1.17.

Scanner Direction

Tape Direction
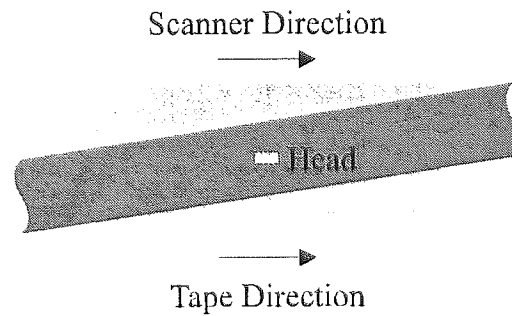
Figure 1.17 Scanner and Tape Rotation in Hi-8 Helical Scan Format

The angle between the tape and drum results in diagonal tracks across the tape, as shown in Figure 1.18, and in the case of Hi-8 video systems, this angle is 4.9° and is sufficient to ensure the length of each individual track describes one complete television field.
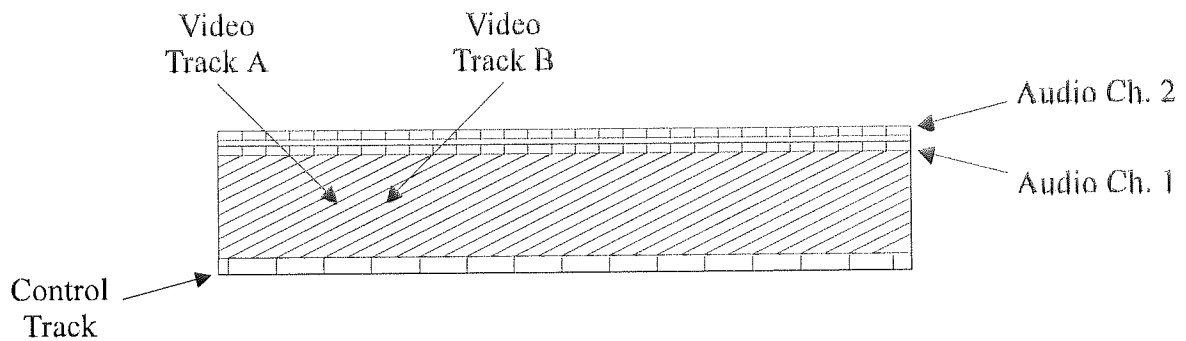
Figure 1.18 Position of Tracks on a Tape when using a Hi-8 Video System

A summary of the specifications for the Hi-8 video system is given in Table 1.4. Metal evaporated and metal particle media are both suitable for use in such a system although it is recommended that interchanging the two types of tape should be avoided [41].

Drum diameter	0.04 m
Drum Speed	1800 rpm
Writing Speed	3.76 ms^{-1}
Forward Tape Speed	14.35 mms^{-1}
Track Length	0.063 m
Track Angle	4.9^{O}
Video Track Pitch	20.5 μm
Luminance Range	5.7 - 7.7 MHz
Chrominance Sub Carrier Frequency	743 KHz

Table 1.4 Specifications of Hi-8 Video System

1.8 Tribology of Magnetic Recording Systems

Tribology is defined as the science of interacting surfaces in relative motion [42] for which Suh [43] identified three important factors. The physical and chemical surface interactions with environmental constituents, such as the lubricant; the response of the material in the near surface region of the interface, when acted on by external forces; and finally, the generation and transmission of forces between surfaces in contact. Each of these factors can cause the surface topography of a sample to change through the generation of wear particles.

However, the tribology of magnetic media differs considerably from that of conventional tribology. The trend of using thinner magnetic coatings, smaller read/write head dimensions, narrower track widths and a smaller spacing between the head and media has produced tribological contact problems which now threaten to hinder the projected increase in storage densities of flexible magnetic media. One way of achieving higher recording densities is to minimise the spacing losses between the media and the head. The smallest spacing loss will be realised when the distance between the magnetic part of the media and the head is reduced to zero. i.e. when the two surfaces are in intimate contact with each other.

It is the mechanical contact problems caused by intimate contact which are now, and that will in the future, be one of the most influential factors in restraining the development of high density recording media. To date, most of the problems related to tribological contact have been overcome by using harder head materials in combination with lower contact pressures and improved lubricants. In addition to do this, the laws of tribology have been favourable since they tend to naturally assist low wear rates (1.8.2 Friction in Polymers).

The drives used in the latest generation of recording systems have a smaller power rating than those used in previous systems due to the continual trend towards miniaturisation of system components. However, this fact has now placed a further emphasis on the importance of friction since if it is too high, the performance of the system could be impeded through variations in tape speed or ultimately through failure of the drive motors. Friction can be characterised into static and dynamic friction with static friction being the force required to initiate motion whereas dynamic friction is the force required to maintain it. Generally, static friction is higher than dynamic friction because the force required to initiate movement is greater than that needed to sustain it. This is particularly true for recording systems such as tape drives, in which the head rests on the magnetic media during start up. A high frictional force may exist which will ultimately cause the initial movement of the media to be uneven and jerky. This phenomena is known as stick-slip and in severe cases can result in the tape being unable to move. Rigid disk drives are also prone to problems caused by stick slip because there is physical contact between the disk and head slider during start up. The high initial friction can lead to start/stop acceleration problems which may cause head slider instability, damage the disk and ultimately lead to head crash. If the high frictional force exceeds the spindle motor torque, the drive will be unable to start and hence the system will be redundant. Clearly, high friction is detrimental to the performance of a recording system and must be minimised if an efficient system is to be produced.

1.8.1 Fundamental Laws of Friction

The first fundamental law of friction states that when two sliding surfaces are in relative contact with each other, the frictional force, F, is proportional to the normal load, W, such that

$$F = \mu W \qquad (1.3)$$

where μ is the coefficient of friction.

The second fundamental law of friction states that the frictional force between to contacting bodies is independent of the apparent area of contact, A_a, since nearly all materials have a rough surface on a micro scale. Furthermore, contact actually occurs at asperity tips such that normally, the real area of contact, A_r, will be much smaller then the apparent area of contact, as shown in Figure 1.19.
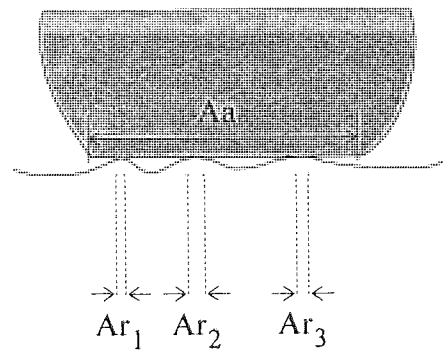
Figure 1.19 Real and Apparent Areas of Contact at a Sliding Interface

When two surfaces are in contact under normal pressure, the total load will be supported on the real area of contact leading to high areas of stress at the contacting asperity tips. If the contact areas are unable to support the load, the asperities will plastically deform until a new state is reached in which the area of contact is sufficient to be able to support the load. The yield pressure for plastic flow, p_0, at which deformation of the softer material will take place is given by Equation 1.4.

$$p_0 = \frac{W}{A_r} \qquad (1.4)$$

This theory was originally developed by Bowden and Tabor [44] for two interacting metals in which p_0 is the yield pressure for plastic flow of the softer metal. However, in the case of a polymeric material, the deformation will not always be plastic but partly elastic since some of the deformation may only be temporary and can be recovered after the load has been removed.

The type of deformation of the asperities depends on the mechanical properties of the interaction and the topography of the surfaces. Greenwood and Williamson [45] defined a plasticity index, ψ, in order to provide an indication of the mode of deformation, as given in Equation 1.5

$$\psi = \frac{E_c}{H}\left(\frac{\sigma_p}{R_p}\right)^{1/2} \qquad (1.5)$$

where

E_c = Effective elastic modulus of the surfaces which interact

H = Hardness of the softer material

σ_p = Standard deviation of the peak height distribution

R_p = Effective radius of curvature of the contact asperity

They concluded that the deformation mode would be plastic if ψ was greater than 1.0 and elastic if ψ was less than 0.6. However, Bhushan [46] later developed a plasticity index for polymers, ψ_p, defined in Equation 1.6 as

$$\psi_p = \left(\frac{E_c}{Y}\right)\left(\frac{\sigma_p}{R_p}\right)^{1/2} \qquad (1.6)$$

where

E_c = Composite modulus

Y = Tensile yield strength of the polymer

σ_p = Standard deviation of peak height distribution

R_p = Composite radius of asperity on rough surface

Composite modulus, E_c is given by Equation 1.7

$$\frac{1}{E_c} = \frac{(1 - v_1^2)}{E_1} + \frac{(1 - v_2^2)}{E_2}$$
(1.7)

where

E_1 and E_2 = Young's moduli of elasticity for the interfacing surfaces

v_1 and v_2 = Poisson's ratios for the interfacing surfaces

If the plasticity index for polymers, ψ_p is greater then 2.6, then the contact will be plastic whereas if ψ_p is less than 1.8, the contact will be elastic. The mode of deformation cannot not be accurately predicted when ψ_p is between 1.8 and 2.6 since this is a region of transition in which the mode of deformation can be influenced by the stress levels which act on the asperities. Bhushan [47], and Bhushan and Doerner [48] have shown by substituting experimental data into Equation 1.6 that typically, the contact between recording heads and particulate media is elastic. Using this information, the real area of contact between the two surfaces was shown to be approximately equal to $3.2(W/\psi Y)$.

In this research programme, any deformation of the polymeric part of the magnetic media will primarily occur from contact with the harder materials present in the recording heads, such as ceramic and glass.

1.8.2 Friction in Polymers

The two main sources of friction in polymers are

(a) *adhesion* and subsequent shearing of asperities at the contact interface

(b) displacement, or *deformation*, of the softer material by the harder material.

The total frictional force experienced at an interface is the aggregate of the force due to adhesion and the force due to deformation. Deformation can be either elastic or plastic in nature and also incorporates any displacement that may occur due to ploughing of a softer material by a harder material. For polymers, the deformation component is usually more significant than it is for metals since polymers exhibit viscoelastic-plastic behaviour.

Adhesive wear may arise when two surfaces come into contact and form strong adhesive bonds at the real area of contact. The bonds can either be physical, involving weak Van der Waals bonds, or chemical involving covalent, metallic, hydrogen, electrostatic or ionic bonds.

Van der Waals bonds exist between atoms or molecules which have complete shells so that no valence electrons are available for electrostatic (ionic), covalent or metallic bonding. The forces associated with Van der Waals bonds are long range electrostatic attractive forces and occur when the negative charge of the electrons of a particular atom do not coincide with the centre of the positively charged nucleus. This leads to a dipole within the atom and ultimately to dipole bonds between neighbouring atoms. Unlike the forces which result from chemical interactions, Van der Waals forces are always present and can produce a bond which is comparable in strength to those between the molecular chains of the polymer binder although it is more usual for the covalent bonds of atoms to be stronger than the Van der Waals bonds between chains. Van der Waals forces act over large distances and hence can lead to an increase in the real area of contact by pulling the two surfaces closer together.

Covalent bonds are formed when a pair of atoms share valence electrons, in order to complete the outer shell. This usually occurs when it is energetically unfavourable for the atoms to form bonds through the transfer of electrons, as is the case when atoms have three, four or five electrons in the outer shell, or indeed when a molecule is formed through the bonding of identical atoms. The forces associated with covalent bonds are generally short range, which in the case of organo-metallic bonds, can be of a particularly high strength [49].

Electrostatic (or ionic) forces arise when one or more electrons transfer entirely from one atom to another. When an electron moves between two neutral atoms, the recipient atom will become negatively charged whereas the donor atom will be left with a net positive charge. The atoms may then mutually attract through the formation of chemical ionic bonds within the real area of contact.

Metallic bonds are a combination of electrostatic and covalent bonds since atoms which have loosely bound valence electrons may, when in close proximity to other atoms, transfer valence electrons from one site to another and hence form a zone in which positively charged ions are held in close proximity to each other. Metallic bonds are very characteristic of the bond between two metals but its contribution to the adhesive contact at a head-media interface is usually minimal. The case in which metallic bonds can make a significant contribution to adhesive contact is when a MR head is used in conjunction with ME media, thus giving rise to the possibility of metallic bonds at the head-media interface through contact of the metal MR elements with the metal layer of the magnetic thin film.

1.8.3 Mechanisms of Wear in Polymers

Fatigue, abrasive, corrosive, erosive and adhesive are the five mechanisms responsible for wear in polymeric materials [50].

Fatigue wear may occur when a material is subjected to repeated loading over a single area due to cyclic stressing. This can lead to sub-surface damage, in a similar manner to that of delaminative wear for metals (See Section 1.8.4). Fatigue Wear is particularly likely to occur when microscopic irregularities exist within the structure of a material. According to the molecular-mechanical theory of friction in solid bodies, minimum fatigue wear will occur if the contact is of an elastic nature. However, in the case of polymeric materials, the cyclic stressing will lead to the formation of characteristic waves on the strained material due to tribo-cracking of the polymer molecules [51].

Abrasive wear results in the plastic deformation of a surface due to ploughing and can arise from two different sources. Firstly, if a hard asperity on the surface of one material penetrates into a softer material, material from the softer surface will be removed, giving rise to a wear track. The second scenario arises when a hard asperity becomes trapped between the two contacting surfaces, leading to a three body interaction. In both cases, a higher frictional force results, firstly from the creation of the wear particles through the shearing of chemical bonds and secondly by the increase in resistance to motion as the hard asperity ploughs through the softer material, leading to a build up of debris in front of the head (rather than being removed) [52]. Surfaces that undergo plastic deformation suffer a permanent change in shape due to the material being unable to relax back to the original form. The deformation may consist of the creation of surface ridges, which upon further ploughing will fracture and come away from the surface. In addition to damage to the outer surface, the ploughing process also causes plastic deformation to the sub-surface, through the generation of sub-surface cracks. If these cracks propagate, the

wear rate will increase from that associated with surface ridges, since relatively large wear particles will be created as several sub-surface cracks are linked.

Corrosive wear of a polymeric surface may occur but only if the wear interface is reactive and the local environment is conducive to corrosion. Under these conditions, corrosive reactions may occur with the products remaining on the exposed surfaces. These reaction products are not usually bonded to the surfaces very strongly and thus may be removed fairly easily upon further sliding. In the case of ME thin film media, the reactive constituents are protected by a lubricant [53] and in some cases, a carbon layer [54]. For particulate media, metal particles which are susceptible to corrosion are protected by a non-reactive oxide layer [55] which has had the effect of reducing the problems of corrosive wear in magnetic media to a minimum.

Erosive wear may occur when a surface is damaged through the bombardment of particles in a liquid or gaseous medium. The rate of wear is dependent on the angle of incidence of particle bombardment and also on the nature of the target surface. For brittle surfaces, cracks may form on the outer surface which upon further particle bombardment will propagate leading to the creation of wear particles when the cracks intersect. In the case of ductile materials, the mechanism of wear will be similar to that of abrasion and fatigue although in the case of magnetic media, erosive wear is not likely to occur since particle bombardment of the media is not prevalent.

Adhesive wear may occur when the shear strength of the interface junction is greater than the shear strength of bulk material. It maybe that before adhesive wear can occur, the shear strength of the bulk material has to be reduced through a fatigue process in order for the strength of the interface junction to exceed that of the bulk material. When a polymeric material is in contact with a smooth hard surface (i.e. head/media interface), the load will be supported by the asperities on the polymer which will subsequently deform until the load is fully supported. This will in effect increase the real area of

contact and following further relative motion at the interface, a section of polymer may shear in the bulk thus creating loose wear debris or transferring some polymeric material directly to the smoother hard surface. Polymeric transfer to a metal as a result of repetitive sliding has been observed and can lead to the creation of a polymer film on the metal surface [56,57].

Archard's law [58], as described in Equation 1.8, is the fundamental law of adhesive wear and it describes how materials will wear under various conditions

$$\omega = \frac{kW}{p_m} \qquad\qquad (1.8)$$

where

ω = Wear rate, the volume of material removed per unit distance of sliding.

k = Constant of proportionality (or wear coefficient).

W = Applied load.

p_m = Flow pressure (or hardness).

The wear coefficient, k, is a dimensionless constant of proportionality and is governed by the mechanical and chemical interaction between two contacting surfaces. Systems that use magnetic media as the recording media have evolved using lighter head loads in conjunction with harder head and media materials since this will lead to smaller wear rates, as Archard's law predicts. Further assistance towards improved tribological performance of recording systems comes naturally since the wear coefficient does not remain constant at all loads. Rabinowicz [59] showed that k actually decreases at very low loads and can reach values of between 10^{-3} to 10^{-6} for lubricated surfaces in sliding contact. However, the friction coefficient associated with the system at equivalent loads is not as helpful since it increases, particularly when the surfaces are very smooth. The increased frictional forces which exist at very low loads are now becoming a major

influence on the performance of high density recording systems especially as the trend in the magnetic media industry is to develop systems which operate at very low loads.

In polymers, a high proportion of the total deformation is elastic since the material displacement is only temporary and can be recovered. This leads to hysteresis behaviour in the frictional force such that the interacting body initially causes elastic deformation of the polymer material due to the low elastic modulus of polymeric materials [60]. This deformation translates to stored energy within the polymer and the energy is only released when the interfacing body moves away from the stressed area, allowing the elastic recovery to take place through relaxation. The amount of energy used in deforming the polymer is greater than that released during relaxation with the difference giving rise to an increase in the temperature of the polymer.

1.8.4 Delaminative Wear

Delaminative wear is synonymous with catastrophic failure since it involves the removal of large, slender sheets of wear particles, often revealing an unprotected surface. The theory which explains this process was first proposed by Suh [61], specifically for wear in metals, and it is described by the following sequence of events. Normal and tangential loads are transmitted at the contact points of an interface, as shown in Figure 1.20.
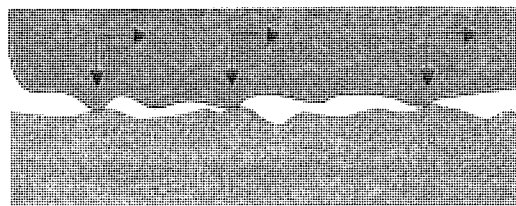
Figure 1.20 Delamination Theory : Normal and Tangential Loads

being Transmitted through Contact Points

These loads result from the adhesive and ploughing actions which occur when two sliding surfaces come into contact. The shape of the asperities on the surface of the softer material will be deformed and eventually fracture, to form small wear particles. Asperities on the surface of the harder material will also be removed but at a slower rate to that of the softer asperities. The repeated loading action will eventually form a relatively smooth surface by either deforming the asperities or removing them from the surface. The asperities which still remain on the harder surface will lead to plastic deformation of the softer material at the contact points of the interface, as shown in Figure 1.21
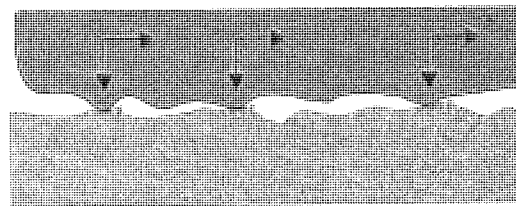
Figure 1.21 Delamination theory : Plastic Deformation of the Surface

The plastic deformation is compounded with each cycle of loading, eventually resulting in sub-surface deformation. This leads to crack nucleation just below the surface, as shown in Figure 1.22, which upon further loading and deformation, will extend and propagate, until neighbouring cracks are joined together.

Sub-Surface
Crack Nucleation
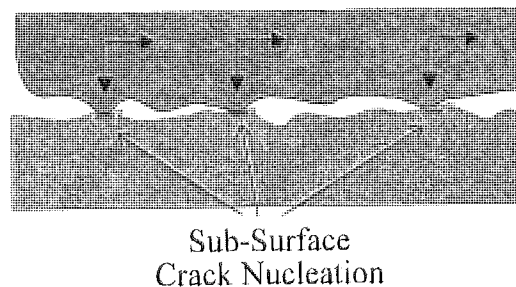
Figure 1.22 Delamination Theory : Sub-Surface Crack Nucleation

The cracks will tend to propagate in a direction parallel to the outer surface at a depth determined by a combination of the properties of the material and the state of loading.

When the cracks finally shear to the surface, long thin wear sheets will delaminate from the material, as shown in Figure 1.23.
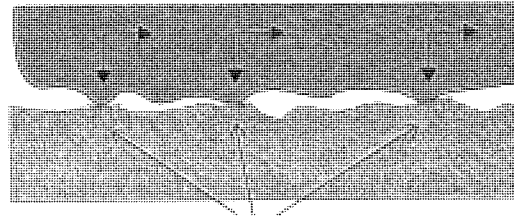
Thin Wear Sheets about to
Detach from the Surface

Figure 1.23 Delamination Theory : Thin Wear Sheets Formed

after Cracks Extend to the Surface

The thickness of each delaminated wear sheet is governed by the position of the sub-surface crack growth. This is influenced by the normal and tangential loads transmitted at the contact points of the interface. The rate of wear is determined by the crack nucleation rate or the crack propagation rate since both processes must occur for delamination to take place. Thus, the wear rate is ultimately governed by the rate at which the slower of these two processes takes place.

1.8.5 Friction and Wear of Magnetic Media

High initial friction in magnetic media can occur as a consequence of several factors. Firstly, at normal operating temperatures, the magnetic layer is in a viscoelastic state so the real area of contact will increase with time and hence the initial frictional force will also increase accordingly. Secondly, Van der Waals forces exist at the interface of the media and head which have the effect of increasing the surface area above that predicted by theory. Each of these effects increase when the system is stationary and they will become more pronounced with time. The problem of high static friction is exacerbated

further under operating conditions of high humidity [62], probably due to a combination of meniscus effects [63] and/or water plasticisation of the polymer [64] (see section 1.8.6).

Briscoe et al. [65] showed that due to a combination of the topography of the interfacing surfaces, the nature of the contact and the viscoelastic tribological characteristics of the magnetic layer, the dynamic friction which occurs when a head is in contact with a particulate magnetic media is due to adhesion since the deformation components of ploughing and hysteresis loss are negligible. Tabor's classical theory of adhesion [66] defines the frictional force due to adhesion for a dry contact as given in Equation 1.9

$$F_A = A_r \tau_a \qquad\qquad (1.9)$$

where

F_A = Frictional force due to adhesion

A_r = Real area of contact

τ_a = Interfacial shear stress

The interfacial shear stress does not remain constant since in general, it will increase with pressure and decrease with temperature. In addition, the frictional force will be dependent on speed of motion at the interface since the elastic properties of the polymer are time dependent and the temperature will increase with velocity.

In the case of particulate media, a fatty acid or equivalent type lubricant is added to the binder system of the media in order to improve the tribological properties of the media. The binder system then acts as a reservoir to protect the media over the projected lifetime. Tabor's classical theory of adhesion also incorporates a law for a lubricated contact, as described in Equation 1.10

$$F_A = A_r \left(\alpha \tau_a + (1 - \alpha) \tau_l \right) \qquad\qquad (1.10)$$

where

τ_a = Interfacial shear stress of the dry contact.

τ_l = Interfacial shear stress of the lubricant.

α = Fractional areal coverage of the lubricant.

The lubricant film typically has a thickness equivalent to 2 or 3 molecular layers with a coverage which can be as small as just 10%. A combination of the low surface energy of polymers and the minimal lubricant coverage results in the lubricant having a negligible effect on reducing the problems of friction. The lubricant is primarily included in the binder system of a particulate media to protect the media from wear. However, it should be noted that in the case of a rigid disk or indeed a thin film metal evaporated tape where the media is in general topically lubricated, the effects of friction and wear are both significantly reduced.

In the case of particulate media, friction is largely determined by the properties of the magnetic layer and hence in order to reduce friction between the head and the media, the magnetic layer should have a high hardness and complex modulus but attention should also be given to other material properties that are equally important such as the glass transition temperature and toughness. A rough surface will also give lower frictional forces but only at the expense of decreasing the mechanical durability of the media and increasing the distance between head and media. Thus, the option of using rougher surfaces is not implemented into the design of magnetic media since it is imperative to keep spacing losses to a minimum.

The coefficient of friction for a system using particulate media is known to increase with running time over the first few passes or cycles which is consistent with the idea of the media surface becoming smoother but inconsistent with the assumption that the contact between the head and media is elastic. However, Sharma [67] has shown that although the surface roughness does indeed initially decrease, there is also a chemical change in

the outer layers of the polymeric binder of the media. If it is assumed that the frictional force is due to adhesion (mainly as a result of interfacial Van der Waals physical bonds and chemical electrostatic ionic bonds), the chemical change in the binder may account for the increase in the coefficient of friction whilst still allowing the contacts to be elastic.

Charge transfer occurs at the real area of contact and the amount of charge transferred is dependent on a combination of the actual area of contact, the differences in the work function and by the density of the electronic states at the surface. An additional feature known as the triboelectric effect results in an increase in the fraction of area charged when subjected to a rubbing action [68]. A further electrostatic force, although weaker, can exist between a charged atom and a neutral atom. In this case, the neutral atoms will become polarised since a dipole moment is induced as a result of the proximity of the neighbouring charged atom(s). Bhushan [69] calculated that in an ideal case, the maximum electrostatic force at a head-tape interface is approximately 60 mN. The force would be smaller in a real system since Bhushan assumed the interfacing surfaces to be parallel. This resulted in a higher initial value for the electric field which when used to calculate the electrostatic force, gave a higher value than is the case in a real system. However, the electrostatic force is still a major contributor towards the total friction and could be responsible for the shearing that occurs within the bulk of the magnetic layer. When the polymer of particulate magnetic media is in contact with the ceramic part of a recording head, strong adhesive junctions are likely to form as a consequence of ion-dipole bonds. The atoms within polymer chains are bound together by covalent bonds, typically with energies of 10 eV per atom, whereas the molecular chains are bound by weaker ion-dipole interactions (approximately 0.2 eV per atom). Thus, assuming ion-dipole bonds are responsible for adhesion between the polymer of the media and the ceramic of the head, such junctions may be sufficiently strong to produce shearing of the magnetic layer and ultimately lead to the transfer of material from the media to the head.

Transfer films, which commonly appear as a brown stain on the recording head of a tape, floppy or rigid disk drive, are often formed after several cycles or passes of the media on the head [70]. Such stains, probably mistakenly known as friction polymer [71,72] were thought to occur when there was relative motion between the two surfaces and at least one of the materials at the surface interface was organic, such as the lubricant associated with the media or an environmental contaminant. Analysis of the stains has shown little evidence of chemical interaction and thus the description of the stains as friction polymer is misleading. The films actually consist of iron oxide which is consistent with the transfer of particles from the polymer based media to the head through adhesive wear, followed by ion-dipole interactions in order to hold the particles to the head.

In addition to the brown stains, loose debris is sometimes produced when a head is in contact with the media and this can lead to head clogging. The debris has different properties to the stains and is commonly produced as a result of the removal of surface asperities or the creation of wear particles. A head cleaning agent (HCA) is added to the binder system of particulate media in order to keep the thickness of the stains to a minimum since once the stains have formed, it is very difficult to remove them. Indeed, the stains cannot be removed by simple solvent washing so mechanical methods have to be used such as the application of an abrasive tape. The HCA does not afford the system any protection from head clogging but in addition to minimising the growth of transfer films, its major function is to act as a bearing surface which helps protect the media from the effects of wear, when in contact with a hard surface such as the head or tape guide mechanism.

Head stains have been observed for over 30 years with a distribution coverage ranging from intermittent spots to continuous layers with a thickness of typically 20 nm. These small amounts of material deposit have always hindered attempts to characterise the stains fully since the area of analysis is minimal. However, different surface analytical techniques have recently been employed to analyse the stains. In 1991, Ota et al [73]

used SEM and TEM techniques to investigate the composition of the brown stains found on VCR heads, after playing MP tapes in the deck. They found that the stains only began to form when the VCR was operated in a relative humidity of less than 45% and that head wear decreased with the occurrence of the brown stains. TEM investigations enabled Ota et al. [73] to conclude the stains mainly consisted of small grains of γ-iron oxide, together with a small amount of tape binder.

The composition of the head stains was later confirmed by Reichlmajer [74] when he used TOF-SIMS to analyse the stains formed on a VCR head, when used in conjunction with a MP tape. His investigations led him to conclude the stains were formed when iron from the tape became smeared onto the surface of the head. A small amount of organic material was also identified in the stain which must have been transferred from the tape to the head. Stahle and Lee [75] also used MP tape and found that the humidity in the test area had to be below 30% before any staining of the VCR heads would occur. Their investigations included the use of AES and FTIR techniques for analysing the brown head stains and they concluded that the stains mainly consisted of an inorganic material, composing of ferrite from the head and iron particles from the tape. When a metal-in-gap (MIG) head was used instead of a ferrite head, the brown stain was found to compose of metal particles from the tape. However, in each case, there was still a small trace of organic material within the stain. Head staining may be beneficial in improving the tribological performance of a system since friction and wear are reduced [76] but its existence also detracts from the recording characteristics since there can be a large reduction in the head output signal due to increased spacing losses.

Bhushan and Hahn [77] conducted a series of experiments using MP and Co-Fe_2O_3 tapes in conjunction with MIG heads. They reported observing the appearance of brown stains for both types of tape after the tape had run a distance of 100 km against the head. The deposit associated with the oxide tape was patchy whereas for the MP tape it was a continuous uniform film although in both cases, the deposits were still very difficult to

remove. Chemical analysis of the head stains produced with the Co-Fe$_2$O$_3$ tape revealed the stains consisted of organic material together with iron and oxygen. The stains produced with the MP tape comprised mostly of iron and oxygen, with a small amount of organic material.

Tsuchiya and Bhushan [78] investigated the effect of running ME tape against MIG heads and observed the formation of a spotty deposit on the heads. It consisted of cobalt, nickel and a PFPE lubricant but the deposit was not restricted to the head surface alone since it was also found to be present on the whole of the air bearing surface. It was also possible to remove the deposit by simply applying a solvent and hence the deposit was not classified as a stain. One possible explanation for the existence of this deposit is that unlike particulate media, ME tapes do not contain a head cleaning agent and hence the surface of the head will remain dirty.

The recent investigations outlined above have indicated that brown head stains are produced when MP or barium ferrite tapes are used and that the deposits are made up of mainly iron or iron and oxygen. Thus, it is inappropriate to refer to such stains as friction polymer as the stains primarily consist of an inorganic material. Stahle and Lee [75] were amongst the first to recognise this fact although the actual process leading to the formation of the head stains has still to be determined. Various mechanisms have been proposed but general agreement has yet to be reached. For instance, Narishige and Sato [79] suggested the stain formed as a result of oxidation of the metal present in the head whereas this was contradicted by Stahle and Lee [75] who reported that due to the large amounts of iron found in the stains, the tape was more likely to be the source of the deposits. Indeed, Bhushan and Hahn [77] noted that the stains did not contain any aluminium or silicon - elements which are common to the Sendust metal used in MIG heads.

Hamilton and Goodman [80] showed that when two surfaces are in sliding contact, as is the case in many magnetic media recording systems, the maximum shear stress occurs just below the surface. As the interfacial friction increases, the magnitude of the stress induced by the asperity contact will also increase but at a location nearer to the surface. The depth at which the maximum stress occurs is also affected by the radii of the asperity contact which is itself dependent on the applied load. When an individual asperity on the surface of the tape or head approaches an asperity on the opposing surface, the subsurface region will be under compression whereas when the asperities start to move apart, the region will then be in tension. In the case of a magnetic media recording system, the asperities will experience repeated contact with other asperities as the media passes over the head. This has the effect of subjecting the subsurface region to repeated forces of compression and tension, known as cyclic stressing, which will ultimately lead to the creation of fatigue cracks. These cracks will propagate as the subsurface region is stressed further until eventually, wear particles will be produced. This is a process analogous to, but not the same as Suh delaminative wear.

Plastic deformation in polymers can only occur if the opposing hard surface has a roughness of at least 12 μm [81]. A prerequisite for abrasive wear is that the softer surface must experience plastic deformation below the contacting asperity in a two body interaction or below the third particle in a three body interaction. In a magnetic recording system, neither the head or the tape has a roughness comparable to 12 μm and hence it is impossible for abrasive wear to occur through a simple two body interaction. It is very likely therefore that the scratches and associated damage observed on a tape surface occur as a result of a three body interaction process involving some loose debris that has become trapped between the head and media of a system.

The recording heads used in magnetic recording systems are generally constructed from a hard material which may contain a combination of ceramic, ferrite or metal components. They are characterised as having a high elastic modulus, high chemical and

thermal stability, high fracture strength but also being very brittle. The shear strengths associated with the head junction are very low due to the small interfacial adhesive forces. Thus, the probability of material being transferred from the head to the media is very small. It is far more likely that any wear to the head materials will result from abrasion and/or fatigue.

Reaves and Sullivan [82] showed that the wear rate of manganese zinc ferrite and glass VHS video heads was dependent on the abrasivity of the magnetic media. Chromium dioxide tapes are more abrasive than iron oxide tapes and as such were shown to produce a much higher rate of head wear. The surface of the head worn by the chromium dioxide tape was very smooth and was typical of a surface that had been subjected to a polishing process. In the case of the iron oxide tapes, the head had been polished but in contrast to the previous scenario, there was also evidence of grooves and scratches on the surface, a consequence of plastic deformation. However, it was impossible for the damage to be caused by particles from within the media because no individual particles of a sufficient size exist to produce the damage observed [83]. Hence, the plastic deformation must have arisen as a result of either a three body abrasive interaction between agglomerates of particles from the magnetic media, such as head cleaning agents, or to large asperities in the media surface, similar to those observed by Hahn [84]. In both cases, the load at the whole interface might be supported at a single contact point which would then give rise to a very high temperature. Indeed, surface and interface contact temperatures can be extremely high with flash temperatures reaching 600-900 °C [85]. Such temperatures are easily high enough to account for the plastic deformation sometimes seen on the head surface.

A further problem comparable with head wear caused by plastic deformation is that of differential head wear. When a head is constructed from different materials, as in the case of MIG heads, the rate of wear for each of the head materials is usually different and this can ultimately result in the introduction of spacing losses. For MIG heads, the

differential wear leads to a hollowing out of the head whereas for linear recording heads, high humidity operating conditions can lead to the ceramic material, wearing at a greater rate than that of the ferrite or glass.

Thin film metal evaporated tape has a unique set of tribological contact problems. For instance, the lubricant on a ME thin film tape must provide complete areal coverage but due to the minimisation of spacing losses, it should have a thickness no greater than 4 to 5 nm. It must also protect the magnetic layer from corrosion and be able to do so for a lifetime which is at least comparable to the lifetime of particulate media. A further problem associated with ME tape is that it does not possess the same advantages of good porosity and surface chemistry as particulate media and hence the demands on the lubricant are that much greater.

The wear process of thin film magnetic media is governed by the surface topography of the media, the contact geometry between the media and the head, and the loads applied at each of the interface contact areas. The process by which material is removed from a surface during adhesive wear was described by Samuels et al [86]. Initially, the asperities at the interface are flattened through elastic and plastic deformation until the real contact area is able to support the load. The relative motion between the two surfaces will then result in each of the contact points at the interface experiencing a shear stress. If the shear strengths are above a threshold value, the contacting asperities may rupture, resulting in the removal of material from one surface and subsequent transfer to another. This process can be responsible for the generation of multiple wear fragments so in order to minimise the generation of any other wear fragments, it is imperative that the shear strengths at the interface are distributed equally amongst the contact areas.

In the event that an adhered wear fragment becomes detached from a surface, the fragment will become a debris particle. In the case of thin film magnetic media, the debris particles which have been generated as a result of head-media contact will be

physically characteristic of the surface asperities on the thin film media since this is the softer material and is more likely to rupture in the first place. Continual movement between the head and media will lead to further debris being generated which will eventually become trapped at the interface. At this stage, the debris will either act as the third body in a three-body interaction, or will smear into one of the surface regions.

In the case of particulate media, the magnetic layer which is in contact with the read/write heads of a recording system will mainly exhibit the tribological properties of a filled polymer since the magnetic pigment is bound together in a polymeric resin. The situation is complicated slightly by the presence of substances such as head cleaning and wetting agents, solvents and lubricants. However, although the existence of these components should be recognised, the most important part of the system is the polymeric binder which usually consists of copolymers such as polyurethane-polyester.

Polymers can exist in a crystalline or amorphous state and if the polymer is amorphous, it can be glassy, rubbery or viscous. In the case of particulate media, the polymeric binder usually has a glassy phase to provide some hardness for mechanical stability. A "soft" rubbery phase will then give the media the flexibility needed to negotiate the complex tape guide mechanisms which are commonly found in recording systems.

Adhesive wear occurs at the interface of two sliding surfaces and is dependent on the real area of contact rather than the apparent area. When the polymeric binder of the particulate media is in moving contact with the hard surface of the ceramic, glass, ferrite head, as in the case of helical scan formats, the real area of contact at the interface is small in comparison to the actual apparent area.

When applying the first law of thermodynamics to the interface of the head and media, the external work done by the frictional force at the interface must equate to the total energy dissipated at the interface and any increase in internal energy. It is the dissipation

of energy that causes a surface to change shape, whether it be a permanent change through plastic deformation or only a temporary change due to elastic deformation.

1.8.6 Environmental Effects on Media Wear

Environmental conditions such as temperature and humidity significantly affect the tribological performance of magnetic recording systems [87] since the major components associated with the corrosion of heads and media exist in the atmosphere. Oxygen can lead to oxidation of elements in the magnetic head and to oxidative degeneration of the polymer surface of the media whereas the water vapour may cause further damage through the formation of hydroxides in head constituents, or by breakdown of the polymeric media binder through hydrolysis and chain scission [88].

Commercial MP and ME tapes are more susceptible to material degradation at very high humidities and temperatures than at ambient conditions [89]. In the case of particulate media, high humidity (greater than 45% RH) can lead to binder degradation due to an increased water content in the binder. The products of binder degradation will have a lower molecular weight and thus will be able to migrate to the surface of the tape much quicker than when the binder is intact. This will result in greater adhesion and wear at the head media interface which may in turn lead to stiction due to the formation of strong covalent and electrostatic bonds. Stiction often results in tape failure since the forces present at the interface are greater than those of the tape drive and hence this scenario must be avoided.

The accicular particles in a MP tape typically have an average length of 0.1 μm and an aspect ratio of approximately 5:1 although the latest metal particles are smaller with an aspect ratio of just 3.4:1 and a length of 64 nm [5]. A protective oxide layer is added to the surface of the particles by pretreating them with a non magnetic component such as

Al_2O_3 or SiO_2. Although this has the effect of reducing the magnetisation intensity of each particle, it is still nearly twice that of cobalt-ferric oxide particles, and significantly, the layer helps preserve the magnetisation of the metal particles and gives them oxidation stability. The pre-treated metal particles are dispersed with binder polymers and then coated onto a substrate film. The binder also has a stabilising effect since it surrounds the metal particles and hence forms an additional barrier by protecting the particles from the oxygen and water vapour in the atmosphere. This further reduces the possibility of media degradation through the oxidation of metal particles since in effect, the tape has a double protection layer.

The durability of MP media is further improved by using a double protection layer for the magnetic particles but it is limited by the inclusion of organic polymers such as the lubricant, back-coating, the binder and dispersing agents. It is these organic polymers that gradually degrade although this process increases at higher temperatures and humidities.

The environmental conditions in which thin film ME media are used can significantly influence the tribological properties at the head media interface. In particular, changes in the relative humidity may effect the frictional and adhesive properties of an interface due to the hydrophobic nature of the PFPE lubricant.

Binggeli and Mate [90] applied a 1.5 nm PFPE lubricant layer to a silicon wafer and measured the frictional force experienced by an AFM tip sliding across the wafer as a function of load. This procedure was repeated at several different levels of relative humidity in order to ascertain the relationship between the tribological properties at the tip-PFPE layer interface and changing environmental conditions. The friction and adhesion experienced by the AFM tip both decreased as the relative humidity increased. This response may have been due to the water molecules from the vapour being able to penetrate the contact junction at the interface and hence afford the contacting surfaces

better lubrication. As the relative humidity increased, more water molecules were able to contribute to the overall lubrication and hence the friction and adhesion both decreased. Similar mechanisms may take place in a magnetic recording system using thin film ME media since essentially, the same conditions will be replicated.

Much of the literature published to date about the environmental effects on the tribology of magnetic media deals with particulate media or rigid disk applications. Both of these types of media are significantly different to thin film ME media since in the case of particulate media, the binder forms an integral part and it is particularly susceptible to the effects of the environment (binder degradation), whereas in rigid disk format, stiction is of great importance to the overall durability of a system and is known to increase with humidity. Some recent studies have investigated the effect of various environmental conditions on the durability and performance of ME media [91-93] although extensive research in this area is still fairly limited. For the purposes of this research, a chamber was constructed which enabled durability tests to be performed at different humidity conditions.

CHAPTER 2

EXPERIMENTAL

2.1 Introduction

The apparatus used in this research can be divided into 2 distinct groups. All the equipment associated with sample generation and signal performance monitoring can be considered as one entity, whereas all the surface analysis instrumentation used for evaluating any physical or chemical surface changes can be considered as the other. Lubricant characterisation and the identification of media wear mechanisms formed an integral part of this research and as such, a wide variety of surface analysis techniques were utilised. The characterisation of the lubricant was primarily performed using **X-ray Photoelectron Spectroscopy** (**XPS**) at a series of different analyser take-off angles and **Secondary Ion Mass Spectrometry** (**SIMS**) whereas identification of the media wear mechanisms relied upon **Scanning Electron Microscopy** (**SEM**).

The mechanical measurements needed for sample generation and signal performance evaluation consisted of 2 types of durability test. Stop motion tests were used to give a measure of the durability of a tape in still frame (pause mode) whereas cycling tests were used to give a measure of the durability in repeated playback mode. Two Sony EVO-9500 Hi-8 VCR's were used, one for each type of test, although both VCR's needed to be modified before any experiments could be performed.

2.2 Apparatus for Signal Measurement and Sample Generation

2.2.1 VCR Modifications

The first modification to the VCR's was necessary to enable the 'raw' RF signal to be monitored directly from the tape, rather than from the standard video outputs since the signal from these outputs would have been subjected to corrective signal processing. This modification involved the addition of a bridging amplifier to each of the VCR's with the RF input into the bridging amplifier taken from test point TP031 on the FR-40 board of the VCR as shown in Figure 2.1. Finally, the 'raw' RF output from the bridging amplifier was attenuated in order for it to be possible to monitor the signal using a RF voltmeter and oscilloscope. The bridging amplifier circuit used in this research was designed by the 3M Company, and is illustrated in Figure 2.2.
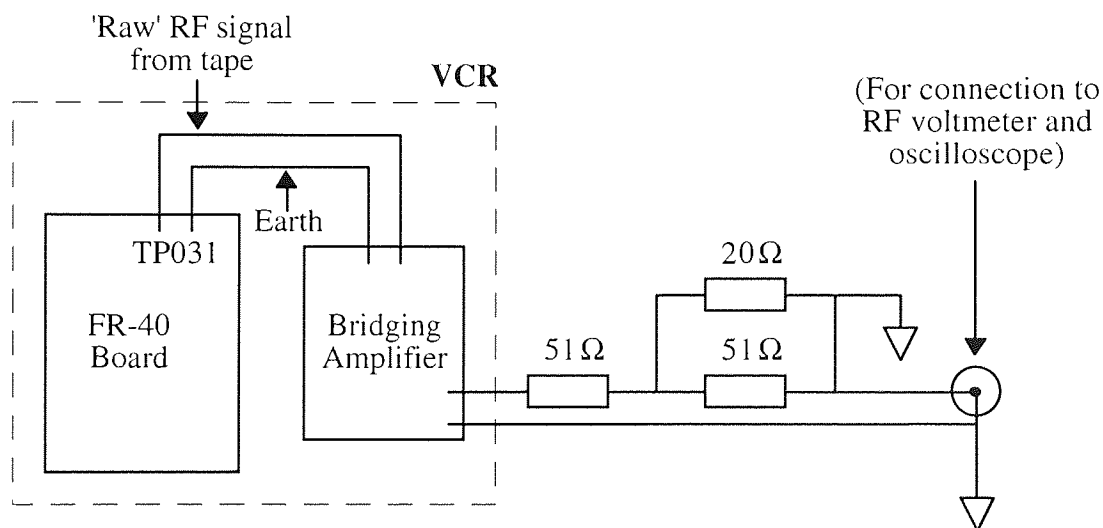
Figure 2.1 Modification to the VCR in order to Monitor the 'Raw' RF Signal from the Tape
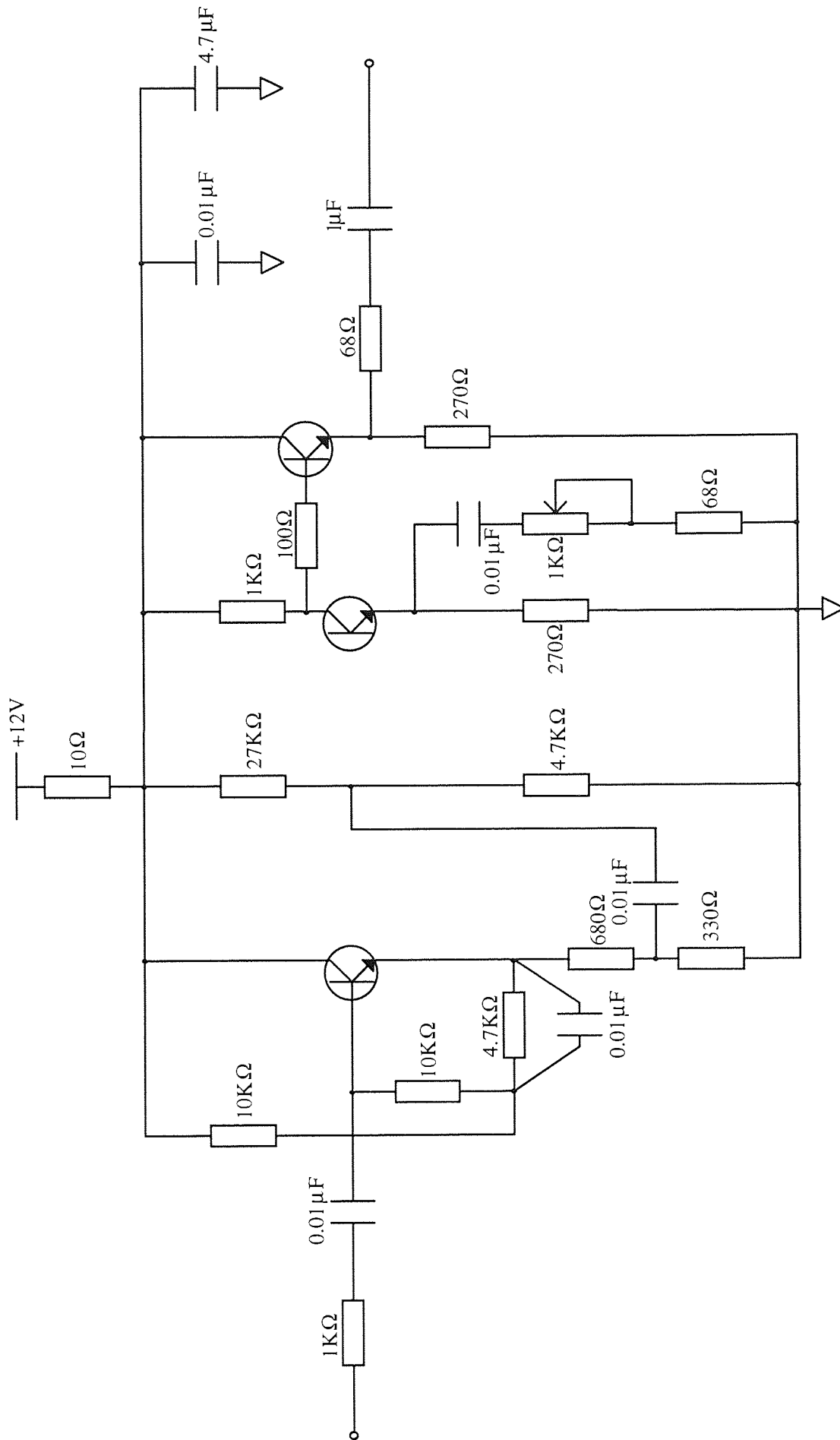
Figure 2.2 Bridging Amplifier Circuit

When a NTSC red field signal was to be applied to the VCR, it was performed in the standard manner by connecting a signal generator to the relevant input at the back of the deck, which then ensured the signal was subjected to the normal video processing. However, in the case of the 3.75 MHz square waveform, it was better to avoid any unnecessary video processing since this could distort the true number of dropouts measured after a tape had been cycled. In order to achieve this, the VCR was modified, as shown in Figure 2.3, so the signal could be applied at a point nearer to the read/write heads.

Normal Video Operation   Read/Write Heads

(Red Field Signal)   (3.75 MHz Signal)

A

200Ω

Function
Generator, Y_{IN} Switch
(3.75 MHz Signal)   51Ω   S1

B
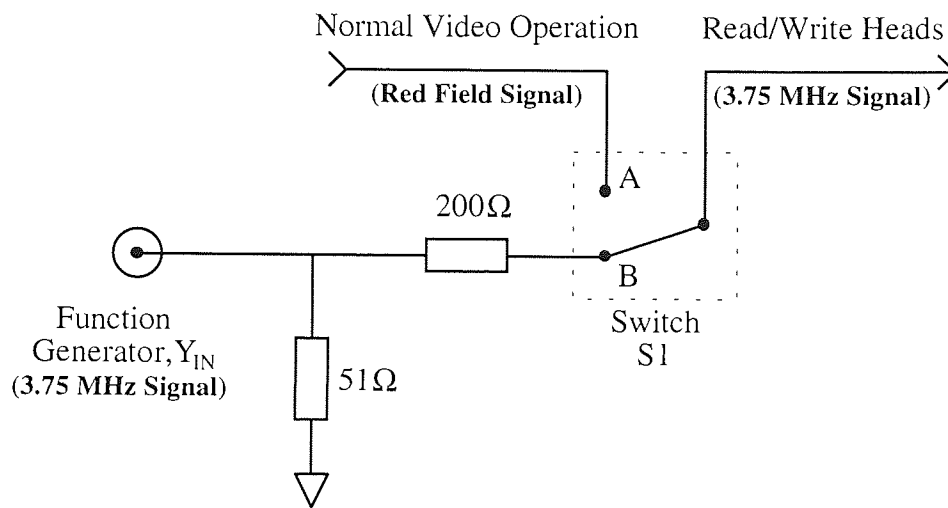
Figure 2.3 Circuit Modification for Injecting a 3.75 MHz Signal near to the Video Heads

When the switch, S1, was in position A, the video was connected for normal operation and a red field could be recorded onto a tape by applying an appropriate signal to the back of the deck. In order to record a 3.75 MHz square wave with minimal video signal processing, the switch had to be changed to position B and an appropriate signal applied at the correct input.

2.2.2 Humidity Chamber

In order to investigate the effects of high and low humidity on the performance of ME and MP tapes during cycling and stop motion durability tests, a humidity chamber was constructed as shown in Figure 2.4.
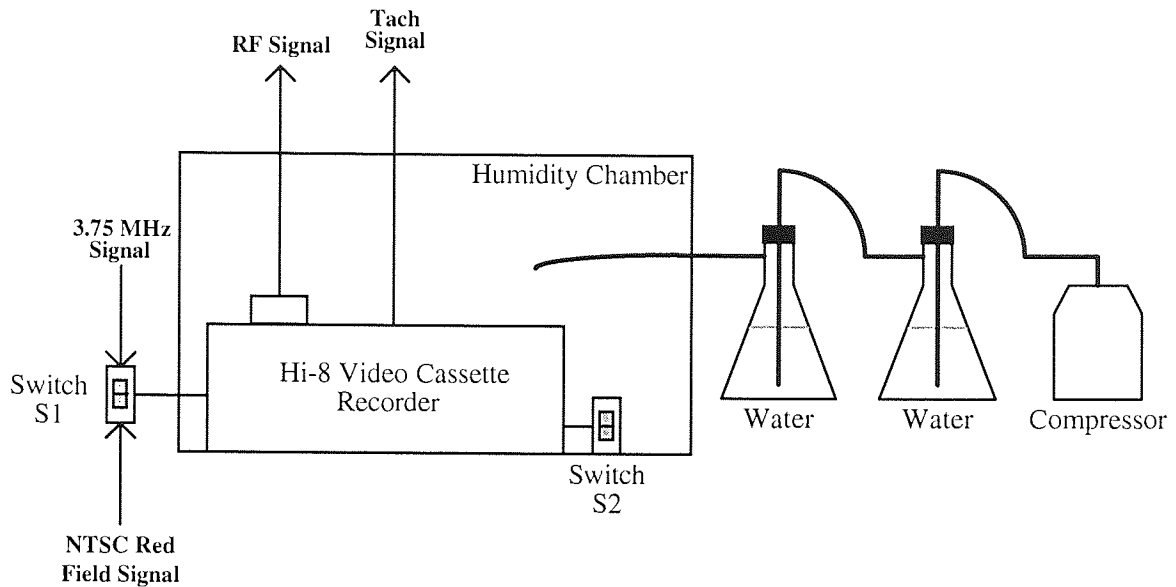
Figure 2.4 Humidity Chamber for Durability Tests

When high humidity conditions were required for a durability test, a compressor was used to push air through 2 water filled flasks. The "wet" air was then fed directly into a closed perspex chamber and typically, within 60 minutes of activating the compressor, the air in the chamber would have stabilised to a relative humidity of approximately 95%. Alternatively, by replacing the 2 water filled flasks with a dreschel bottle of anhydrous $CaSO_4$ drying crystals, it was possible to reduce the humidity of the air in the chamber to less than 10%. Thus, the chamber allowed a more thorough investigation of the durability of ME and MP tapes to be performed, and this was important since the wear of flexible magnetic media is known to be different at high humidity [94-95].

110

2.2.3 Cycling Tests

One of the methods used to assess the quality of a video tape is to monitor the number of dropouts per minute whilst playing back a recorded signal. A dropout is defined as a temporary loss of signal for a given length of time and several instruments have been designed for monitoring the dropout rate [96-98]. However, the instrument used in this research was designed by 3M and custom manufactured by Doradus. The tester separates dropouts into 20 classes, each of which is defined by depth and width, as described in Table 2.1.

Depth (dB)		Width (µs)				
Start	Stop	3.0	10.0	20.0	50.0	100.0
3.0	2.0	Class 1	Class 2	Class 3	Class 4	Class 5
6.0	5.0	Class 6	Class 7	Class 8	Class 9	Class 10
10.0	9.0	Class 11	Class 12	Class 13	Class 14	Class 15
16.0	15.0	Class 16	Class 17	Class 18	Class 19	Class 20

Table 2.1 Classes of Dropout Detected by the Doradus Dropout Tester.

Individual timers are assigned to each of the dropout classes which are then initialised when the signal level falls below a pre-determined start depth and stopped when the signal level rises above a pre-determined stop depth. The dropout will be registered in a class with the greatest depth and width for which it qualifies and this ensures that a dropout will only be counted once, irrespective of its size.

A schematic diagram of the equipment used in a cycling test is shown in Figure 2.5. A 3.75 MHz (450 mV p-p) square waveform was recorded on the tape for 5 minutes 20 seconds. The tape was then rewound back to the beginning and the number of the

dropouts within the first 5 minutes of the tape were measured using a 'Doradus' dropout tester. The tape was then rewound again and a red field from a NTSC pattern generator was recorded on the tape for 5 minutes 45 seconds. This was followed by a further 10 seconds blank section (no input signal) and then finally by a 3.75 MHz square waveform signal of 1 minute duration.
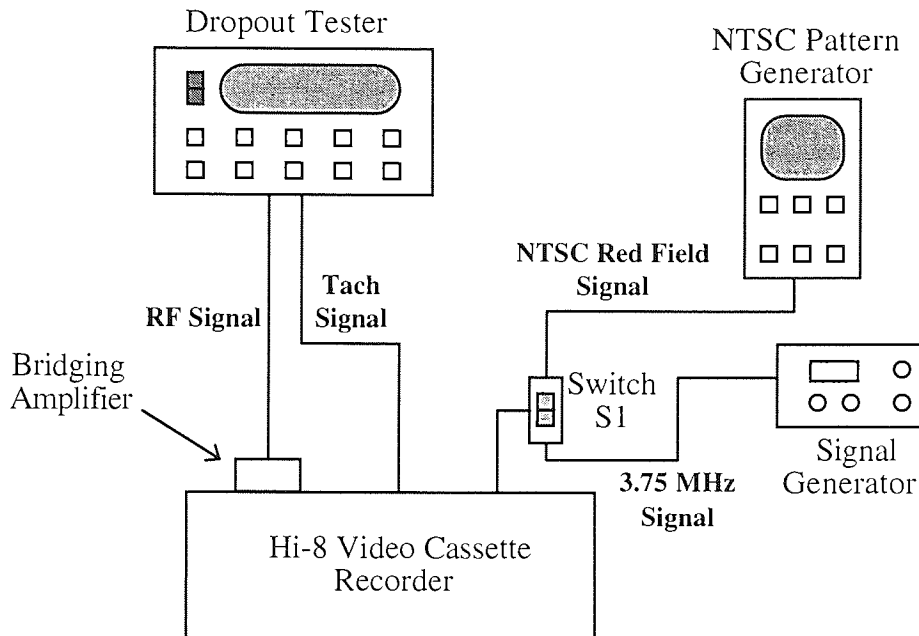
Figure 2.5 *Test Equipment for Cycling Tests*

Each of the VCR's could be switched to a mode known as 'auto-repeat'. In this mode, the VCR would play a tape from the beginning for as long as it detected a recorded signal. If the tape then reached a point where no signal had been recorded for a few seconds, typically 10 seconds, the VCR would automatically stop playing the tape, rewind back to the beginning, and then start to play the tape again. However, the VCR's do not recognise the 3.75 MHz signal as a television signal and hence the auto-repeat mode would not respond to any changes in the square wave signal. This was the primary reason for recording a red field from the NTSC pattern generator when cycling was required although the choice of a red television signal was not imperative - it merely had to be an NTSC television signal.

The VCR was placed in 'auto-repeat' mode so that cycling of the tape could commence and the cycling was stopped every 50 cycles (5 hours) so that the total number of dropouts could be measured. This was achieved by re-recording a 3.75 MHz (450 mV p-p) square waveform at the beginning of the tape for 5 minutes 20 seconds, after which the dropout tester was used to monitor the different classes of dropouts.

After measuring the dropouts, a red field from the NTSC pattern generator was again recorded on the tape for 5 minutes 45 seconds followed by a further 10 second blank section. Cycling of the tape could then begin again for another 50 cycles after which the number of dropouts were measured. This process was repeated until a catastrophic growth in the number of dropouts had been observed. At this point, the tape was wound forward to the previously uncycled 1 minute section (3.75 MHz square waveform signal) and the output signal was tested for dropouts. The relative number of dropouts present on this section of tape should have been similar to those observed before any cycling had been performed on the 5 minute 45 section of the tape. This test would confirm that any degradation in the output signal was due to changes in the tape and not to any deterioration of the heads in the VCR.

2.2.4 Stop Motion Test

In the case of the stop motion test, the VCR had been designed to allow a maximum stop motion time of one hour. This had been incorporated into the design of the deck by the manufacturer in order to prevent any accidental damage to tapes by prolonged operation in 'pause' mode. However, the very nature of a stop motion test required an indefinite stop motion time so the performance of the lubricant on a tape could be fully assessed. The VCR was modified by the simple addition of a switch and capacitor, as illustrated in Figure 2.6.
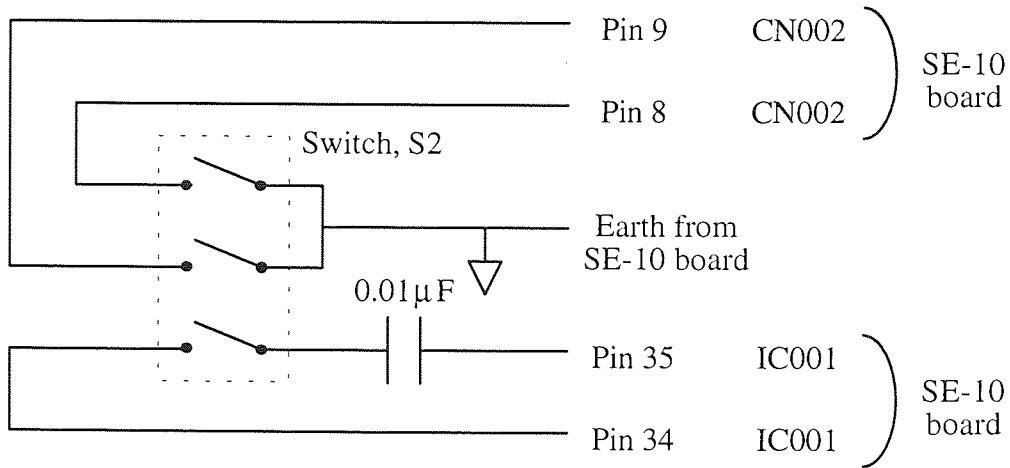
Figure 2.6 Modification of VCR Required for Indefinite Stop Motion Operation

This alteration gave rudimentary control over the oscillator that drove the mode control integrated circuit, IC001, which in turn enabled the clock on the VCR to be controlled externally so the timing could either be overridden or remain operational. When switch S2 was set to override the oscillator, indefinite stop motion times could be achieved. If, on the other hand, the switch was left in the open position, the VCR would continue to perform as per normal with a maximum stop motion time of approximately 1 hour.

For the stop motion tests, a 3.75 MHz (450 mV p-p) square waveform was recorded on the tape for 110 frames. The tape was then rewound to frame 50 and the VCR placed in extended pause mode. This was achieved by activating the pause button on the VCR so that the video heads would continually contact the same track on the tape. The internal clock of the VCR was then stopped by closing switch, S2, and an oscilloscope was used to check that good contact had been made between the two read/write heads and the tape. A chart recorder enabled the output signal from the tape to be monitored continuously and a tape was deemed to have failed once a 6 dB drop in the output signal had been observed. The test was then repeated at frame 100 so that the findings of the first test could be confirmed. A schematic diagram of the test equipment for a stop motion test is shown in Figure 2.7.

RF Voltmeter

Chart Recorder

DC Signal

DC Signal

Oscilloscope

RF Signal

Bridging
Amplifier

RF Signal

Tach
Signal

3.75 MHz
Signal

Hi-8 Video Cassette
Recorder

Signal
Generator

Digital
Voltmeter

Switch
S2
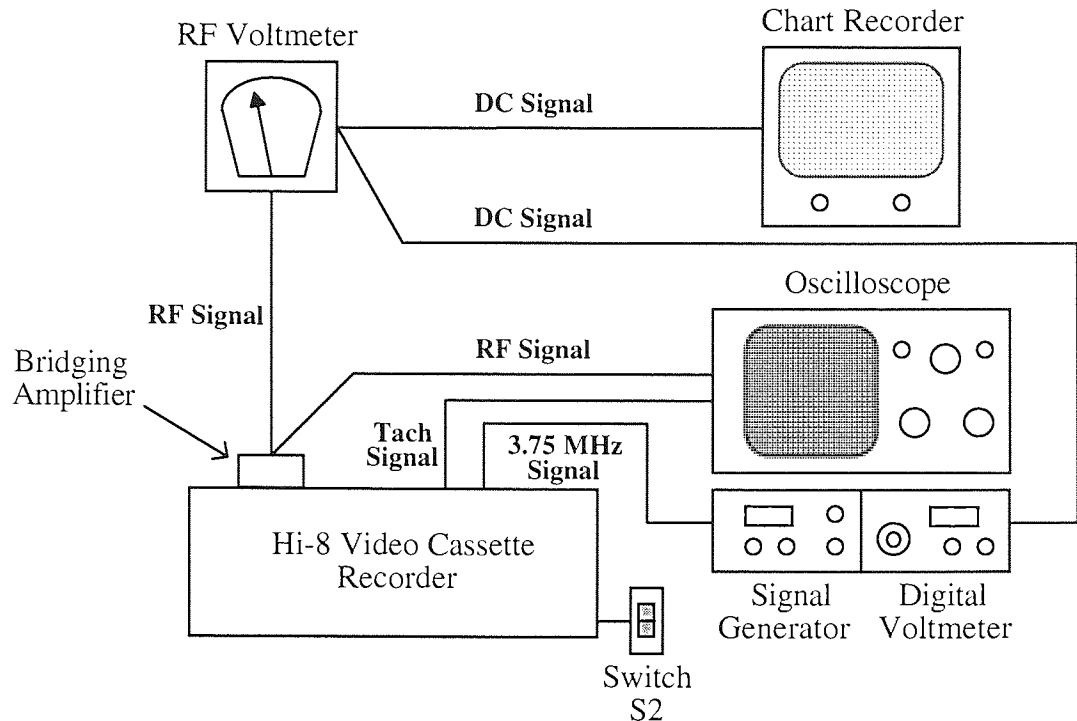
Figure 2.7 *Test Equipment for Stop Motion Tests*

The three heads on the rotating drum, (2 read/write heads and an erase head) ensured that a single track on the tape would be subjected to 324,000 head passes per hour. Thus, the stop motion test provided a very demanding examination of the durability of a tape.

2.3 Analytical Techniques

Surface analysis incorporates a wide range of analytical techniques which are used to gain physical and chemical information about the surface (top layer of atoms) and near surface region (up to several atomic layers beneath the top layer) of a sample. For instance, the elemental composition and associated chemical states of a surface can be determined through x-ray photoelectron spectroscopy, and when angle resolved XPS is utilised, depth information about a surface may also be derived. Further chemical information about a compound can be revealed through the application of secondary ion mass spectrometry and this technique is particularly useful when the chemical structure of a sample is relatively complex.

Scanning electron microscopy is used to obtain physical information about the outer layer of a sample surface and is an excellent tool for determining the dimensions of surface features on a micron scale. However, a thorough surface analytical investigation of a sample usually requires several of the aforementioned techniques to be used in conjunction with one another since chemical and physical information are often both needed for a complete surface diagnosis.

2.3.1 X-Ray Photoelectron Spectroscopy, XPS

X-ray photoelectron spectroscopy is based on the principal of the photoelectron effect, where the sample under investigation is usually irradiated with K_α aluminium or K_α magnesium monoenergetic photons, as shown in Figure 2.8.
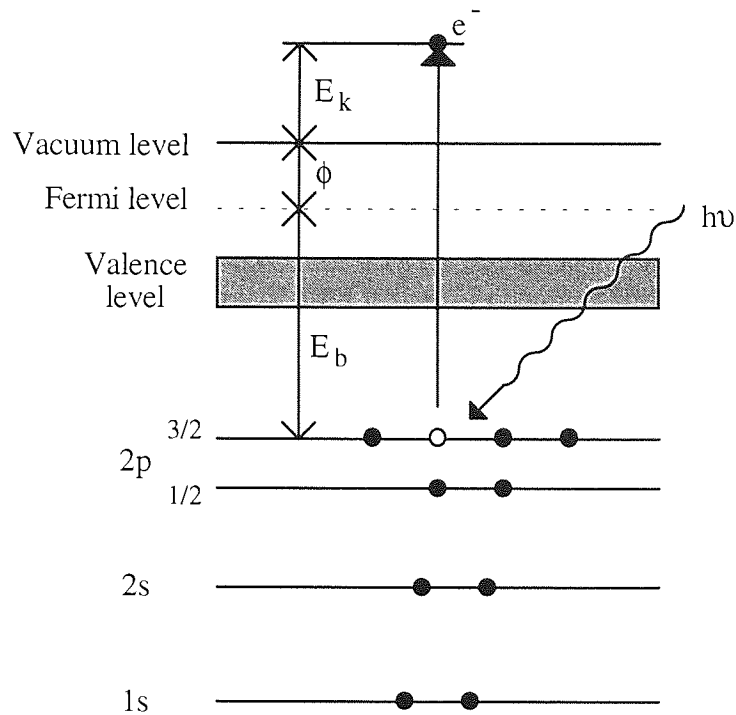
Figure 2.8 X-ray Photoelectron Spectroscopy

Core level electrons of atoms in close proximity to the sample surface will be excited by the incident x-rays to such an extent that they may be able to surmount the binding energy of the nucleus. If the energy of the excitation x-rays, $h\upsilon$, is sufficient, the photoelectrons will gain enough energy to overcome the specimen work function, ϕ, and escape from the sample surface. Thus, by analysing the kinetic energy of the ejected photoelectrons, E_k, the relevant binding energy, E_b, can be determined using Equation 2.1.

$$E_k = h\upsilon - \phi - E_b \tag{2.1}$$

The binding energy of the emitted core level electrons, corresponds to a particular species of atom and thus by measuring the number of electrons at a given binding energy, the atomic concentration of an element may be determined. The work function, ϕ, is the difference in energy between the Fermi level of a specimen sample and the energy of free space (Vacuum level). Thus, the work function can be considered to be the amount of

energy (in electron volts) required to remove an electron from the highest occupied energy level from within the sample, to a position under vacuum, away from the sample surface.

One of the most important features of XPS is that of chemical shifts in the photoelectron lines. Identical atoms in different chemical structures will have different binding energies due to differences in the valence electron charge densities and electrostatic effects from neighbouring atoms. A partial decrease in the valence electron density of a species of atoms results in an increase in the binding energy and this ultimately enables the chemical states (or bonding) of an element to be determined. Near neighbour effects can also be considerable, if less easy to predict.

The depth of analysis for XPS is limited by the escape depth of the core level electrons and the relative angle between the surface plane of the sample and the analyser of the spectrometer. The maximum inelastic mean free path, λ, of the photoelectrons emerging from core atoms is about 3.5 nm although in most cases, it is significantly less. Thus, since approximately 95% of all the photoelectrons will have been derived from a distance of 3λ within the sample, the maximum detection limit of XPS can be considered to be about 10 nm.

2.3.2 Angular Resolved X-ray Photoelectron Spectroscopy

One of the main attributes of angle resolved XPS is the ability to produce a non-destructive depth profile of the top few atomic layers of a sample surface. The intensity of the emerging photo-electrons is dependent on the composition of the sample and its variation with depth. Thus, by varying the angle at which the photoelectrons escape

from the sample, a change in the sampling depth can be produced, as illustrated in Figure 2.9.
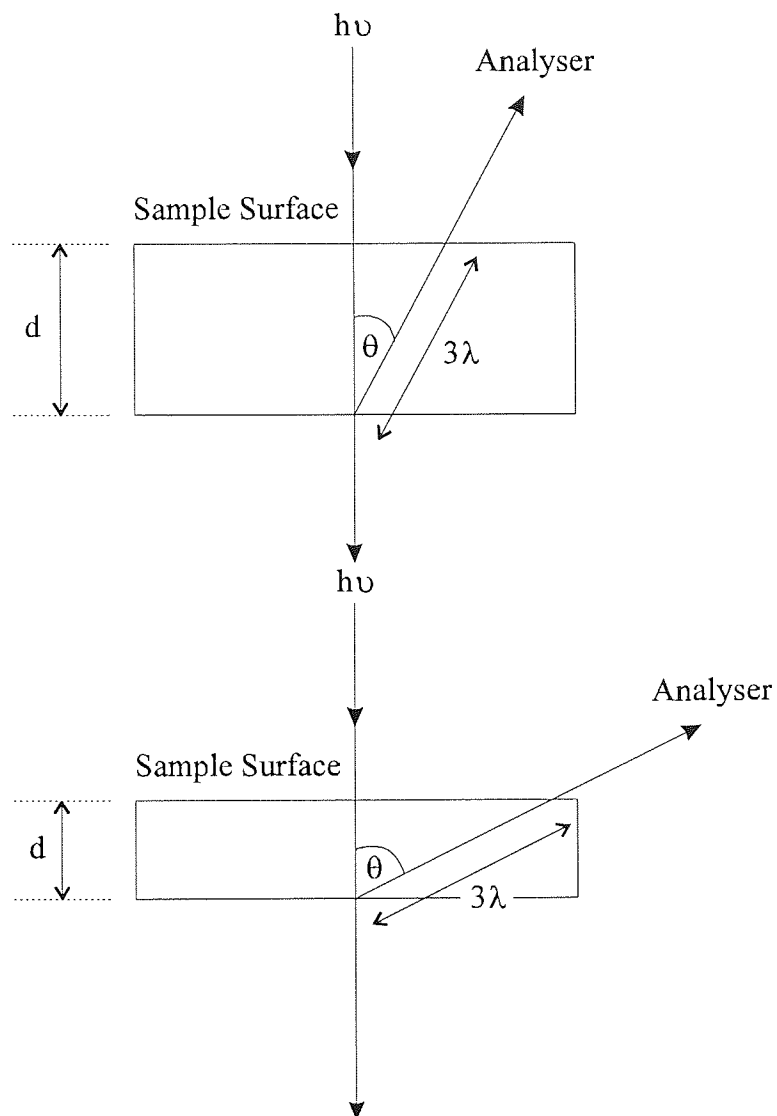
Figure 2.9 *Depth Profile as a Function of Analyser Take-off Angle*

The vertical depth sampled is given by Equation 2.2

$$d = 3\lambda \cos\theta \qquad\qquad (2.2)$$

where

$\lambda =$ The inelastic mean free path of the photoelectrons from the core atoms.

$\theta =$ Analyser take-off angle between the surface normal and the trajectory of the photoelectrons.

For a substrate covered with a thin uniform overlayer of thickness t, the angular variation of the intensity of the photoelectron signal is given by

$$I'_s = I_s e^{-\frac{t}{\lambda \cos \theta}} \qquad\qquad \text{from the substrate}$$

$$I'_o = I_o \left(1 - e^{-\frac{t}{\lambda \cos \theta}} \right) \qquad \text{from the overlayer}$$

Briggs and Seah [100] showed that in an ideal case, the angular dependency of the signal intensity is described by the curves illustrated in Figure 2.10.
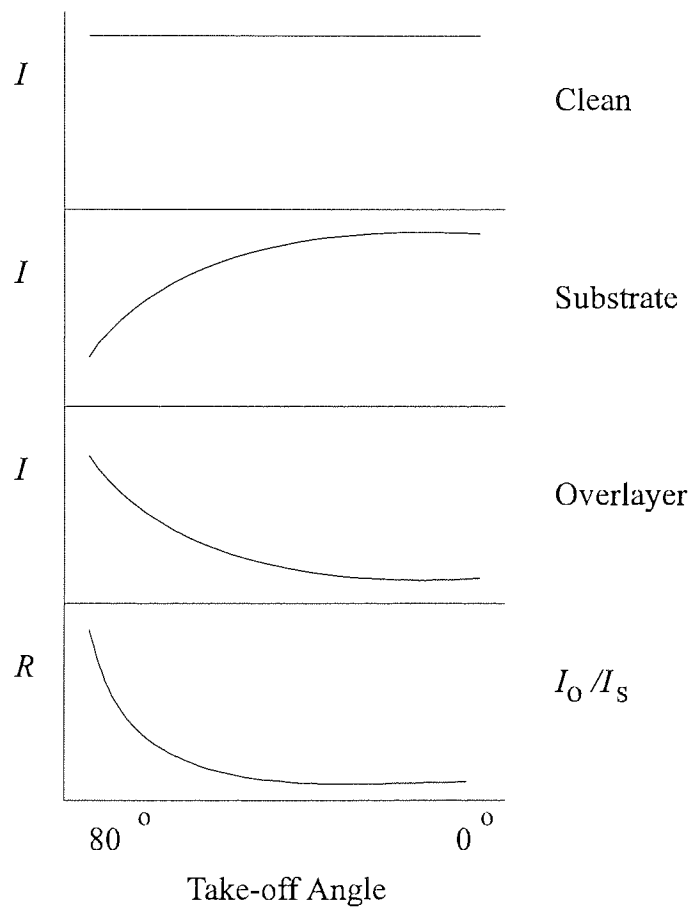
Figure 2.10 *Angular Dependency of the Signal Intensity for XPS Analysis*

Chemical analysis of tape surfaces in this research was conducted by means of X-ray photoelectron spectroscopy and Secondary Ion Mass Spectrometry in a Fisons Instruments VG ESCALAB 200-D multi-technique spectrometer. The change in surface lubrication and surface composition after running durability tests was investigated using XPS whereas the backbone and end-group of the lubricants on commercial ME tapes was identified using SIMS analysis. Angle resolved X-ray photoelectron spectroscopy (ARXPS) was used to determine further characteristics of the tape surfaces such as elemental atomic concentrations and integrated depth profiles. This technique was also used to determine the thickness of the lubricant on thin film metal evaporated media and the relative thickness of material covering the magnetic pigment in metal particulate tapes. Analytical methods for the determination of these quantities will be covered in Chapter 3.

Al K_α X-radiation was employed for the XPS examination, at a source excitation energy of 15 keV and emission current of 20 mA. The area of analysis was chosen to be 2 x 3 mm in the majority of the analyses except for where the region around a wear scar was to be examined. For these cases, in which the wear scar occurred as a result of a stop motion durability test, the area of analysis was circular with a 150 μm diameter.

Survey scans were first recorded for all samples at take off angles of 0° (normal to the analyser) in order to ascertain which elements were present on the surface of a given sample. Once the elements had been identified, narrow region energy scans were collected at normal incidence and at a series of increasing "take off angles". The data from each of these angles enabled depth information to be resolved, and hence integrated depth profiles of a sample surface could be constructed. In order to reduce the effect of radiation induced loss of fluorine from the ME tape surfaces, a different sample was used for each angle measured and the fluorine spectrum was always collected first. Similarly, in the case of the MP tape, the first spectrum to be collected was that of chlorine and in all cases, sample to sample variability was negligible.

Relative atomic concentrations were calculated for each angle from the intensities of the major photoelectron spectral lines by means of codes incorporated in the VG 5250 instrument data system using Schofield cross sections. Multiple scans were used for the constituents in the surface, in order to improve the statistics, and the base pressure within the spectrometer during examinations was always better than 8×10^{-10} mbar. This ensured that all the signals detected by the analyser were from the sample surface and not due to system contamination.

2.3.3 Secondary Ion Mass Spectrometry

In Secondary Ion Mass Spectrometry, the surface of a sample is bombarded with primary rare gas ions, in the energy range 15-20 KeV. This results in the emission of secondary ions and molecules, as shown in Figure 2.11, which are then mass analysed using a quadrupole mass spectrometer.
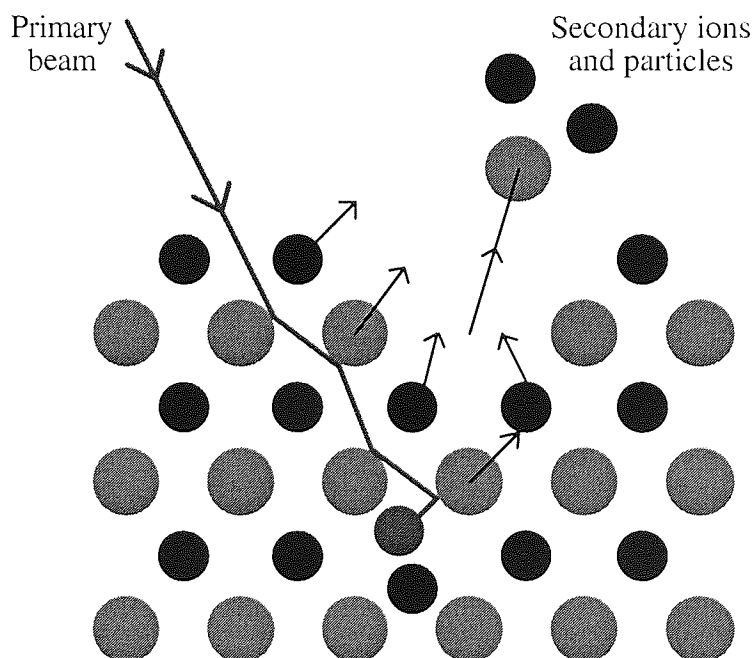

Figure 2.11 Secondary Ion Mass Spectrometry

All elements and isotopes can be detected using SIMS and the detection limit is in the range 1 ppm to 1 ppb, although quantification was not possible for the samples used in this investigation. For these analyses, a technique known as static SIMS was employed. In this mode, the primary beam of argon ions had a low current density of the order of 10^{-9} Acm^{-2} and in this case, the surface monolayer lifetime was sufficient to allow time for the original surface to be analysed before it was removed. Thus, a mass spectrum from the outermost surface layer could be generated, and from this, detailed chemical information was gained.

All the positive SIMS experiments in this research were performed using a 5 keV Ar primary ion source with a current density of 1 nAcm^{-2}. For such a current density, static SIMS conditions applied for all examinations, and the resultant secondary ions produced from the ion bombarded surface were analysed using an 800 amu quadrupole mass spectrometer. The spectra resulting from these analyses were compared with reference spectra [100] which then enabled the backbone and end-group of the lubricants on commercial ME tapes to be identified.

2.3.4 Scanning Electron Microscopy, SEM

When the surface of a sample is to be analysed using Scanning Electron Microscopy, a beam of electrons is generated using an electron gun, accelerated towards an anode and then directed towards a magnetic lens. The beam is subsequently focused to a fine point by the electromagnets and can be rastered across the surface of a sample by applying a variable voltage to a set of scanning coils. The voltage energises the coils and creates a magnetic field which deflects the focused electron beam in a controlled manner. The variable voltage is synchronous with the cathode ray tube since the voltage applied to the scanning coils of the microscope is also applied to the coils of the cathode ray tube.

When the focused electron beam hits the surface of a sample, secondary electrons are generated which are then detected, converted to a voltage and amplified. This amplified voltage is applied to the grid of the cathode ray tube to enable an image to be viewed as illustrated in Figure 2.12.
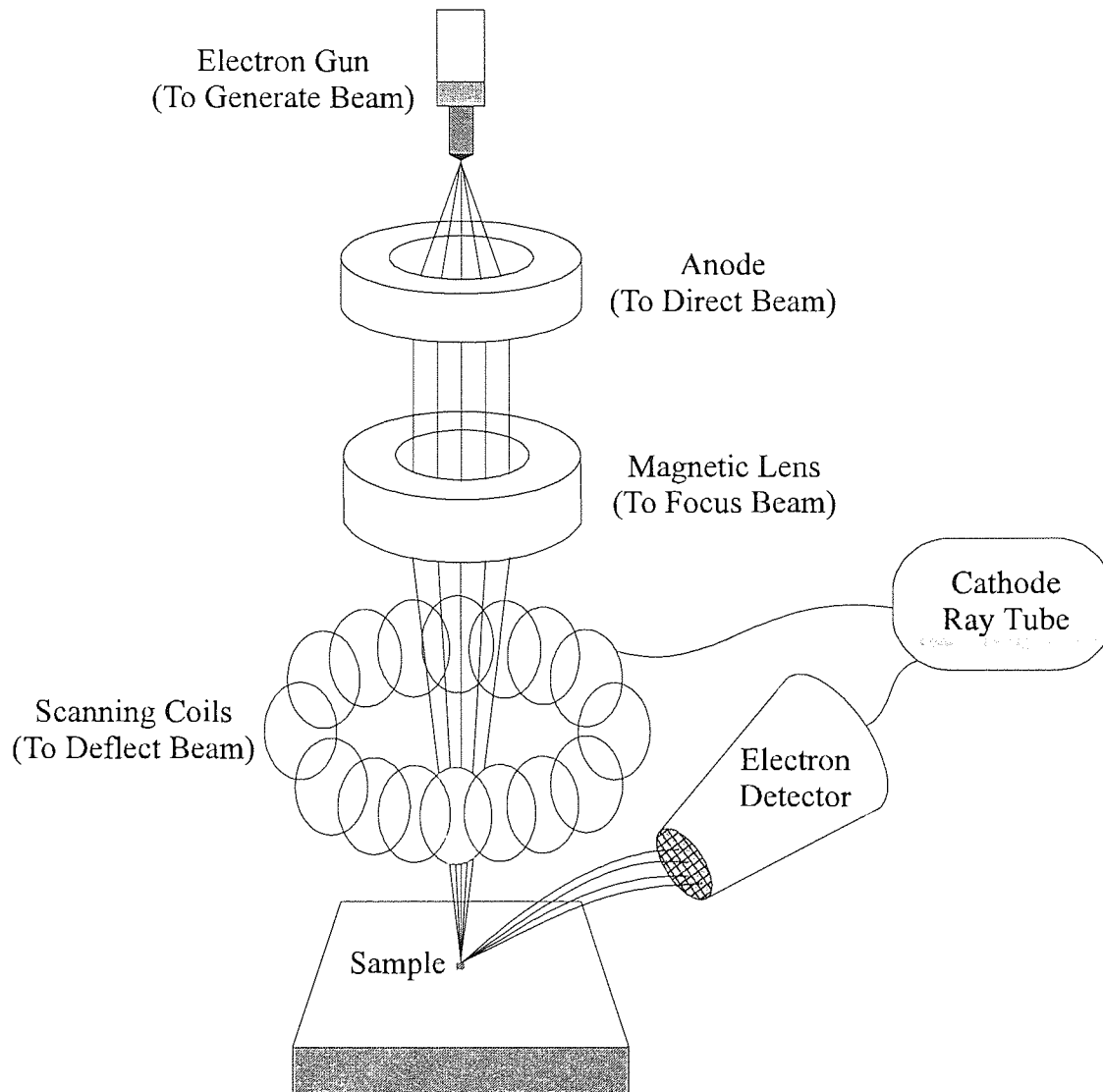

Figure 2.12 *The Scanning Electron Microscope*

The brightness of the cathode ray tube is modulated by the detected secondary electron current which is itself mainly dependent on the angle between the incident electrons and the contours of the sample. The image displayed on the cathode ray tube consists of

thousands of spots of light with varying intensities and is a topographical representation of the sample surface.

Analysis of the tape surfaces in this research was conducted by means of a Cambridge S100 Scanning Electron Microscope in order to investigate any physical changes which occurred to a tape surface following stop motion and cycling durability tests. The samples were firmly mounted on metal stubs using double-sided sticky tape and silver paint was applied to the perimeter of the tape samples and to the edge of the metal stubs. This ensured that there was a good contact between the two surfaces which ultimately minimised the problem of sample charging. The need for coating the surface of the tapes through gold sputtering was thus eliminated since image drifting did not occur.

Images illustrating the surface of ME and MP tape samples were recorded on Polaroid film, in order to provide a permanent record of the wear damage. The area of analysis illustrated on each photograph varied depending on the relative size of the wear feature but surface damage as small as 2 to 3 μm in length was easily resolved.

2.4 Tape Samples

2.4.1 Metal Evaporated Thin Film Tape Samples

The commercial metal evaporated tape samples used in this research were produced by two different manufacturers with tapes ME#1 and ME#3 produced by one manufacturer and tape ME#2 by another. However, in each case, there were important structural differences between each tape, as listed in Table 2.2.

Tape	Magnetic Layer	Protective Film	Substrate Thickness
ME#1	Single	PFPE lubricant	10 μm
ME#2	Dual	PFPE lubricant	10 μm
ME#3	Single	PFPE lubricant & Carbon overlayer	6.7 μm

Table 2.2 Properties of Commercial ME Tapes

The substrates used in the construction of tapes ME#1 and ME#2 were of equal thickness whereas a thinner substrate was used for tape ME#3 [41]. This reduced the total thickness of the tape and increased the capacity by enabling more tape to be supplied in the Hi-8 cassette. Also, tape ME#3 contained a DLC protective coating between the PFPE lubricant layer and the magnetic thin film and this was likely to afford the tape better protection and hence improve the durability characteristics of the tape.

Another significant difference between the tapes arose from the number of magnetic layers since tapes ME#1 and ME#3 were both constructed using a single magnetic layer whereas tape ME#2 had a dual layer. Magnetic multitilayer structures and very thin substrates is believed to have a significant effect on the overall durability of ME media.

2.4.2 Metal Particle Tape Samples

In addition to the metal evaporated tape samples, a commercial metal particle tape was subjected to exactly the same tests and analyses in order to provide comparative data about the durability of the metal particle tape, relative to that of the metal evaporated tapes. The metal particle tape chosen for this study was produced by the same manufacturer as that for the metal evaporated thin film tapes, ME#1 and ME#3.

2.5 Experiments

The durability of the commercial metal evaporated tapes ME#1, ME#2 and ME#3 was evaluated using a series of cycling and stop motion tests. Two identical video cassette recorders were available for use in this research and hence one was allocated for cycling tests whilst the other was only used for stop motion tests.

Interchanging metal evaporated tape with particulate tape within the same VCR causes excessive head and tape wear due to the tapes forming different head shapes during VCR operation [41]. Thus, one set of scanners was allocated for use with ME tapes whilst another set was used for experiments involving MP tapes. This ensured that any wear that might have occurred through interchanging different types of tape was eliminated.

When a cycling test was to be performed on a metal particle tape, either a new scanner was fitted to the VCR, or an existing scanner in which the heads were still in good condition was used. If a scanner had been used for a previous durability test, a standard procedure was followed in order to clean the scanner and heads before a new test was commenced. This was performed by the careful application of ethanol to the scanner, heads and any readily accessible parts of the tape guide system. The VCR was then left for a few minutes to allow time for the ethanol to evaporate before finally, lapping tape was played in the VCR for approximately 10 seconds in order to remove any remaining debris. This was deemed to be the best method for ensuring comparable experimental conditions since it was not possible to use a new scanner for each durability test due to the prohibitive cost this would have incurred.

CHAPTER 3

DETERMINATION OF LUBRICANT THICKNESS

3.1 Introduction

Thin film magnetic recording media rely on a topical lubricant layer to minimise the effects of wear, caused when the recording heads and tape guide system are in contact with the media. In the Hi-8 video system, the drum carrying the heads, rotates at a speed of 1800 rpm, and since the heads on the drum are in intimate contact with the tape, severe wear would occur at the head-media interface without the presence of a suitable lubricant. The lubricant layer must be as thin as possible in order to minimise spacing losses but it must still afford the tape excellent protection from the effects of friction. Thus, it is essential that the lubricant can be characterised in terms of thickness and areal coverage in order to facilitate the optimisation of lubricant layers.

The determination of the thickness of a lubricant layer through ellipsometry techniques requires a smooth and reflective outer surface since the measured properties of changes in phase and amplitude of polarised light depend upon the reflection of the light at the surface. Theoretically, it should be possible to calculate the thickness of the lubricant layer on a metal evaporated tape using ellipsometry. However, although the surface of ME media appear glossy to the naked eye, it is microscopically rough and this can interfere considerably with the reflected light beam, resulting in a loss of amplitude in the polarised light. The delta and psi parameters measured during ellipsometry contain information related to the optical properties of the material and surface films under investigation and also to properties of the surface roughness. The problem of distinguishing quantitatively between these different properties is extremely difficult and leads to unrealistic values for the thickness of the lubricant layer [101].

Angle resolved XPS experiments inherently include depth information about a sample and hence it should be possible to use this technique to determine the thickness of the lubricant layer on a ME tape. A series of general models have been postulated for calculating the thickness of overlayers, based on ARXPS experiments which have ranged

from assuming a uniform layer to films which have a regular, but non-uniform surface topography.

In the case of particulate media, a continuous magnetic film does not inherently exist within the media so a different model has to be used to those developed for continuous thin films. Indeed, rather than calculating the thickness of the lubricant layer, it is more appropriate to determine the thickness of overlayers (such as binder material, lubricant and carbonaceous films) above the top magnetic particles since this will effect the spacing losses and durability of the media.

3.2 Models Based on XPS Techniques

3.2.1 Uniform Lubricant Layer Model

In this model, it was assumed that the lubricant consisted of a uniform layer, covering the magnetic thin film, as illustrated in Figure 3.1.
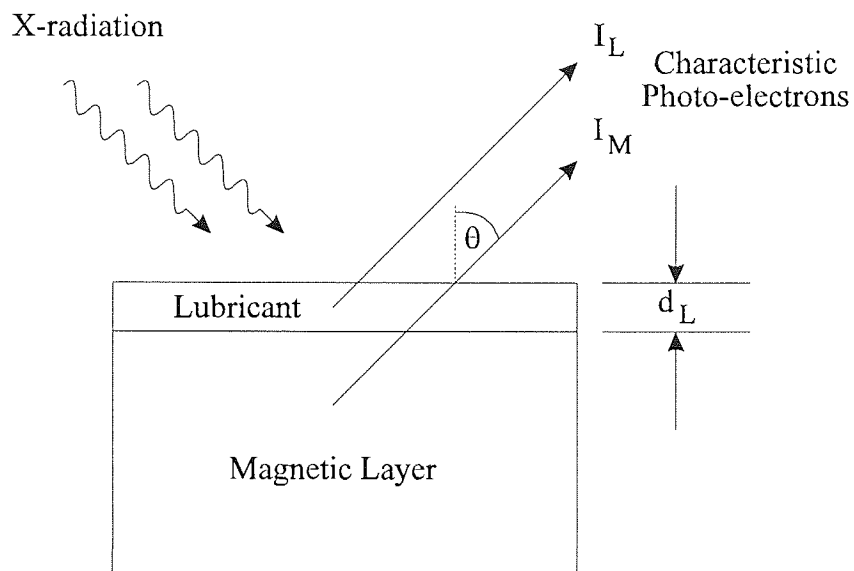

Figure 3.1 Uniform Lubricant Model

Briggs and Seah [102] described a method, based on ARXPS, for determining the thickness of a carbon or hydrocarbon contamination layer on the surface of a sample. They postulated that in the absence of elastic scattering, the photoelectron signal from the substrate B of a sample, I_B, covered by a fractional monolayer α_A is given by Equation 3.1.

$$I_B = I_B^0 \left\{ 1 - \alpha_A + \alpha_A \exp\left[-\frac{d_A}{\lambda_A(E_B)\cos\theta} \right] \right\}$$

(3.1)

where

I_B^0 = Signal from an element in the substrate, in the absence of a contamination layer.

d_A = Thickness of the contamination layer.

The same principles can be used to calculate the thickness of a general overlayer which in the case of a thin film ME tape, is the lubricant layer. Thus, the photoelectron signal from an element in the magnetic film, in the presence of a lubricant layer is given by Equation 3.2.

$$I_M = I_M^0 \left\{ 1 - \alpha_L + \alpha_L \exp\left[-\frac{d_L}{\lambda_L(E_M)\cos\theta} \right] \right\}$$ (3.2)

where

I_M^0 = Signal from an element in the magnetic film, in the absence of the lubricant.

α_L = Fractional coverage of the lubricant.

d_L = Lubricant thickness.

$\lambda_L(E_M)$ = Inelastic mean free path of photoelectrons from the magnetic film.

θ = Analyser take-off angle, normal to the analyser.

For a ME tape, there must be complete areal coverage of the magnetic layer by the lubricant. Otherwise, high frictional forces would occur at the head/tape interface which would then cause the tape to fail. Thus, by assuming $\alpha_L = 1$, Equation 3.2 becomes

$$I_M = I_M^0 \exp\left[-\frac{d_L}{\lambda_L(E_M)\cos\theta} \right]$$ (3.3)

$$\ln I_M = \ln I_M^0 - \frac{d_L}{\lambda_L(E_M)\cos\theta}$$ (3.4)

$$\ln I_M = -\frac{d_L}{\lambda_L(E_M)\cos\theta} + \ln I_M^0$$ (3.5)

Therefore, a graph of $\ln I_M$ against $\frac{1}{\cos\theta}$ will have a gradient equal to $-\frac{d_L}{\lambda_L(E_M)}$, from which the thickness of the lubricant can be readily determined.

Manipulation of Equation 3.2 in a different manner leads to Equation 3.6.

$$\frac{I_M}{I_M^0} = 1 - \alpha_L + \alpha_L \exp\left[-\frac{d_L}{\lambda_L(E_M)\cos\theta} \right]$$

(3.6)

By making the same assumption that there is complete areal coverage of the magnetic layer by the lubricant film, Equation 3.6 reduces to Equation 3.7 and ultimately to Equation 3.8.

$$\frac{I_M}{I_M^0} = \exp\left[-\frac{d_L}{\lambda_L(E_M)\cos\theta} \right]$$

(3.7)

$$\ln\left(\frac{I_M}{I_M^0} \right) = -\frac{d_L}{\lambda_L(E_M)\cos\theta}$$

(3.8)

Thus, a graph of $\ln\left(\frac{I_M}{I_M^0} \right)$ against $\frac{1}{\cos\theta}$ will have a gradient equal to $-\frac{d_L}{\lambda_L(E_M)}$

A second uniform layer model, similar to that illustrated in Figure 3.1, was proposed by Kimachi et al. [103] in which a lubricant layer of constant thickness, d_L, completely covers the magnetic film. If it is assumed that the magnetic thin film layer is very flat and the elemental atoms in the lubricant layer are evenly distributed [104], the ratio of the signals from the characteristic photo-electrons, for the uniform model is given by Equation 3.9.

$$\frac{\left(\frac{I_L}{I_M} \right)}{k} = \frac{1 - \exp\left(-\frac{d_L}{\lambda\cos\theta} \right)}{\exp\left(-\frac{d_L}{\lambda\cos\theta} \right)}$$

(3.9)

and

$$k = \frac{S(E_L,\theta)\sigma_L n_L \lambda_L}{S(E_M,\theta)\sigma_M n_M \lambda_M}$$

(3.10)

where

$S(E_i, \theta)$ = Spectrometer detection efficiency.

E_L = Kinetic energy of the photoelectrons from an element in the lubricant.

E_M = Kinetic energy of the photoelectrons from an element in the magnetic layer.

σ_L = Photo-ionisation cross section for the core level of an atom in the lubricant.

σ_M = Photo-ionisation cross section for the core level of an atom in the magnetic layer.

n_L = Atomic density of an element in the lubricant.

n_M = Atomic density of an element in the magnetic layer.

λ_L = Inelastic mean free path of photoelectrons from the lubricant.

λ_M = Inelastic mean free path of photoelectrons from the magnetic layer.

Any photoelectrons that have been detected by the spectrometer and that had originated from the magnetic layer must also have passed through the lubricant. Thus, Kimachi et al. [103] assumed that the inelastic mean free path of the photoelectrons from the magnetic layer is equivalent to the inelastic mean free path of photoelectrons from the lubricant. Based on this assumption, Equation 3.9 simplifies to Equation 3.11.

$$\ln\left(\frac{(I_L/I_M)}{k} + 1\right) = \frac{d_L}{\lambda_L \cos\theta} \tag{3.11}$$

If the lubricant layer is of constant thickness, a graph of $\ln\left(\frac{(I_L/I_M)}{k} + 1\right)$ against $\frac{1}{\cos\theta}$ should be a linear plot with a gradient of $\frac{d_L}{\lambda_L}$.

Linder and Mee [105] described a method for measuring the average thickness of the fluorocarbon lubricant film on magnetic disk media. The method involved the use of XPS to measure the signal from the lubricant, which would increase with increasing lubricant thickness, and the signal from the resin, which would decrease with increasing lubricant thickness. They obtained a profile of the disk by initially analysing a sample

disk using XPS, followed by a period of argon ion etching. This process of XPS analysis followed by ion etching was then repeated several times so that eventually the lubricant would be removed and a profile of the near surface region could be established.

The XPS profiles, together with some SIMS analysis of the disk indicated that part of the outer resin had mixed with the fluorocarbon layer. Further information about the surface structure was gained through angle resolved XPS analysis since these results indicated that on average, the fluorocarbon layer was above the resin. Linder and Mee [105] summarised the main features of these results by proposing a surface structure for the disk, as illustrated by Figure 3.2.
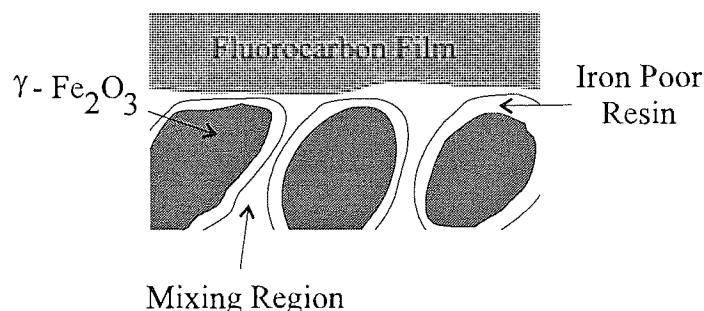

Figure 3.2 Surface Structure of a Lubricated Magnetic Disk

The complex structure of an outer fluorocarbon layer, followed by a resin/fluorocarbon transition region, above a region of γ-Fe$_2$O$_3$/resin enclosed in a poor iron resin was not particularly conducive to efficient modelling. Thus, a simplified model was developed by making two assumptions which still retained the essential features of the surface structure but which ultimately enabled the structure to be modified to a simpler form.

Firstly, the typical loading factors for γ-Fe$_2$O$_3$ gave a similar carbon density to that of the pure resin, and since the γ-Fe$_2$O$_3$ was coated with a pure resin, it was deemed that the carbon signal before argon etching was not significantly affected by the presence of the γ-Fe$_2$O$_3$. Secondly, the transition, or mixing region as shown in Figure 3.2, was

very thin and since it was also bounded by pure materials, its presence was considered to be irrelevant in terms of the model and hence it was neglected. These assumptions gave rise to a far simpler surface structure, as illustrated in Figure 3.3.
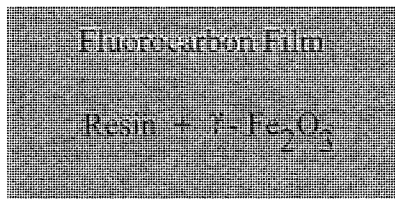

Figure 3.3 Simplified Surface Structure of a Lubricated Magnetic Disk

The thickness of the fluorocarbon film in the simplified model is given by Equation 3.12.

$$d_L = \lambda \cos\theta \ln(aR + 1)$$ (3.12)

where

d_L = Thickness of the fluorocarbon layer.

λ = Inelastic mean free path of the photoelectrons from the resin and γ-Fe_2O_3.

θ = Analyser take-off angle, normal to the analyser.

a = Ratio of the carbon atom density in the resin and γ-Fe_2O_3 to that in the fluorocarbon layer, when analysing the constituents separately.

R = Ratio of the carbon atom density in the resin and γ-Fe_2O_3 to that in the fluorocarbon layer, when analysing the complete disk.

This simplified model of the magnetic disk is very similar to that of a ME thin film tape since they both have a layered structure. The fluorocarbon film in the disk model is equivalent to the lubricant layer on the ME tape whereas the magnetic layer on the tape is represented by the resin and γ - Fe_2O_3 region on the disk. Thus, by simple analogy to the model of the Winchester disk, the thickness of the lubricant layer on a ME tape can be determined using Equation 3.12, but with the variables defined as

d_L = Thickness of the lubricant layer.

λ = Inelastic mean free path of the photoelectrons from the magnetic layer.

θ = Analyser take-off angle, normal to the analyser.

a = Ratio of the carbon atom density in the carbon protective layer to that in the fluorocarbon layer, when analysing the constituents separately.

R = Ratio of the carbon atom density in the carbon protective layer to that in the fluorocarbon layer, when analysing the complete disk.

Thus, Equation 3.12 can be modified to give Equation 3.13.

$$d_L = \lambda \cos\theta \ln\left\{\left(\frac{R_1/R_2}{R_3/R_4}\right) + 1\right\} \qquad (3.13)$$

where

R_1 = C-F peak area of the C 1s XPS spectrum.

R_2 = C-C + contamination peak area of the C 1s XPS spectrum for the carbon protective layer only.

R_3 = C-F peak area of the C 1s XPS spectrum when analysing just the lubricant.

R_4 = C-C + contamination peak area of the C 1s XPS spectrum for the carbon protective layer only.

3.2.2 Non-Uniform Lubricant Layer Model

Several analytical models for quantifying the lubricant layer on magnetic recording media have been developed based on a non uniform lubricant distribution, as illustrated in Figures 3.4 - 3.7. [103]
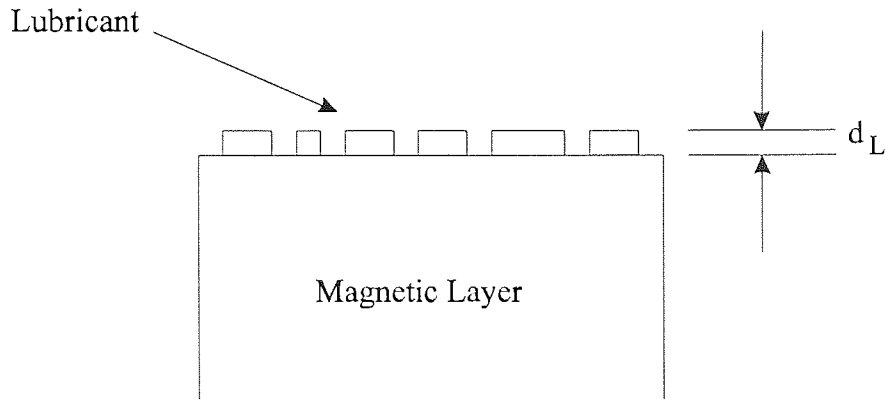
Lubricant

Magnetic Layer

d_L

Figure 3.4 *Island Lubricant Distribution Model*

In the island model, it was proposed that the lubricant does not provide complete areal coverage of the magnetic layer but in fact forms discrete lubricant islands of constant thickness, d_L.
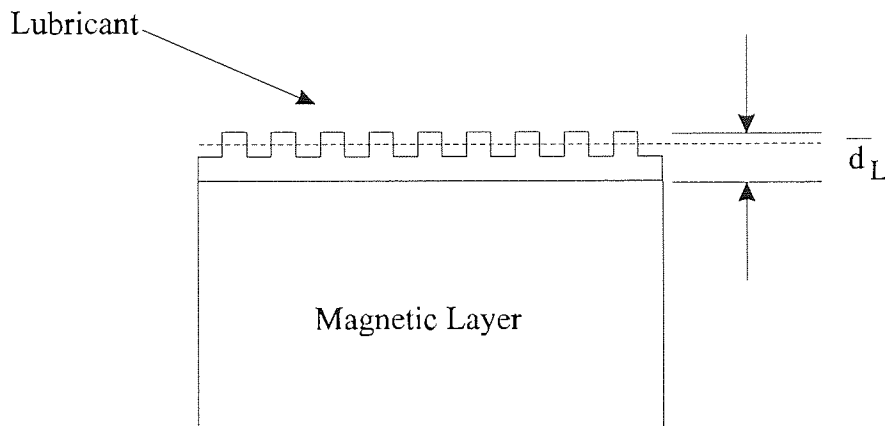
Lubricant

Magnetic Layer

$\overline{d}_L$

Figure 3.5 *Stranski-Krastanov Lubricant Distribution Model*

Lubricant

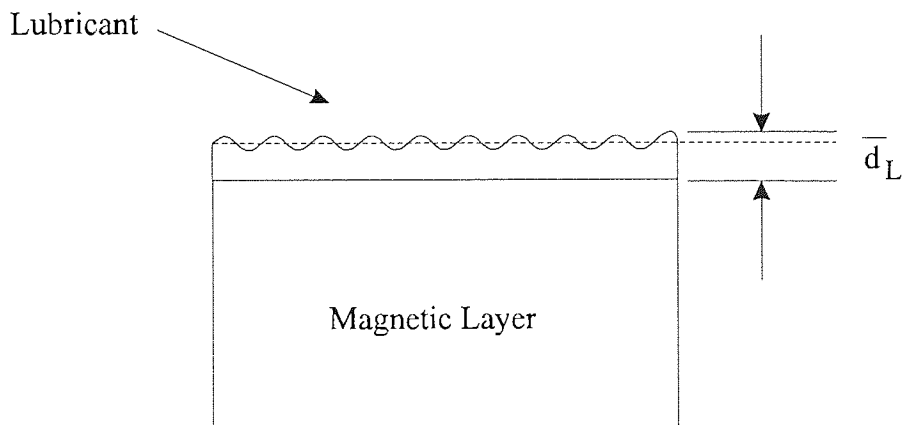Magnetic Layer

$\overline{d}_L$

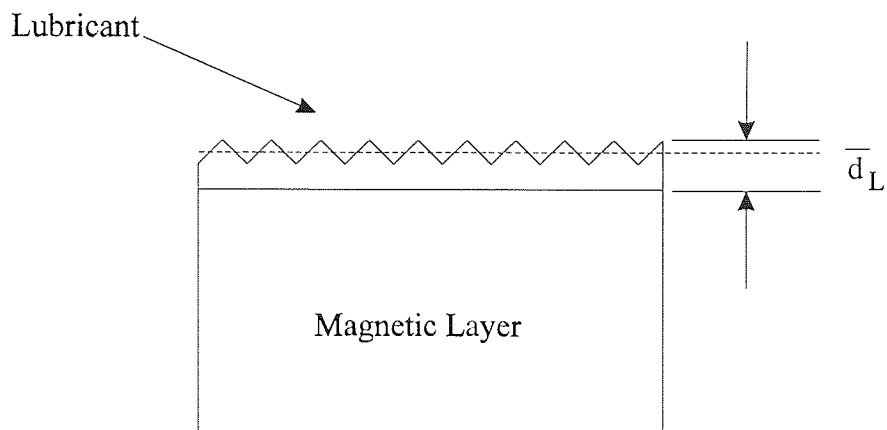**Figure 3.6** *Sinusoidal Overlayer Lubricant Distribution Model*

Figure 3.7 Notched Overlayer Lubricant Distribution Model

The Stranski-Krastanov, Sinusoidal overlayer and Notched overlayer models have the common feature of a periodic lubricant distribution on top of a uniform lubricant layer. Thus, each of these models assume complete areal coverage but with different surface topographies.

For each of the models, it was assumed that once the photoelectrons had passed through the lubricant layer, they did not re-enter the lubricant at any other time. Uniformity parameters were defined for each of the models, as illustrated in Table 3.1, where the average thickness of the lubricant layer is equal to the product of the lubricant thickness and the uniformity parameter.

Model	Uniformity Parameter	Average Thickness
Island	Θ	Θd
Stranski-Krastanov	α	αd
Sinusoidal	β	βd
Notched	γ	γd

Table 3.1 Uniformity Parameters for Non-Uniform Models

Equation 3.9 can be adapted for the island model [103] to give the photoelectron intensity ratio, $(I_L / I_M) / k$, as defined by Equation 3.14.

$$\frac{(I_L / I_M)}{k} = \frac{\Theta(1 - \exp(-d_L / \lambda_L \cos\theta))}{(1 - \Theta) + \Theta \exp(-d_L / \lambda_M \cos\theta)}$$ (3.14)

Equation 3.14 can be modified for each of the other non-uniform models by simply substituting the relevant uniformity parameter. Kimachi et al. [103] simplified Equation 3.14 by assuming $d_L < \lambda_L$. However, the thickness of lubricants used in current ME tapes has been reduced to such an extent that this assumption no longer holds and hence it cannot be used to simplify Equation 3.14. Re-arranging Equation 3.14 leads to Equation 3.15.

$$\Theta\left\{1 + \frac{(I_L/I_M)}{k} - \exp\left(-\frac{d_L}{\lambda_L\cos\theta}\right) - \left(\frac{(I_L/I_M)}{k}\right)\exp\left(-\frac{d_L}{\lambda_M\cos\theta}\right)\right\} = \frac{(I_L/I_M)}{k} \quad (3.15)$$

Assuming, $\lambda_L = \lambda_M$, Equation 3.15 can be simplified to give

$$\exp\left(-\frac{d_L}{\lambda\cos\theta}\right) = \frac{\Theta + \Theta\left(\dfrac{(I_L/I_M)}{k}\right) - \left(\dfrac{(I_L/I_M)}{k}\right)}{\Theta\left(1 + \left(\dfrac{(I_L/I_M)}{k}\right)\right)} \quad (3.16)$$

Thus, the thickness of the lubricant layer can be expressed in the form of Equation 3.17

$$d_L = -\lambda\cos\theta\ln\left\{1 - \frac{\left(\dfrac{(I_L/I_M)}{k}\right)}{\Theta\left(1 + \left(\dfrac{(I_L/I_M)}{k}\right)\right)}\right\} \quad (3.17)$$

In the Stranski-Krastanov model, the lubricant coverage on the uniform layer is fixed at 0.5. Thus, Equation 3.17 reduces to Equation 3.18

$$d_L = -\lambda\cos\theta\ln\left\{\frac{1 - 3\left(\dfrac{(I_L/I_M)}{k}\right)}{1 + \left(\dfrac{(I_L/I_M)}{k}\right)}\right\} \quad (3.18)$$

However, the topographical surface of thin film media will vary from sample to sample and in reality, none of the non-uniform lubricant layer models will provide an accurate representation of the surface of a ME tape. Thus, none of the aforementioned models can be deemed to produce significantly better measurements than any one of the other non-uniform models.

3.2.3 Reconstruction of Depth Profiles from ARXPS Data

Another approach that could be used to determine the lubricant thickness is by extracting depth profile information from ARXPS data. A reconstructed depth profile of a ME tape would allow the thickness of the lubricant layer to be measured by simply observing the depth at which the fluorine content falls to zero. Unfortunately, the task of deconvoluting a depth profile from XPS data is by no means a straight-forward task.

The concentration depth profile of a sample is dependent on the cosine of the analyser take-off angle. Thus, a series of XPS spectra, collected at a range of different take-off angles will contain a convolution of the entire depth profile. The angular distribution, $I_j(\theta)$, of photoelectrons that escape from the jth element in a sample is given by Equation 3.19

$$I_j(\theta) = \int_0^\infty c_j(x)\varphi(x,\theta)dx \qquad (3.19)$$

where

$\varphi(x,\theta)$ = Depth distribution function.

$c_j(x)$ = Concentration depth profile.

x = Depth from the sample surface.

The depth distribution function is defined as the probability that a photoelectron originating from a depth x will escape to the sample surface without losing any energy.

If elastic scattering is insignificant, the depth distribution function, $\varphi(x,\theta)$, can be approximated to

$$\varphi(x,\theta) = e^{\frac{-x}{\lambda\cos\theta}} \tag{3.20}$$

which when substituted into equation (3.19), gives a Beer-Lambert type of equation

$$I_j(\theta) = \int_0^\infty c_j(x)e^{-\frac{x}{\lambda_j\cos\theta}}dx \tag{3.21}$$

The conversion from ARXPS data (intensity against take-off angle) to a deconvoluted depth profile is one of mathematics "ill-posed" problems since there is no unique solution to Equation 3.21 [106]. Any solution is extremely sensitive to experimental uncertainties and consequently, a small error in the ARXPS data can lead to large variations in the resultant depth profile.

Several algorithms have been proposed for extracting depth profiles from ARXPS intensities. Holloway and Bussing [107] used a forward Laplace transform method in which the sample surface is initially partitioned into several layers whose thickness can be made infinitely small. A concentration step function is then assigned to each of the layers, which enables an ARXPS data set of intensity against take-off angle to be calculated, using a forward Laplace transform. The forward transform of a step function is explicitly defined and the position of the step function in real space (i.e. depth profile) is transformed into a smooth varying function in angle space (take-off angle). Thus, in theory, it should be possible to extract the composition depth profile information contained within the ARXPS data. The residual errors between the ARXPS experimental data set and the calculated data set are then used to calculate a series of correction factors for modifying the concentration profile. Once the modified concentration profile has been determined, an updated intensity against take-off angle data set is calculated which is then used to obtain a new set of residual errors. This

iterative process is repeated until the sum of the squared errors is less than a value pre-determined by the user. The concentration profile obtained at this point is considered to be the final solution.

Another approach to generating depth profiles from ARXPS data was initiated in 1963 by Tikhonov [108] and Twomey [109] when they each proposed that Equation 3.21 could be modified by adding a regularisation parameter, α. This had the effect of converting Equation 3.21 into a more stable equation which had a single minimum value for non-zero α. However, the regularisation factor is a discretionary parameter which if not assigned an appropriate value, can smooth the reconstruction to such an extent that real features are lost or indeed, fail to stabilise the solution. Butler et al. [110] developed this original work by limiting the regularisation technique to non-negative values. This was a natural progression to the algorithm since it was meaningless to consider a negative concentration of any element in a reconstructed depth profile. Tyler et al. [111] then modified the algorithm of Butler et al. [110] by introducing further criteria for selecting the optimal value of α. They tried to ensure that the appropriate amount of smoothing was applied to the reconstruction by implementing the non-negative constraint in an iterative manner. They found that their algorithm was more stable to noise than previous regularisation techniques and that the reconstructions were more accurate at the near surface regions.

Livesey and Smith [112] used the principles of maximum entropy to extract elemental depth profiles from ARXPS data. Maximum entropy, S, (a negative quantity) is based on statistical theory and is a measure of the disorder of a system. Gull and Skilling [113] defined entropy as that given in Equation 3.22.

$$S = \sum_{j} \sum_{i} n_{j,i} - m_{j,i} - n_{j,i} \log(n_{j,i} / m_{j,i}) \tag{3.22}$$

where

$n_{j,i}$ = the proportion of element j at a depth i.

$m_{j,i}$ = the initial estimate for the proportion of the element j at a depth i.

The logarithmic term, $-n_{j,i} \log(n_{j,i} / m_{j,i})$, ensures that the elemental proportions in the reconstruction will be positive and this eliminates the need to impose restrictions such as those required in the Regularisation algorithm. When applied to the problem of deconvoluting a depth profile, the entropy can be considered as the minimum amount of information contained within the reconstruction, but which is still consistent with the XPS data. In order to determine how the composition of the sample varies with depth, a model structure is assumed, consisting of an arbitrary number of layers of constant thickness, t, as shown in Figure 3.8.
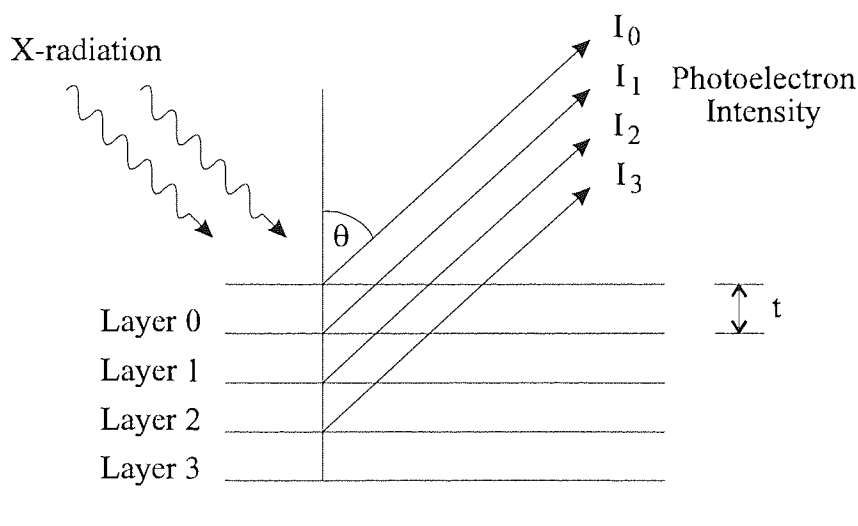
Figure 3.8 Model Structure used in the Reconstruction of a Depth Profile using Maximum Entropy Data Analysis.

The deconvoluted depth profile is obtained by maximising the entropy in Equation 3.22 for all the elemental proportions in each layer, so that a smooth overall depth profile can be reconstructed. This was achieved by utilising a suite of general entropy maximisation subroutines, originally developed by Skilling [114-115] and Gull [116]. The mathematics behind the subroutines is based on the Bayesian theory of maximum entropy, an outline

of which is described by Livesey and Smith [112]. These form the base of an iterative algorithm which allows the reconstruction to be modified until the maximum entropy solution is reached.

The technique was improved further when the effects of elastic scattering were incorporated into the algorithm. Originally, the angular distribution, $I_j(\theta)$, was predicted using Equation (3.22). However, Werner et al. [117-119] showed that this approach was rather to simplified for certain structures. They used Monte-Carlo calculations to model the effects of elastic scattering on the depth distribution and obtained good agreement between experimental data and the predictions of their model [120]. They proposed a new depth distribution function consisting of the summation of 2 exponential terms. This incorporated the effects of elastic scattering into the depth distribution function with the first term representing the photoelectron straight line paths, whilst the second term accounted for the photoelectrons which had travelled in random directions due to elastic scattering.

$$\varphi(x,\theta) = -a_1 e^{\frac{-x}{\lambda_t \cos\theta}} + a_2(\theta)e^{\frac{-x}{\lambda_a \cos\theta}} + a_3(\theta)e^{\frac{-x}{\lambda_a \cos\theta}} \tag{3.23}$$

where

$$a_1 = \left(\frac{\lambda_t}{\lambda}\right)\left(\frac{\lambda - \lambda_a}{\lambda_a - \lambda_t}\right) \tag{3.24}$$

$$a_2(\theta) = 1 + a_1 - a_3(\theta) \tag{3.25}$$

$$a_3(\theta) = \frac{\cos\theta}{1 - \cos\theta}\left(\frac{\lambda_t}{\lambda}\right)\left(\frac{\lambda - \lambda_a}{\lambda_a}\right) \tag{3.26}$$

$$\lambda_a = \frac{\lambda\lambda_{tr}}{(\lambda + \lambda_{tr})}\upsilon_0 \tag{3.27}$$

where

λ_t = Total mean free path of the photoelectrons.

λ_{tr} = Transport mean free path, calculated using a quasi classical formula.

v_0 = unity to within 3% in the energy range of relevance for XPS

The third term in Equation 3.23 represents the trajectories of photoelectrons at deep depths in the sample and only has a weak angular dependence at large depths and contains little information [121]. The effects of elastic scattering were incorporated into the maximum entropy reconstruction method by encoding the distribution function, as described in Equation 3.23, into the entropy routine [121].

3.2.4 Electron Attenuation Length

The attenuation lengths of electrons in a solid material are of great importance in electron spectroscopy since they are required for quantitative surface analysis, such as determining the depth of material through which the detected photoelectrons have travelled. The inelastic mean free path (IMFP), attenuation length (AL) and escape depth are often used to describe the same quantity although they each have a separate and precise definition.

The inelastic mean free path is defined as the mean distance an electron can travel in a material before it looses energy through an inelastic collision and is usually calculated through theoretical calculations, whereas values for the attenuation length of a material are usually obtained from experiments based on overlayer films and incorporate the effects of elastic collisions. Finally, the escape depth of photoelectrons from a sample material, as often referred to in XPS experiments, is equivalent to the product of the AL and the cosine of the angle between the analyser and the surface normal of the sample. Previously, the attenuation length was considered to be equivalent to the inelastic mean

free path because elastic collisions were not thought to contribute to the overall distance travelled. However, attenuation lengths are typically shorter than the corresponding inelastic mean free path by between 15% and 30% and thus for electron spectroscopy techniques, the depth of analysis is less when elastic collisions are taken into account.

Briggs and Seah [122] originally referred to λ as the inelastic mean free path although this was later amended to the attenuation length [123] in order to include the effects of elastic scattering. Given the importance of λ, accurate values must be used in any quantitative calculations. Seah and Dench [124] provided a set of equations for calculating the attenuation lengths for different classes of material, in the kinetic energy (E) range 1 eV to 6 keV, by fitting universal curves to a set of measured attenuation length data.

For elements:

$$\lambda = 538E^{-2} + 0.41(aE)^{1/2} \text{ monolayers} \tag{3.28}$$

For inorganic compounds

$$\lambda = 2170E^{-2} + 0.72(aE)^{1/2} \text{ monolayers} \tag{3.29}$$

For organic compounds

$$\lambda = 49E^{-2} + 0.11E^{1/2} \text{mgm}^2 \tag{3.30}$$

where the monolayer thickness, a, is given by Equation 3.31

$$a = \sqrt[3]{\frac{A}{1000\rho N_A}} \tag{3.31}$$

and

A = The atomic weight of matrix atoms

N_A = Avogadro's Number (6.023 x 10^{23} per gram mole)

ρ = The bulk density (Kgm^{-3})

Table 3.2 lists the attenuation lengths for the elements found in the commercial tapes ME#1, ME#2 and ME#3 when calculated using Seah and Dench equations.

Element	Atomic Weight, A	Density, ρ_M (Kg m-3)	Atom Size (nm)	Energy, E (eV)	λ (nm)
Carbon	12.0	2000	0.22	1199.6	1.4
Oxygen	16.0	1429	0.27	955.6	1.7
Fluorine	19.0	1696	0.27	800.6	1.6
Cobalt	58.9	8900	0.22	705.6	1.1
Nickel	58.7	8900	0.22	631.6	1.1

Table 3.2 Attenuation Lengths of C, O, F, C and Ni Calculated using Seah and Dench Equations [124]

A method of determining the inelastic mean free path, based on theoretical calculations was provided by Tanuma et al. after they extended an algorithm originally developed by Penn [125], to calculate the IMFP of elements in the energy range 50-2000 eV [126]. Values for the IMFP of the 5 elements present in thin film metal evaporated tape are listed in Table 3.3.

Element	Binding Energy (eV)	Kinetic Energy (Al X-Ray Source)	IMFP (nm)
Carbon	287	1199.6	3.1
Fluorine	686	800.6	2.2
Oxygen	531	955.6	2.6
Cobalt	781	705.6	1.2
Nickel	855	631.6	1.1

Table 3.3 IMFP of elements in ME Tape, based on theory of Tanuma et al. [126]

There is a difference between the values of λ depending on which method was used to determine them and it was imperative that the same values were used throughout any quantitative analysis in order that any relative changes between samples were genuine. Equations 3.28-3.30 may not provide the most accurate values for λ since they are based on curves of best fit to experimental data. For this reason, it was decided to use values generated from first principles by Tanuma et al. [126] although these values were modified in order to provide a more realistic representation of ME tapes. The photoelectrons originating from the cobalt and nickel (magnetic layer) would have passed through the organic PFPE lubricant layer before being detected by the analyser. Thus, for angle resolved XPS experiments, the majority of the signal from the magnetic layer will have been attenuated by organic material rather than by metals. Hence, values for the IMFPs should be of cobalt and nickel when passing through a layer of fluorocarbon lubricant rather than when passing through just cobalt and nickel. Tanuma et al. [126] calculated the IMFPs for 14 organic compounds in the energy range 50-2000 eV, from which an average value for the IMFP of the 14 organic compounds could be calculated. The kinetic energies of the detected photoelectrons from cobalt and nickel, using a K_{α} Aluminium radiation source, are 705.6 and 631.6 eV respectively and the average IMFPs of the 14 organic compounds at an electron energy of 600, 700, and 800 eV were calculated to be 2.1, 2.3 and 2.6 nm respectively. Thus, using linear interpolation, the IMFPs of cobalt and nickel, when passing through an organic layer, can be considered to be 2.3 and 2.1 nm respectively, as summarised in Table 3.4.

Element	IMFP (nm) (no organic overlayer)	IMFP (nm) (with organic overlayer)
Cobalt	1.2	2.3
Nickel	1.1	2.1

Table 3.4 IMFP of Cobalt and Nickel, with and without an Organic Overlayer

These values need to be modified further to incorporate the effects of elastic scattering within the material since the IMFP is known to be larger than the AL for most elements by about 15-30%, depending on the atomic number and electron energy. Assuming in the case of cobalt and nickel, the increase is of the order of 20%, whereas for carbon, fluorine and oxygen, the increase is 15%, then the AL's to be used in any quantitative surface analysis of ME tapes will be as listed in Table 3.5

Element	Attenuation Length (nm)
Carbon	3.11 - 15% = **2.6**
Fluorine	2.23 - 15% = **1.9**
Oxygen	2.57 - 15% = **2.2**
Cobalt	2.33 - 20% = **1.9**
Nickel	2.14 - 20% = **1.7**

Table 3.5 *Attenuation Lengths to be used in Quantitative Surface Analysis of ME Tapes*

3.2.5 Best Method to Calculate Lubricant Thickness

If XPS is to be used as a tool to determine the thickness of the lubricant layer on ME media, there are essentially two options that can be used. Firstly, either a model has to be assumed which can be used to simulate the features of the surface of the tape or secondly, a deconvoluted depth profile has to be reconstructed from angle resolved XPS data. The lubricant thickness could then be deduced from the depth at which the fluorine content reduces to zero.

In the case of the depth profile reconstruction from XPS data, there are several methods for calculating a deconvoluted depth profile [107-112] but each has its limitations and cannot be relied upon to give an accurate reconstruction due to the sensitivity of the

reconstruction to instrumental and experimental errors [127]. The maximum entropy method [121] was used in conjunction with ARXPS data from tapes ME#1 and ME#2 in order to ascertain the viability and reproducibility of deconvoluted depth profiles and the results are shown in Chapter 4.

The main reason for using non-uniform models in the determination of overlayer thickness is to compensate for the non-uniform surface structure of real samples. However, Gunter et al. [128] have shown the apparent existence of a "magic" angle to minimise the surface roughness effects in quantitative XPS. One of the major problems associated with ARXPS analysis of a rough surface is that of shadowing. At analyser take-off angles which graze the sample surface, the surface roughness can significantly effect the properties of the detected photoelectrons since the analyser cannot be seen from all parts of the surface. The errors associated with ARXPS vary depending on the roughness of the sample surface and the angle at which the analysis is performed. However, calculations based on 3-dimensional model rough surfaces have shown the errors are minimised for an analyser take-off angle of $45°$ and the thickness of an overlayer can be determined with an error of less than 10% [128].

The alternative method of determining the lubricant thickness on ME tapes using a model will also be examined irrespective of whether the deconvolution method proves to be successful. The non-uniform models [103] can be discounted as being no more suitable for lubricant quantification than those which use a standard uniform model [102, 103, 105] since they only add complexity without any real gains in replication of the tape surface.

In addition to calculating the actual lubricant thickness, it is also possible to calculate the relative overlayer thickness of the lubricant and this may provide a better guide as to changes in the lubricant thickness between different tape samples. Furthermore, this concept may be extended to particulate media such as tape MP#1 in order to calculate

the relative thickness of the layers covering the magnetic pigment at different stages of cycling. Each thickness can be calculated from the electron attenuation of Fe 2p3 electrons in the overlayer but these values should not be taken as absolute thicknesses due to the assumptions that need to be made in order to simplify the complex matrixes in the tape. However, they may be regarded as a reliable indicator of the relative thickness of the layer covering the magnetic pigment at different stages of cycling. Each calculated thickness is the total mean thickness of the layers covering the magnetic pigment which is likely to include lubricant, binder and possibly any material such as a carbonaceous overlayer, formed as a result of wear debris.

CHAPTER 4

RESULTS

4.1 Stop Motion Results

Stop motion tests were performed on a series of commercial tapes at low (10% RH, 25°C), ambient (40%, 25°C), and high (85%, 25°C) humidity conditions. The tapes comprised of three metal evaporated thin film tapes (ME#1, ME#2 and ME#3) and 1 MP tape (MP#1). Each test was repeated using a new virgin section of tape and good contact between the read/write heads and the tape was ensured by monitoring the output signal from the tape on an oscilloscope. A typical signal output for good contact is shown in Figure 4.1 in which each "envelope" represents the signal from one head on the tape. A stop motion test was only continued if the initial contact between both heads and the tape was good. In some cases, only one head initially made good contact when the VCR was placed in pause mode and thus the test was stopped and a new section of tape tested. Once good contact had been established, any subsequent change in the signal level corresponded to a change in the amplitude in one or both of the signal envelopes. However, accurate signal response was monitored through the use of a DVM and chart recorder.
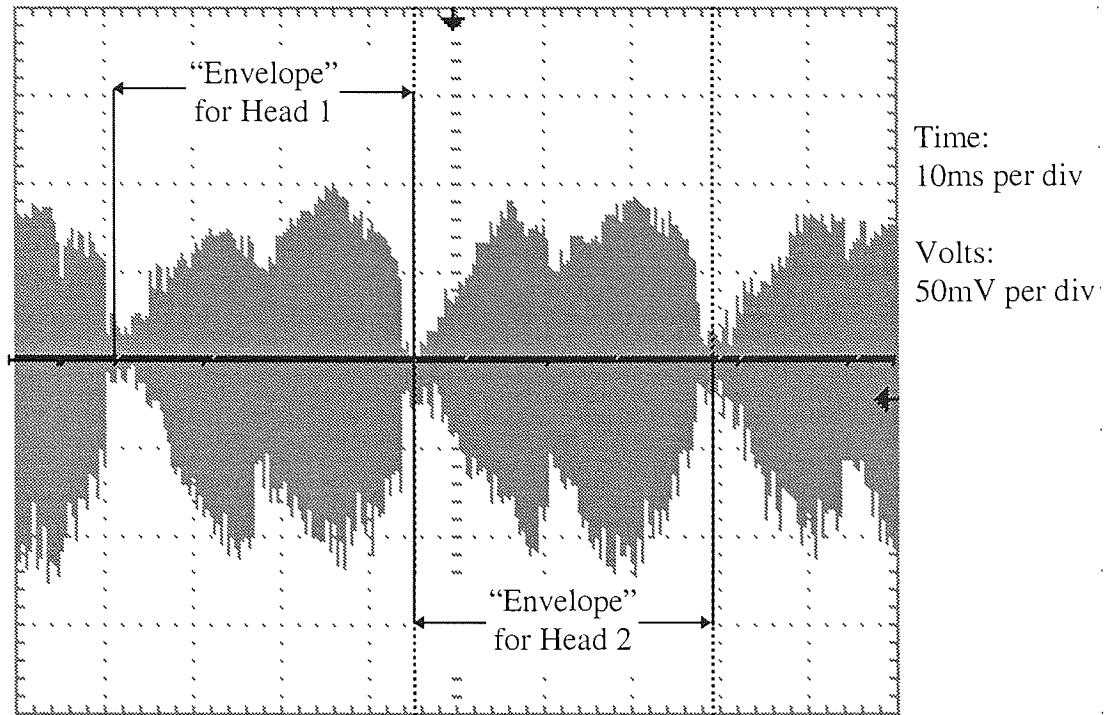
Figure 4.1 A Typical Waveform for Good Contact During a Stop Motion Test in which
each "Envelope" Represents the Signal from a Head in Contact with the Tape

4.1.1 Tape MP#1

Typical stop motion test results at low and ambient humidity conditions for tape MP#1

are shown in Figures 4.2 and 4.3 respectively with each figure illustrating how the

extremes of the recorded signal varied with time. A tape was deemed to have failed the

stop motion test when the signal had fallen by 6 dB.

Time (Hours)
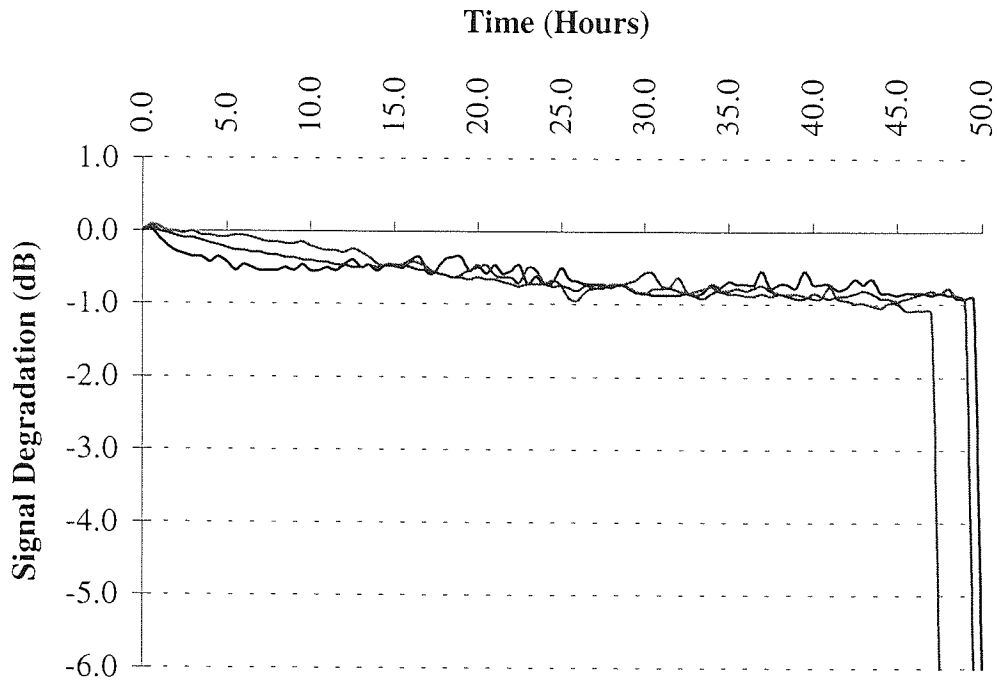
Figure 4.2 Stop Motion Test Showing Signal Degradation with Time for

Tape MP#1 under Low Humidity Conditions

Time (Hours)
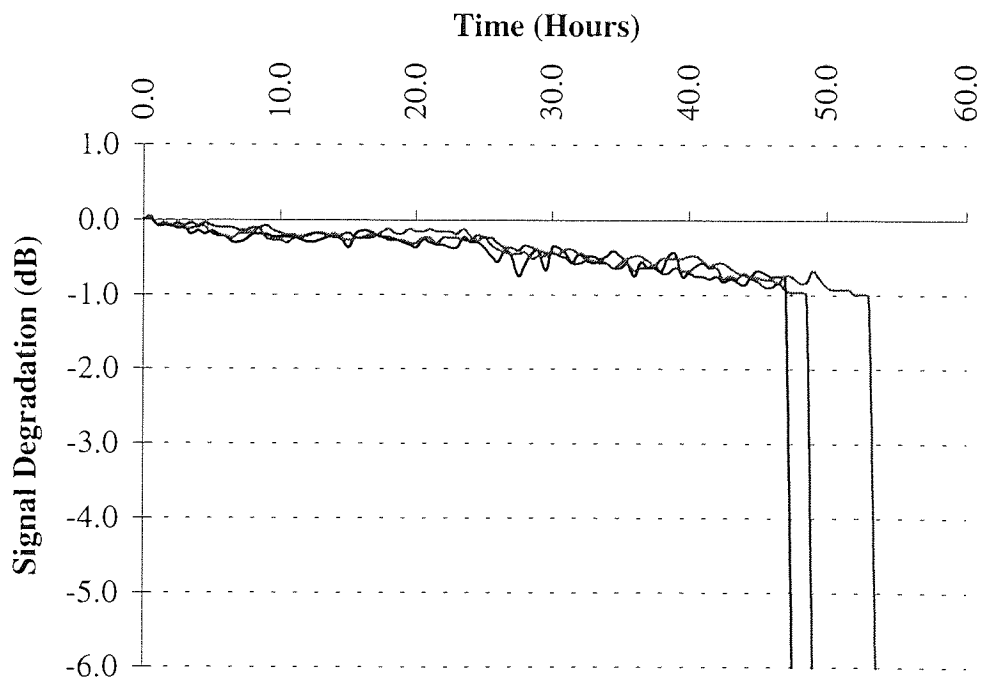
Figure 4.3 Stop Motion Test Showing Signal Degradation with Time for

Tape MP#1 under Ambient Conditions

The stop motion tests gave similar results for tape MP#1 at low and ambient humidity conditions in each of the above cases with the signal remaining within a 1 dB band for between 45 and 50 hours. Total signal failure occurred instantaneously corresponding to severe wear of the tape surface to such an extent that there was a complete loss of signal.

In the case of the stop motion tests performed at high humidity conditions, the extremes of the variation of signal with time were quite different to those for low and ambient conditions, as illustrated in Figure 4.4. The response was far more erratic with the signal fluctuating within a 3 dB band although the tape regularly survived the stop motion tests for a longer period of time before total signal failure occurred. On some occasions, the time to failure was up to 90 hours, far greater than the case for low and ambient humidity conditions.
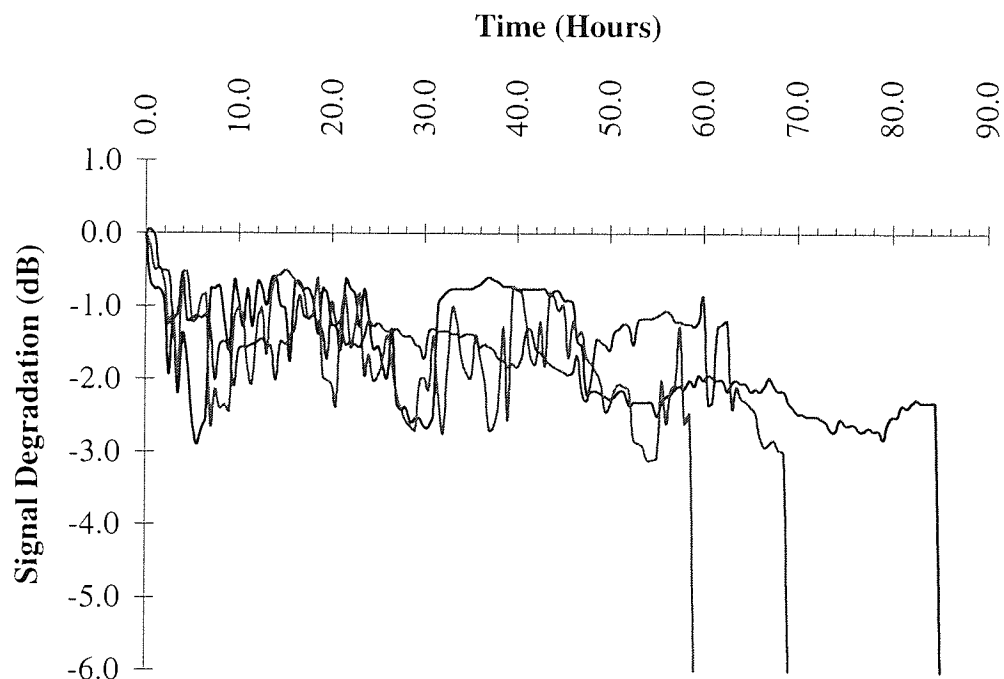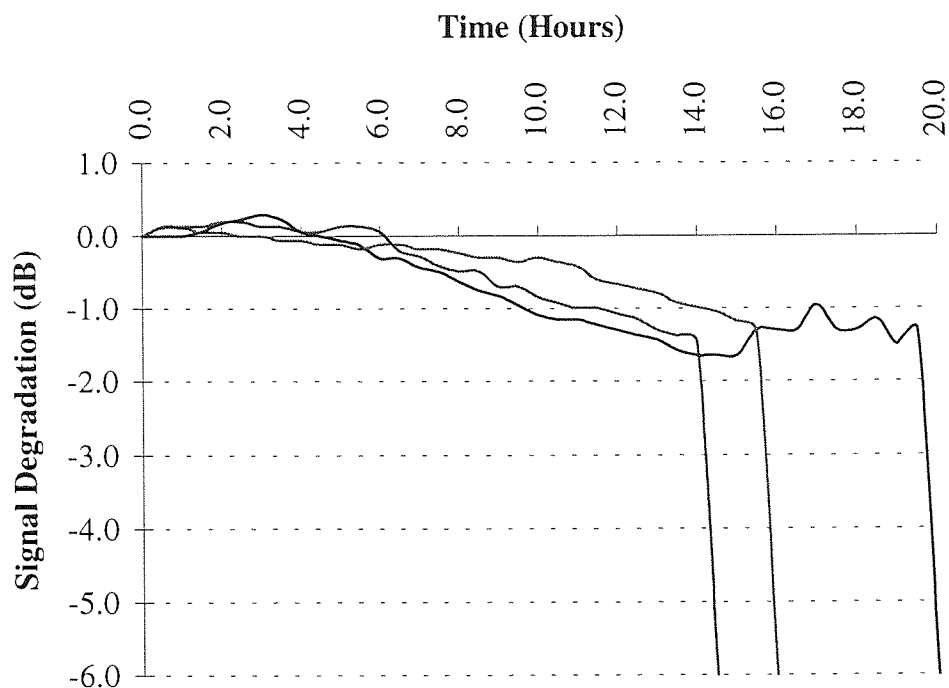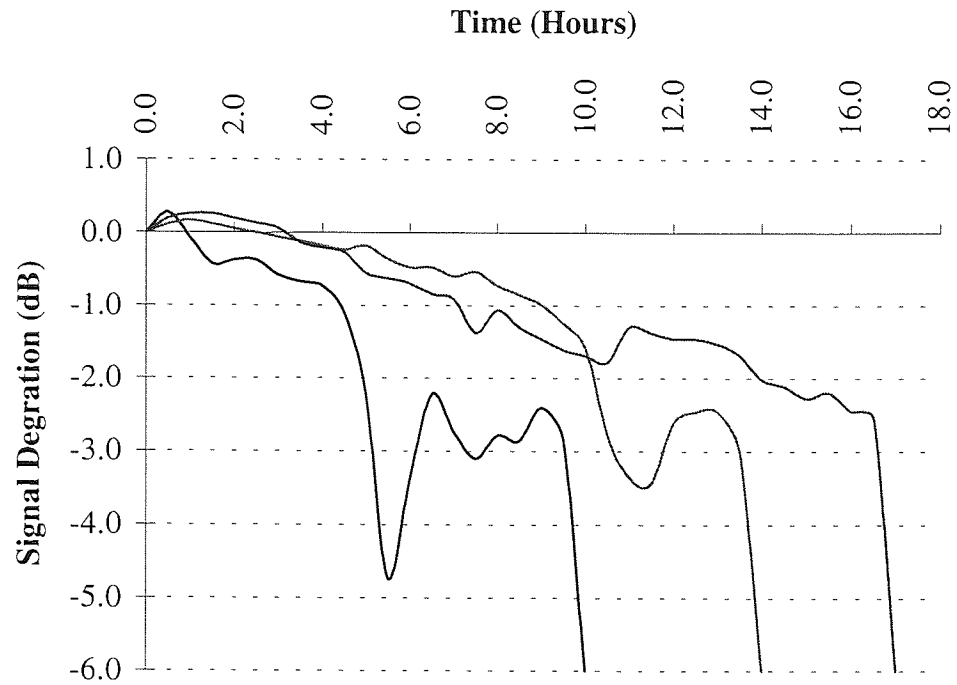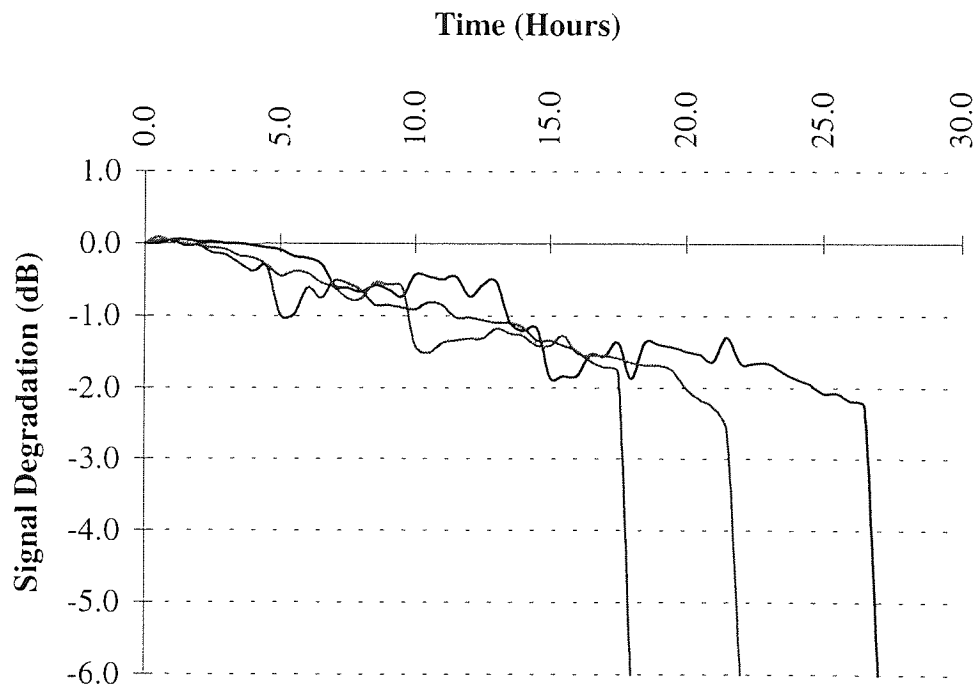

Figure 4.4 Stop Motion Test Showing Signal Degradation with Time for

Tape MP#1 under High Humidity Conditions

4.1.2 Tape ME#1

The stop motion test results for tape ME#1 tape are illustrated in Figure 4.5 with the

signal routinely remaining within a 1 dB band for the duration of the test. The tape

typically survived for between 6 and 9 hours before total failure occurred and this was

true for both low and ambient humidity conditions. However, when stop motion tests

were performed under high humidity conditions, the length of time before failure

occurred was generally in excess of that for the tests performed at low and ambient

humidity, as shown in Figure 4.6. The signal also remained within a 1 dB band prior to

total signal loss which as Figure 4.4 illustrated, was not the case for the particulate tape

under identical high humidity conditions.

Time (Hours)
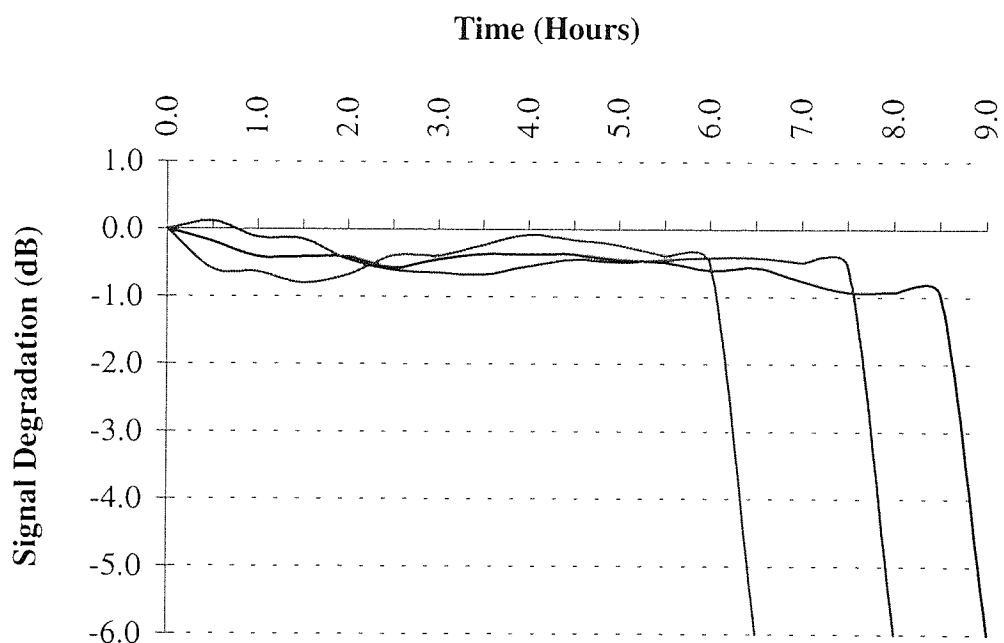
Figure 4.5 *Stop Motion Test Showing Signal Degradation with Time for*

Tape ME#1 under Ambient Humidity Conditions

Time (Hours)
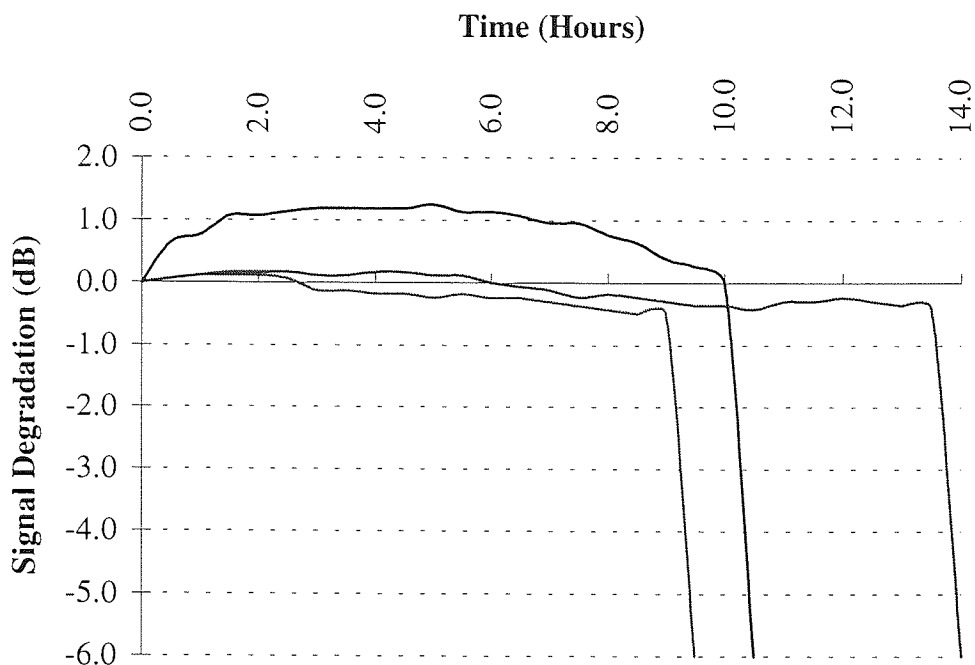
Figure 4.6 Stop Motion Test Showing Signal Degradation with Time for

Tape ME#1 under High Humidity Conditions

4.1.3 Tape ME#2

For tape ME#2, the results of the stop motion tests were the poorest of all the tapes

tested with both the shortest times to failure and signal degradation profiles which

showed little sign of any temporary signal recovery. Indeed, after an initial period of

signal increase (which was common to all tests irrespective of the type of tape under

investigation), the signals consistently decreased with complete failure usually occurring

when the signal had fallen by 3 dB. Typical results at ambient humidity conditions are

shown in Figure 4.7 with each graph illustrating the extremes of recorded signal.

Time (Hours)
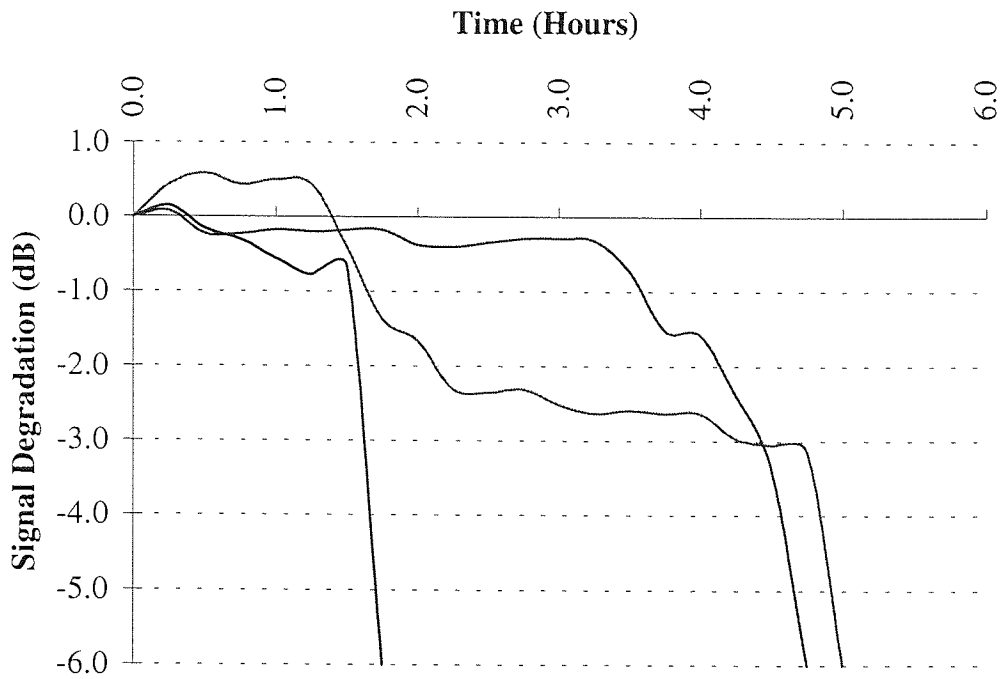
Figure 4.7 Stop Motion Test Showing Signal Degradation with Time for

Tape ME#2 under Ambient Humidity Conditions

At high humidity conditions, the performance of the tape in the stop motion tests

improved and in the best case, the time to failure was nearly 20 hours. The variation of

the signal was also better with a 2 dB band defining the maximum fluctuation of the

signal. Typical signal responses as a function of running time for tape ME#2 under high

humidity conditions are shown in Figure 4.8.

Time (Hours)

Figure 4.8 *Stop Motion Test Showing Signal Degradation with Time for*

Tape ME#2 under High Humidity Conditions

4.1.4 Tape ME#3

The signal response of tape ME#3 in ambient conditions had a varied response with the best time to failure results for any of the ME tapes under identical test conditions although the signal did tend to fluctuate wildly and in some cases, by as much as 5 dB before total failure occurred. Figure 4.9 shows the response of 3 typical tests for tape ME#3 under ambient conditions and illustrates how temporary signal recovery often occurred prior to complete signal failure. At high humidity conditions, the time to failure was longer than for at ambient conditions and the fluctuation in extremes of signal for tape ME#3 were less, typically within a 2 dB band, as shown in Figure 4.10.

Time (Hours)

Figure 4.9 Stop Motion Test Showing Signal Degradation with Time for

Tape ME#3 under Ambient Conditions

Time (Hours)

Figure 4.10 Stop Motion Test Showing Signal Degradation with Time for

Tape ME#3 under High Humidity Conditions

4.2 Tape Cycling Results

Tape cycling tests were performed on the same series of ME and MP tapes at ambient (40%, 25°C) and high (85%, 25°C) humidity conditions. Each test was repeated using a virgin section of tape and 15 classes of dropout were measured over the first 5 minutes of tape at regular intervals. In the case of the three ME tapes, this was after every 50 cycles until a catastrophic growth in the number of dropouts had been observed. This coincided with the tape becoming "tacky" and thus it became impossible for any further cycling of the tape to be performed. In the case of the MP tape, dropouts were measured after every 100 cycles up to a maximum of 5000 cycles.

At the end of each cycling test, the tape under investigation was advanced to a virgin section, at which point the number of dropouts per minute were again measured for all categories of dropout. It was then possible to confirm that any increase in the dropout rate was due to media deterioration rather than head wear.

4.2.1 Tape MP#1

Figure 4.11 illustrates typical 6 dB dropout growth under ambient conditions for tape

MP#1. There was a general increase at each width (3 μs, 10 μs, 20 μs, 50 μs and 100

μs) with increasing number of cycles. The greatest number of dropouts per minute fell

into the narrow 3 μs class whereas the smallest number of dropouts per minute fell into

the broad 100 μs class.
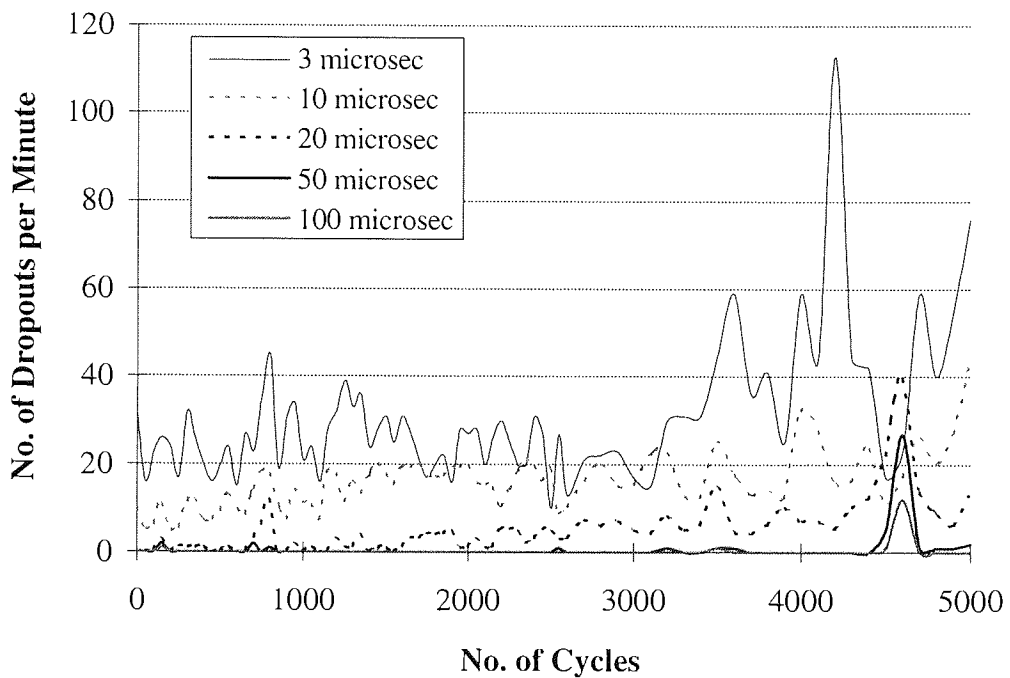
Figure 4.11 *6 dB Dropout Growth under Ambient Conditions over 5000 Cycles for Tape MP#1*

In the 10 dB class of dropout, there was also a steady increase in the number of dropouts

per minute with increasing number of cycles, as illustrated in Figure 4.12. However,

after approximately 2500 cycles, the relative number of shorter dropouts (3 μs, 10 μs

and 20 μs) fluctuated with no individual class of dropout particularly dominant. At the

same stage, there was a small increase in the number of dropouts in the broader 50 μs

and 100 μs classes although the total number was still negligible at less than 5 dropouts

per minute.
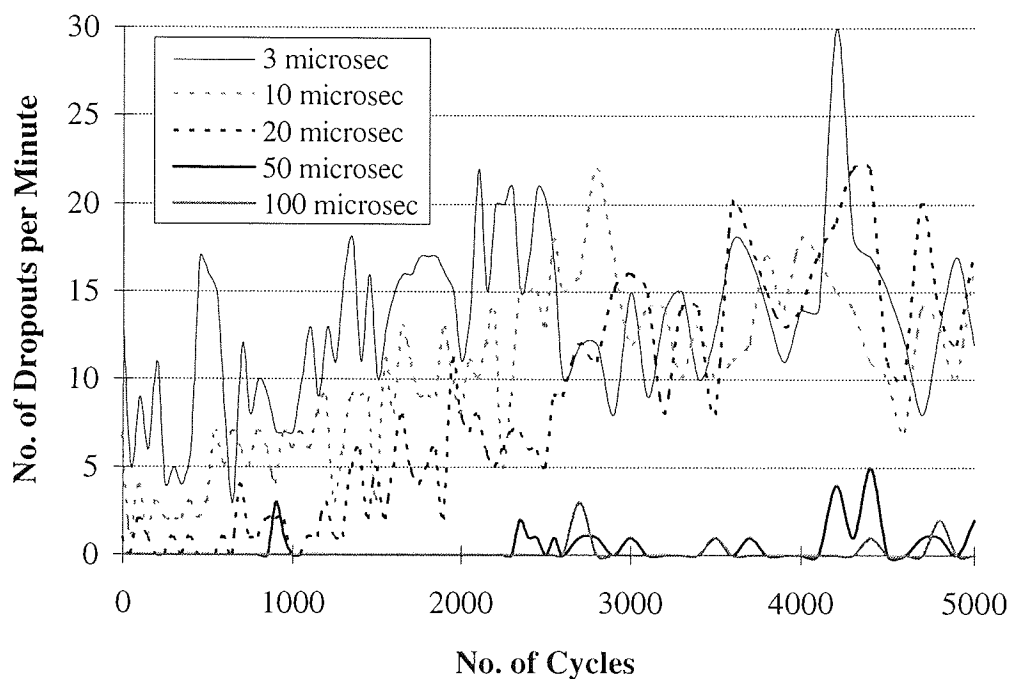
Figure 4.12 *10 dB Dropout Growth under Ambient Conditions over 5000 Cycles for Tape MP#1*

In the case of the 16 dB dropout growth, there was a significant growth in the number of

dropouts per minute for all widths after approximately 2500 cycles, as shown in Figure

4.13. The most significant growth was in the medium 20 µs and 50 µs classes of

dropout which indicated a probable change to the surface of the tape. This was later

confirmed by SEM and XPS analysis of the tape surface.
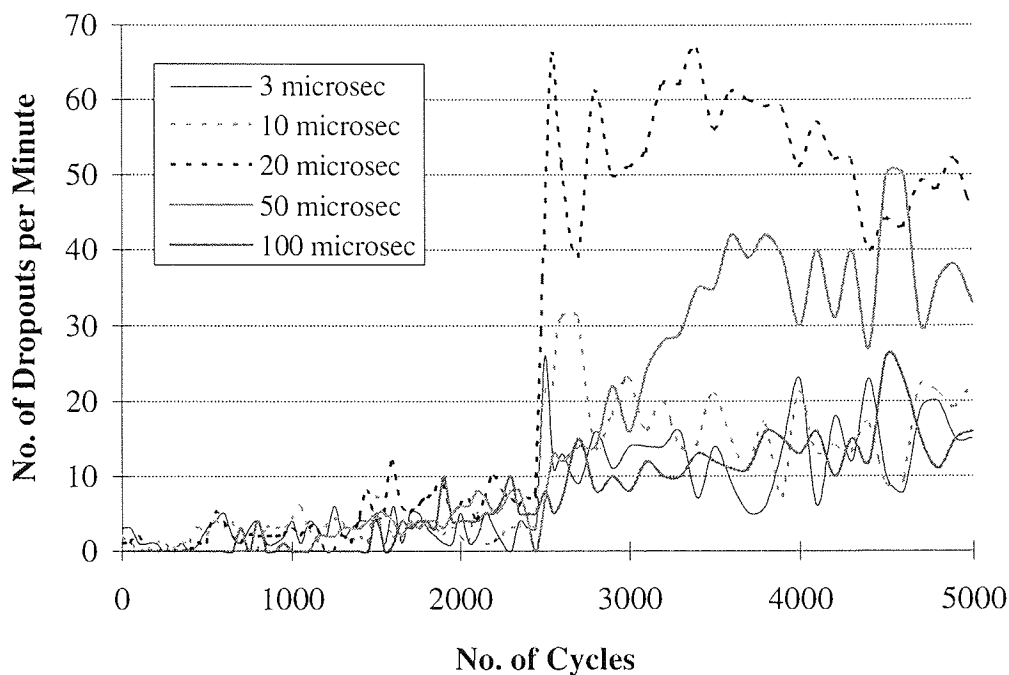
Figure 4.13 16 dB Dropout Growth under Ambient Conditions over 5000 Cycles for Tape MP#1

After 5000 cycles had been completed for all the MP cycling tests, each tape was advanced to a virgin section at which point the number of cycles per minute were again measured for all categories of dropout. The number of dropouts per minute at 6 dB, 10 dB and 16 dB were similar in magnitude to those measured prior to commencement of the 5000 cycles. Thus, the increase in the dropout rate at each depth and width was due to media deterioration rather than head wear.

After cleaning the heads and tape guide system of the VCR with ethanol, the cycling experiments were repeated using new virgin tape samples in high humidity conditions. Figures 4.14 - 4.16 show the 6 dB, 10 dB and 16 dB dropout growth with increasing number of cycles for tape MP#1 at high humidity.

In the 6 dB dropout class, the number of dropouts per minute peaked at 4700 cycles before falling back again. This increase was probably due to temporary poor head-to-tape contact rather than any permanent damage to the tape since the signal soon returned to its previous level. The same phenomena was probably responsible for the high initial number of dropouts, especially as when the experiment was repeated, similar high dropout rates were not detected at any stage of the cycling test.

The general shape of the dropout growth at high humidity, shown in Figure 4.14, differed from the equivalent profile at ambient conditions since apart from the two erroneous peaks at the start and end of the test, the maximum number of dropouts at high humidity conditions occurred at approximately 2500 cycles whereas at ambient conditions, the maximum dropout rate occurred towards 5000 cycles. The presence of

broad 50 µs and 100 µs dropouts was minimal for both ambient and high humidity test

conditions.
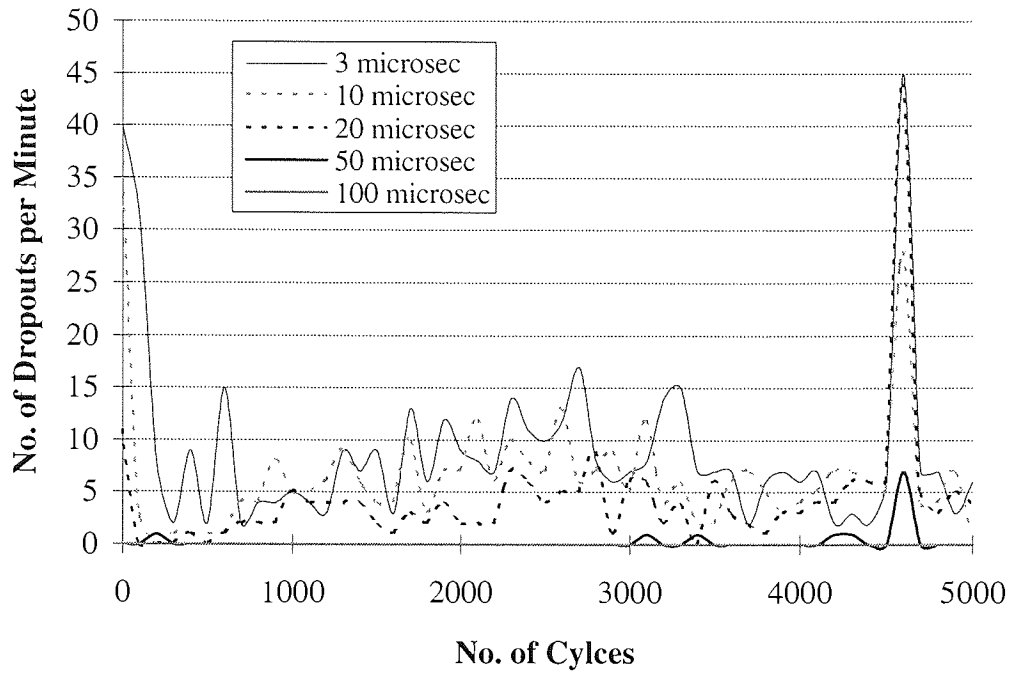
Figure 4.14 *6 dB Dropout Growth under High Humidity Conditions over 5000 Cycles for Tape MP#1*

For the 10 dB class of dropout at high humidity conditions, as illustrated in Figure 4.15, there were again no broad 100 μs classes of dropout which was in contrast to the equivalent experiments performed at ambient conditions. However, the general trend for the narrow 3 μs, 10 μs and 20 μs dropouts was similar to that of the 6 dB dropouts at high humidity conditions with the rate of dropouts increasing up to approximately 2500 cycles, before falling back as the number of cycles approached 5000 cycles. However, the rate of dropouts were still relatively small throughout the duration of the tests.
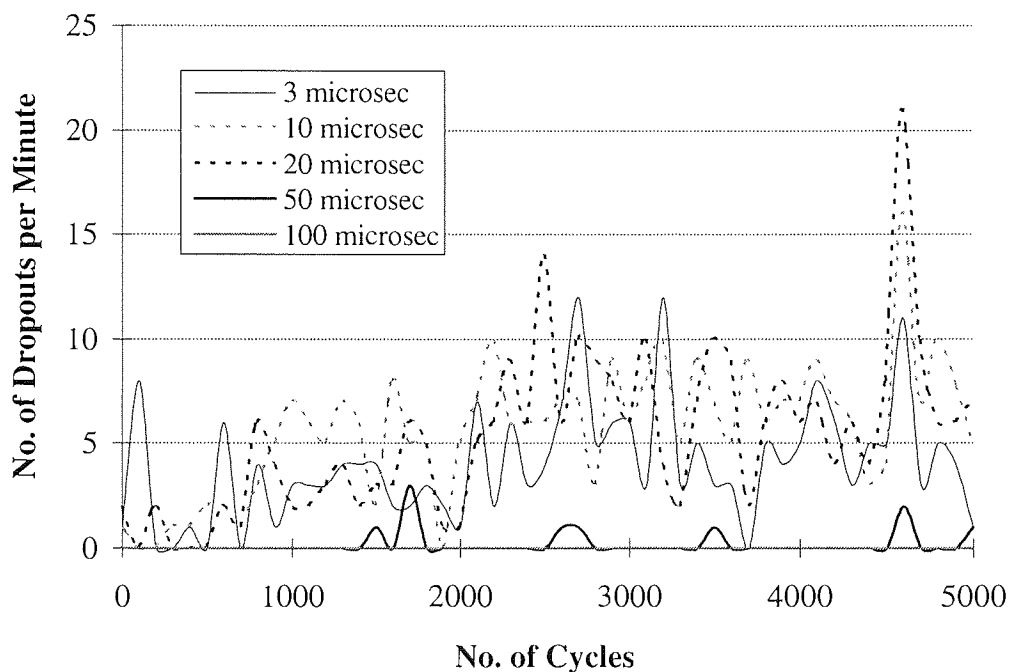
Figure 4.15 *10 dB Dropout Growth under High Humidity Conditions over 5000 Cycles for Tape MP#1*

The increase in the number of dropouts with increasing number of cycles was very pronounced with the 16 dB dropout. Every width of dropout was evident and with the broader widths of 20 µs, 50 µs and 100 µs, the number of dropouts increased steadily with number of cycles from approximately 1000 cycles onwards. The 16 dB class was the most significant depth for dropout growth in both ambient and high humidity conditions. However, at ambient conditions, the substantial growth did not occur until 2500 cycles whereas at high humidity conditions, initiation of the dropout growth occurred at a much earlier stage in the cycling. In addition, the 20 µs class of dropout was the most abundant at depths of 16 dB for both ambient and high humidity conditions.
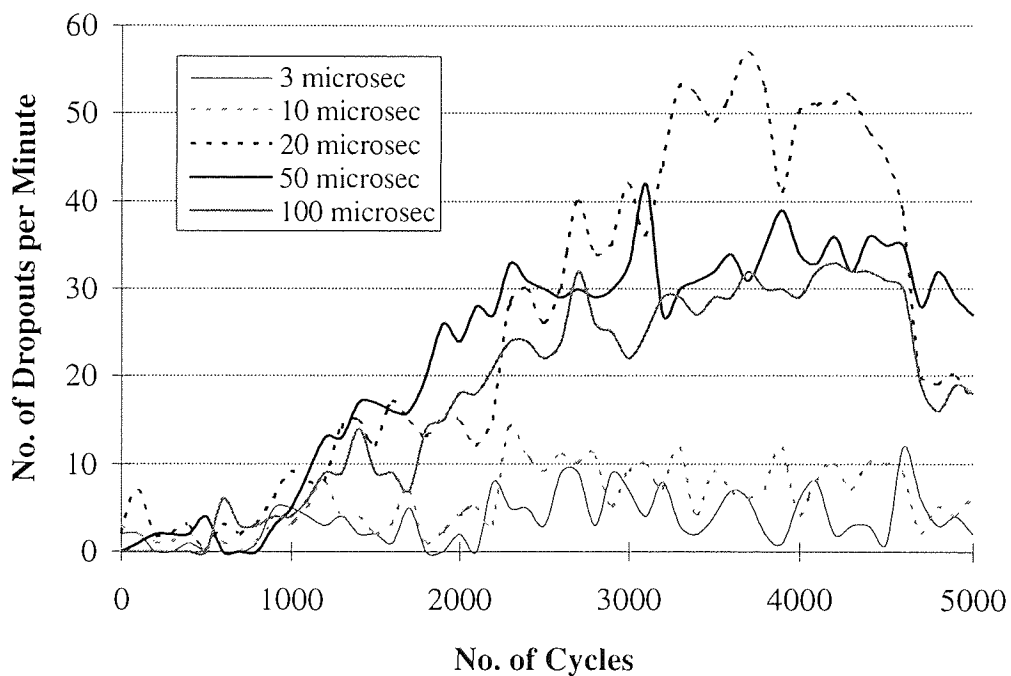
Figure 4.16 *16 dB Dropout Growth under High Humidity Conditions over 5000 Cycles for Tape MP#1*

4.2.2 Tape ME#1

The number of dropouts per minute for tape ME#1 were measured every 50 cycles until a catastrophic growth had been observed. Figure 4.17 shows the dropout growth at depths up to 6 dB, at ambient conditions, in which the number of dropouts at widths of 50 µs and 100 µs were negligible throughout the test and catastrophic growth of dropouts at the 3 narrower widths occurred at 300 cycles. Furthermore, the highest number of dropouts at depths of 6 dB were in the 20 µs class.
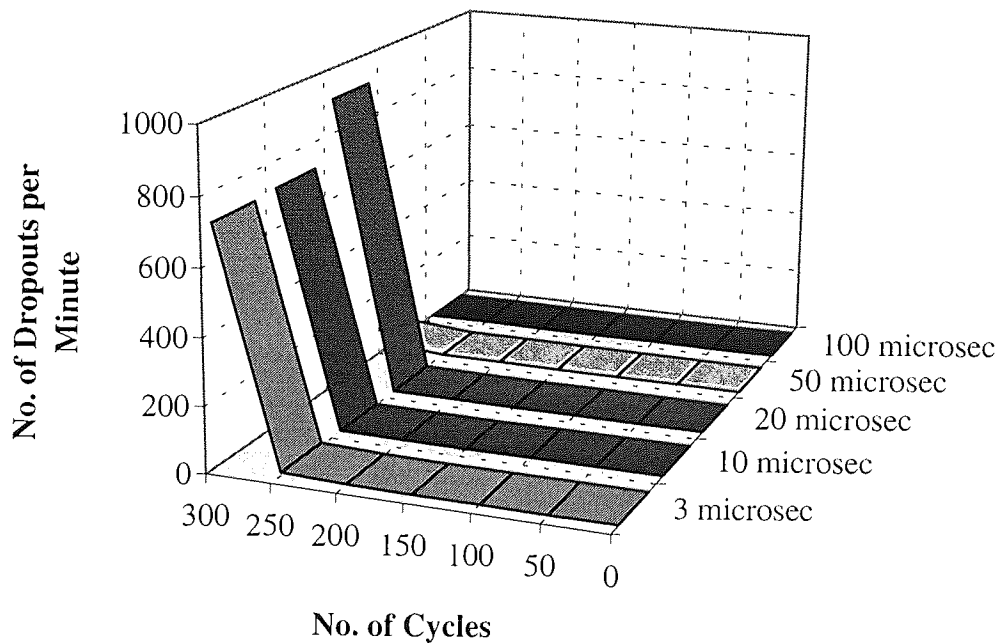
Figure 4.17 *6 dB Dropout Growth under Ambient Conditions for Tape ME#1*

The 10 dB dropout growth at ambient conditions for tape ME#1 is illustrated in Figure 4.18 and shows similar trends to that of the 6 dB dropout growth profile. Again, the number of dropouts in the 50 μs and 100 μs classes was negligible throughout the test and the relative magnitudes of the remaining widths were the same as those for the 6 dB class. However, the actual number of dropouts when catastrophic growth occurred was less than in the 6 dB class.
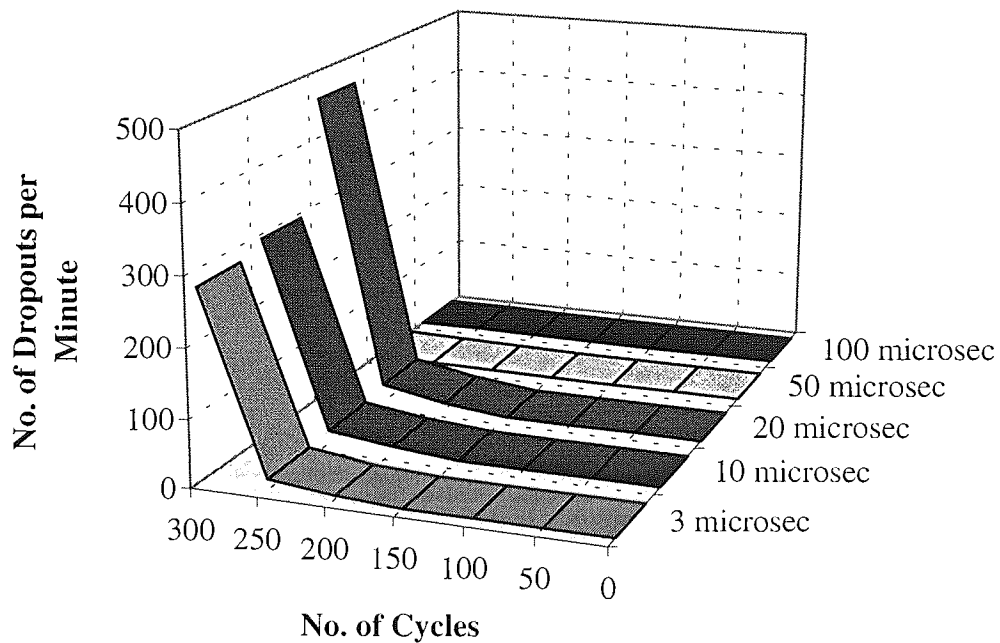
Figure 4.18 *10 dB Dropout Growth under Ambient Conditions for Tape ME#1*

The 16 dB dropout growth for tape ME#1 at ambient conditions is shown in Figure 4.19. There was slight growth in the number of dropouts between 250 and 300 cycles but the most substantial growth was again in the 20 μs class. The relative dropout rate at a depth of 16 dB was less in the narrow width classes than for the corresponding classes at depths of 6 dB and 10 dB.
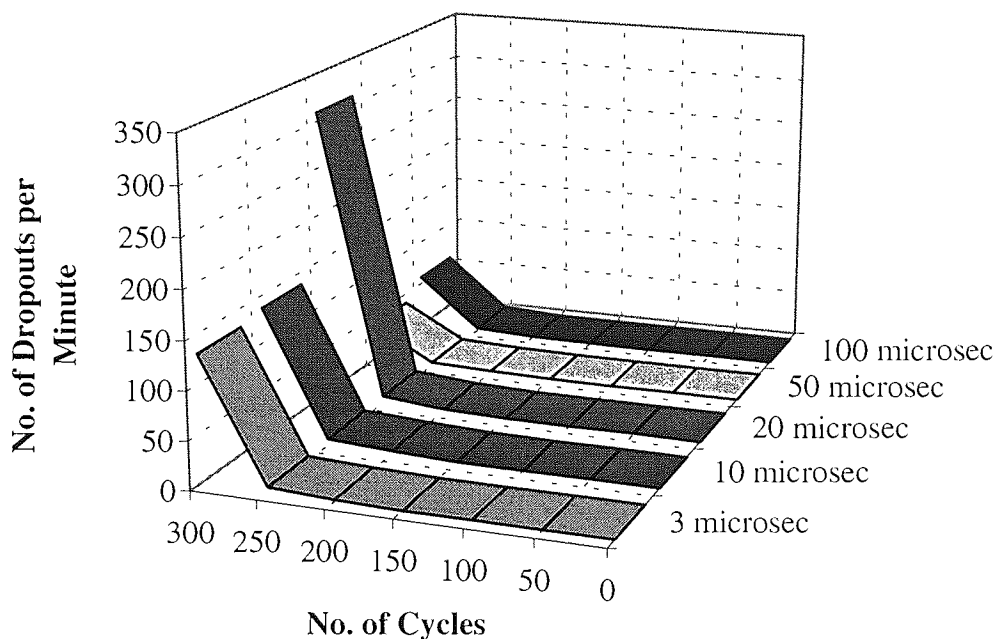
Figure 4.19 16 dB Dropout Growth under Ambient Conditions for Tape ME#1

Identical cycling experiments were performed using tape ME#1 at high humidity conditions with the results of a typical test illustrated in Figures 4.20 - 4.22. The most apparent difference from the tests conducted at ambient conditions was the increased number of cycles that could be performed before catastrophic failure of the tape ensued. Indeed, there was no apparent dropout growth at any width in the 6 dB class prior to 400 cycles. As Figure 4.20 shows, the number of dropouts then gradually increased until at 600 cycles, significant growth occurred particularly in the narrower width classes, culminating in catastrophic growth at 800 cycles. The relative number of dropouts after

800 cycles was far in excess of those when failure occurred under corresponding tests at ambient conditions. Indeed, tape ME#1 routinely failed after 300 cycles at ambient conditions and thus the higher humidity conditions were clearly beneficial to the durability of the tape.
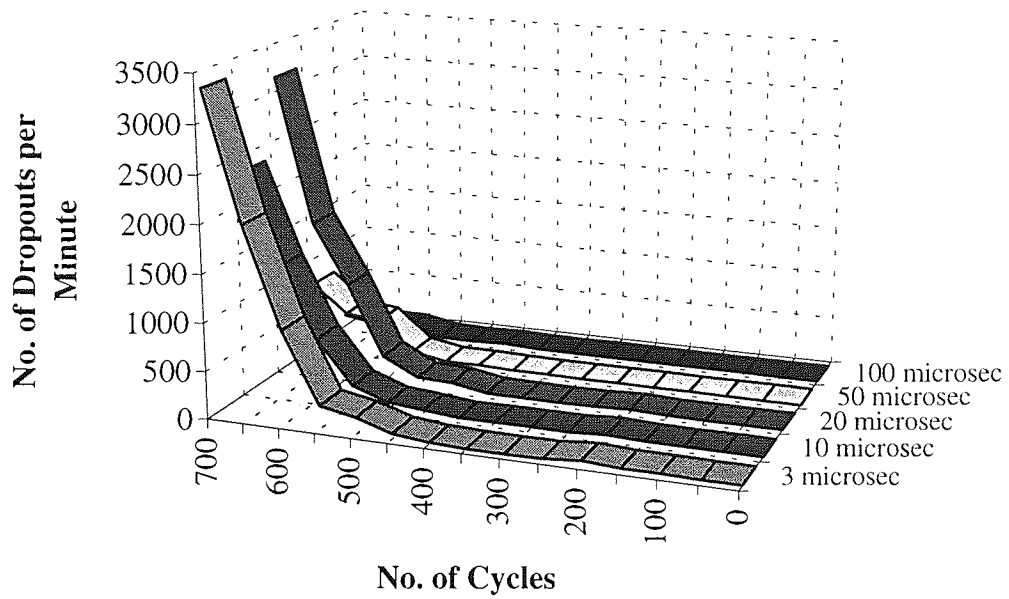
Figure 4.20 6 dB Dropout Growth under High Humidity Conditions for Tape ME#1

The same basic features of the 6 dB dropout growth profile were evident in the 10 dB profile, as illustrated in Figure 4.21. Once the dropout rate had started to increase, significant growth continued with increasing number of cycles until failure finally occurred at 800 cycles. The shorter classes of dropout at 3 μs, 10 μs, and 20 μs were again the most abundant although in contrast to identical tests at ambient conditions, there was some growth in the number of dropouts in the broader classes of 50 μs and 100 μs.
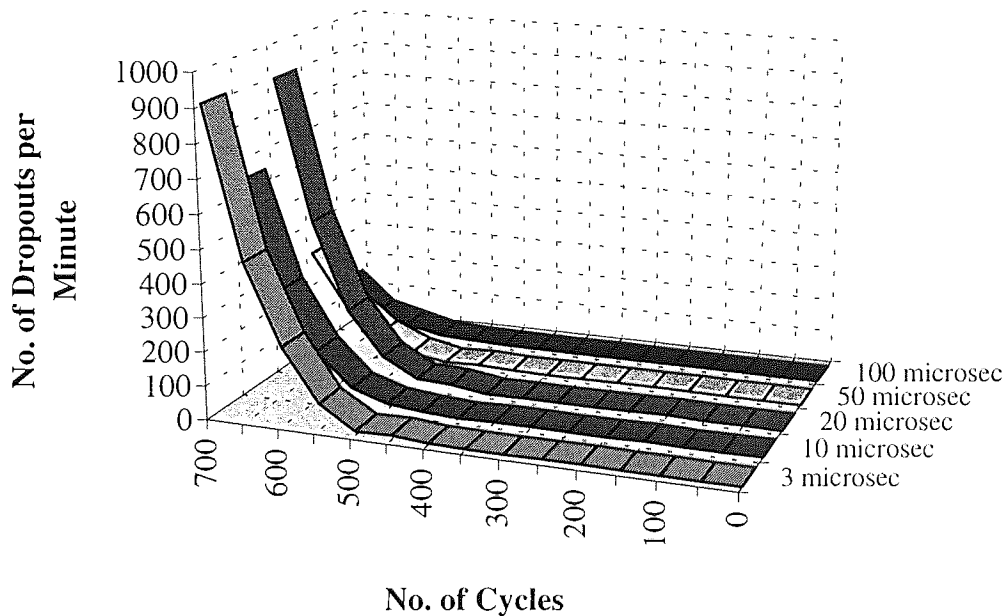
Figure 4.21 *10 dB Dropout Growth under High Humidity Conditions for Tape ME#1*

Figure 4.22 shows the 16 dB dropout growth for tape ME#1 at high humidity conditions. The number of dropouts per minute remained negligible up to 500 cycles at which point the dropout rate in each class increased with further cycling. At 800 cycles, catastrophic dropout growth occurred with the highest number of dropouts falling into the 100 μs class. This was in contrast to the dropout growth at 6 dB and 10 dB depths where the dropout rate in the 100 μs class was usually zero for the duration of the tests, irrespective of the test conditions.
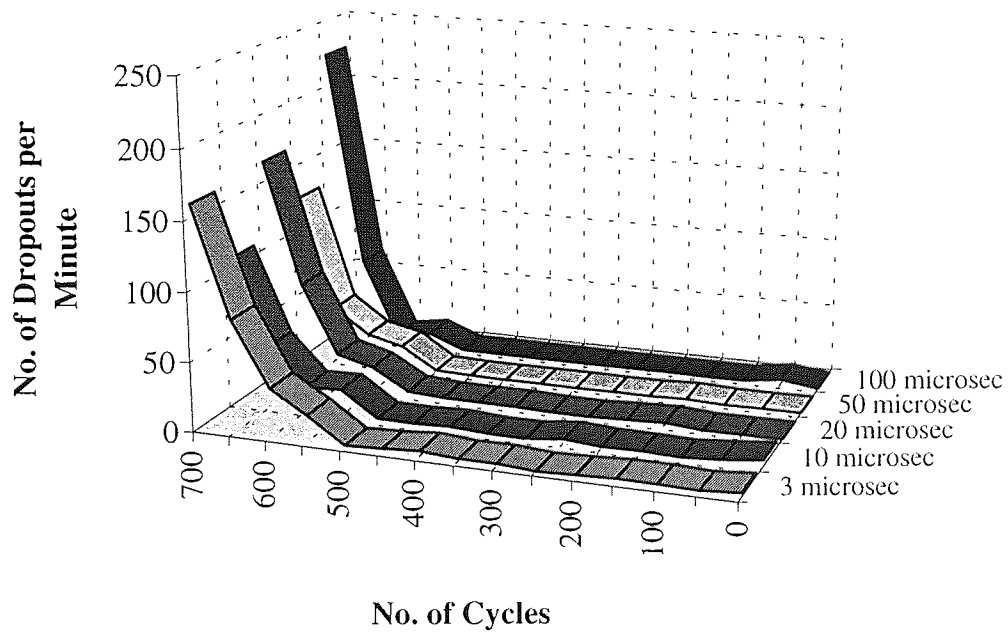
Figure 4.22 *16 dB Dropout Growth under High Humidity Conditions for Tape ME#1*

4.2.3 Tape ME#2

Tape ME#2 exhibited the poorest results for a series of cycling tests at ambient conditions with both high levels of dropout and the shortest number of cycles to catastrophic dropout growth, as shown in Figure 4.23. There was little growth in the broad 50 μs and 100 μs dropout classes but the narrower classes each showed significant dropout growth, with the greatest increase in the 3 μs and 10 μs width classes.
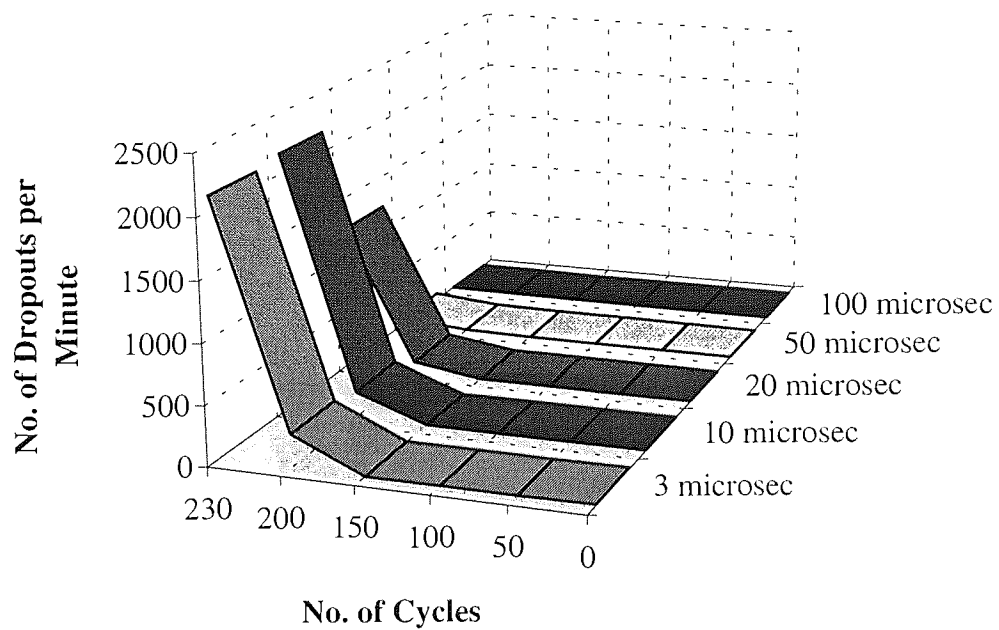
Figure 4.23 6 dB Dropout Growth under Ambient Conditions for Tape ME#2

The 10 dB dropout growth profile, illustrated in Figure 4.24, has similar characteristics to the 6 dB dropout profile with negligible growth in the broad 50 µs and 100 µs classes and catastrophic growth in the narrower classes after 230 cycles. The highest number of dropouts were the narrow 3 µs and 10 µs classes which mirrored the 6 dB dropout growth pattern. The feature of higher dropouts in the narrow 3 µs and 10 µs classes was different to that of tape ME#1 under identical test conditions since the results from tape ME#1 showed the maximum number of dropouts consistently occurred in the 20 µs dropout class.
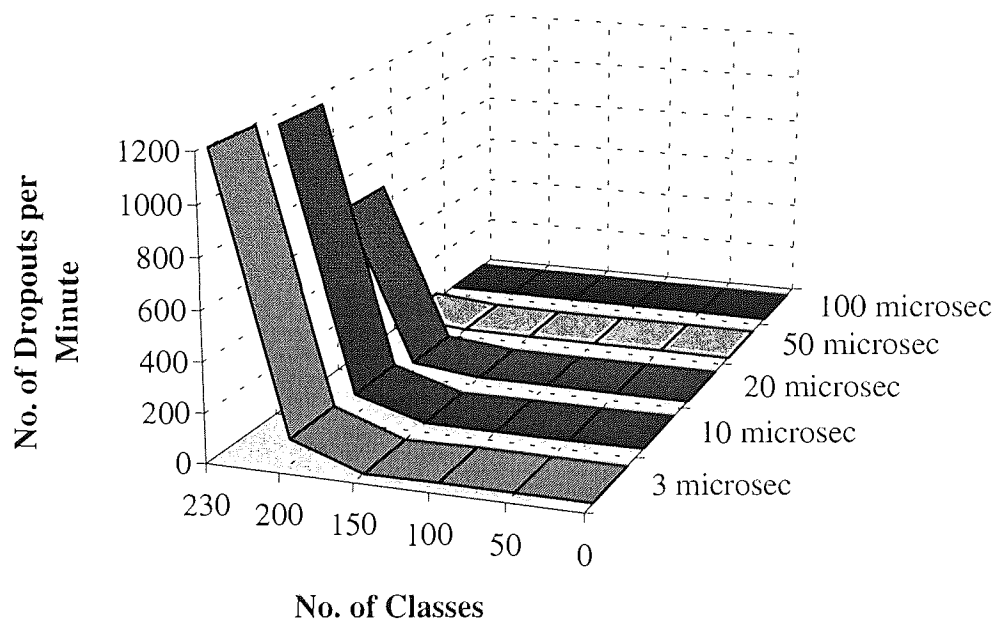
Figure 4.24 *10 dB Dropout Growth under Ambient Conditions for Tape ME#2*

Figure 4.25 shows the 16 dB dropout growth for tape ME#2 under ambient test conditions. The 16 dB class showed slightly different trends to the profiles at 6 dB and 10 dB with the 20 μs width showing the greatest dropout rate. Broader 50 μs dropouts were also observed between 200 and 230 cycles - the first time this had occurred at any signal depth for tape ME#2.
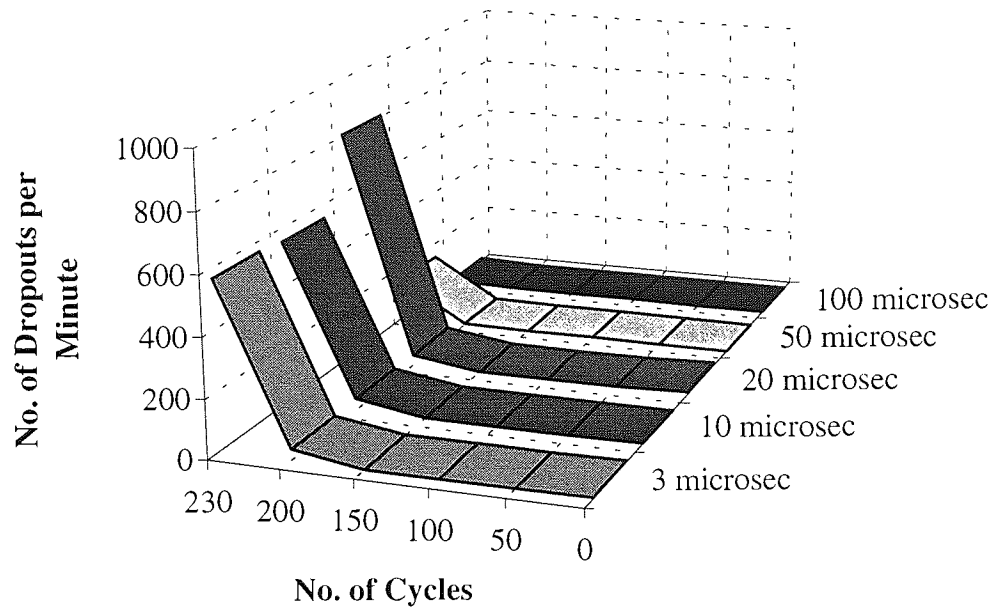
Figure 4.25 16 dB Dropout Growth under Ambient Conditions for Tape ME#2

The cycling tests performed using tape ME#2 at high humidity showed an improved

performance over similar tests performed at ambient conditions. Indeed, the tape last for

a greater number of cycles before catastrophic growth occurred and when such growth

did occur, the number of dropouts per minute was not as great as for the tests at ambient

conditions. Figure 4.26 shows the 6 dB dropout growth at high humidity conditions for

tape ME#2 with the maximum dropout rate occurring at the 3 μs class.
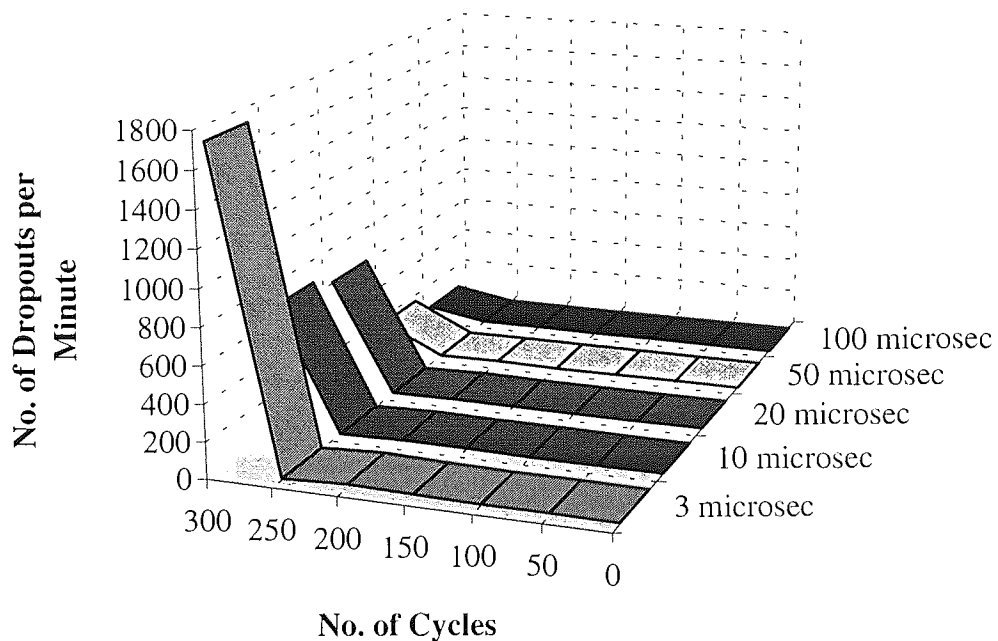
Figure 4.26 *6 dB Dropout Growth under High Humidity Conditions for Tape ME#2*

Figure 4.27 illustrates the 10 dB dropout growth for tape ME#2 at high humidity conditions. Again, the maximum dropouts occurred in the narrow 3 μs class but the actual number of dropouts were significantly lower than for tests performed at ambient conditions. Indeed, the dropout rate corresponding to catastrophic growth at high humidity conditions was typically half that observed at ambient conditions. Thus, the high humidity conditions appeared to have a significant beneficial effect on the cycling durability performance of tape ME#2.
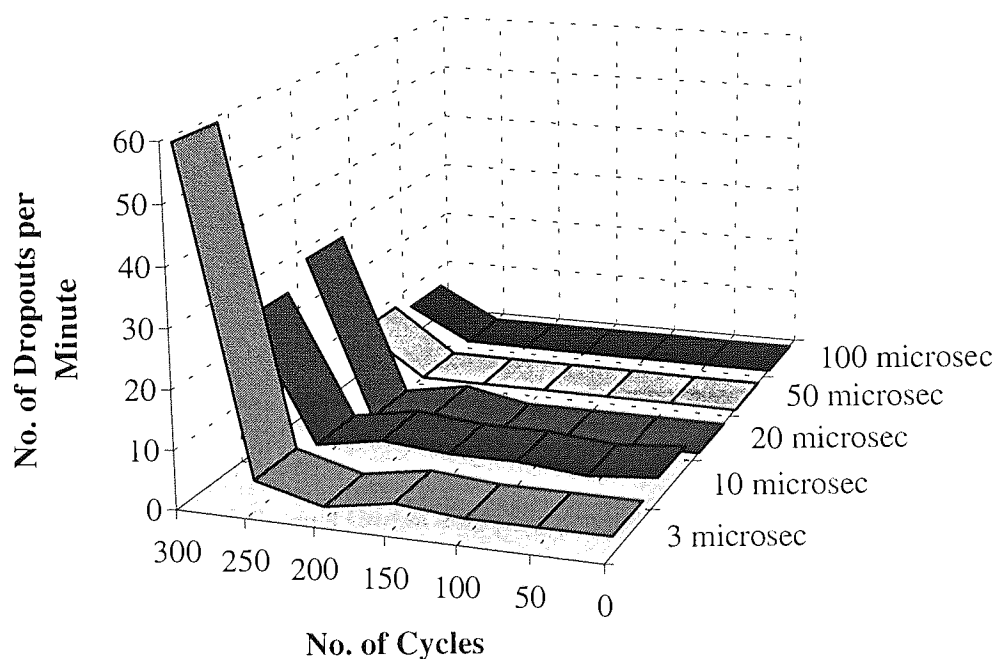
Figure 4.27 *10 dB Dropout Growth under High Humidity Conditions for Tape ME#2*

The 16 dB dropout growth at high humidity conditions for tape ME#2 is illustrated in

Figure 4.28. The number of dropouts per minute in each class was extremely small and

negligible when compared to the level of dropouts in each equivalent class when identical

tests were performed at ambient conditions.
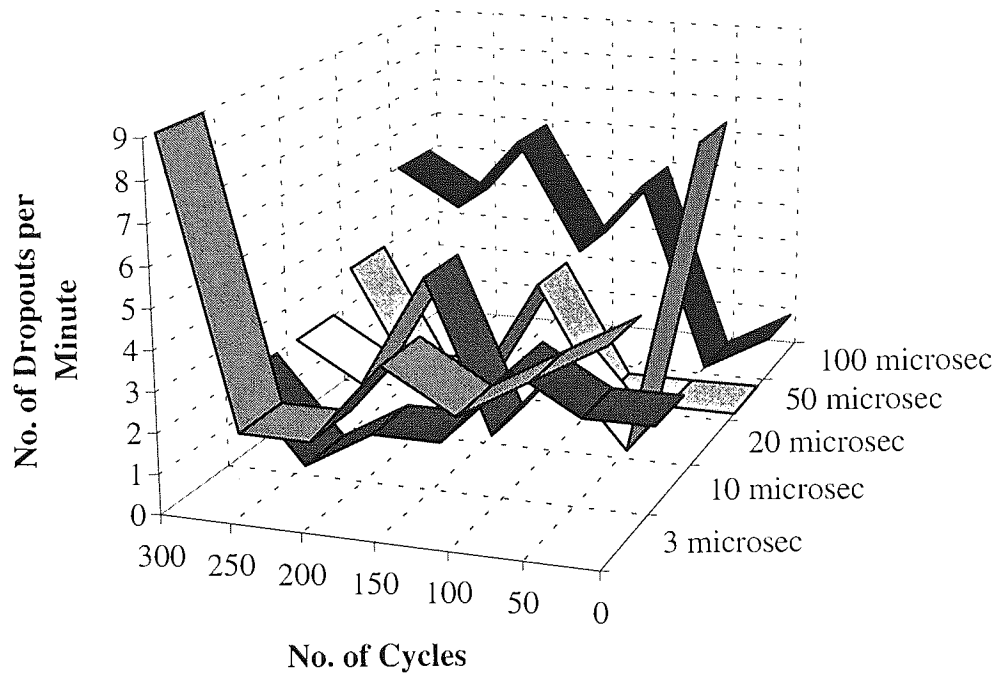
Figure 4.28 16 dB Dropout Growth under High Humidity Conditions for Tape ME#2

4.2.4 Tape ME#3

The 6 dB dropout growth for tape ME#3 at ambient conditions is illustrated in Figure 4.29. Catastrophic dropout growth did not occur until 400 cycles and even then, it was only the narrow 3 μs dropout class that increased, rising to over 120 dropouts per minute. At 400 cycles, tape ME#3 showed significantly better durability than tape ME#1 or tape ME#2 under identical test conditions.
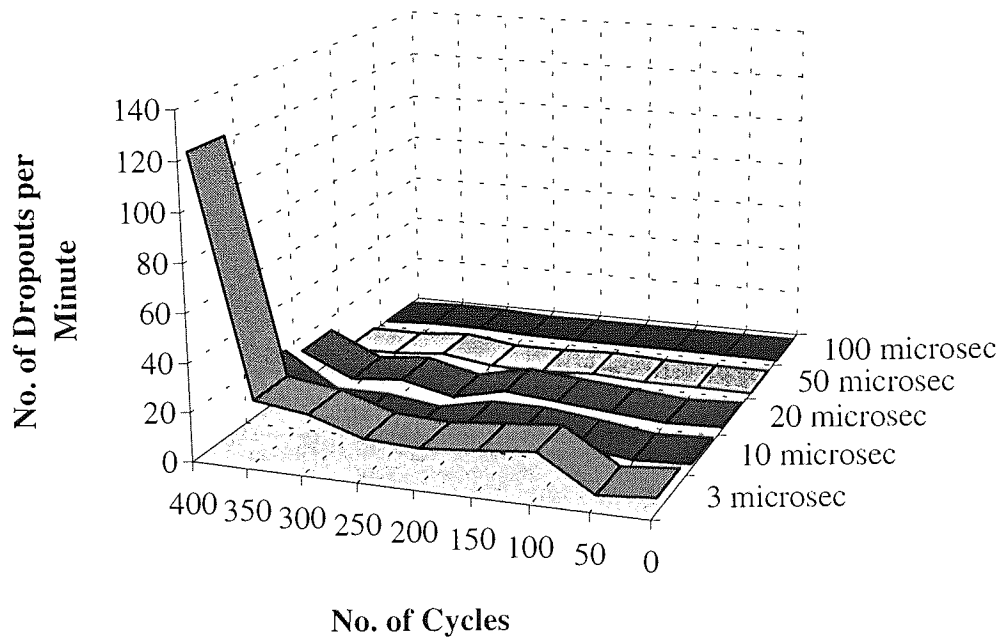
Figure 4.29 6 dB Dropout Growth under Ambient Conditions for Tape ME#3

The 10 dB dropout growth for tape ME#3 at ambient conditions remained fairly low throughout the test, with none of the classes showing significant growth. The dropout profile is illustrated in Figure 4.30, with the maximum number of dropouts per minute again occurring at the narrow 3 μs class. However, at 15 dropouts per minute, this cannot be classed as catastrophic growth.
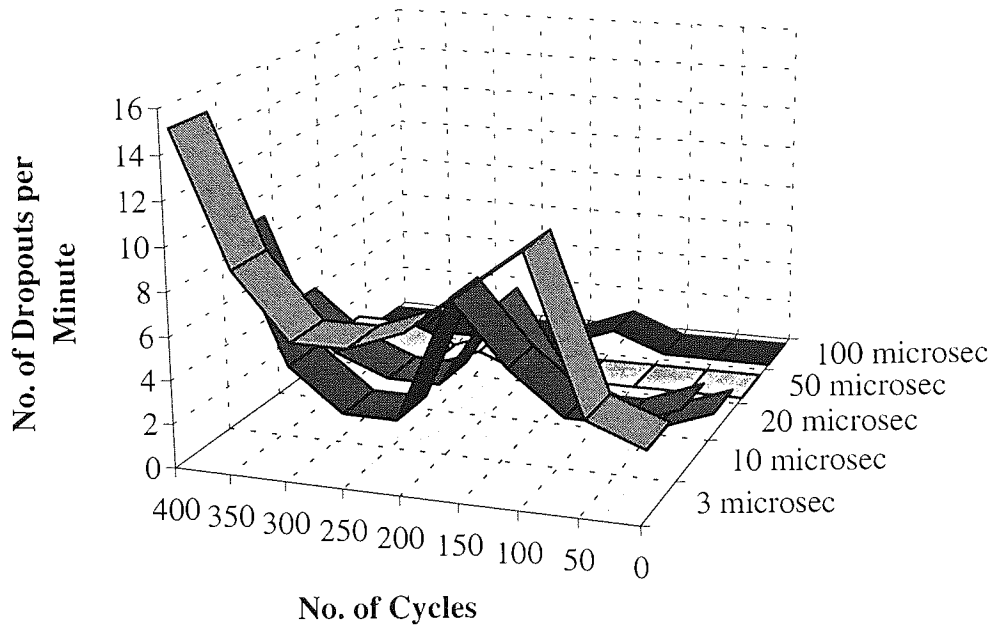
Figure 4.30 10 dB Dropout Growth under Ambient Conditions for Tape ME#3

As Figure 4.31 shows, the 16 dB dropout growth for tape ME#3 fluctuated with increasing number of cycles but the number of dropouts per minute were again at a low level. Thus, the change in number of dropouts after each series of 50 cycles was probably due to statistical error rather than any change to the tape surface since when the tests were repeated, the absolute number of dropouts per minute were similar, showing small variations with increasing number of cycles.
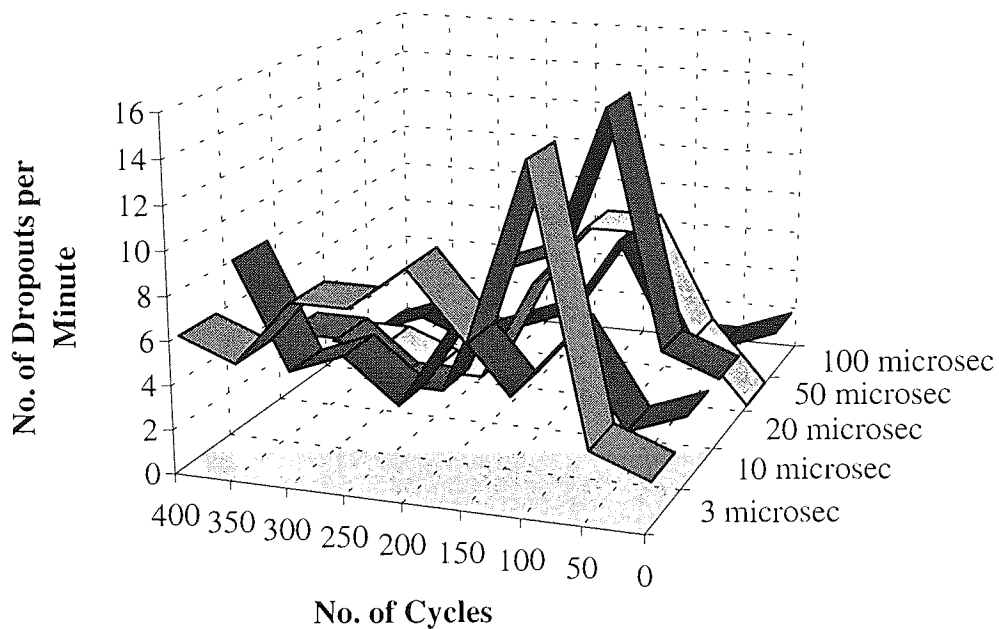
Figure 4.31 16 dB Dropout Growth under Ambient Conditions for Tape ME#3

Figures 4.32 - 4.34 show the 6 dB, 10 dB and 16 dB dropout growth for tape ME#3 when cycled at high humidity conditions. In each category, the dropout rate remained negligible throughout the cycling tests and even when catastrophic dropout growth finally occurred at 800 cycles, the dropout rate was significantly lower than the rates observed for tapes ME#1 and ME#2, irrespective of the climatic conditions at which the tests were performed. In addition, the results of the cycling tests for tape ME#3 at high humidity conditions were superior to those observed at ambient conditions since the dropout rate was consistently lower and generally, catastrophic dropout growth did not occur until almost twice the number of cycles had been completed.
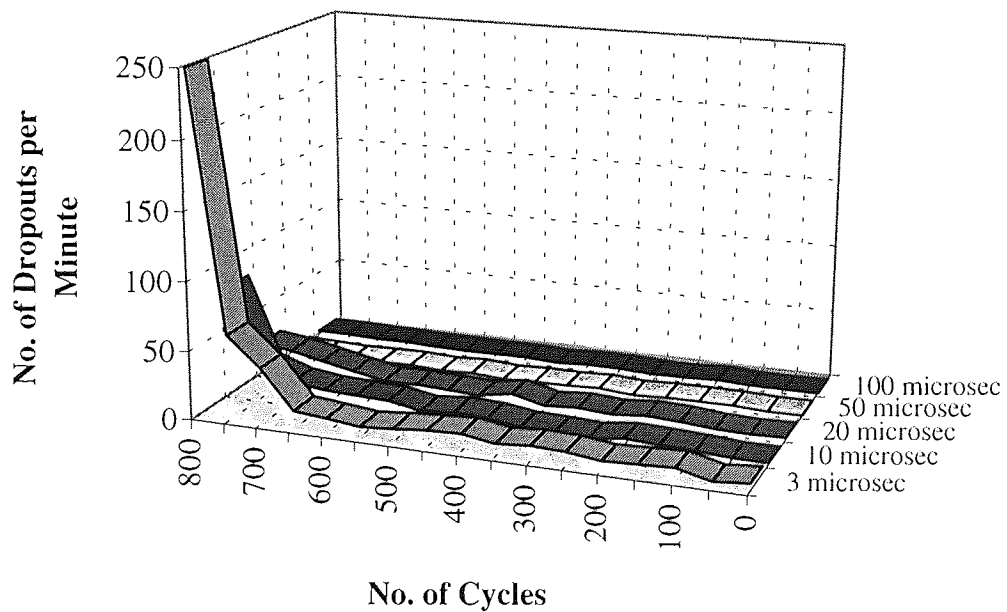
Figure 4.32 *6 dB Dropout Growth under High Humidity Conditions for Tape ME#3*
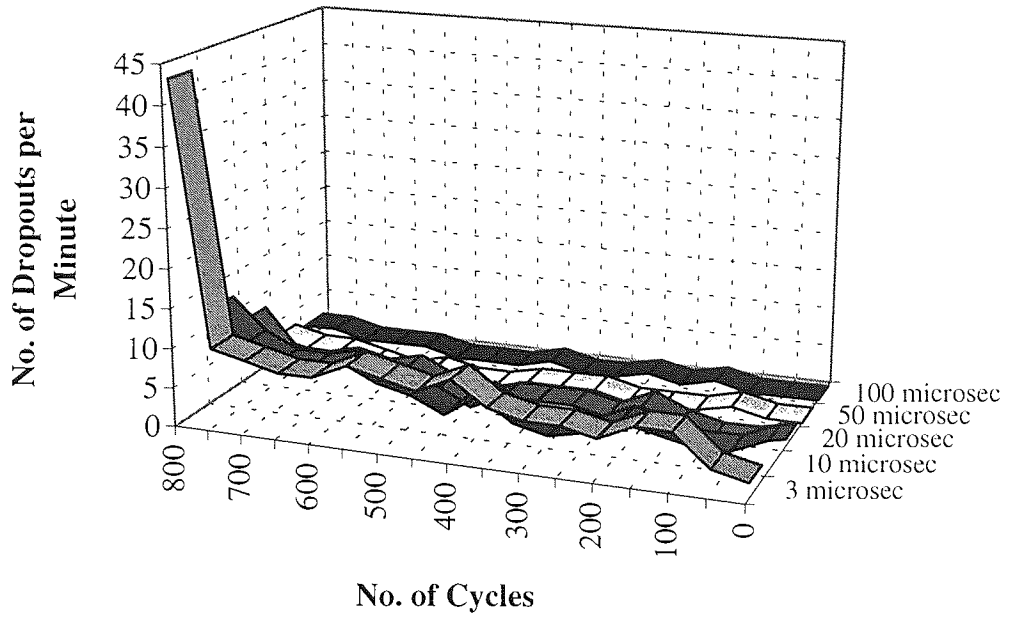
Figure 4.33 *10 dB Dropout Growth under High Humidity Conditions for Tape ME#3*
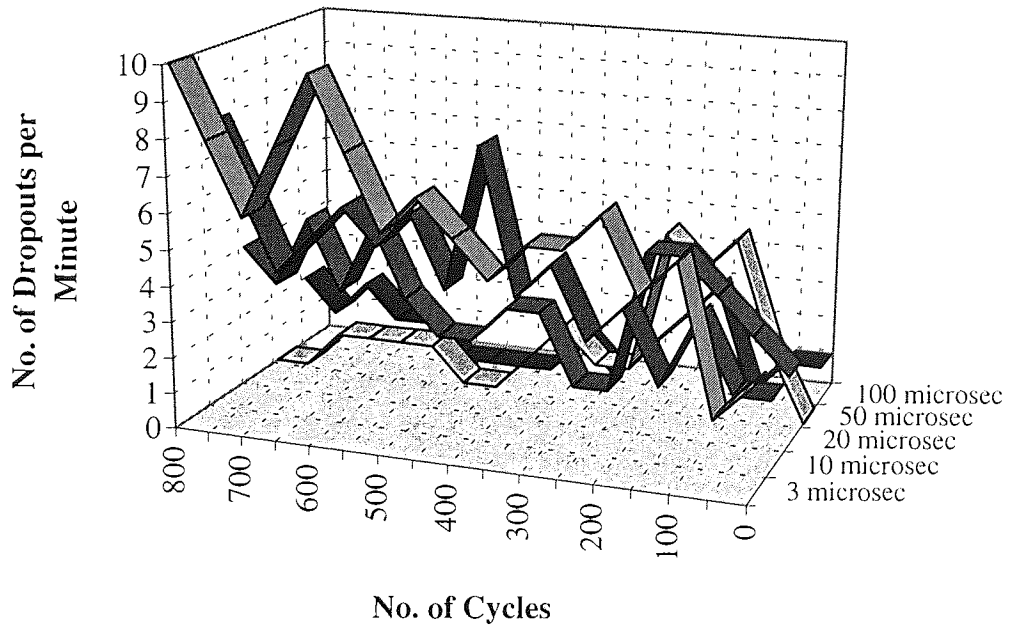
Figure 4.34 *16 dB Dropout Growth under High Humidity Conditions for Tape ME#3*

4.3 Scanning Electron Microscope Analysis

4.3.1 Tape MP#1

A series of micrographs were obtained using SEM in order to show the progression of wear from the initiation of surface scars to severe wear corresponding to tape failure in stop motion tests and catastrophic dropout growth in cycling tests.

Figure 4.35 shows the surface of a virgin sample of tape MP#1 prior to any cycling or stop motion durability tests. As expected, there are no apparent markings on the surface since the tape was in excellent condition.
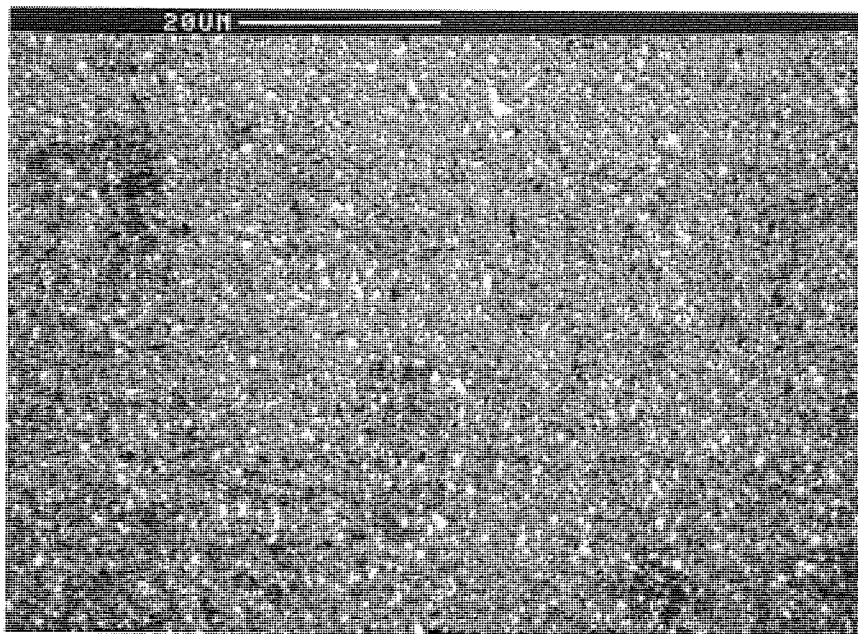
Figure 4.35 *Virgin Tape MP#1 prior to Durability Tests*

A sample of the tape was the subject of several stop motion durability tests in ambient and high humidity conditions. After the tape had been operated in pause mode for a number of hours at ambient conditions, the tape sample was analysed using SEM to determine whether any surface changes had occurred. This procedure was repeated in order to obtain a series of micrographs which depicted the different stages leading to catastrophic failure of the tape and ultimately to help identify the mechanism responsible for failure. Figure 4.36 shows the probable onset of plastic flow with a wear scar in the track direction clearly visible after 7 hours of a stop motion test.

Figure 4.36 *Wear scar Clearly Visible after 7 Hours of a Stop Motion Test at Ambient Conditions*

After 20 hours of a continuous stop motion test at ambient conditions, the wear scar was clearly visible to the naked eye and when analysed using SEM, it had become far more pronounced across the tape, in a direction corresponding to a helical scan on a single track. Figure 4.37 illustrates such a wear scar and the severity of damage resulting from the stop motion test. However, even this degree of damage to the tape did not result in the tape failing the stop motion test since the signal had only fallen by 1 dB when the tape was analysed for surface damage.
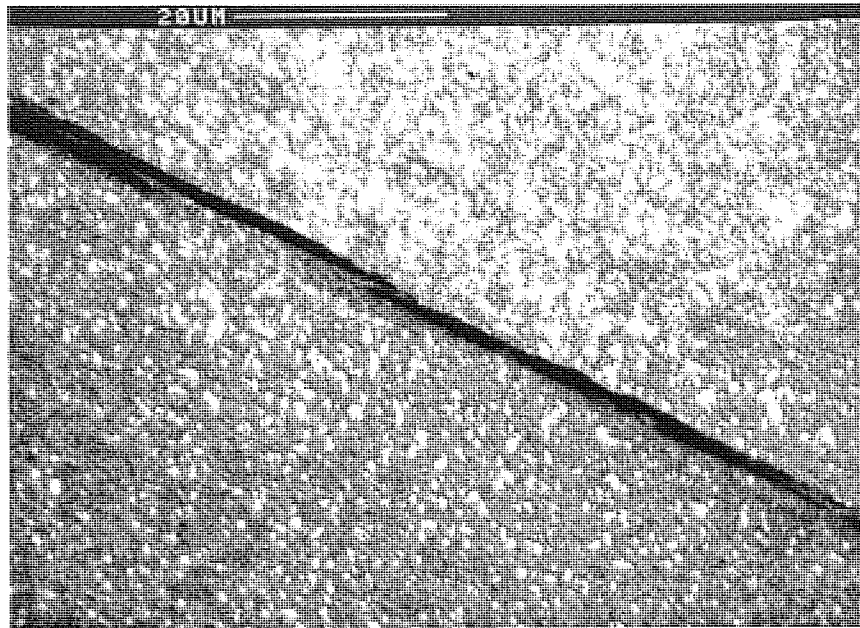
Figure 4.37 *Wear Scar clearly Visible after 24 Hours of a Stop Motion Test at Ambient Conditions*

Closer inspection of the main wear scar after 24 hours of continuous pause mode operation, as illustrated in Figure 4.38, showed substantial deterioration to the tape surface. Large areas of the surface have been worn away resulting in a patchy tape surface in the vicinity of the track.

Figure 4.38 *Wear Scar after 24 hours of a Stop Motion Test at Ambient Conditions*

After 40 hours of a stop motion test at ambient conditions, the width of the wear scar

had increased from approximately 3 μm to about 40 μm, as shown in Figure 4.39. There

were also scratches on the surface of the tape at locations several microns away from the

main wear scar. These could be as a result of loose debris becoming entrapped between

the tape and head, leading to 3-body abrasion.
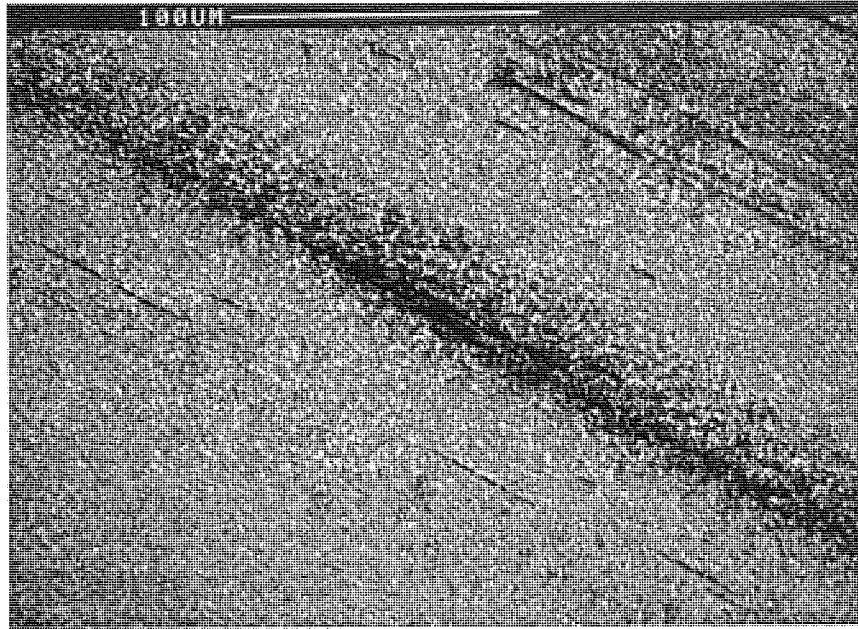
Figure 4.39 *Wear Scar after 40 Hours of a Stop Motion Test at Ambient Conditions*

The micrograph shown in Figure 4.40 illustrates the tape surface after the tape had failed the stop motion test. Severe wear had occurred resulting in the formation of grooves and an abundance of debris. The debris would have contributed to the plastic deformation of the tape surface and ultimately to the total loss of signal.
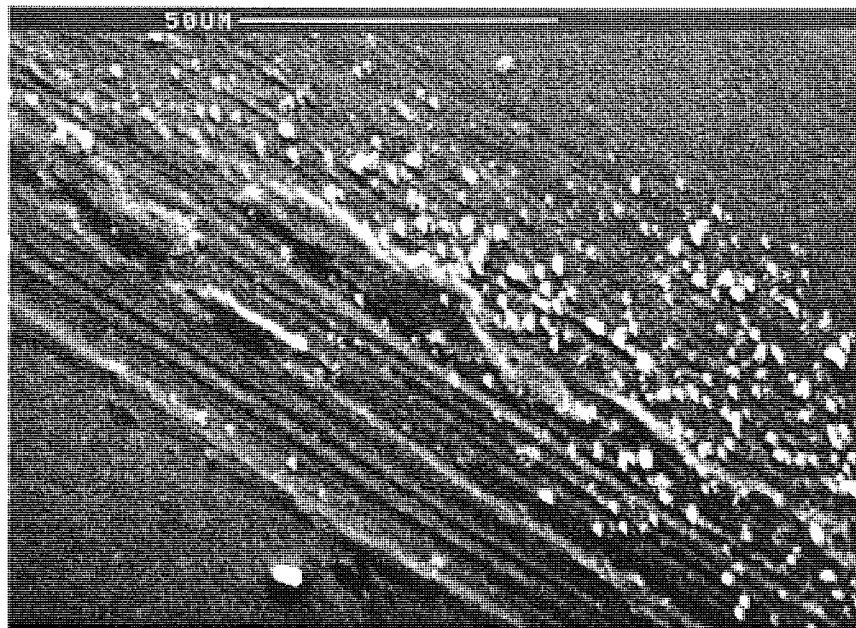
Figure 4.40 *Wear Scar after Stop Motion Test Failure at Ambient Conditions*

The degradation to the surface of tape MP#1 that occurred as a result of the cycling durability tests appeared to be of a different nature to the damage resulting from stop motion tests.

Prior to 2500 cycles, the only change to the surface of the tape was the formation of a

few scratches as illustrated in Figure 4.41. This coincided with an increase in the narrow

3 µs, 10 µs and 20 µs classes of 10 dB dropout at ambient conditions.
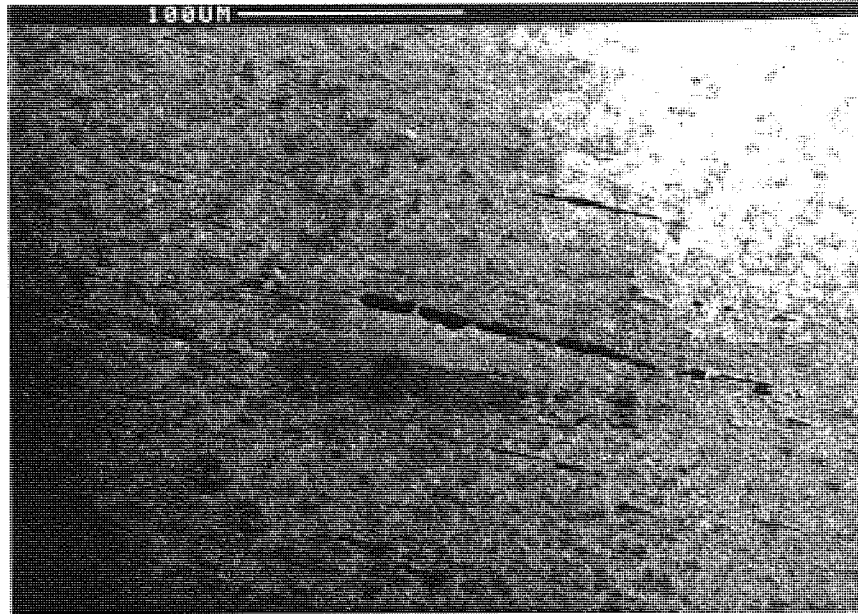
Figure 4.41 *Wear Scars on Tape MP#1 after 2500 Cycles at Ambient Conditions*

When the cycling tests performed at ambient conditions were terminated at 5000 cycles, the wear scars had become far more pronounced, as illustrated in Figure 4.42. The scratches ran parallel to the helical scan direction and typically had a maximum length of 20 μm. Such wear scars could account for the relatively large number of 16 dB dropouts at 5000 cycles.
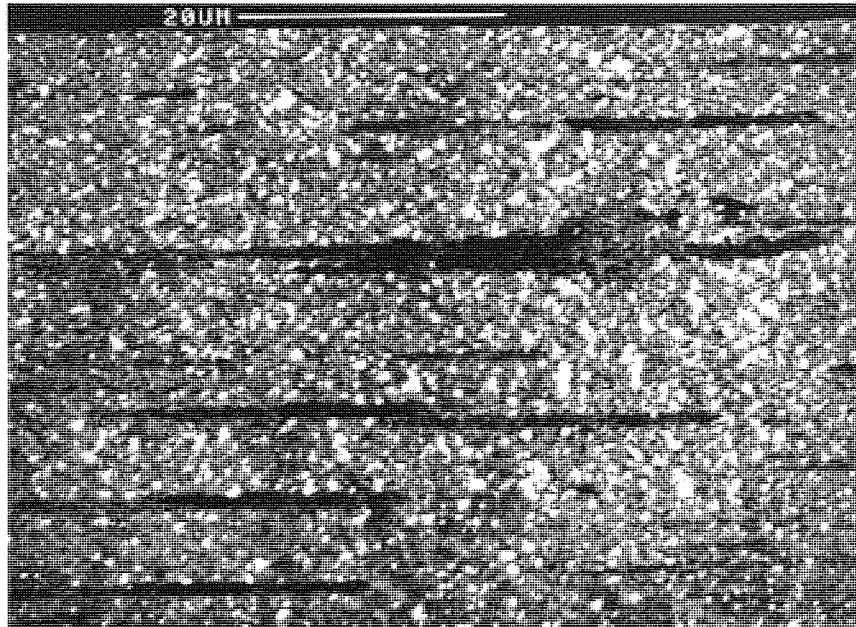
Figure 4.42 *Wear Scars on Tape MP#1 after 5000 Cycles at Ambient Conditions*

A typical micrograph of the surface of tape MP#1 after 2500 cycles at high humidity conditions is shown in Figure 4.43. Wear scars in the form of scratches were clearly evident on the tape surface and the general direction was the same as that for helical scan. Thus, the creation of these scars was probably due to the contact between the heads on the rotating drum and the moving tape.
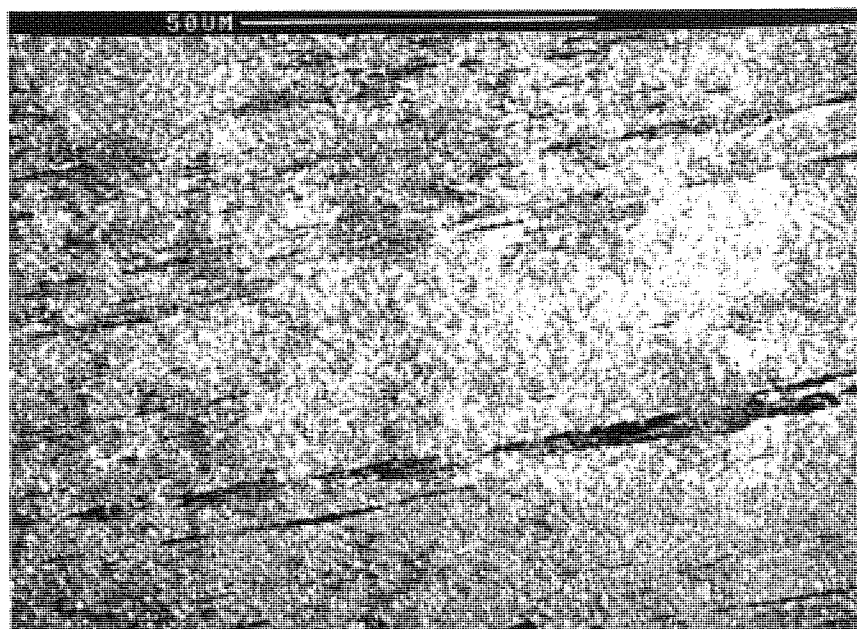
Figure 4.43 *Wear Scars on Tape MP#1 after 2500 Cycles at High Humidity Conditions*

After 5000 cycles at high humidity conditions, scratches were still clearly visible on the tape surface, as illustrated in Figure 4.44. However, in addition to these scratches, several large scars also existed and the formation of these scars coincided with the increase in dropouts. Figure 4.45 shows a closer view of a typical worn area on the tape surface in which the main scar had a length of approximately 25 μm and width of 3 μm.
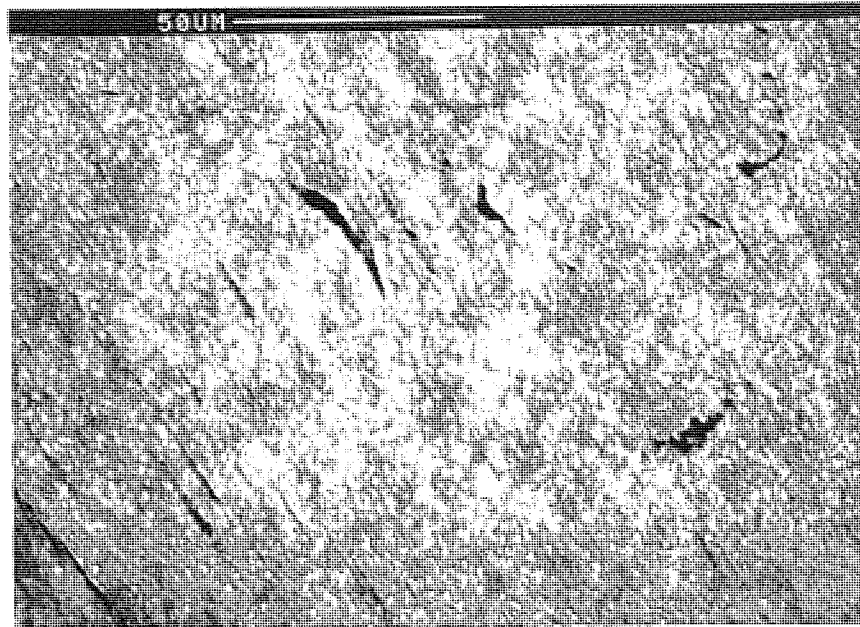

Figure 4.44 Wear Scars on Tape MP#1 after 5000 Cycles at High Humidity Conditions
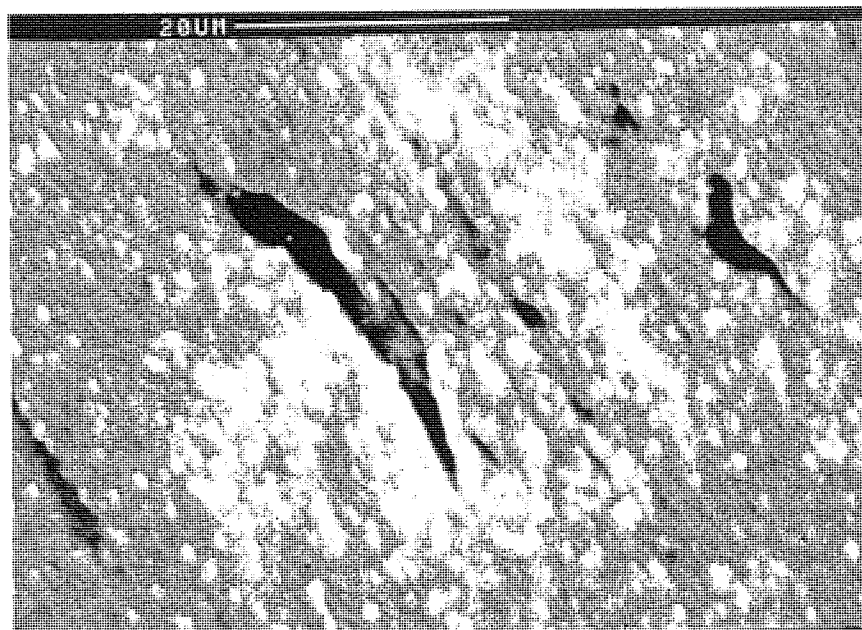
Figure 4.45 Wear Scars on Tape MP#1 after 5000 Cycles at High Humidity Conditions

4.3.2 Tape ME#1

The typical surface features observed on tape ME#1 after a durability test at ambient conditions were similar to those features observed on an identical tape when tested at high humidity conditions, irrespective of the type of test. The main difference arising from the different test conditions was the time at which certain phenomena occurred with high humidity conditions often delaying the progression of wear. However, the time at which these wear features occurred also varied even when the same tape was tested under identical environmental conditions. Thus, the times (re: stop motion tests) given in the following section should only be used as a guide and not as a defining point at which certain wear phenomena will definitely occur.

The micrographs from tapes ME#1 and ME#2 had similar surface features for each type of test although the actual wear scars were significantly different depending on whether the tape had been the subject of a stop motion or cycling test.

A virgin sample of tape ME#1 appeared featureless to SEM and even after the tape had

been the subject of a stop motion test for two hours, the surface still remained fairly

featureless. However, after three hours of the stop motion test, some wear to the surface

of the tape became apparent, as shown in Figure 4.46. There was slight scarring to the

surface which could coincide with a small drop in the playback signal. In the case of tape

ME#1, the signal typically fell by up to 1 dB before total signal loss occurred.
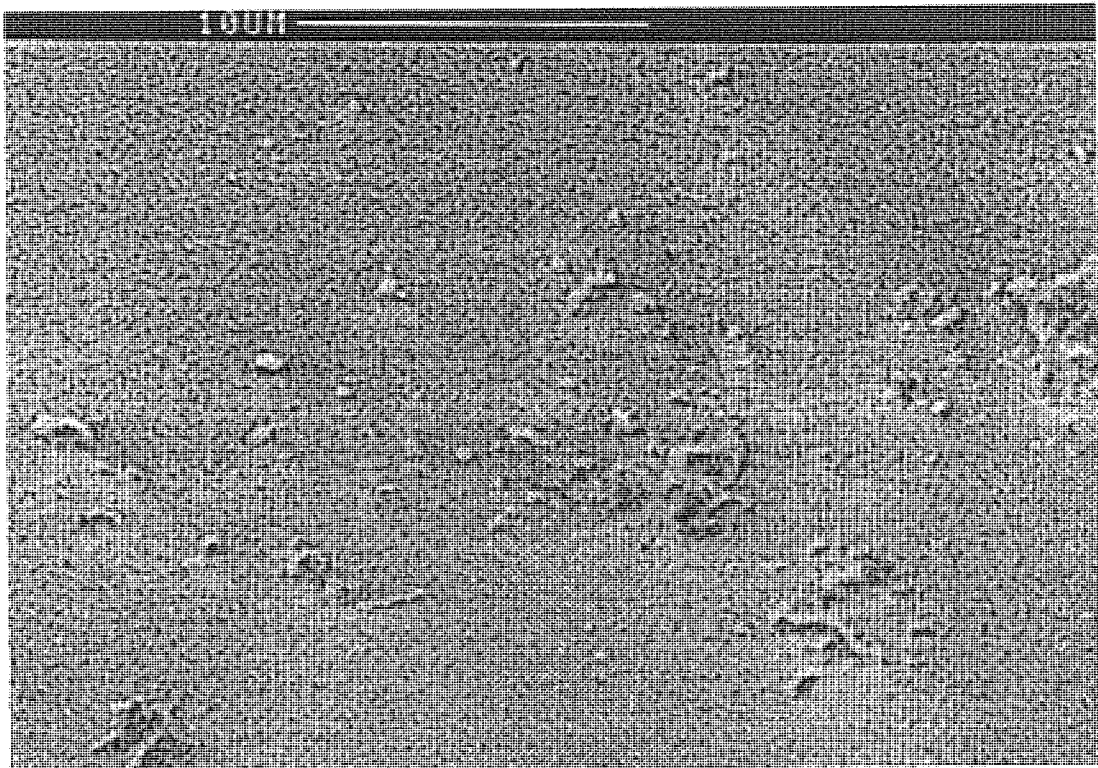
Figure 4.46 Slight Surface Damage to Tape ME#1 after 3 Hours of Stop Motion Test

After 4 hours of stop motion test, the tape began to exhibit signs of surface degradation, as shown in Figure 4.47. A wear track was visible in the direction corresponding to that of a helical scan.

Figure 4.47 Significant Surface Damage to Tape ME#1 after 4 Hours of Stop Motion Test

At 5 hours of continuous stop motion test, the surface had deteriorated to such an extent that sections of the top surface layer began to crack forming debris that would subsequently be removed from one area of the tape and be deposited on another. A classic example of this is shown in Figure 4.48 in which a section of the tape experienced severe wear, leading to flakes of debris and small wear particles. The edge of the track was visible at the top of the micrograph, represented by a patchy black line.
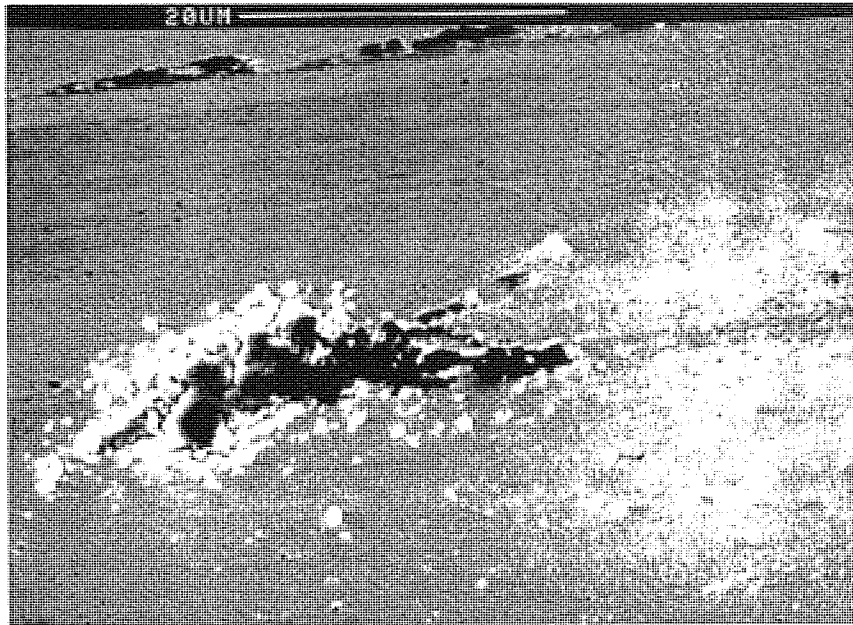
Figure 4.48 *Severe Surface Damage to Tape ME#1 after 5 Hours of Stop Motion Test*

At between 7 and 9 hours, tape ME#1 typically failed the stop motion test and as Figure

4.49 illustrates, catastrophic wear had occurred to the tape surface, leading to total

signal loss. The whole of the track had suffered severe wear eventually exposing the

magnetic layer to the head. At this point, instant catastrophic failure occurred.
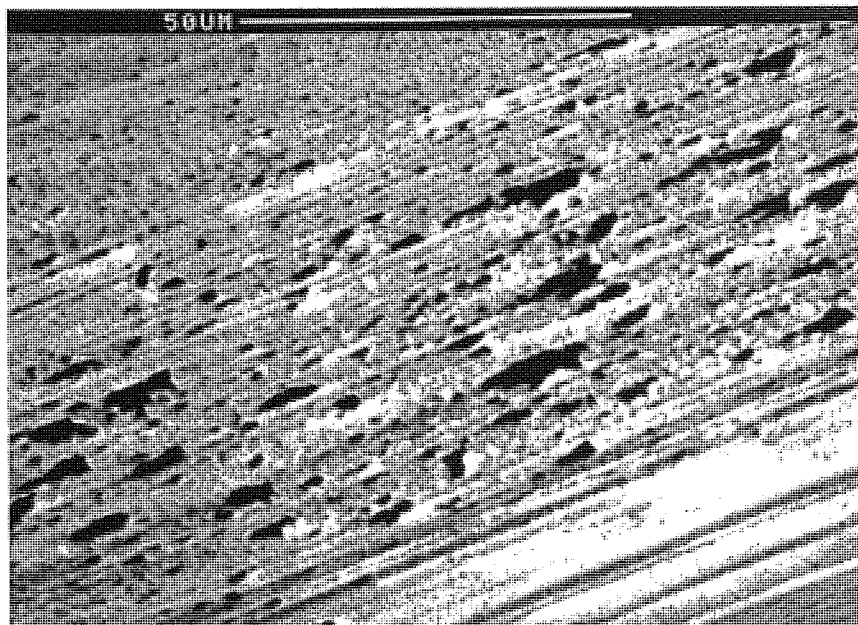

Figure 4.49 *Catastrophic Surface Damage to Tape ME#1 between 7 and 9 Hours of Stop Motion Test*

In the case of the cycling tests, surface damage was also progressive and increased with the number of cycles. However, most of the damage must have occurred in the sub-surface region since there was no significant change to the appearance of the tape when analysed using SEM. This corresponded to the negligible dropout growth for tape ME#1 until at 300 cycles, when catastrophic dropout growth was observed. The surface of the tape was then analysed again using SEM techniques and as Figure 4.50 illustrates, small random patches of the surface had worn across the whole of the tape.
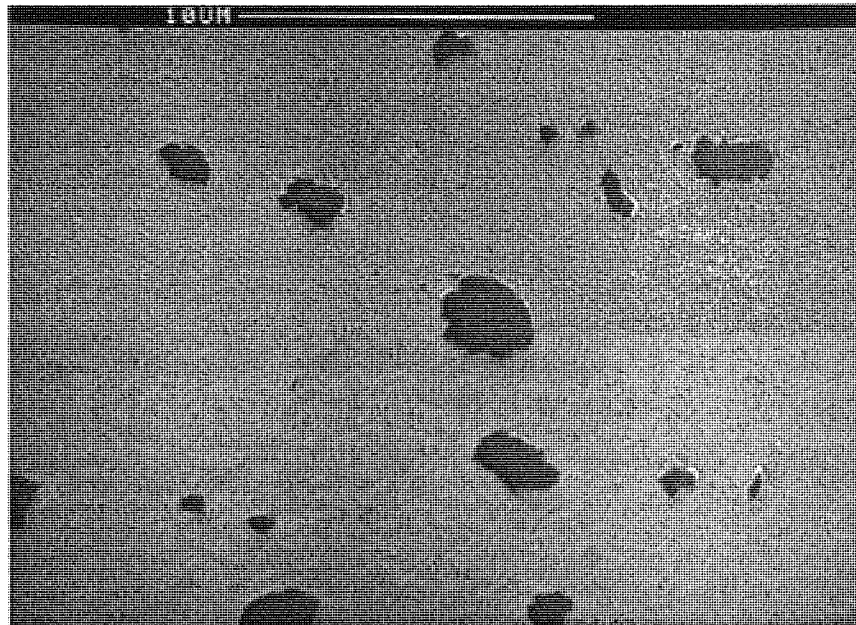

Figure 4.50 Surface Damage to Tape ME#1 Corresponding to Catastrophic Dropout Growth
after 300 Cycles of a Durability Test

4.3.3 Tape ME#2

The micrographs depicting the progression of wear as a result of stop motion tests for tape ME#2 were similar to those for tape ME#1 although the relative time at which each stage occurred was shorter for both ambient and high humidity conditions. For instance, the time at which loose wear debris was observed on the surface of tape ME#2, as illustrated in Figure 4.51, was typically within two hours of a stop motion test.

Figure 4.51 *Significant Surface Damage to Tape ME#2 after 2 Hours of a Stop Motion Test*

A source of loose debris is shown in Figure 4.52 in which a section of the tape surface was clearly breaking up. If the test had not been stopped prematurely, the debris would have been moved to another part of the tape leading to spacing errors and further damage to the tape surface.
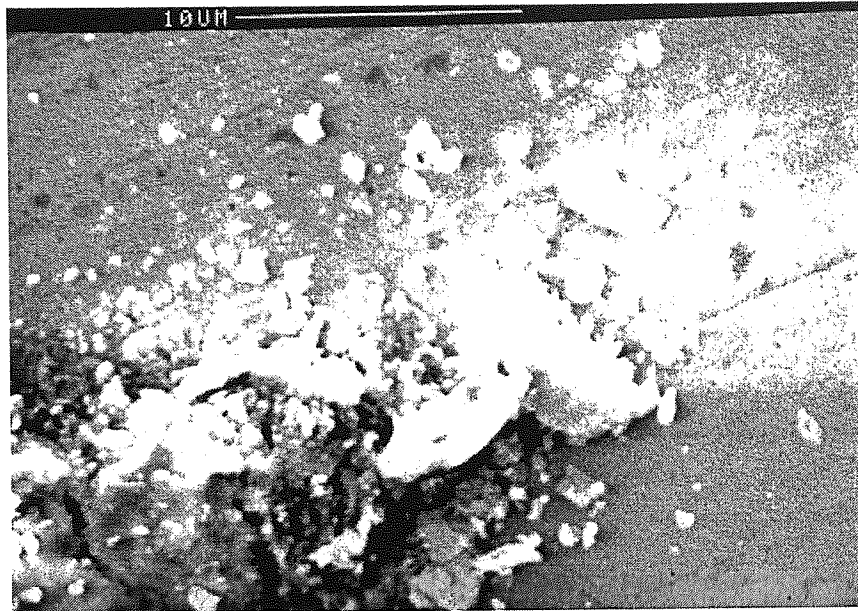
Figure 4.52 Creation of Loose Debris and Surface Damage to Tape ME#2

after 2 Hours of a Stop Motion Test

One such piece of debris was found during SEM analysis at an area on the tape well away from the worn track. As Figure 4.53 shows, the thin debris particle had a laminated appearance and was relatively large with a maximum diameter of approximately 20 μm. The section of tape from where the particle originated would be heavily scarred and the magnetic layer probably left unprotected.
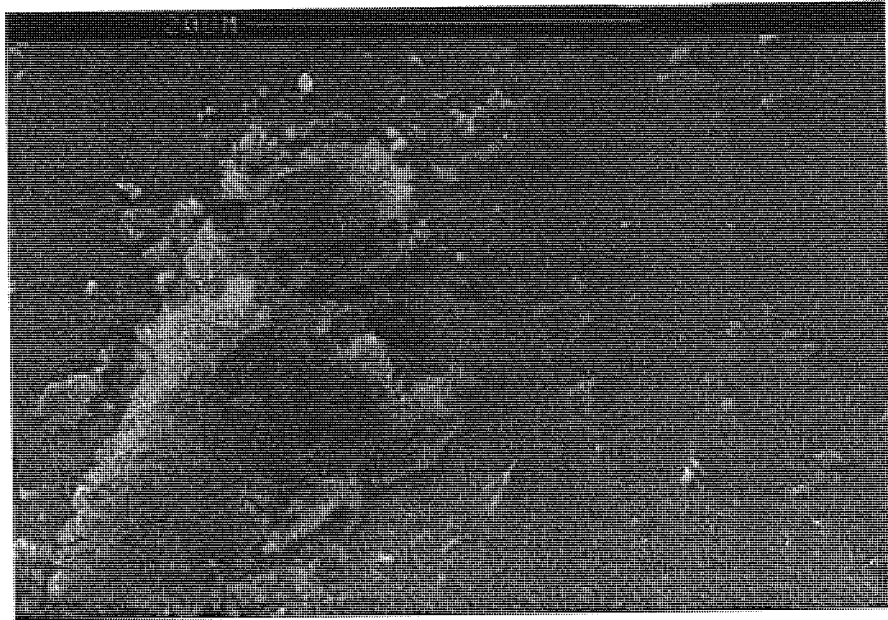
Figure 4.53 *Creation of Loose Debris and Surface Damage to Tape ME#2*

When tape ME#2 had failed the stop motion test, subsequent SEM analysis of the tape

revealed a severely worn surface, as illustrated in Figure 4.54. Catastrophic breakdown

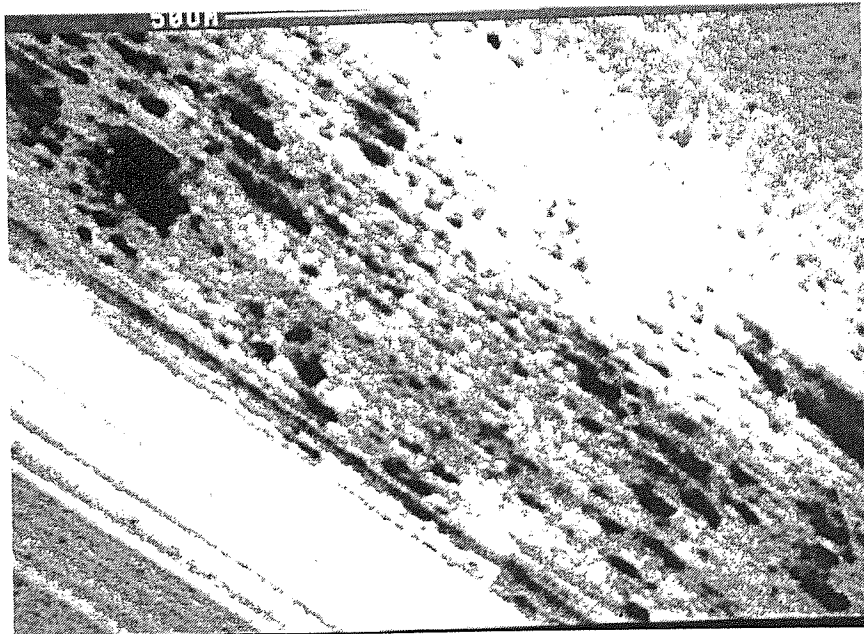of the lubricant and fatigue cracking had resulted in total signal loss

Figure 4.54 *Severe Wear of Tape ME#2 Surface Resulting in Catastrophic Signal Failure*

In the case of the cycling tests, the SEM micrographs which charted the progression of wear with increasing number of cycles were very similar to those of tape ME#1. There was little change to the appearance of the tape surface until catastrophic dropout growth occurred, at 230 cycles. At this point, wear scars such as those shown in Figure 4.55 were observed.
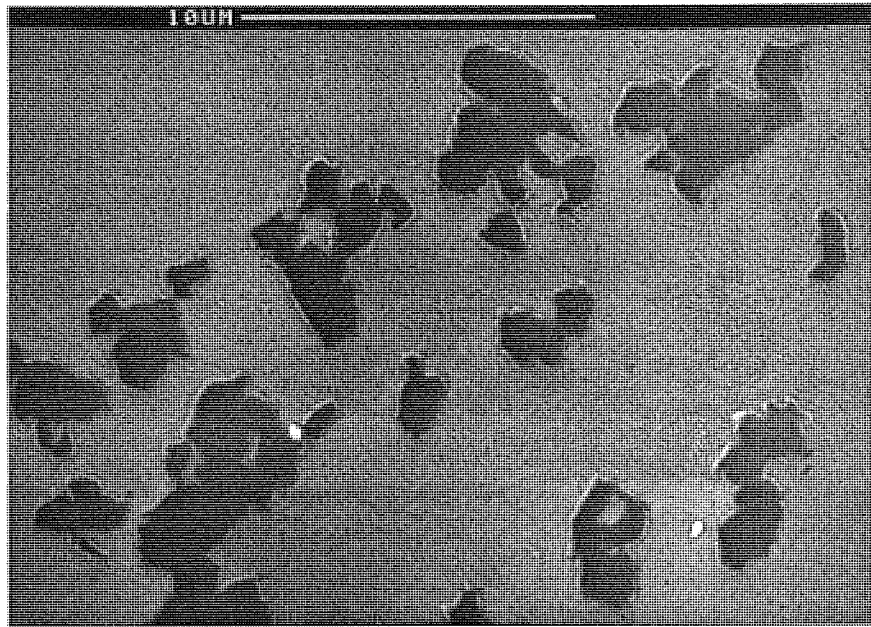

Figure 4.55 *Surface Damage to Tape ME#2 Corresponding to Catastrophic*

Dropout Growth after 230 cycles of a Durability Test

4.3.4 Tape ME#3

The substrate used in the construction of tape ME#3 was more flexible than those used in either of tapes ME#1 or ME#2 and this was reflected in the improved durability results. In the case of the stop motion tests, there was typically no apparent change to the surface of the tape after 2 hours of operation as illustrated in Figure 4.56. The surface was fairly featureless and it was not possible to identify any wear tracks.
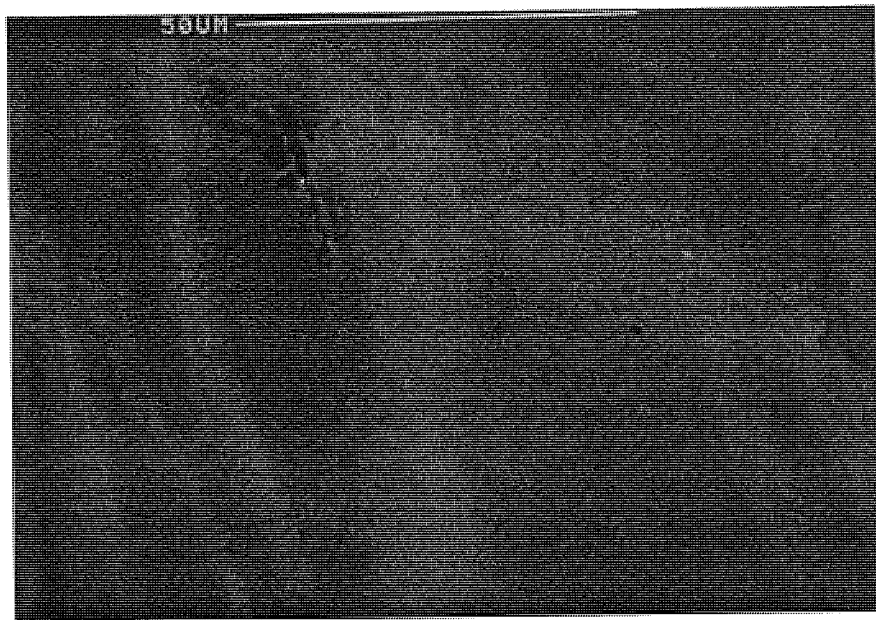

Figure 4.56 No Apparent Change to the Surface of Tape ME#3 after 2 Hours of a Stop Motion Test

The progression of wear to failure followed a similar trend to that of the other ME tapes with a wear track becoming more apparent with increasing stop motion times. However, the times at which each phenomena occurred were longer in the case of tape ME#3. For instance, the creation of wear particles typically only occurred beyond 4 hours in ambient conditions and after 6 hours at high humidity conditions. A distinct wear track

corresponding to the helical scan direction of the heads on the tape also became apparent

during SEM analysis, as illustrated in Figure 4.57.

Figure 4.57 *Wear Track on Tape ME#3 Resulting from Stop Motion Test*

Stop motion times in excess of 10 hours resulted in severe wear to the tape surface and ultimately to total signal failure. A typical micrograph of the surface of tape ME#3 at the point at which signal failure occurred is shown in Figure 4.58. Large areas of the tape surface have been removed, revealing unprotected sections which had previously been covered by a lubricant layer. If sufficiently large, these sections would cause the tape to fail when in contact with a head.
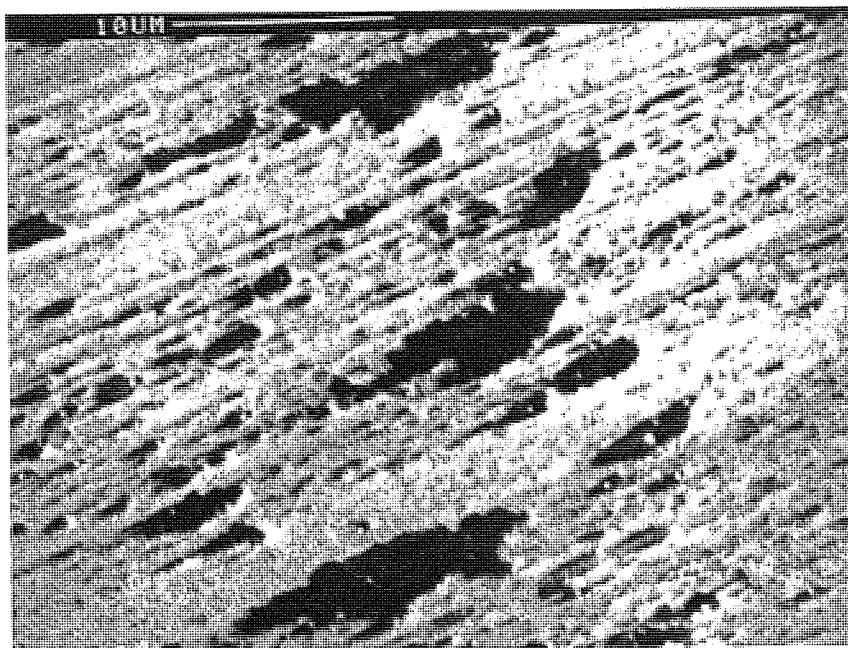

Figure 4.58 Severe Wear on Surface of Tape ME#3 following Stop Motion Test Failure

The micrographs of the surface of tape ME#3 during and after cycling tests revealed a different structure to those observed during equivalent tests on tapes ME#1 and ME#2. At 200 cycles under ambient conditions, a slight change to the surface was observed, as illustrated in Figure 4.59. Feint parallel lines existed which ran across the tape in a direction equivalent to that of the video heads in helical scan format. There were also small discrete areas of damage giving the surface a pitted structure.
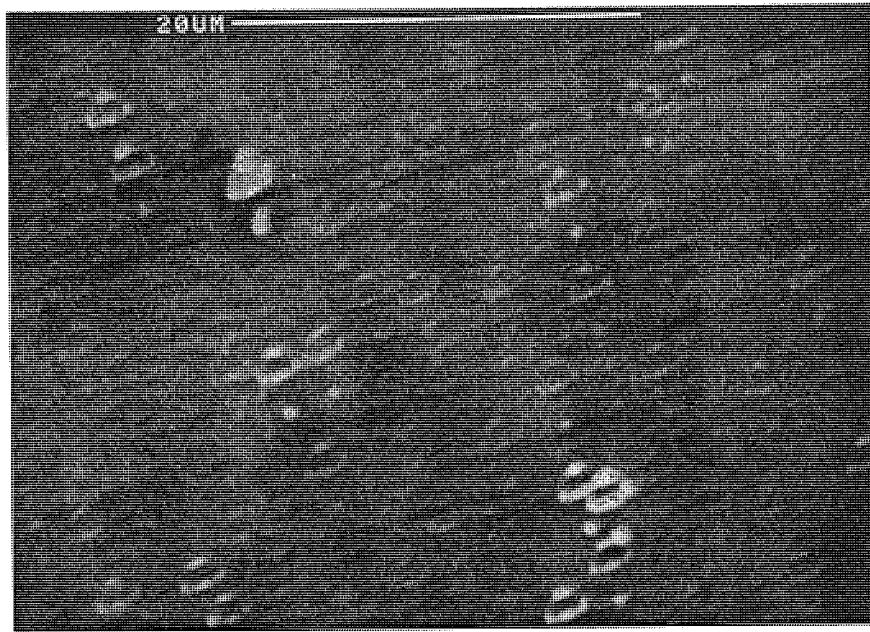

Figure 4.59 Slight Damage to the Surface of Tape ME#3 after 200 Cycles

At 400 cycles, the appearance of the surface had changed significantly, as shown in Figure 4.60, with numerous parallel lines running across the tape. These scars, although different to those on tapes ME#1 and ME#2 probably corresponded to a catastrophic growth in the dropout rate. The greater flexibility of the substrate in tape ME#3 probably contributed towards the different structure of the wear scars and for the better performance in the durability tests.
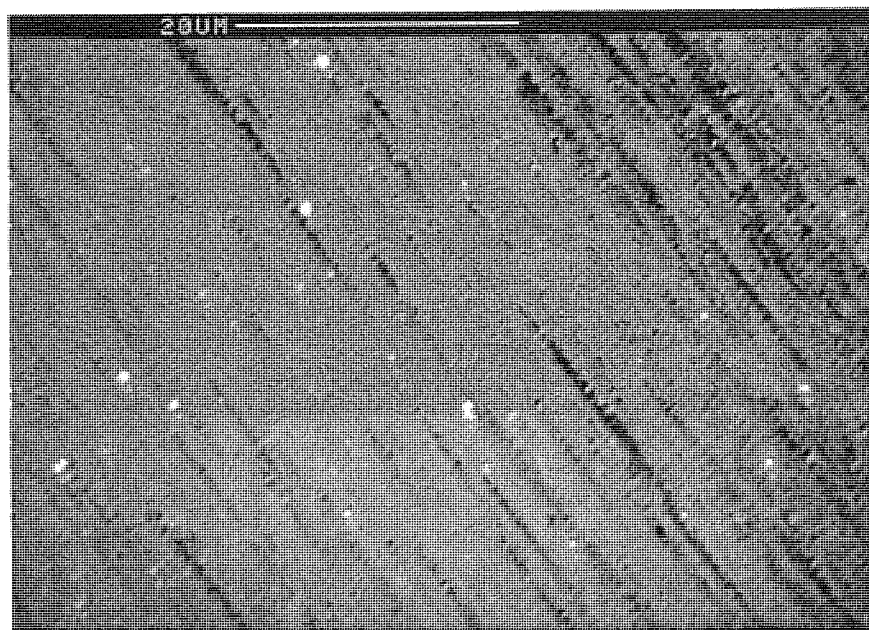

Figure 4.60 *Significant Surface Damage to Tape ME#3 Corresponding to Catastrophic*

Dropout Growth after 400 Cycles of a Durability Test

4.4 Results of XPS Analysis

In XPS, the photoelectron peak position is dependent on the elemental core level, but also on the chemical state and chemical environment of the element from which it originates. Hence, careful measurement of the peak position and peak shifts gives information on the chemical state and bonding of elements in the tape surfaces. To gain such information, it is normally necessary to use a peak synthesis routine on the spectra from a knowledge of expected binding energies and peak half widths. Survey scans were first recorded for all samples at a take-off angle of $0°$ (normal to the analyser). A typical "wide scan" spectrum for tape MP#1 is shown in Figure 4.61. The same six elements of iron, oxygen, nitrogen, carbon, chlorine and aluminium were detected on every wide scan, irrespective of the condition of the tape.
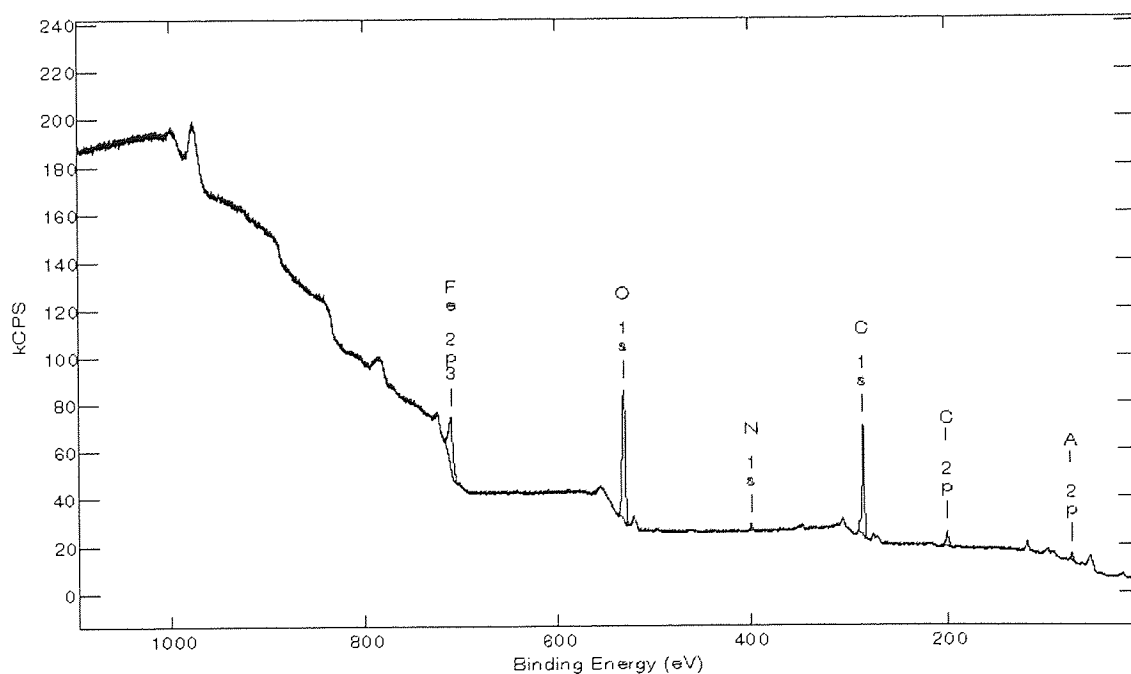
Figure 4.61 Wide Scan Spectrum for Virgin Tape MP#1

In the case of the three ME tapes, wide scans revealed the same 5 elemental constituents

of carbon, oxygen, fluorine, cobalt and nickel although in different quantities depending

on the type of tape and the condition of the tape when it was analysed. A typical wide

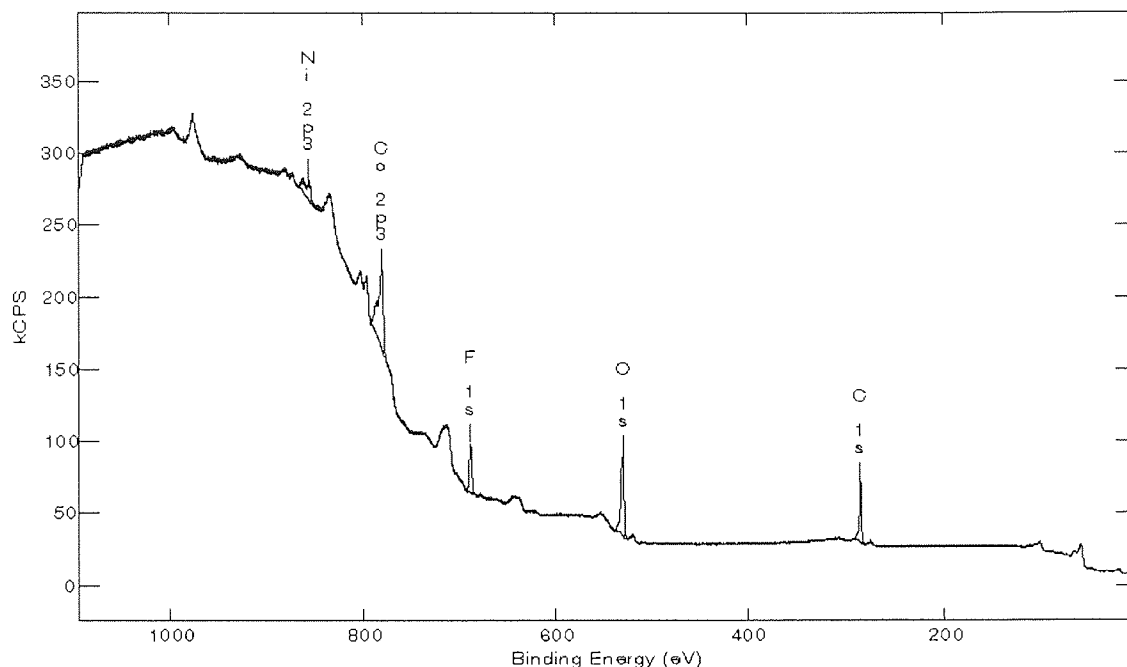scan spectrum for virgin tape ME#1 is shown in Figure 4.62.

Figure 4.62 *Wide Scan Spectrum for Virgin Tape ME#1*

Narrow region energy scans were collected at normal incidence for each element and at a

series of increasing "take-off" angles in order to give depth resolved information. During

preliminary XPS examinations of the ME tape samples, it was found that exposure to the

primary X-ray beam caused the relative atomic concentrations of each element to change

with increasing exposure time. This is illustrated in Figure 4.63 for tape ME#1 and

Figure 4.64 for tape ME#2. In order to minimise the effects of radiation, a different tape

sample was used for each angle measured and in the case of the ME tapes, the fluorine

peak was collected first since the preliminary experiments had shown fluorine to be the

most susceptible to X-ray exposure.
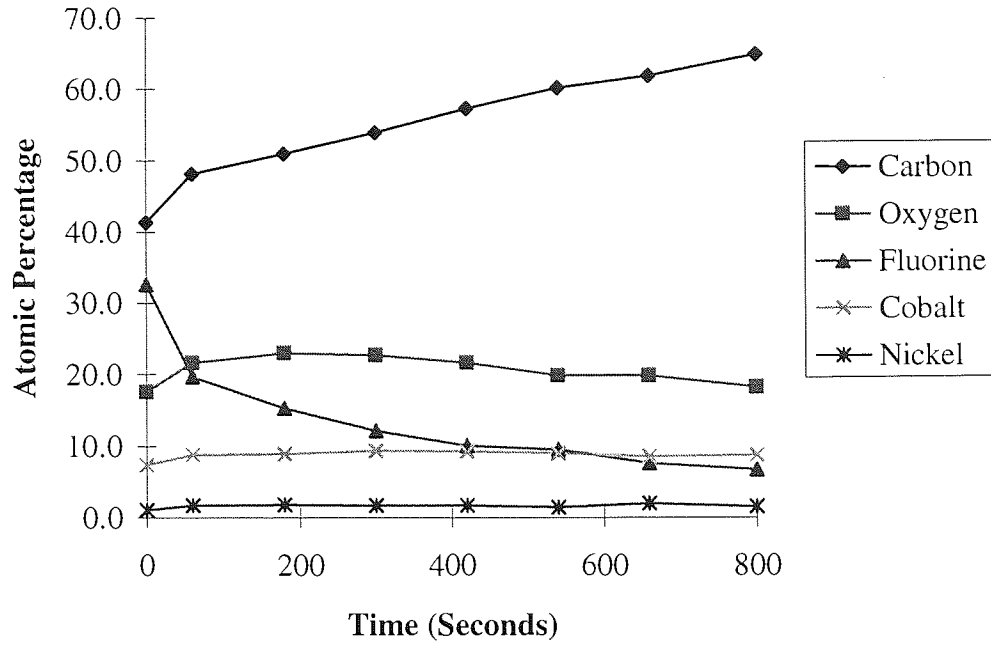
Figure 4.63 *Change in Relative Atomic Concentrations for Tape ME#1*

with Increasing X-ray Exposure Time
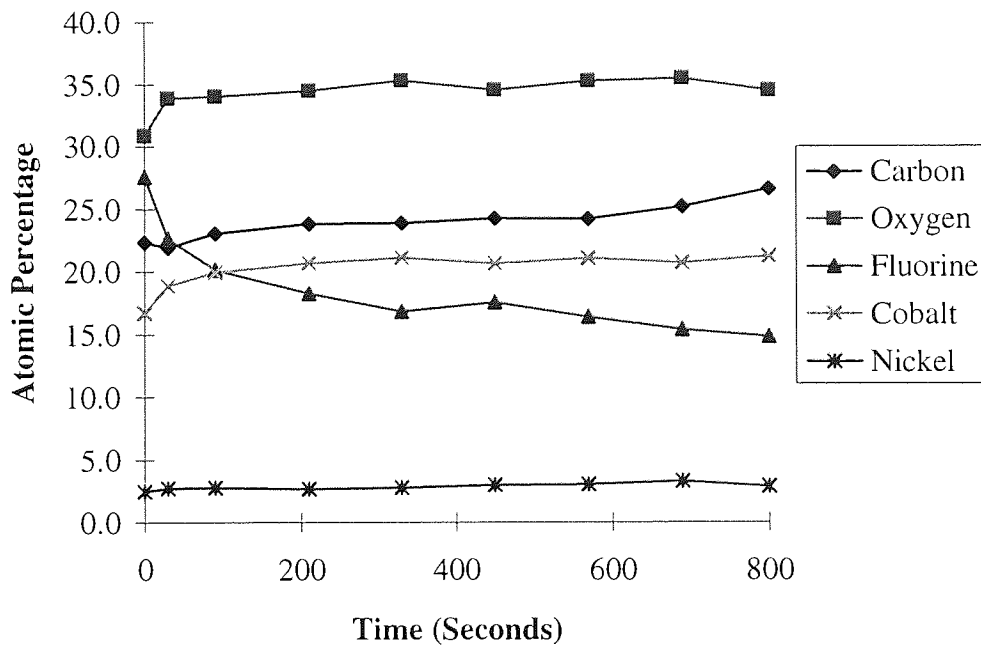
Figure 4.64 *Change in Relative Atomic Concentrations for Tape ME#2*

with Increasing X-ray Exposure Time

4.4.1 Tape MP#1

Integrated depth profiles from ARXPS experiments are shown in Figures 4.65 - 4.68 for

tape MP#1 at 0, 300 and 5000 cycles at ambient conditions and for 5000 cycles at high

humidity conditions. The analysis at 300 cycles was performed in order to ascertain

whether any changes had occurred to the chemical nature of the tape, and in particular to

the binder after just a few hundred cycles. The profiles illustrated in Figures 4.65 - 4.68

show the same basic trends with an increase in oxygen and decrease in carbon, with

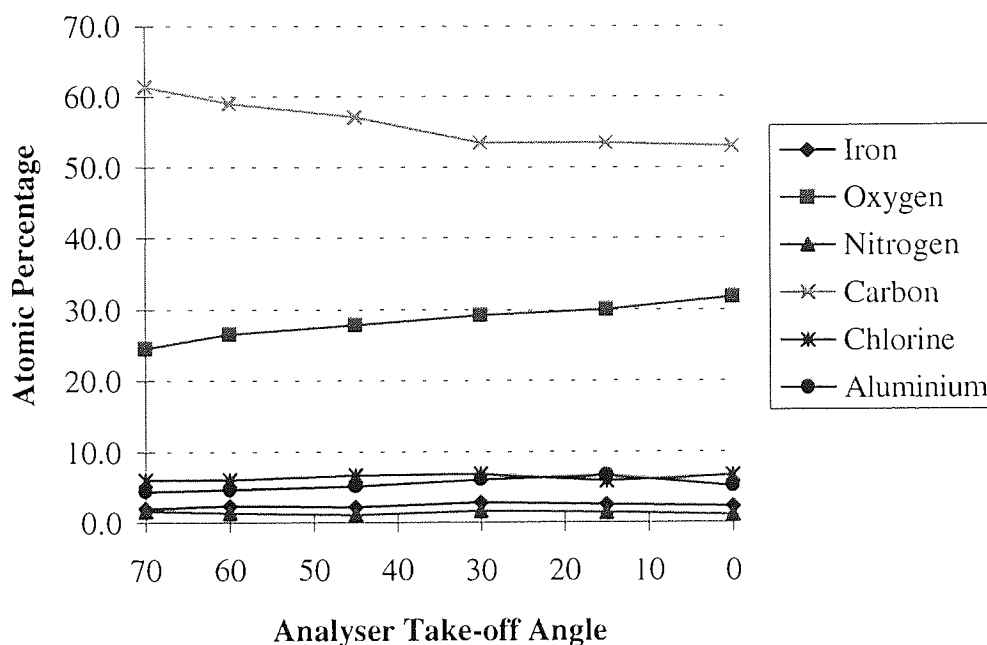decreasing take-off angle (increasing depth).

Figure 4.65 *Integrated Concentration Profile of the Virgin Surface of Tape MP#1*
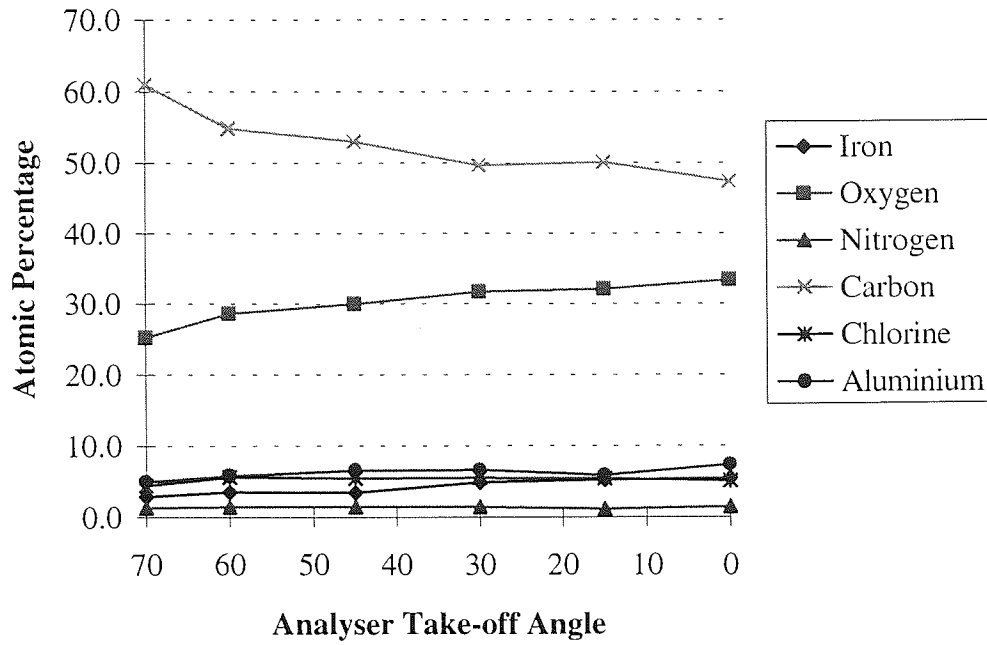
Figure 4.66 *Integrated Concentration Profile of the Surface of Tape MP#1*

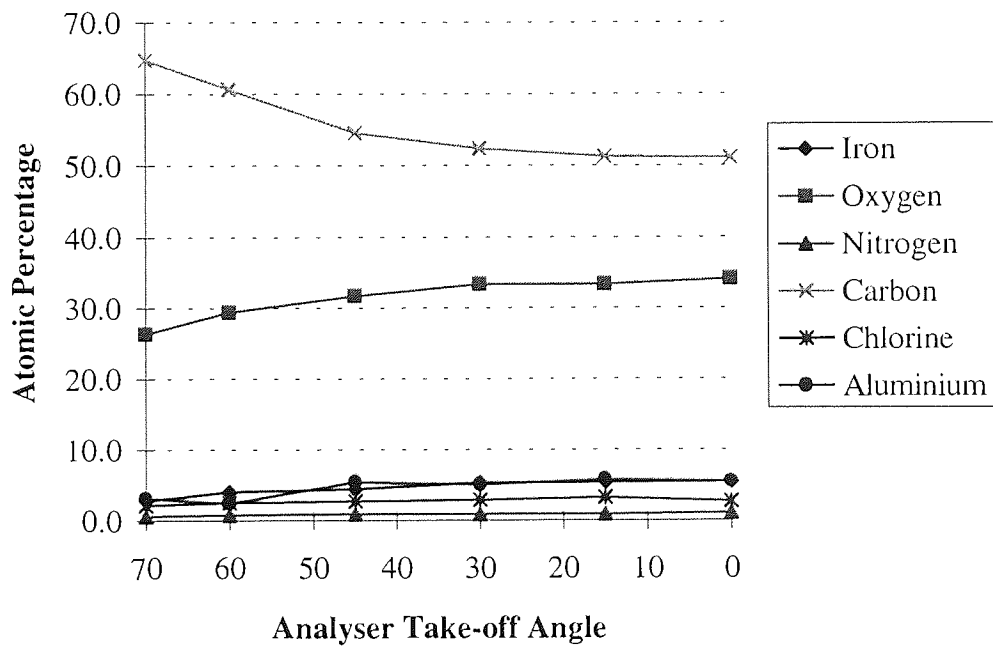*after 300 Cycles at Ambient Conditions*

Figure 4.67 *Integrated Concentration Profile of the Surface of Tape MP#1*

after 5000 Cycles at Ambient Conditions
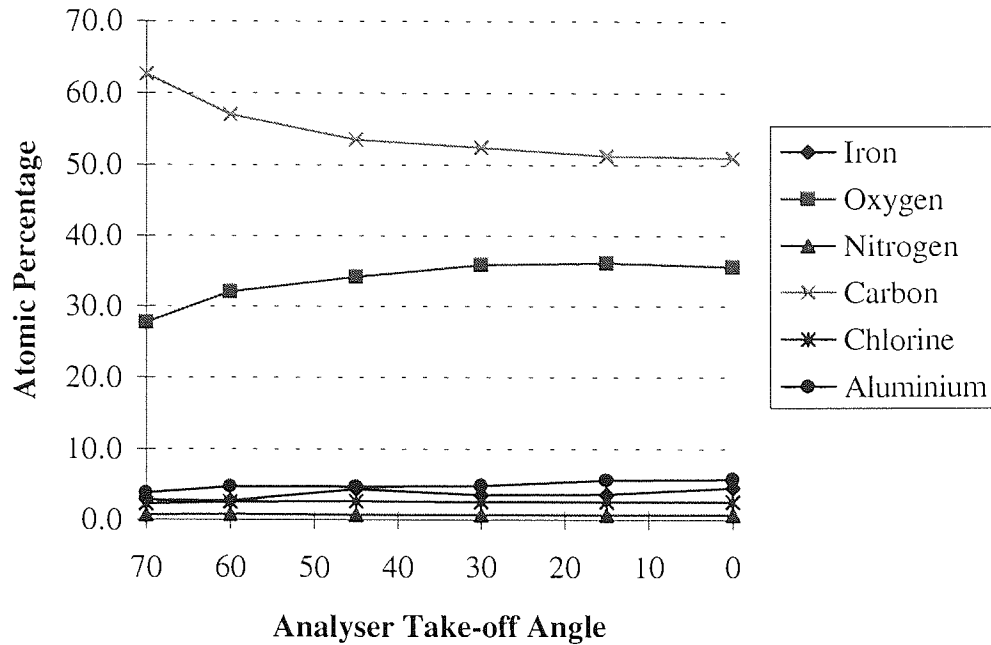
Figure 4.68 Integrated Concentration Profile of the Surface of Tape MP#1

after 5000 Cycles at High Humidity Conditions

Peak synthesis of the oxygen spectra enabled the FeO content to be determined for tape samples at each of the four different conditions. Figure 4.69 shows a typical oxygen spectrum for the MP tape with a FeO peak at a binding energy of 529.6 eV. The two remaining peaks, O1 and O2, did not correspond to any particular chemical state of oxygen but were used to determine the proportion of FeO in the total oxygen spectrum.

Figure 4.69 Synthesis of an Oxygen Spectrum into Individual Peaks in order to Ascertain the

Proportion of FeO Present in the near Surface Region of Tape MP#1

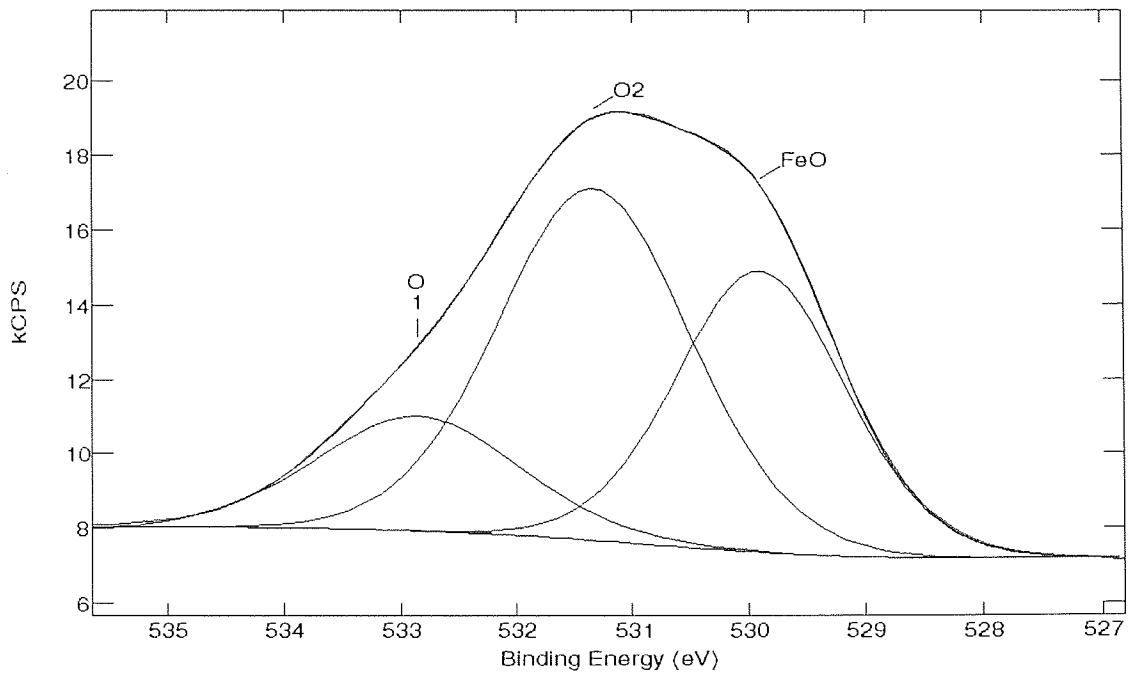Figure 4.70 shows how the FeO content varied with analyser take-off angle for the tape

samples at the four different conditions. The FeO content was a minimum for each of

the tape samples when the analyser take-off angle was 70° (i.e. grazing angle). In each

case, the percentage of FeO generally increased with increasing take-off angle. The

take-off angle of 0° corresponded to the greatest analysis depth and this case, the virgin

tape was found to have the lowest concentration of FeO. Thus, the subsequent cycling

of tape MP#1 appeared to change the surface structure by increasing the amount of

material between the pigment and the outer surface of the tape.

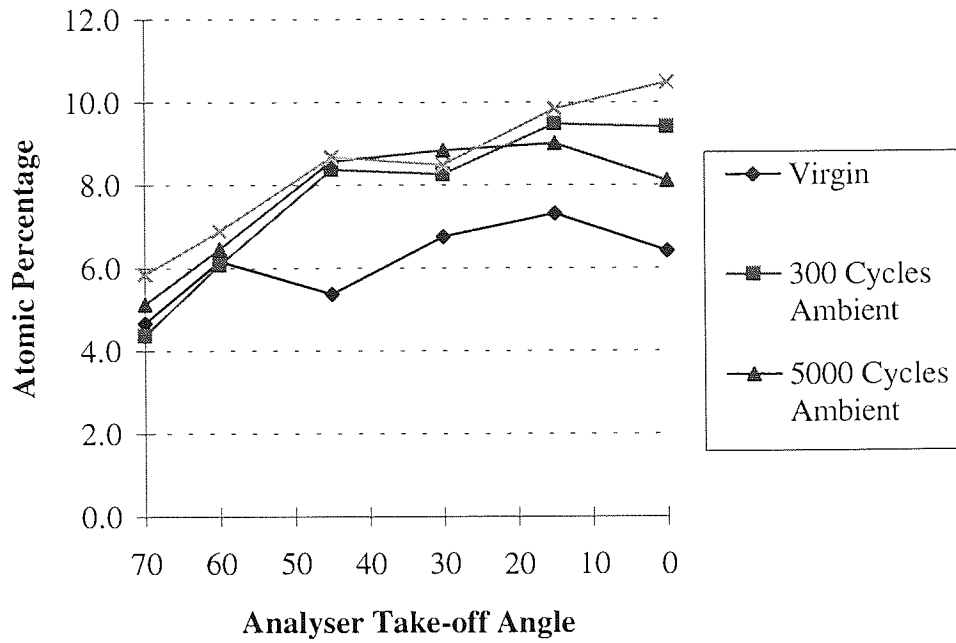Figure 4.70 Variation in FeO Content with Depth for Tape MP#1 at 4 Different Conditions

Peak synthesis of the C spectra was performed for spectra from tape MP#1 and as Figure

4.71 shows, five different chemical states contributed to the total C peak.
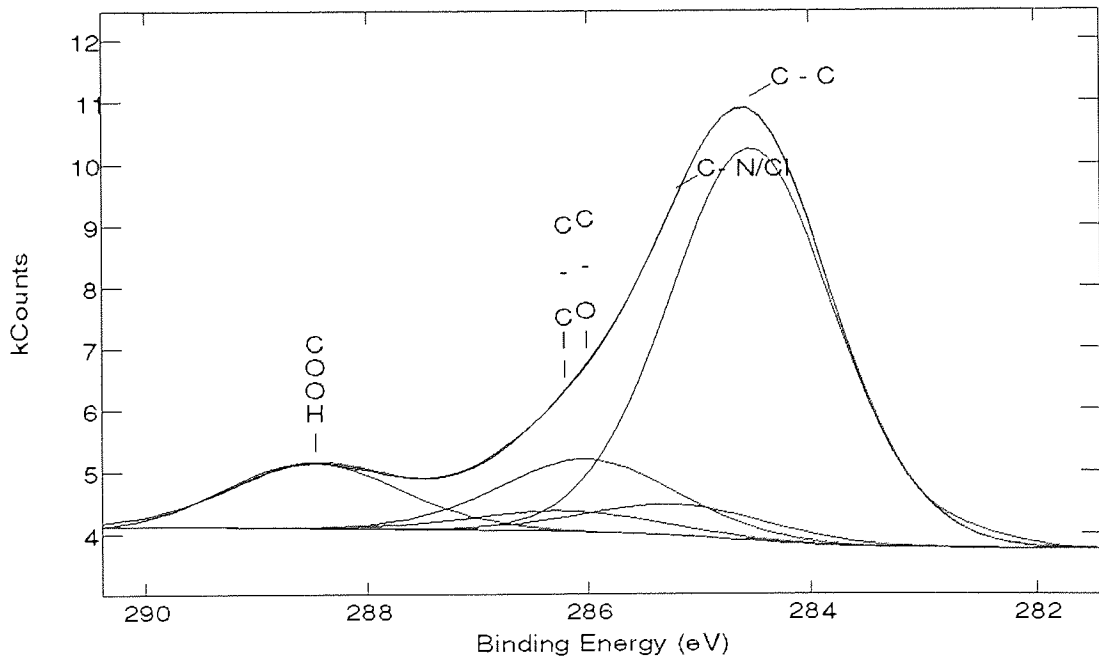
Figure 4.71 Synthesis of a Carbon Spectrum into Individual Peaks in order to Determine the Different

Chemical States of Carbon in Tape MP#1

The C-Cl bonds occurred at two separate energies, one of which coincided with the binding energy of C-N. However, since the two Cl peaks were known to be of equal magnitude, it was possible to separate the C-N/C-Cl peak into C-Cl and C-N bonds.

Synthesis of the carbon spectra for each sample of tape MP#1 at 6 different take-off angles enabled the chemical states to be identified as a function of analyser take-off angle. Figures 4.72-4.75 show the changes in atomic concentration of the five different C bonds in the near surface region of tape MP#1 for virgin tape, after 300 cycles, 5000 cycles and 5000 cycles at high humidity, respectively.

Figure 4.72 *Change in Atomic Concentration of C Bonds in the Near Surface Region*

of Tape MP#1 for Virgin Tape as a Function of Analyser Take-off Angle

Figure 4.73 *Change in Atomic Concentration of C Bonds in the Near Surface Region*

of Tape MP#1 after 300 Cycles as a Function of Analyser Take-off Angle

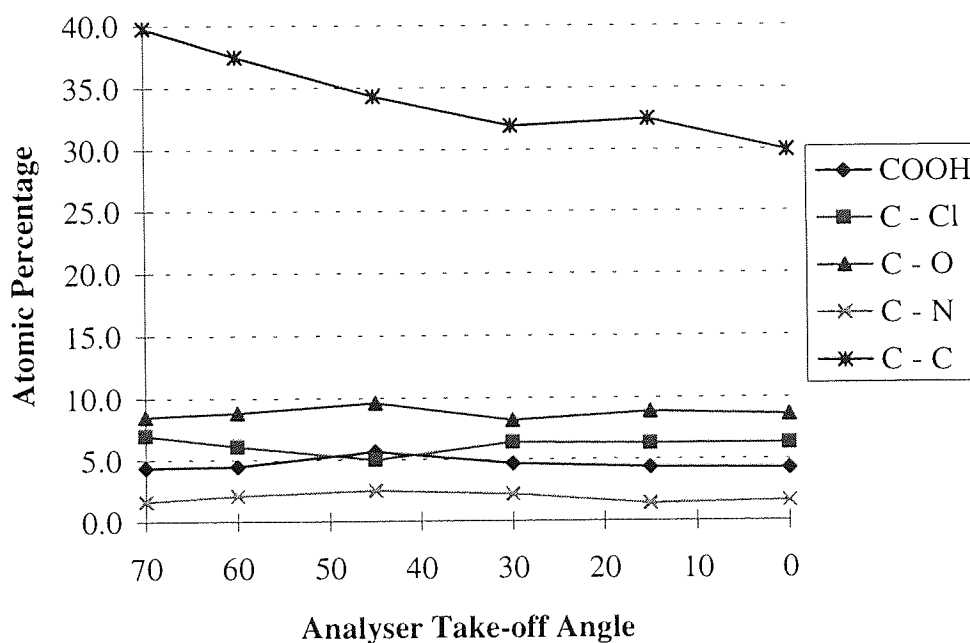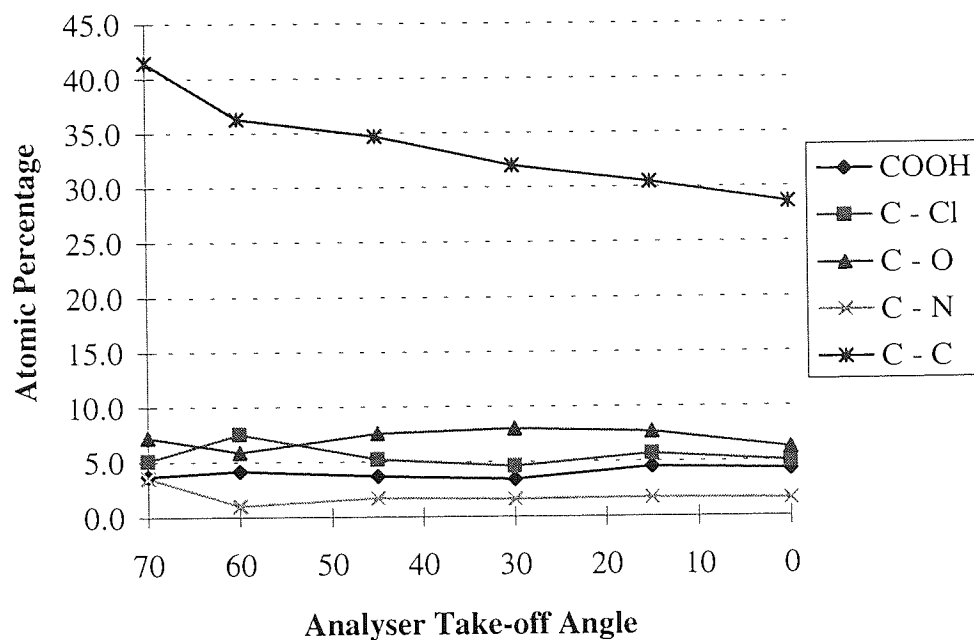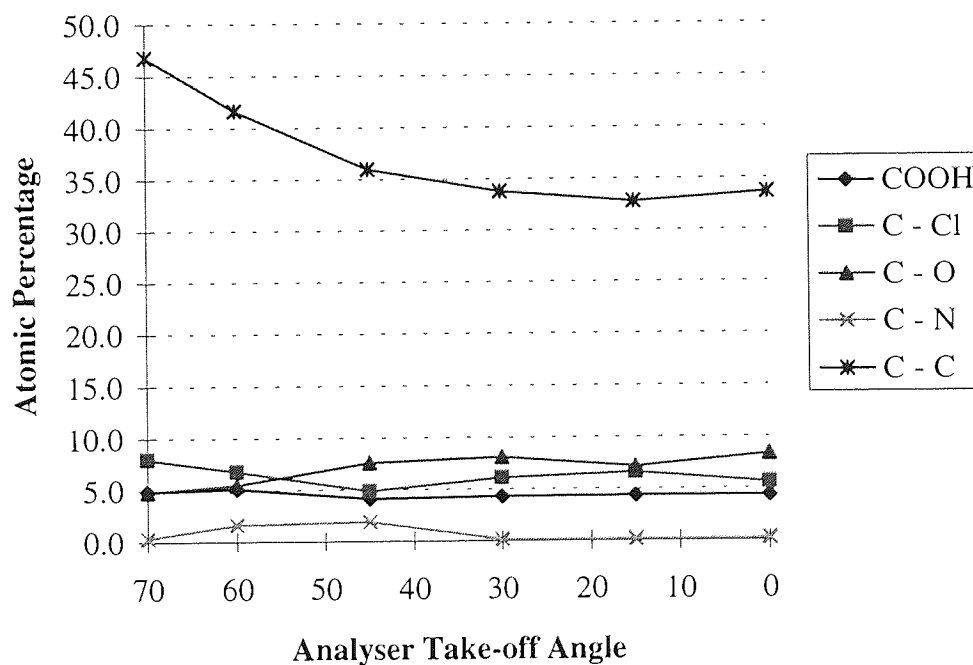**Figure 4.74** *Change in Atomic Concentration of C Bonds in the Near Surface Region*

of Tape MP#1 after 5000 Cycles as a Function of Analyser Take-off Angle
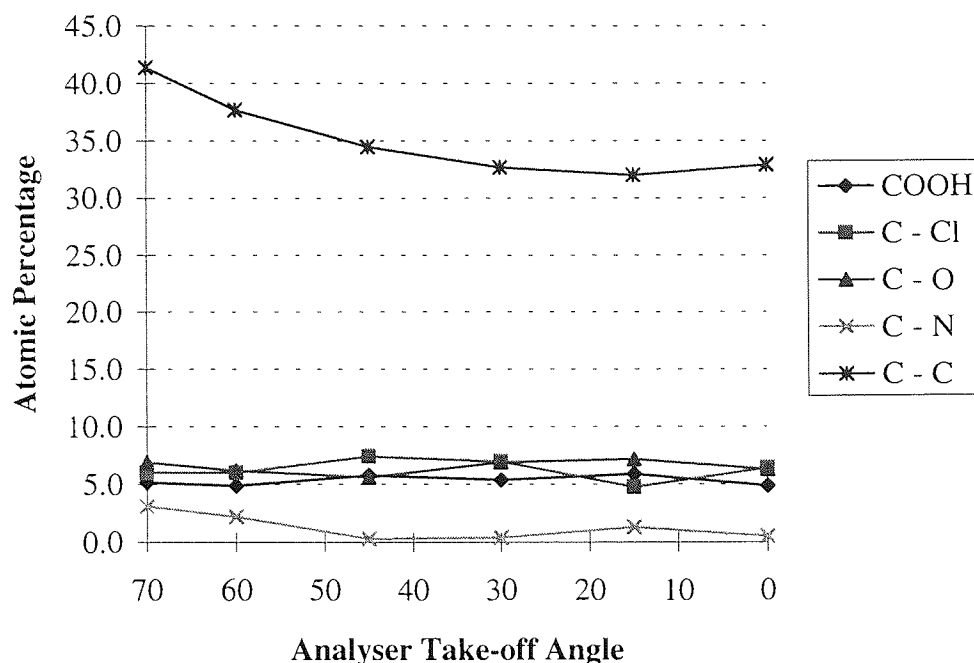
Figure 4.75 *Change in Atomic Concentration of C Bonds in the Near Surface Region*

of Tape MP#1 after 5000 Cycles at High Humidity as a Function of Analyser Take-off Angle

Historically, angle resolved XPS experiments have been used extensively to analyse the surface of particulate magnetic media. However, the validity of such experimental practice is questionable since the irregular non-homogeneous surface of the media could significantly effect the accuracy of any subsequent results. Thus, in order to ensure accurate results, all XPS data originating from particulate media will be limited to that corresponding to an analyser take-off angle of 0° (normal to the analyser).

Analysis of relative elemental concentrations is not a particularly good indicator of total surface change since it is often difficult to judge whether a given sample is more particle rich than another sample by simple reference to measured relative concentrations. A more reliable method is to compare the ratio of one element to another and in particular to the concentration of Fe to elements found in the binder and lubricant of the tape, as

shown in Figures 4.76 - 4.79. Each Figure compares virgin and cycled MP#1 tape at

different environmental conditions and at various number of cycles.
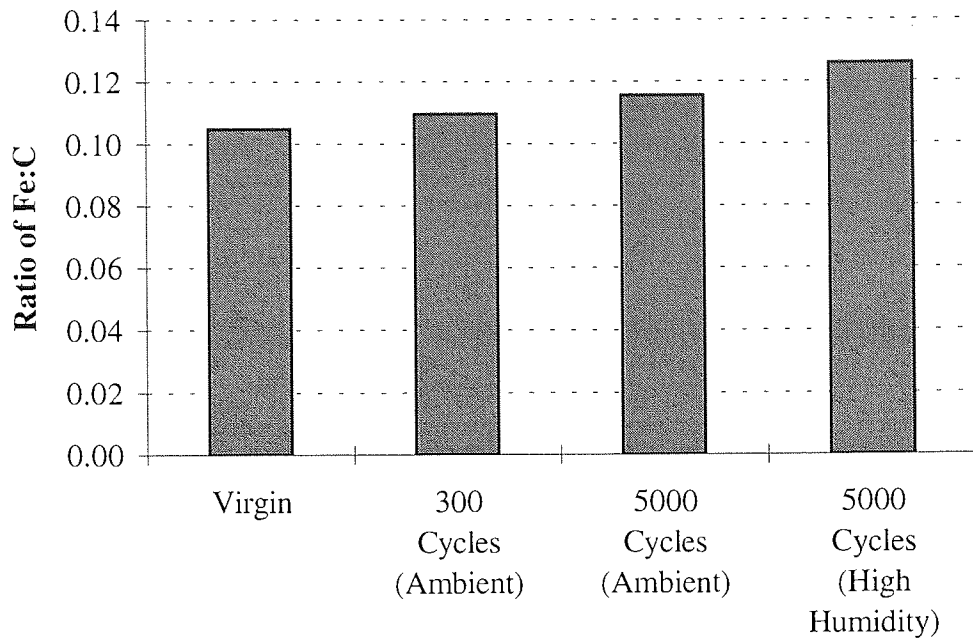
Figure 4.76 Ratio of Fe:C for Tape MP#1
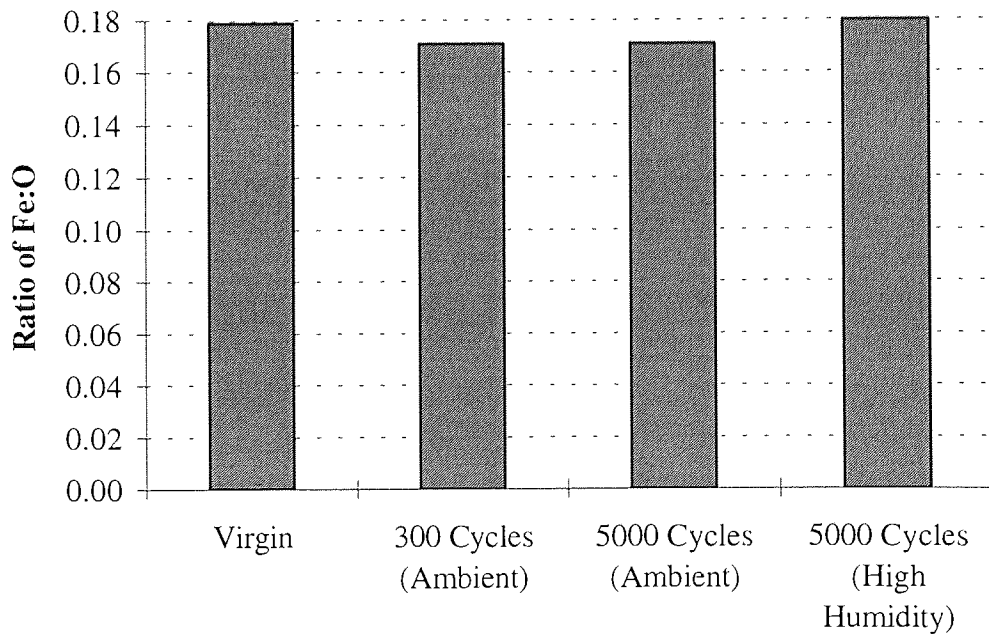
Figure 4.77 Ratio of Fe:O for tape MP#1

224
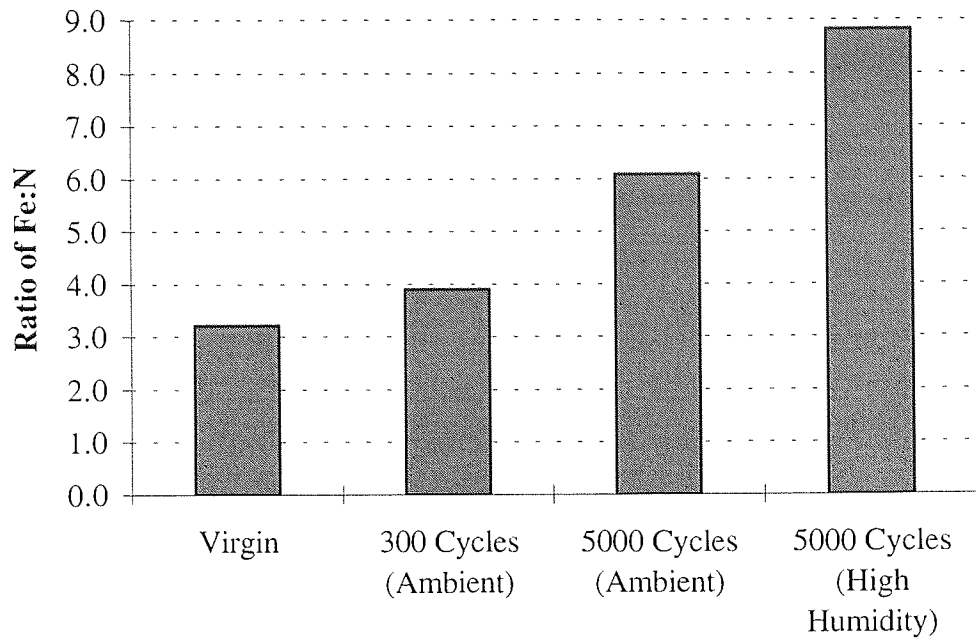
Figure 4.78 Ratio of Fe:N for Tape MP#1
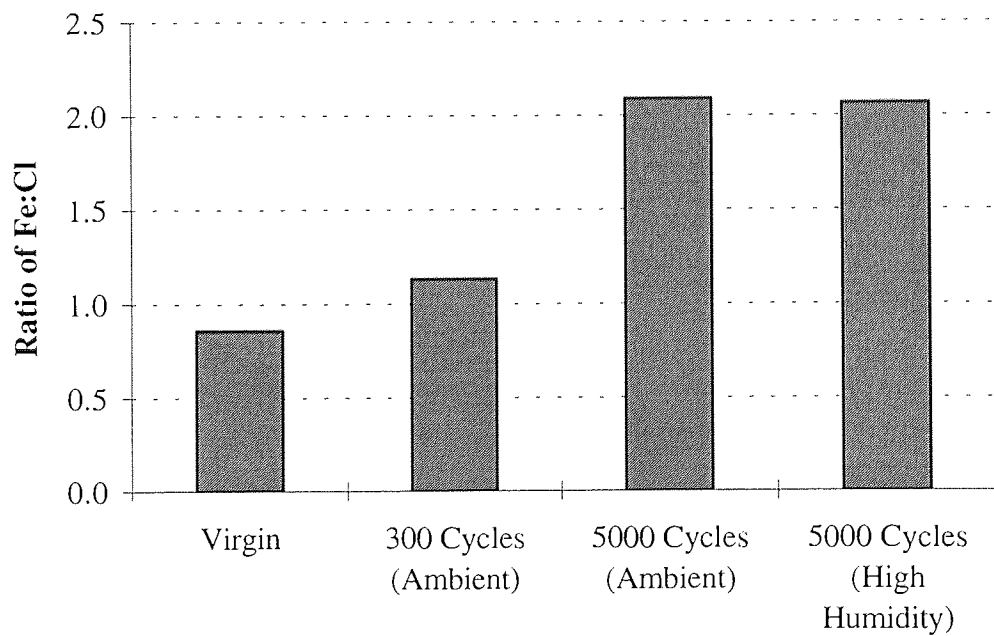
Figure 4.79 Ratio of Fe:Cl for Tape MP#1

Figure 4.80 and 4.81 show the ratio of Cl:C and N:C for tape MP#1 at virgin, 300 cycles

(ambient), 5000 cycles (ambient) and 5000 cycles (high humidity) conditions,

respectively.
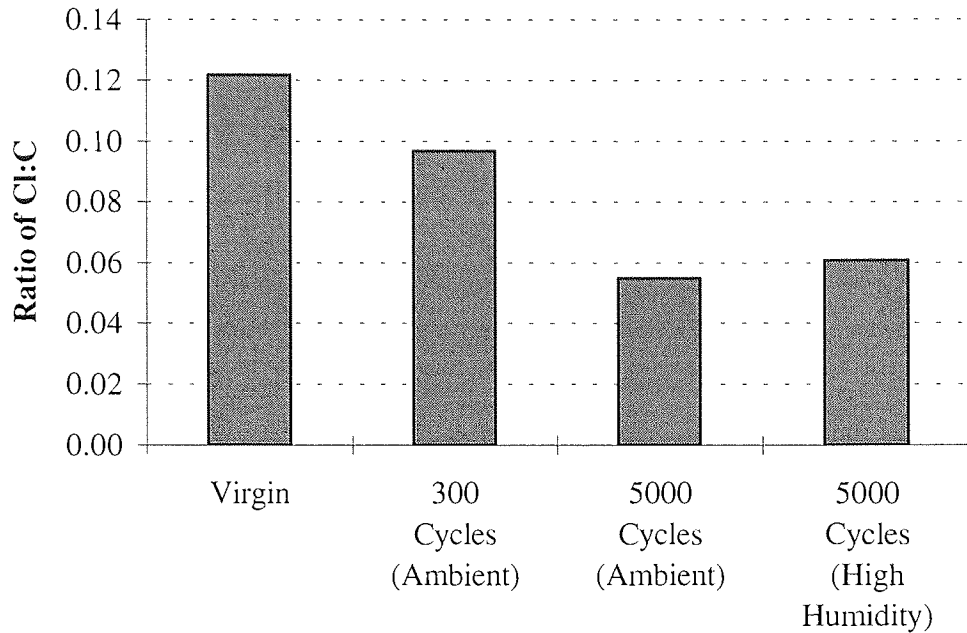
Figure 4.80 Ratio of Cl:C for Tape MP#1
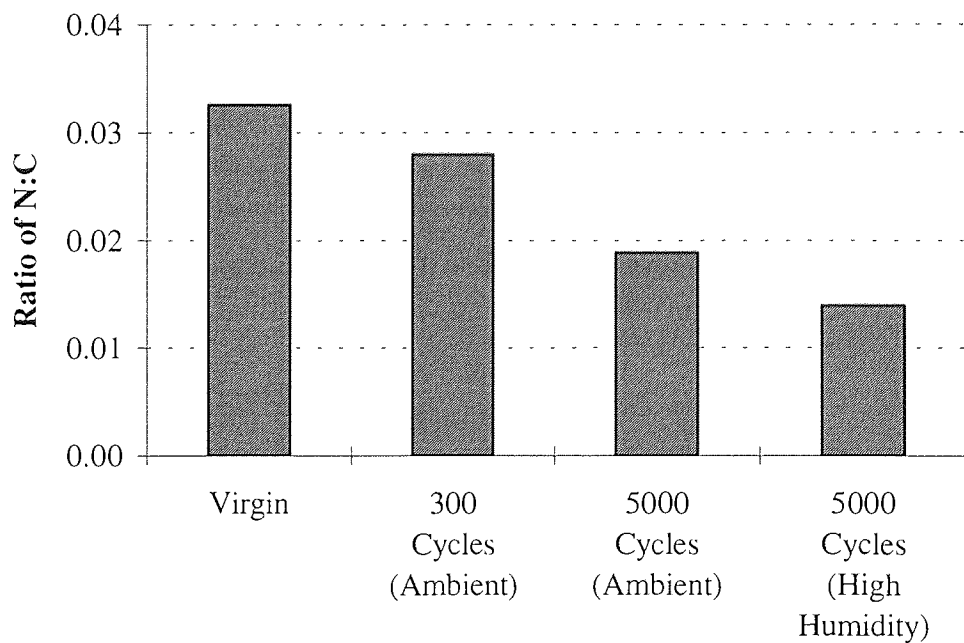
Figure 4.81 Ratio of N:C for Tape MP#1

4.4.2 Tape ME#1

In the case of thin film ME tapes, the results from the angle resolved XPS experiments can be considered to be valid at all analyser take-off angles due to the homogeneous nature and layered structure of the media. A change in the analyser take-off angle will alter the effective depth of analysis without introducing erroneous errors as in the case with particulate media.

The XPS elemental concentration profile of the near surface region of tape ME#1 as a function of take-off angle is shown in Figure 4.82.
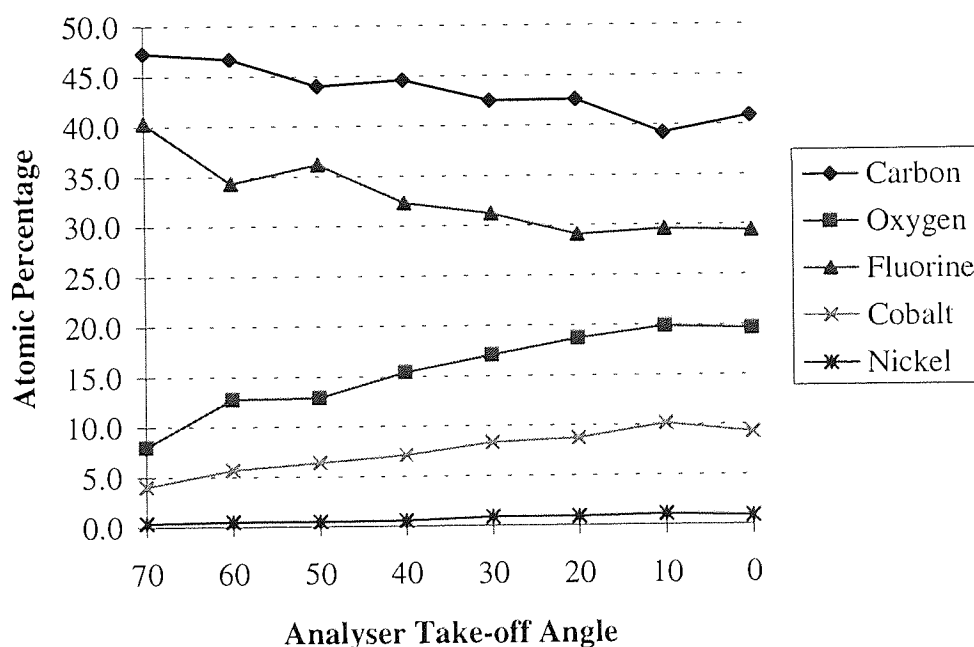
Figure 4.82 Integrated Concentration Profile of the Near Surface Region of Tape ME#1

In order to gain chemical state information, a peak synthesis routine was implemented on the spectra from a knowledge of expected binding energies and peak half widths. This procedure was conducted for the F 1s , O1s and C 1s photoelectron peaks. In the case

of F 1s, two chemical states were revealed as illustrated in Figure 4.83. The fluorine-

metal bond remained constant with increasing (relative to normal) analyser take-off angle

whereas the carbon-fluorine bond decreased.
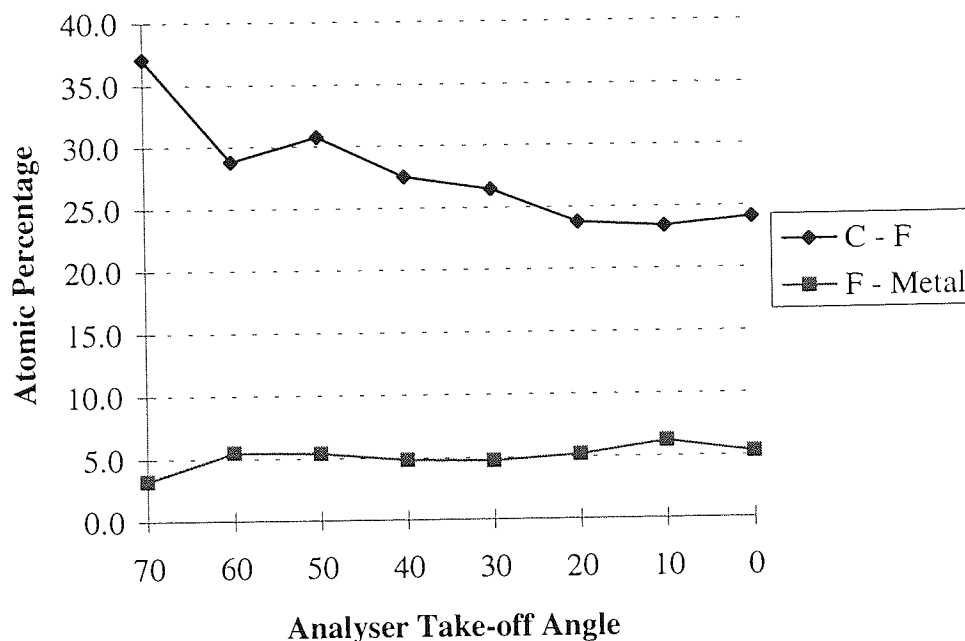
Figure 4.83 *Integrated Depth Profile of Fluorine Content at the Surface of Tape ME#1*

Following Synthesis of Fluorine ARXPS Spectra

Peak synthesis of the oxygen spectra at each analyser take-off angle enabled the different

chemical states of oxygen to be revealed, such as that illustrated in Figure 4.84. Peak O1

corresponded to the fluorine-oxygen bonds from the topical lubricant overlayer and the

presence of this peak was the major difference in shape between the oxygen spectra for

ME media and the oxygen spectra for tape MP#1. Peak O4, at a binding energy of 529.6

eV, corresponded to metal oxide bonds of CoO, NiO and Co_3O_4 since reference spectra

[129] confirmed each of these bonds could occur at a binding energy of 529.6 eV. It

was not possible to corroborate this peak assignment through synthesis of cobalt and

nickel spectra because the spectra were too noisy for accurate peak fitting. However,

the absence of any suitable alternative bonds at the same binding energy from elements

known to exist within the media was sufficient to conclude the original assignment to be

correct.
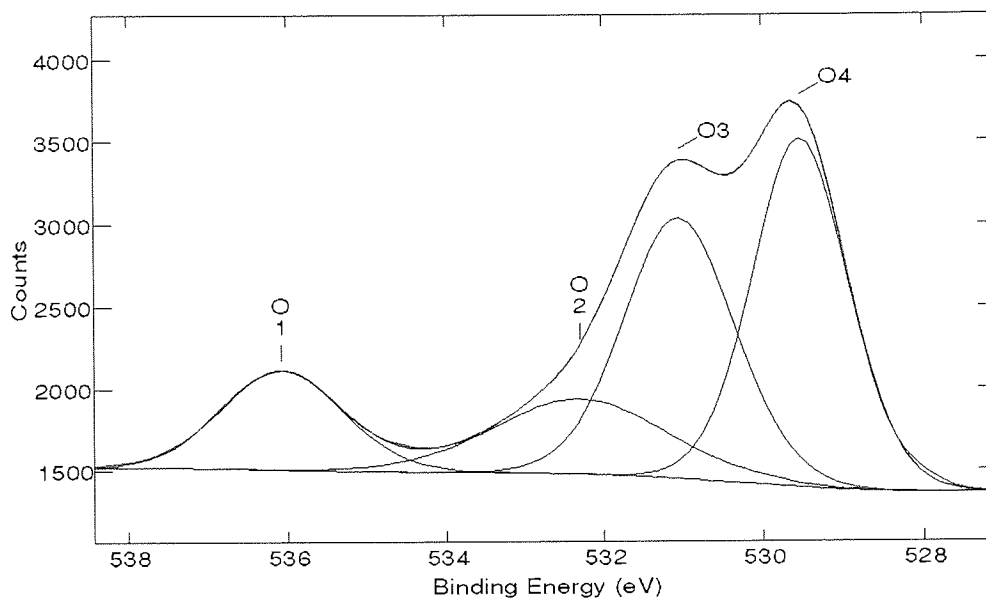
Figure 4.84 Synthesis of Oxygen Spectrum into Individual Peaks for Tape ME#1

Figure 4.85 shows the atomic percentage of metallic-oxygen in comparison to the

remaining oxygen bonds for tape ME#1 at increasing analyser take-off angles.   The

oxygen-metallic bonds contributed less to the total oxygen content in the near surface

region than the aggregate of the remaining oxygen peaks (organic oxide) although they

still formed a significant proportion of the total oxygen within the tape.
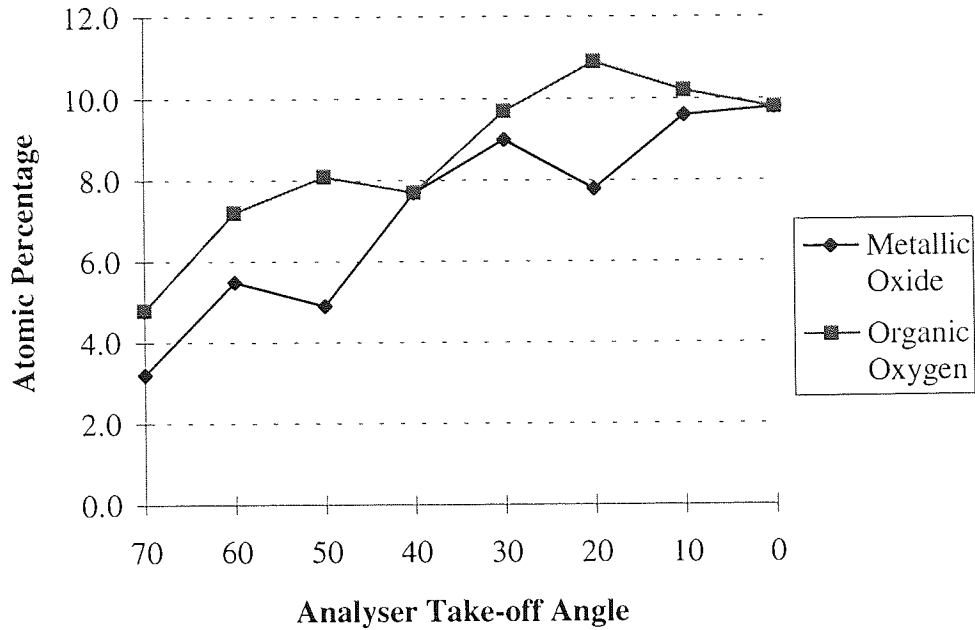
Figure 4.85 Integrated Depth Profile of Oxygen Content at the Surface of Tape ME#1

Following Synthesis of Oxygen ARXPS Spectra

Figure 4.86 shows a typical peak profile following synthesis of a carbon spectrum for

tape ME#1. Peaks C1 and C2 corresponded to fluorine bonds resulting from the

presence of a topical PFPE lubricant. These two peaks were used to establish the

proportion of fluorocarbon in the total carbon spectrum although in reality, far more

peaks would be needed for an exact fit of the fluorocarbon. The software used in the

synthesis of carbon limited the number of peaks to six and hence it was only possible to

use two peaks to fit the fluorocarbon energy range since the remaining four peaks were

needed to successfully allocate peaks to the lower energy range of the carbon spectrum

(291 eV - 281 eV). Indeed, in order to correctly synthesise the carbon spectrum for

Fomblin (a typical fluorocarbon lubricant), 5 peaks would need to be used in conjunction

with a high resolution XPS system [130].
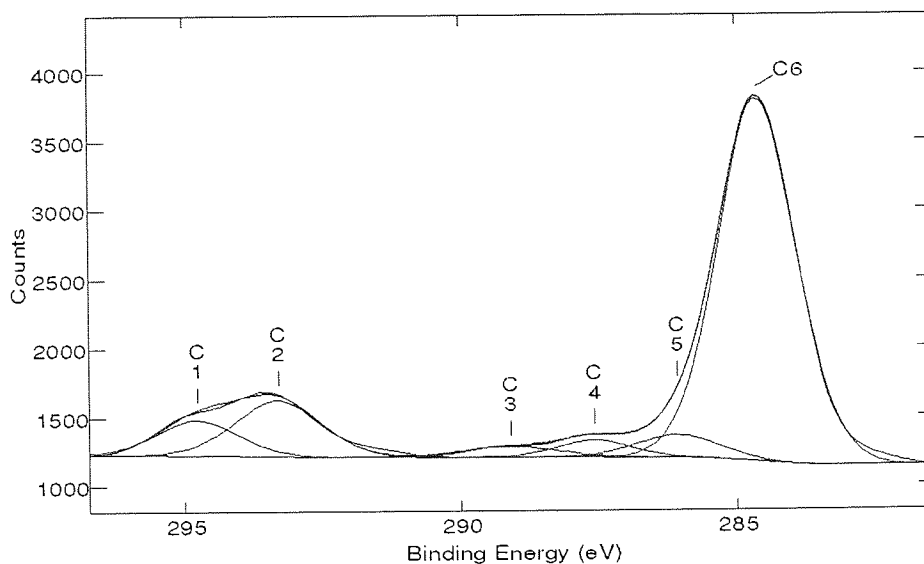
Figure 4.86 *Synthesis of Carbon Spectrum into Individual Peaks for Tape ME#1*

Figure 4.87 shows a profile of the atomic percentages of carbon bonds following synthesis of the carbon spectra for a virgin sample of tape ME#1 at different take-off angles. The fluorocarbon bonds decreased with take-off angle (increasing depth) whereas the other carbon bonds remained at almost constant levels irrespective of angle.

Figure 4.87 *Integrated Depth Profile of Carbon Content at the Surface of Tape ME#1*

Following Synthesis of Carbon ARXPS Spectra

4.4.3 Tape ME#2

The XPS elemental concentration variation with analyser take-off angle of the near surface region of tape ME#2 is shown in Figure 4.88. The atomic concentrations of fluorine and carbon were both at a maximum for an analyser take-off angle of 70° (shallowest depth) whereas oxygen and cobalt were most abundant at greater depths (smaller take-off angles). This was due to the layered structure of the tape with a fluorocarbon lubricant layer above the magnetic thin film.
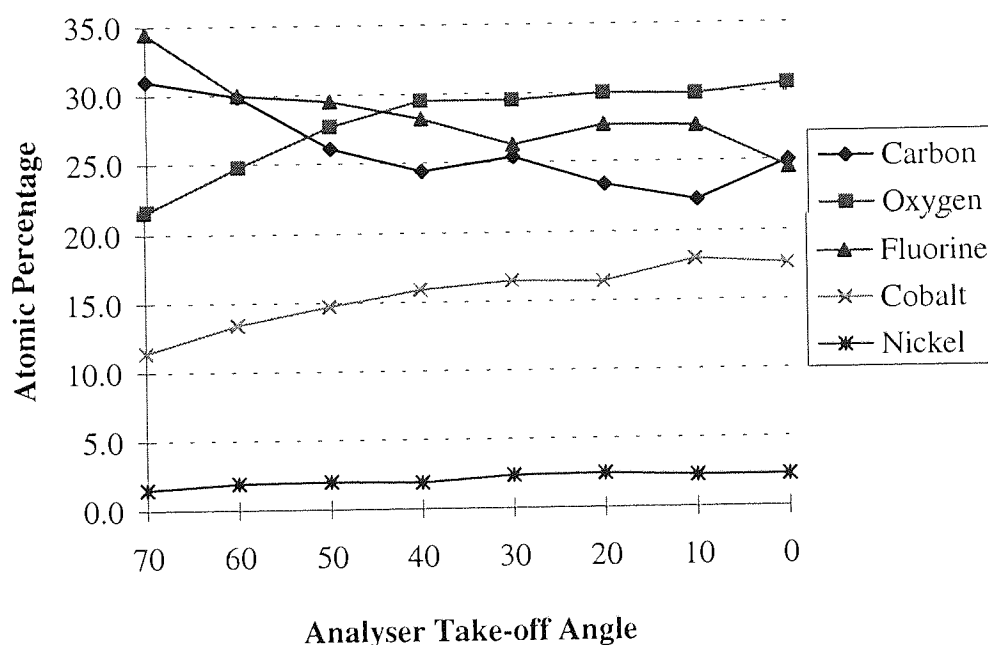
Figure 4.88 Integrated Concentration Profile of the Near Surface Region of Tape ME#2

The variation in fluorine content at the near surface region following peak synthesis is illustrated in Figure 4.89. Two different states were revealed with a fluorine-metal bond at a binding energy of 688.1 eV and a F - C component at 688.9 eV. The fluorine-metal bond contributed only a small amount towards the total fluorine spectrum since the F - C bond was approximately four orders of magnitude greater than the fluorine-metal bond. In addition, the atomic percentage of the fluorine-metal bond remained constant with increasing depth (decreasing angle) whereas the F - C bond decreased with increasing depth.
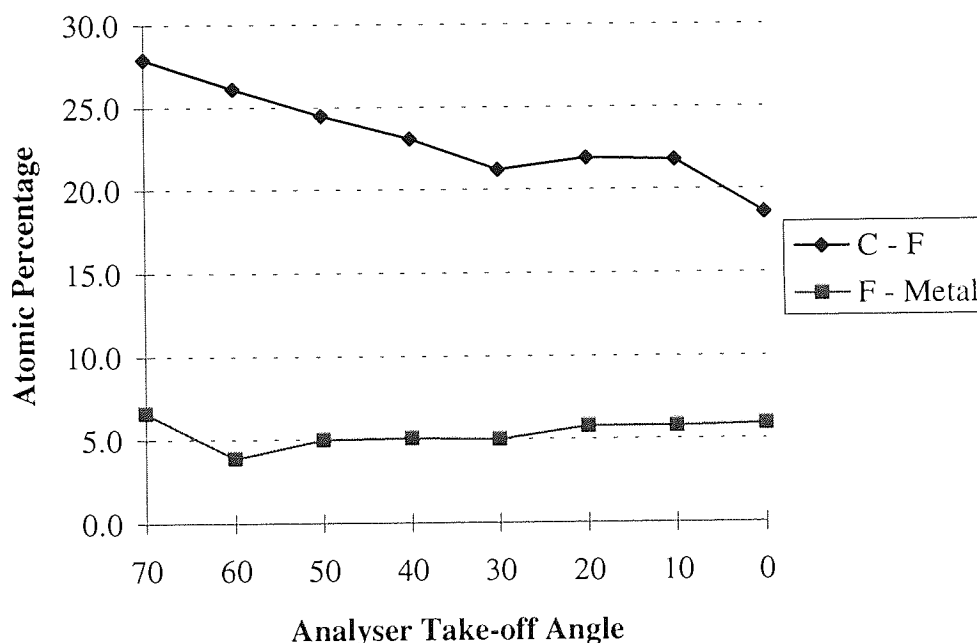
Figure 4.89 Integrated Depth Profile of Fluorine Content at the Surface of Tape ME#2 Following Synthesis of Fluorine ARXPS Spectra

Figure 4.90 shows the variation in oxygen content for tape ME#2 at decreasing take-off angles (increasing integrated depths). There is more organic oxide than metallic oxide at each depth although the difference between the two diminishes with increasing depth. This is to be expected because any metallic oxide bonds should only be present in the sub-surface magnetic layer.
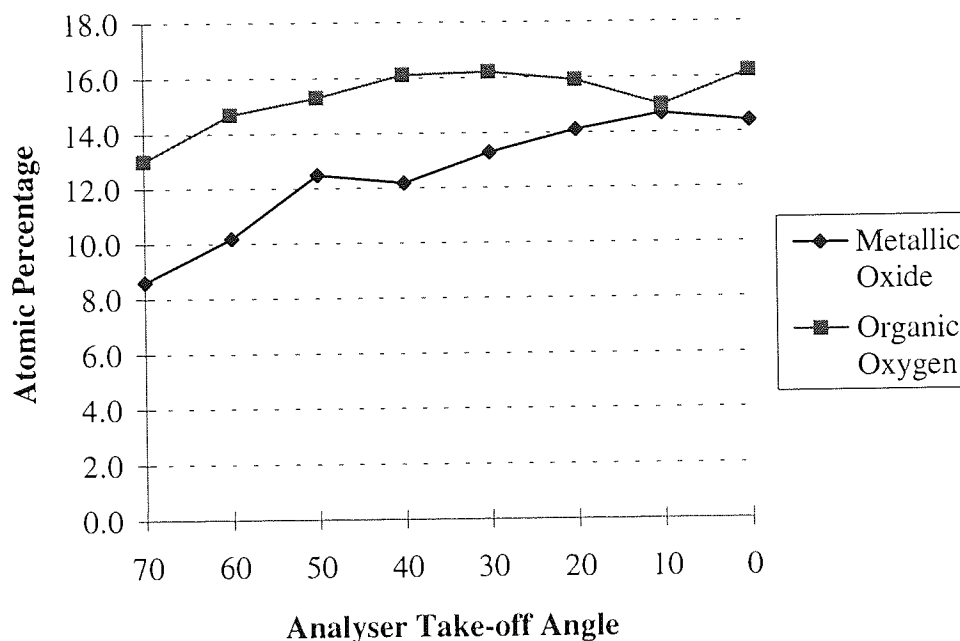
Figure 4.90 *Integrated Depth Profile of Oxygen Content at the Surface of Tape ME#2*

Following Synthesis of Oxygen ARXPS Spectra

Synthesis of the carbon spectra enabled an integrated depth profile of the carbon bonds

in the near surface region of tape ME#2 to be established. As Figure 4.91 shows, the

general trend of the C-C/C-H and fluorocarbon bonds was similar with each bond

decreasing with analyser take-off angle (increasing depth).

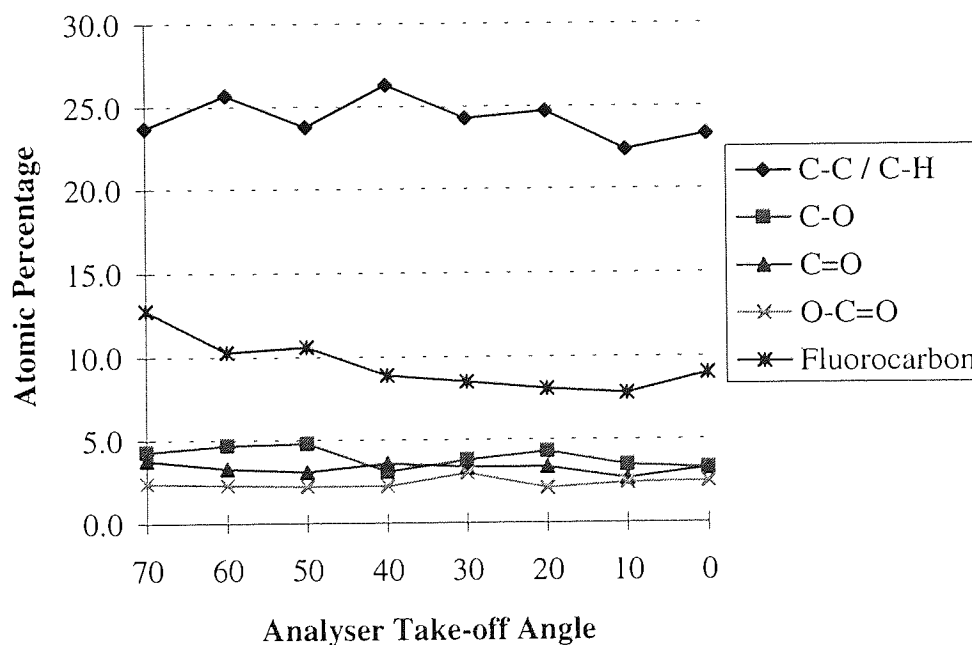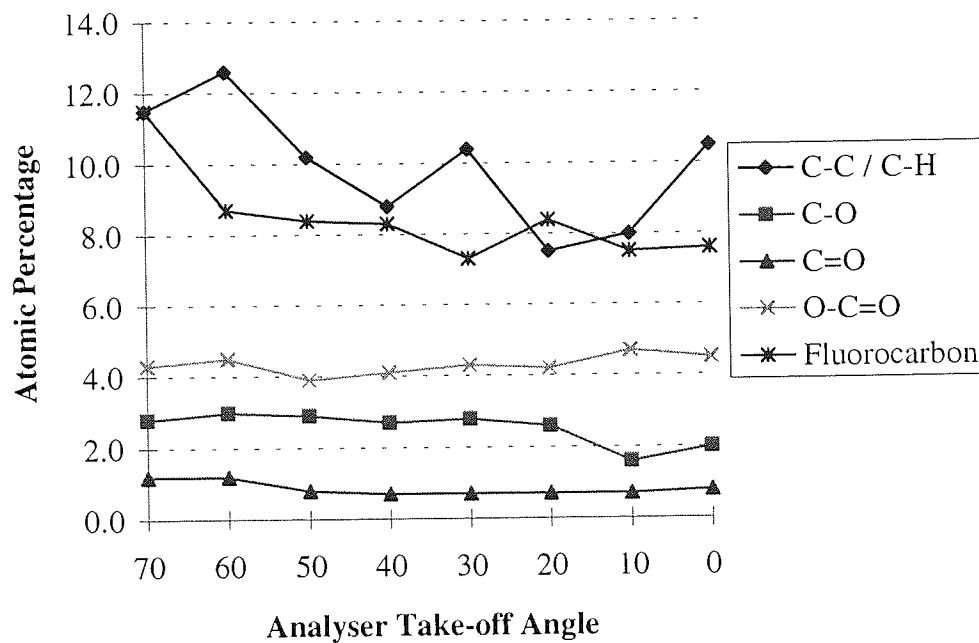*Figure 4.91* *Integrated Depth Profile of Carbon Content at the Surface of Tape ME#2*

Following Synthesis of Carbon ARXPS Spectra

4.4.4 Tape ME#3

Profiles of atomic concentration as a function of analyser take-off angle for virgin and

cycled samples of tape ME#3 are illustrated in Figures 4.92 and 4.93 respectively. The

worn tape had been cycled for 450 cycles at ambient conditions and this corresponded to

catastrophic dropout growth during cycling durability tests.
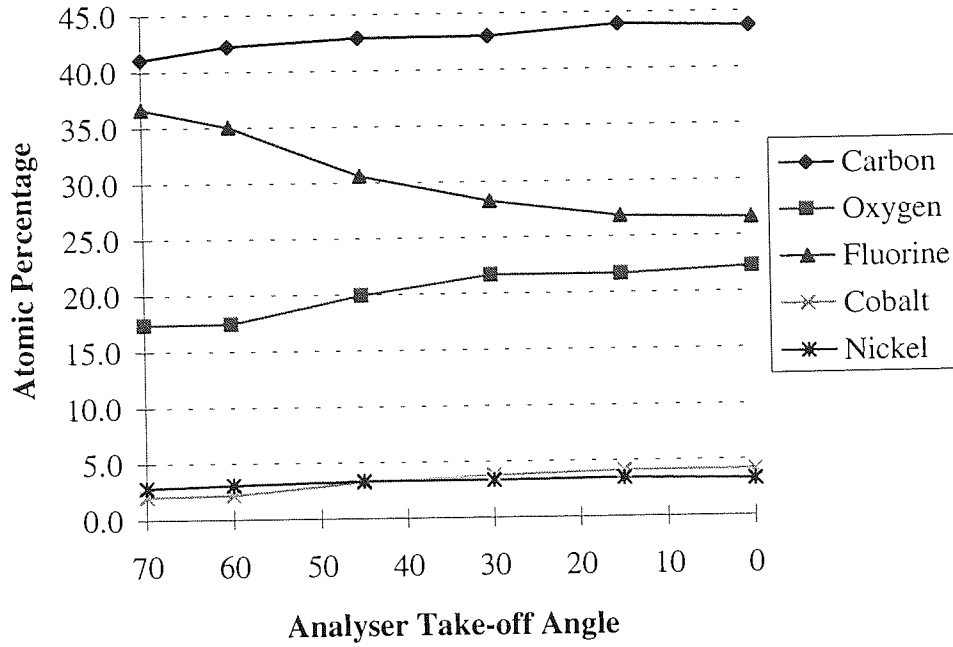
Figure 4.92 *Integrated Concentration Profile of the Near Surface Region of Virgin Tape ME#3*
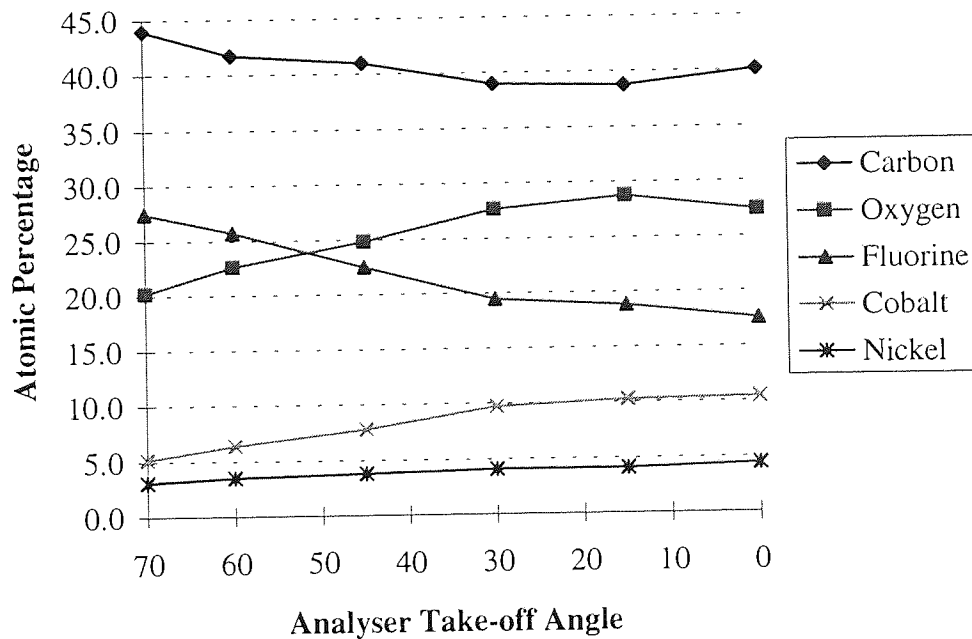
Figure 4.93 *Integrated Concentration Profile of the Near Surface Region of Cycled Tape ME#3*

Peak synthesis of the oxygen spectra enabled the atomic percentage of the F-oxygen and metal-oxygen bonds to be individually determined. The F-oxygen bonds, possibly $H_4C_5O_3F_6$, corresponded to peak O1 (re: Figure 4.84), at a binding energy of 535.7 eV whereas the metallic-oxygen bonds corresponded to peak O4 at 529.9 eV, as listed in Table 4.1. The values for the FWHM and centre energy of these two peaks were maintained for each analyser take-off angle in order to give accurate synthesis results. It was necessary to give a little freedom when allocating FWHM's to peaks O2 and O3 since these did not correspond to specific bonds but were used to ensure the whole spectrum was completely fitted. This allowed correct proportions of the bonds corresponding to O1 and O4 to be determined and ultimately to the correct atomic percentage for each specified bond.

Peak	Centre Energy (eV)	FWHM (eV)
O1 (F - Oxygen)	535.7	1.9
O2	533.2	2 - 2.8
O3	531.6	1.9 - 2.1
O4 (FeO, Fe_2O_3)	529.9	1.6

Table 4.1 Values used in the Peak Synthesis of the Oxygen Spectra for Tape ME#3

Figure 4.94 shows the variation of the F-oxygen bonds with analyser take-off angle for virgin and cycled tape ME#3. Each analysis confirmed a reduction had occurred in the percentage of F-oxygen bonds after catastrophic dropout growth at 450 cycles.
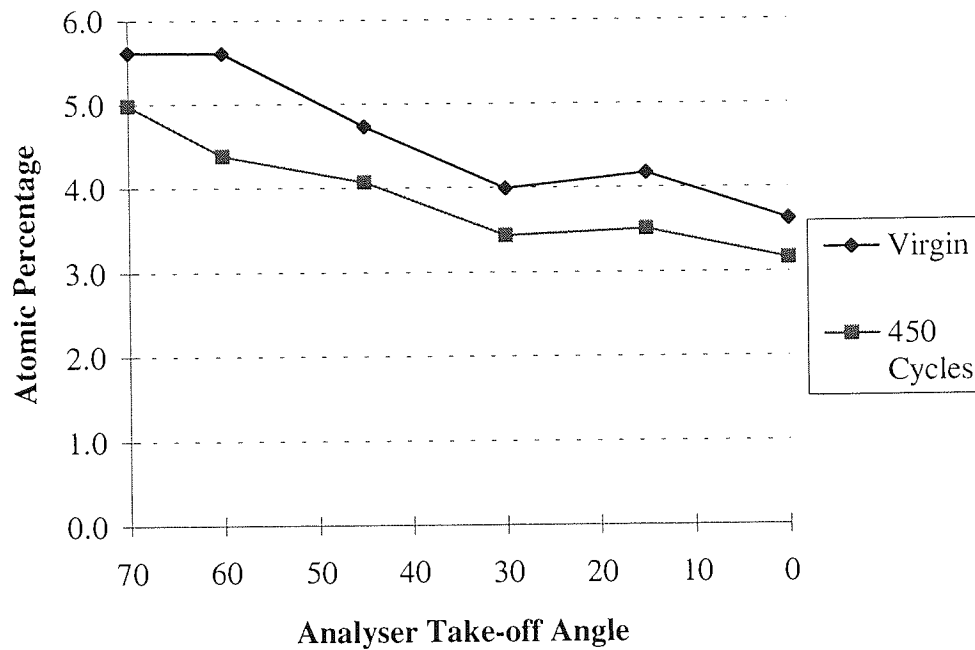
Figure 4.94 *Variation in F-oxygen Bonds with Analyser Take-off Angle*

for Virgin and Cycled ME#3 Tape

Figure 4.95 shows the variation in metal-oxygen bonds with analyser take-off angle for tape ME#3 in virgin state and after 450 cycles. The percentage of metal-oxygen bonds was greater at the surface of the virgin tape than for the cycled tape and the difference between the two tapes increased as the analyser take-off angle was reduced to zero (maximum depth).
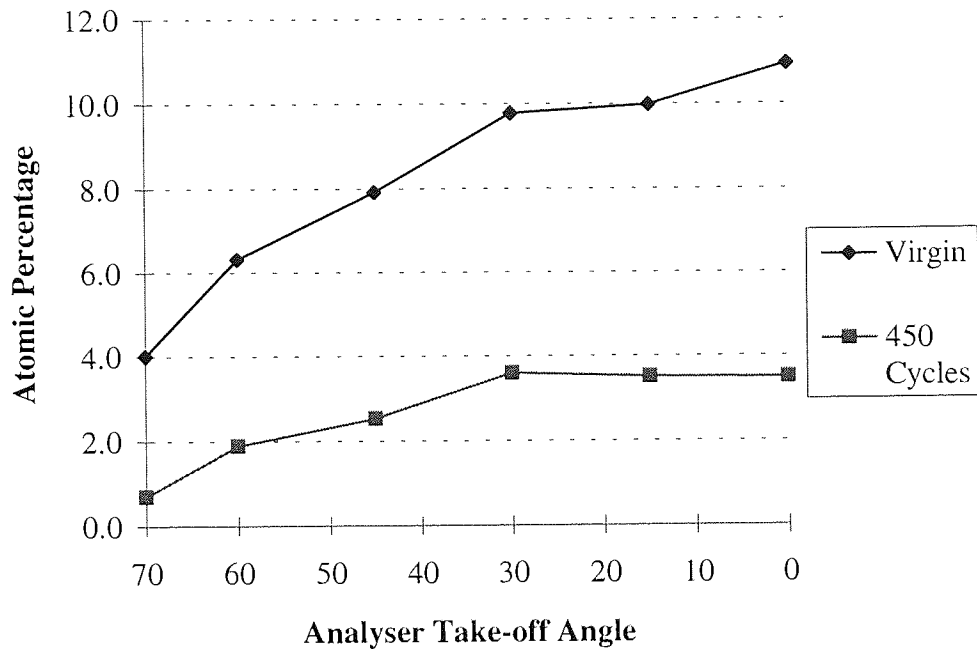
Figure 4.95 Variation in Metal-Oxygen Bonds with Analyser Take-off Angle
for Virgin and Cycled ME#3 Tape

4.4.5 Comparisons between Tapes ME#1, ME#2 and ME#3

As with the results from XPS analysis of tape MP#1, it is better to compare the ratio of one element to another rather than by simple comparison of measured relative atomic concentrations. Figure 4.96 shows the ratio of F:Co at $0°$ take-off angle (normal to the analyser) for the 3 virgin ME tapes and tape ME#3 at 450 cycles. It can be deduced that of the three virgin tapes, tape ME#3 had the greatest thickness of lubricant (including DLC layer in the case of tape ME#3) covering the magnetic layer since the ratio of F:Co was at a maximum for this tape. In the case of the worn tape, the ratio of F:Co was substantially lower than for the corresponding virgin tape, indicating that either the cobalt content had increased (unlikely), or the thickness of the protective overlayer (lubricant and DLC layer) had decreased (likely).
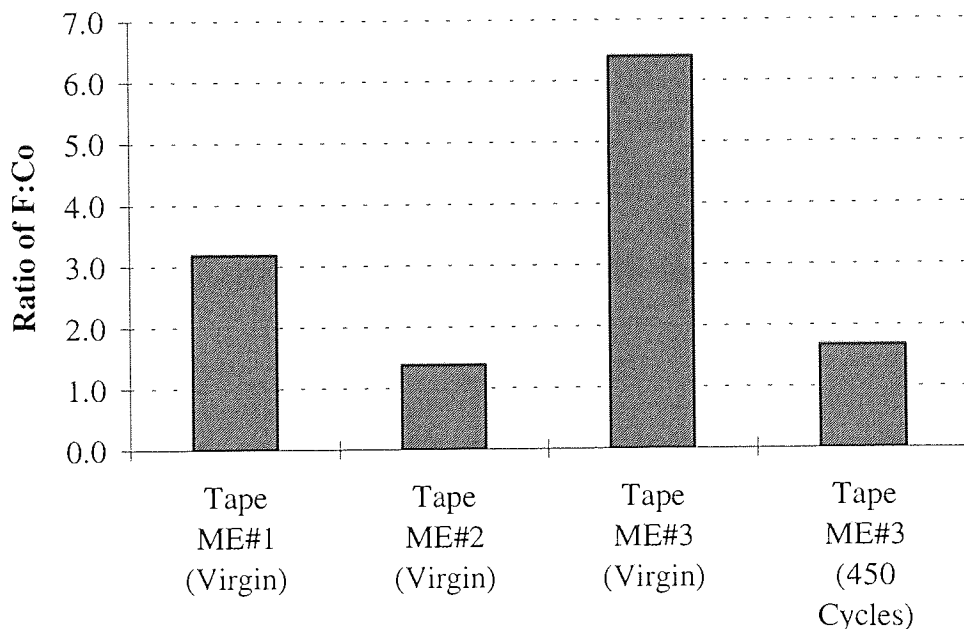
Figure 4.96 Ratio of F:Co for ME Tapes

The ratio of C:Co for each of the different ME tape samples is shown in Figure 4.97.

The C:Co ratio was greatest for virgin ME#3 tape but it then decreased significantly after

450 cycles. This reduction was possibly due to a decrease in the protective overlayer

thickness since this would have enabled more characteristic photoelectrons from the

magnetic layer to be detected during XPS analysis. Tape ME#2 had the lowest ratio

value and thus possibly the thinnest lubricant covering.
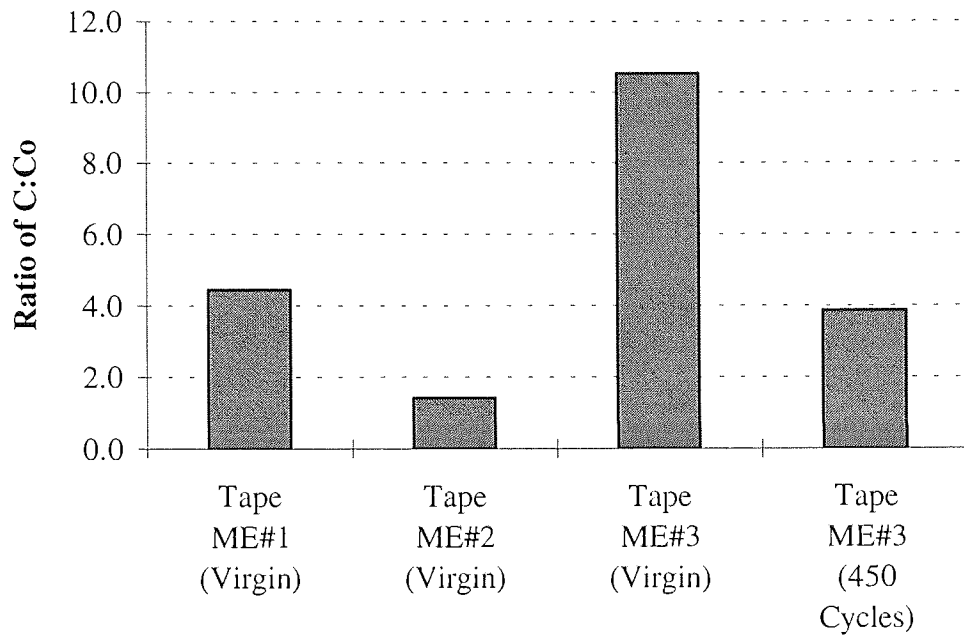
Figure 4.97 *Ratio of C:Co for ME Tapes*

Figure 4.98 shows the two chemical states of fluorine for tapes ME#1 and ME#2. The percentage of the F - metal bond in each tape is approximately the same but in the case of the F - C component, tape ME#1 has a greater proportion than tape ME#2. This may simply be the result of a greater perfluorpolyether film thickness on tape ME#1, but could also suggest a greater proportion of mobile component present on the surface of tape ME#1.
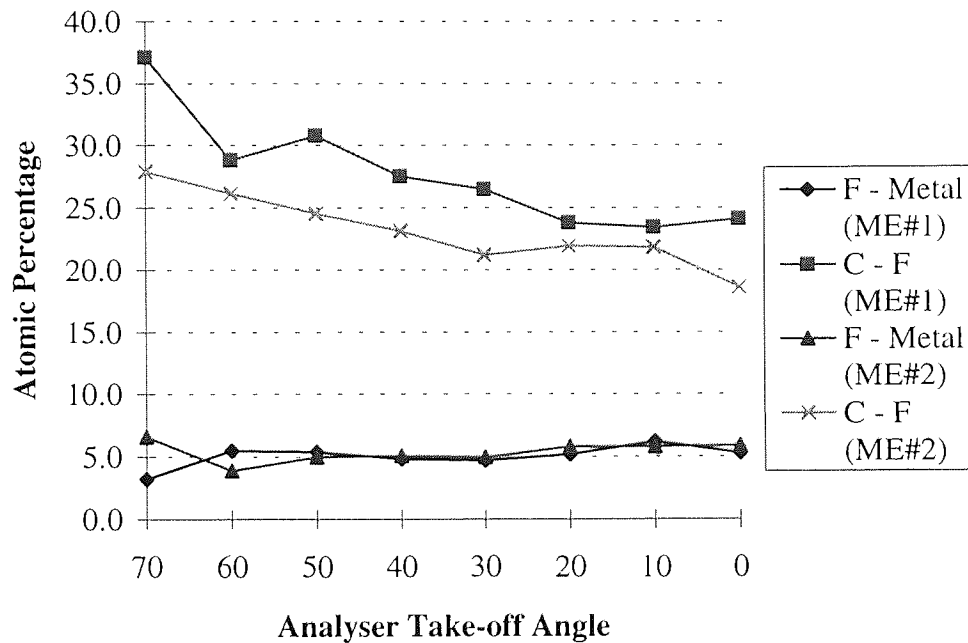
Figure 4.98 *Integrated Depth Profile of Fluorine Content at the Surface of Tapes ME#1 and ME#2*

Following Synthesis of Fluorine ARXPS Spectra

XPS was used to analyse the scars on tapes ME#1 and ME#2 after stop motion test failure whilst further analysis was performed on virgin tapes under identical experimental conditions. This enabled any changes in the concentration of elements to be determined, as illustrated in Figures 4.99 and 4.100 for tapes ME#1 and ME#2 respectively. The analysed area was 150 μm compared with a typical wear scar width of 120 μm and the stop motion tests were performed at ambient conditions (40% RH, $25^{\circ}C$).
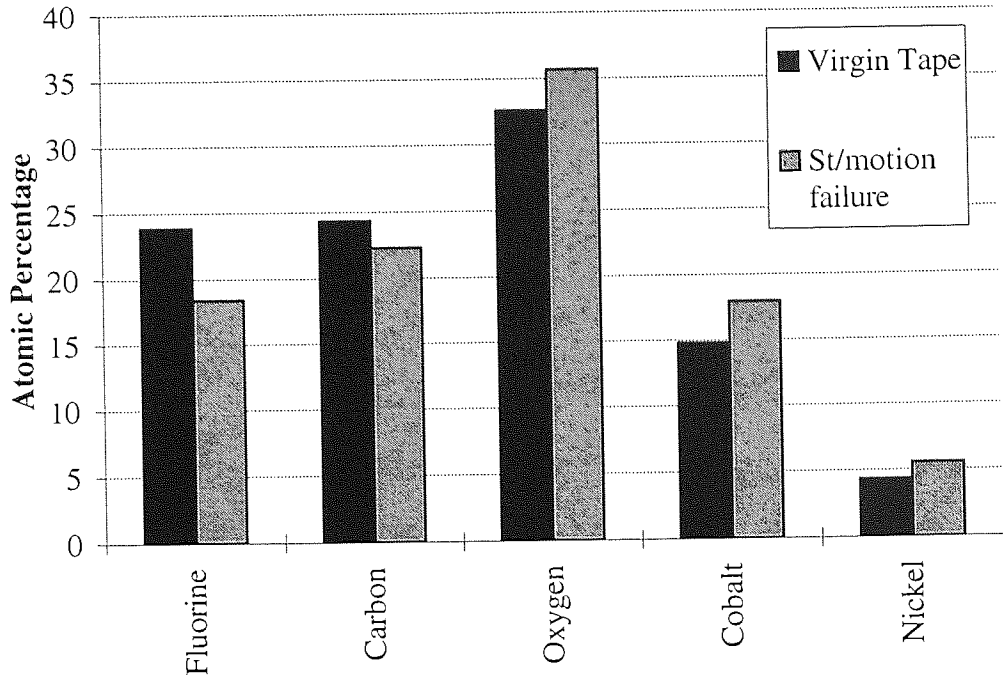
Figure 4.99 *Relative Concentration of Elements on Stop Motion Failure Scar*

and Corresponding Virgin ME#1 Tape
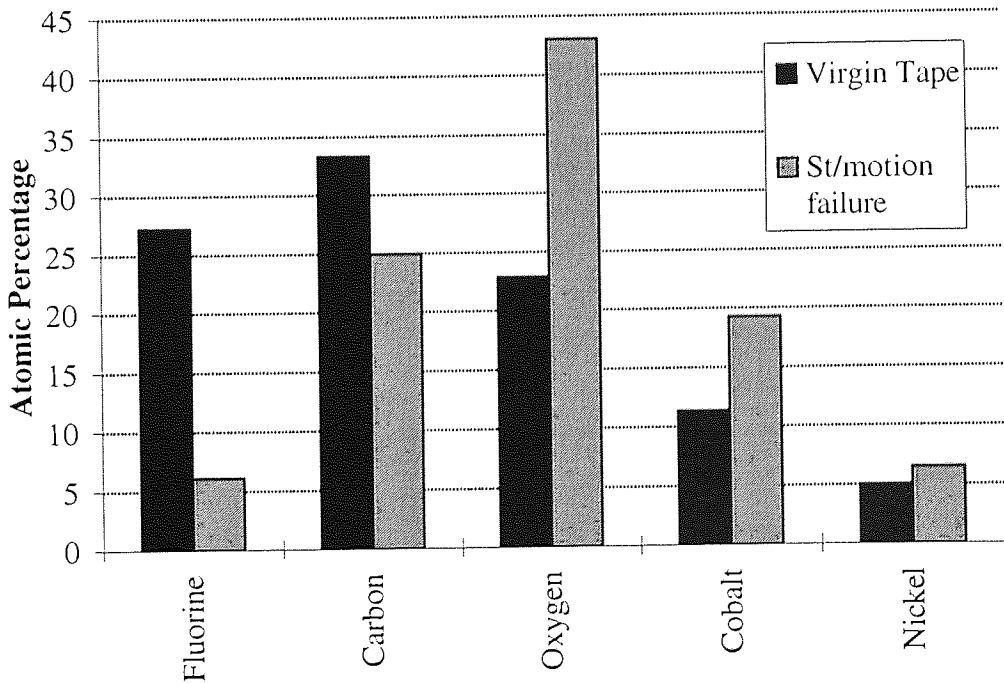
Figure 4.100 *Relative Concentration of Elements on Stop Motion Failure Scar*

and Corresponding Virgin ME#2 Tape

4.5 Results of SIMS Analysis

4.5.1 Tape ME#1

Static SIMS experiments were used to gain information regarding the lubricant type on tapes ME#1 and ME#2. The SIMS spectra obtained from tape ME#1 had characteristic peaks which showed good correlation with Z-deal and Z-dol reference spectra [131]. Figures 4.101 - 4.102 show the spectra for tape ME#1 for 0 - 100 amu and 100 - 200 amu respectively. There was an unusually high peak (1.5×10^4 counts per second) at a mass of 59 which could not be entirely attributed to the presence of cobalt. Part of this peak must have been due to the lubricant end-group of the form

$$CH_2- \underset{\underset{OH}{|}}{C} = O$$
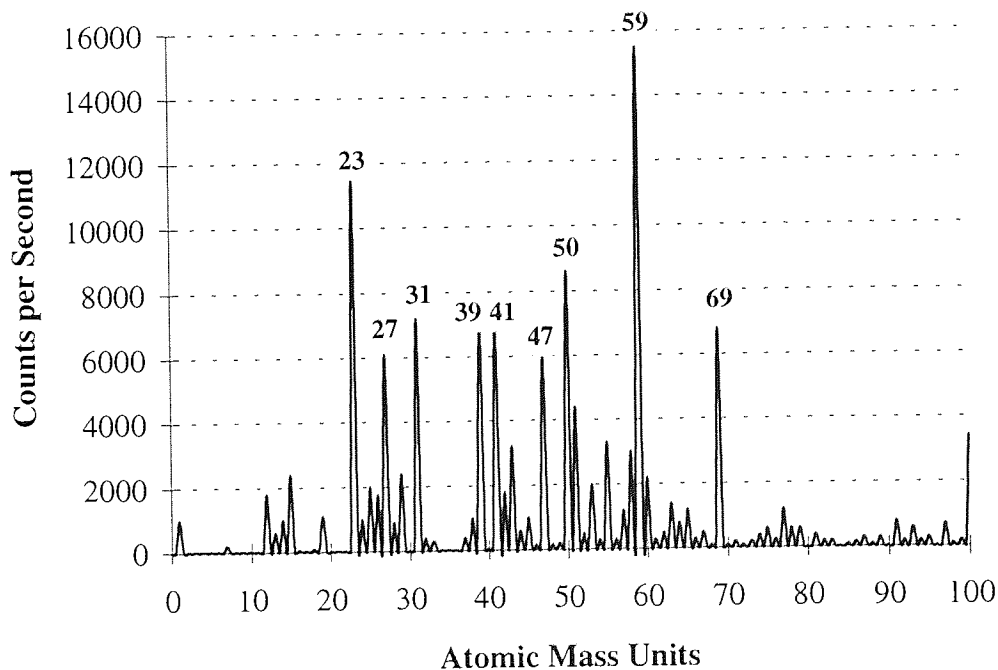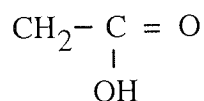
Figure 4.101 Positive SIMS Spectrum for Tape ME#1 (0 - 100 amu)
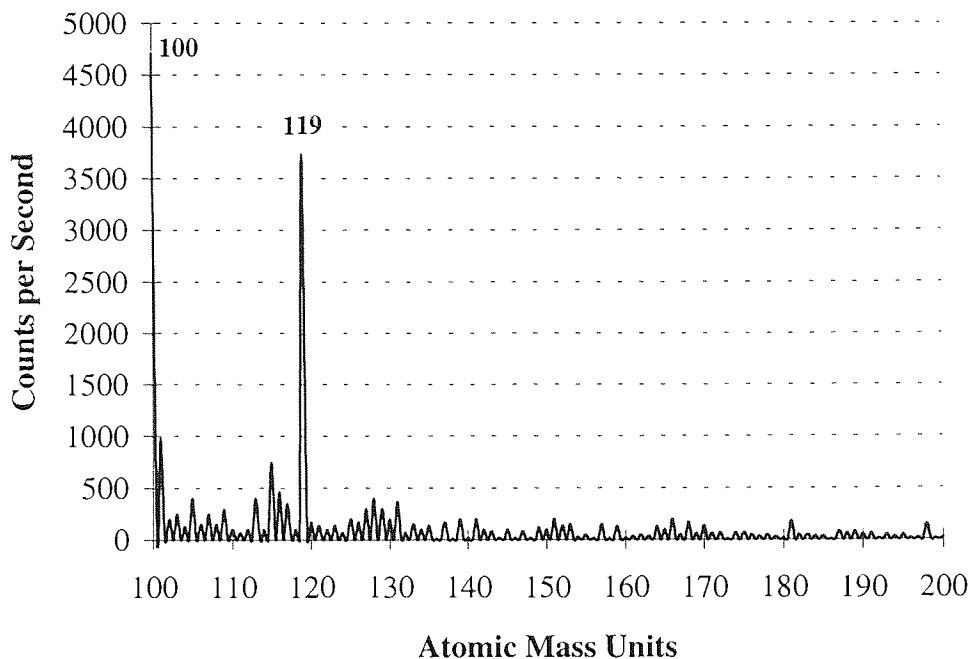
Figure 4.102 *Positive SIMS Spectrum for Tape ME#1 (100 - 200 amu)*

4.5.2 Tape ME#2

The spectra for tape ME#2, collected under identical conditions, again showed the existence of a relatively large peak at mass 59 (see Figure 4.103), similar to that for tape ME#1. However, as Figure 4.104 illustrates, peaks at masses of 131, 150 and 169 were also present in the spectra and this was not consistent with those of tape ME#1, but correlated closely to that of a Krytox type lubricant, with a backbone structure of the same as Krytox 157 [131]

$$CF_2 - CF - O$$
$$|$$
$$CF_3$$

245
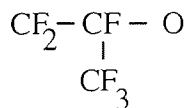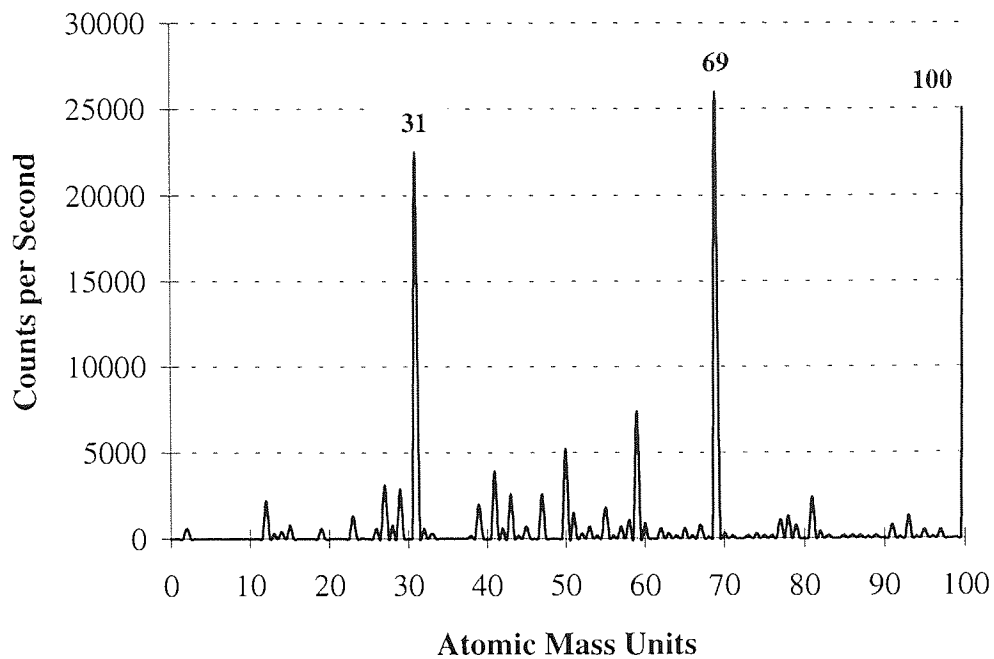
Figure 4.103 Positive SIMS Spectrum for Tape ME#2 (0 - 100 amu)
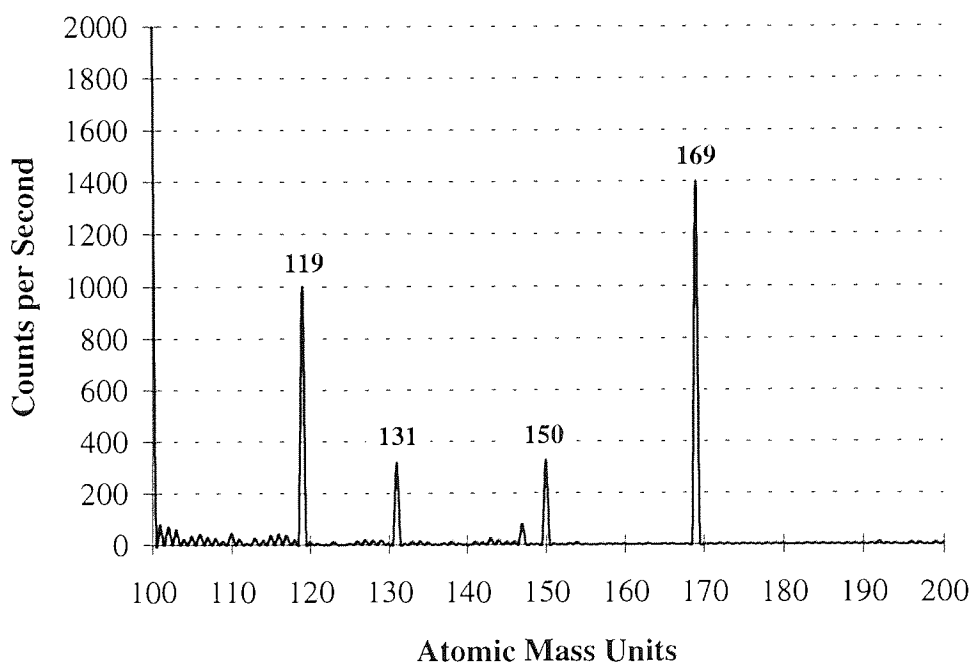
Figure 4.104 Positive SIMS Spectrum for Tape ME#2 (100 - 200 amu)

4.6 Lubricant Thickness Measurements

Several models were described in Chapter 3 which could be used to determine the thickness of the topical lubricant on a thin film ME tape. In this section, the results from XPS analysis on tapes ME#1 and ME#2 are applied to a selection of the best models in order to ascertain the effectiveness of each model for determining the lubricant thickness.

In addition, the relative thickness of the overlayers covering the magnetic pigment in tape MP#1 will be determined by assuming an exponential attenuation of characteristic photoelectrons in overlayers above the magnetic pigment.

4.6.1 Uniform Lubricant Layer Models

The uniform lubricant layer described by Briggs and Seah [102] has been used to determine the thickness of the lubricant layer on tapes ME#1 and ME#2. Equation 3.5 suggested a graph of $\ln I_M$ against $1/\cos\theta$ would have a gradient of $-(d_L/\lambda_L)$ where d_L is the thickness of the lubricant layer and λ_L is the attenuation length of photoelectrons escaping from the magnetic film and through the lubricant layer. In this case, cobalt was used as the characteristic photoelectrons since cobalt was the most abundant element in the magnetic film and thus would provide the best signal to noise ratio. Graphs of $\ln I_M$ against $1/\cos\theta$ are shown in Figures 4.105 and 4.106 for tapes ME#1 and ME#2 respectively.
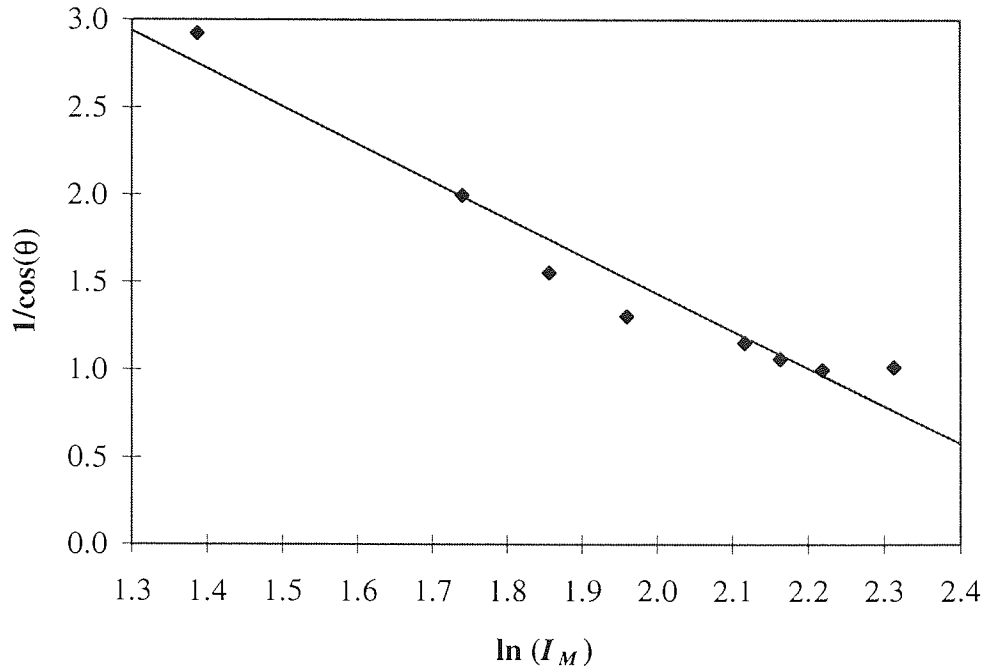
Figure 4.105 *Determination of Lubricant Thickness on Tape ME#1*

based on Uniform Model by Briggs and Seah
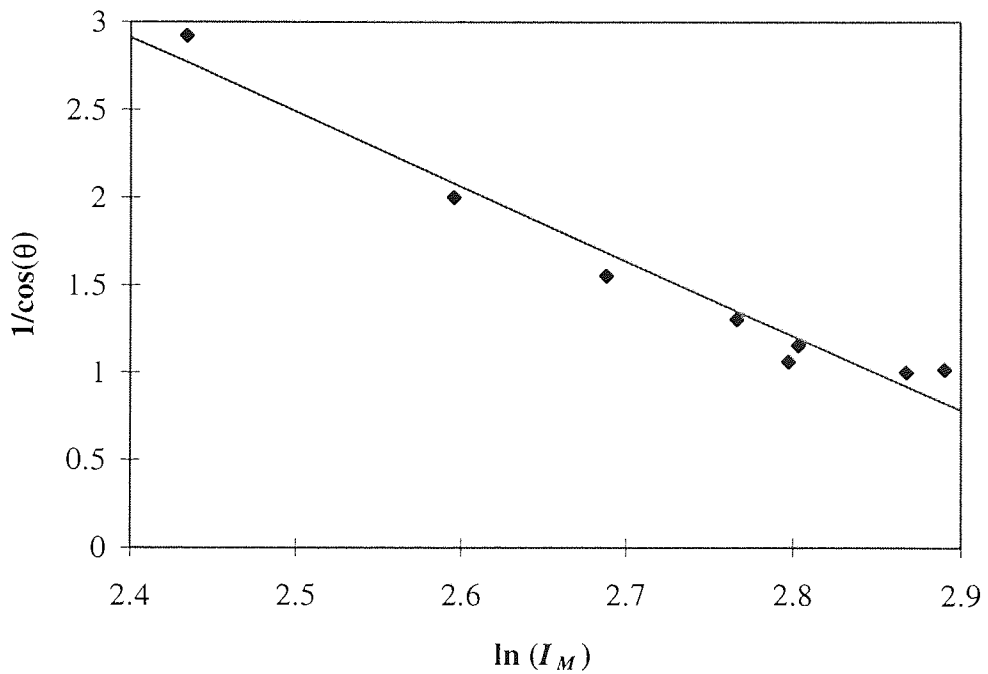
Figure 4.106 *Determination of Lubricant Thickness on Tape ME#2*

based on Uniform Model by Briggs and Seah

The plot for tape ME#1 had a gradient of -4.3 (r^2=0.98, Standard Error=0.13) whereas

for tape ME#2, the gradient was calculated to be -2.1 (r^2=0.97, Standard Error=0.17). If

however, the grazing angle of 70° is ignored the gradient of the lines of best fit for tapes

ME#1 and ME#2 are -3.5 (r^2=0.98, Standard Error=0.10) and -1.7 (r^2=0.96, Standard

Error=0.13) respectively. Assuming the attenuation length of cobalt when covered by an

organic lubricant layer is 1.9 nm, the thickness of the lubricants on tapes ME#1 and

ME#2 were calculated to be as listed in Table 4.2.

	Lubricant Thickness (nm)	
	ME#1	ME#2
Using Angles 0° - 70°	8.2	4.0
Using Angles 0° - 60°	6.7	3.2

Table 4.2 Thickness of Lubricants on Tapes ME#1 and ME#2,

based on Uniform Lubricant Layer Model by Briggs and Seah

A second uniform model for determining the lubricant thickness [103], based on

Equation 3.11 suggests a graph of $\ln\left(\dfrac{(I_L/I_M)}{k}+1\right)$ against $\dfrac{1}{\cos\theta}$ will be a linear plot

with a gradient of d_L/λ_L. I_L and I_M were atomic concentration percentages of fluorine and

cobalt characteristic photoelectrons, respectively. Equation 3.10 defined k as

$$k = \frac{S(E_L,\theta)\sigma_L n_L \lambda_L}{S(E_M,\theta)\sigma_M n_M \lambda_M}$$

Attenuation length of photo-electrons (lubricant), λ_L = 1.9 nm

Attenuation length of photo-electrons (metal), λ_M = 1.9 nm

Spectrometer detection efficiency (lubricant), $S(E_L,\theta)$ = 0.78 [132]

Spectrometer detection efficiency (metal) $S(E_M,\theta)$ = 0.87 [132]

Photo-ionization cross section (lubricant), σ_L = 4.43 [133]

Photo-ionization cross section (metal), σ_M = 12.62 [133]

Atomic density of element (lubricant), n_L = 1696 kgm^{-3}

Atomic density of element (metal), n_M = 8900 kgm^{-3}
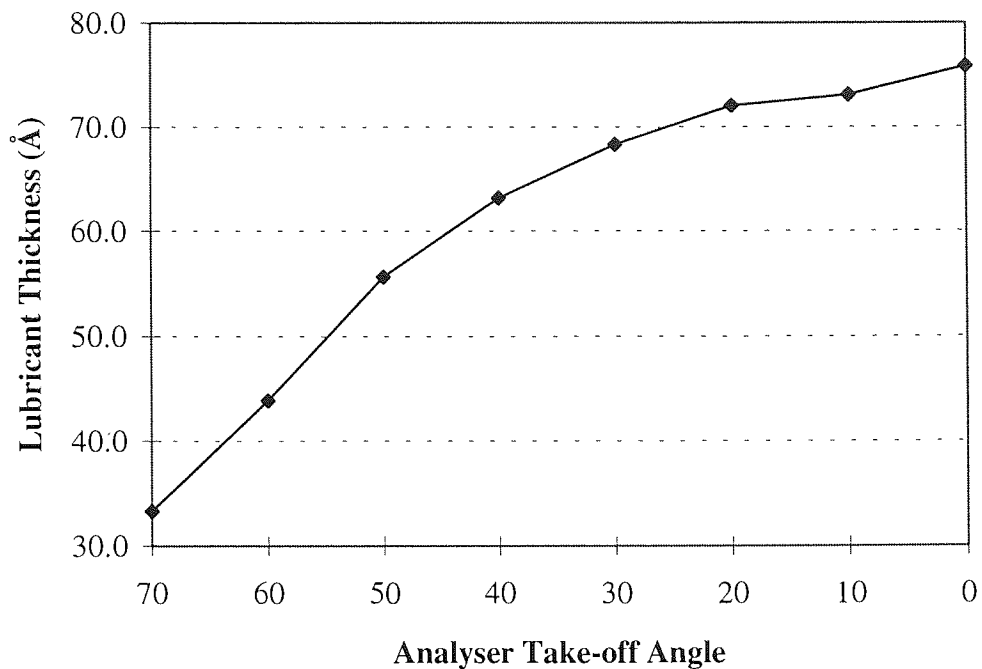
Figure 4.107 Determination of Lubricant Thickness on Tape ME#1

based on Uniform Model by Kimachi [103]
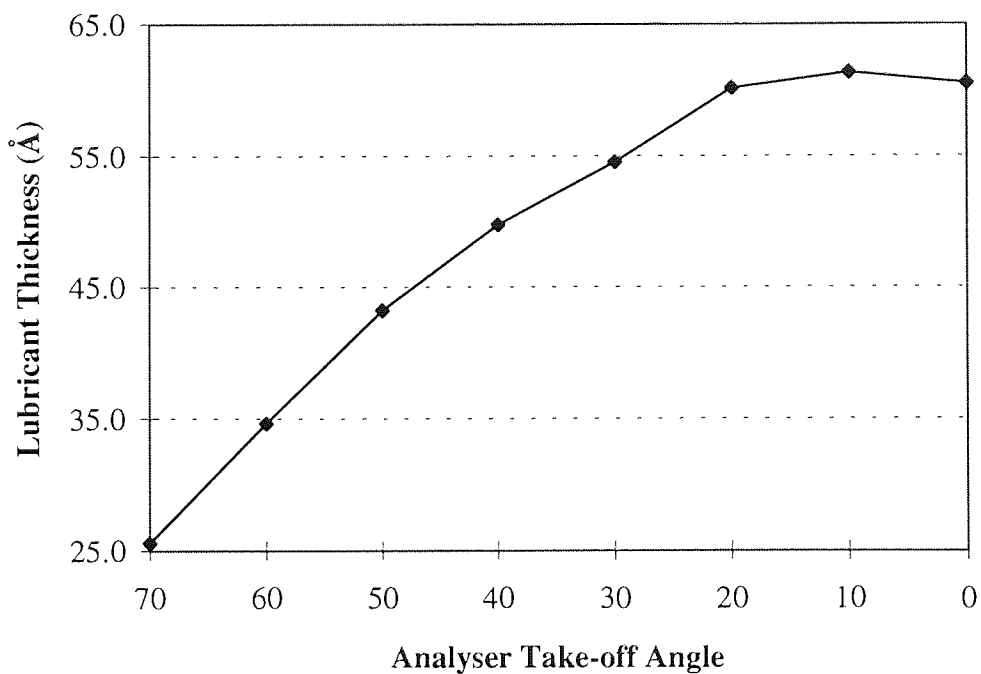
Figure 4.108 Determination of Lubricant Thickness on Tape ME#2

based on Uniform Model by Kimachi [103]

The results from the Kimachi uniform model, illustrated in Figures 4.107 and 4.108 for tapes ME#1 and ME#2 respectively, indicated the lubricant thickness was a function of take-off angle for tapes ME#1 and ME#2. Thus, it can be concluded that the Kimachi uniform model does not provide an accurate method of calculating the lubricant thickness on thin film media.

Linder and Mee [105] suggested a uniform model for calculating the thickness of a lubricant on a magnetic thin film disk. This model could have been easily adapted for thin film ME media since each has a layered structure. However, the model required analysis of the sample without a lubricant in order for the signal from the magnetic film to be quantified. The only way of achieving this with commercial samples was to remove the lubricant prior to XPS examination. However, the application of Hexane to the surface of ME media samples was not successful in removing the lubricant layer and stronger solvents left the tape surface with a patchy appearance. Thus, it was not possible to remove the lubricant in a controlled manner and hence the Linder and Mee model could not be evaluated with any confidence.

4.6.2 Reconstruction of Depth Profiles from ARXPS Data

The routine developed by Livesey and Smith [112] for reconstructing depth profiles from ARXPS data was tested on tapes ME#1 and ME#2. The routine required the user to describe a prior model for the sample surface in order for the algorithm to have a good starting point. In the case of the ME tapes, the top surface layer was assumed to consist of fluorine, carbon and oxygen in equal quantities whereas the base material was deemed to comprise of cobalt (64%), nickel (16%) and oxygen (20%). Values for the attenuation length of carbon, fluorine, oxygen, cobalt and nickel were defined as 2.6, 1.9, 2.2, 1.9 and 1.7 nm respectively. Given this basic information, it was possible to use the algorithm to reconstruct a depth profile from XPS data at a series of increasing analyser

take-off angles. A profile reconstructed in this manner from data for tape ME#1 is
shown in Figure 4.109.
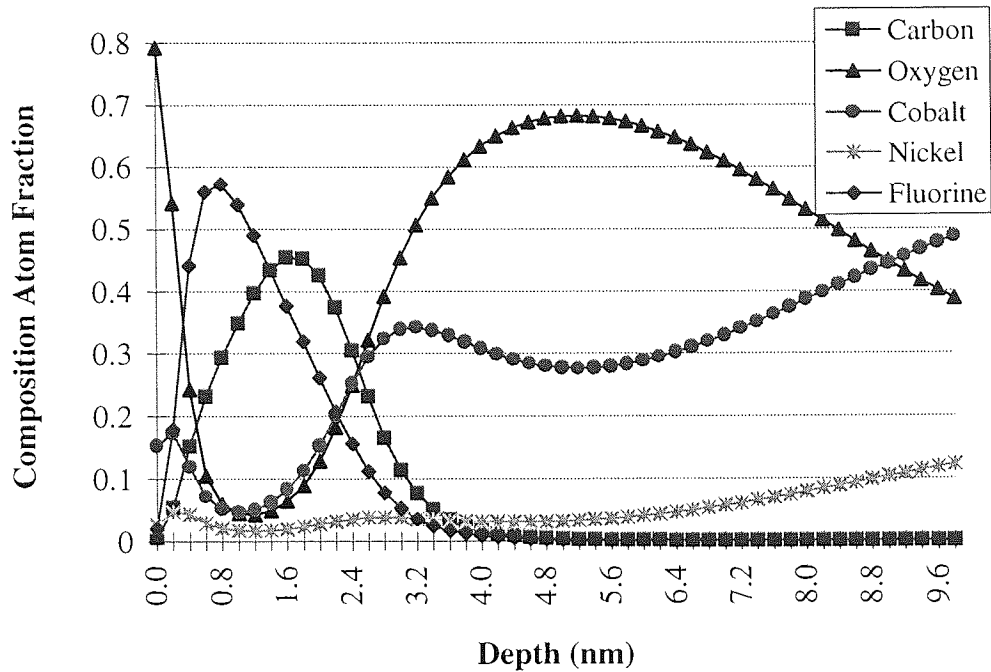
Figure 4.109 Determination of Lubricant Thickness on Tape ME#1 based on Reconstruction of Depth Profile from ARXPS Data

The depth profile of the near surface region of tape ME#1 enabled the thickness of the
lubricant layer to be determined by simple reference to the fluorine signal. The point at
which the fluorine signal fell to zero can be considered to be the boundary between the
lubricant layer and the magnetic thin film structure. Thus, for tape ME#1, the lubricant
had a thickness of 4 nm since this was the depth at which the fluorine signal fell to zero.
The profile seemed to fit very well with one that might have been expected since the
atomic concentration of oxygen and cobalt both increased together just as the fluorine
signal was reaching a minimum. This would represent the transition depth at which the
lubricant layer was in contact with the magnetic thin film.

The reconstruction over the first 1 nm had to be ignored since the errors associated with
this part of the reconstruction were too great due to scattering of the photoelectrons

from XPS analysis at the grazing angle. Similarly, the signal to noise ratio was too small at depths beyond 5 nm and thus the algorithm automatically tried to fit the reconstruction to the prior model. For this reason, the profile beyond 5 nm had to be disregarded.

The reconstructed profile for tape ME#1 suggested the maximum entropy method may have been the best way of determining the lubricant thickness. However, other depth reconstructions suggested that this was not the case. The final reconstruction was extremely sensitive to the attenuation lengths described in the prior model and to the initial ARXPS data. For instance, small changes in the attenuation length values of elements in the prior model resulted in major changes to the profile. The depth at which the fluorine signal decreased to zero often changed significantly and the general shape of the reconstructed profile was sometimes completely different even though it was generated from exactly the same ARXPS data.

The most realistic profile for tape ME#2 is shown in Figure 4.110 but it did not provide a reliable reconstruction. Similarly, other profiles of tape ME#1 showed similar fluctuations in elemental concentrations which would not be expected in a model representation of the tape.
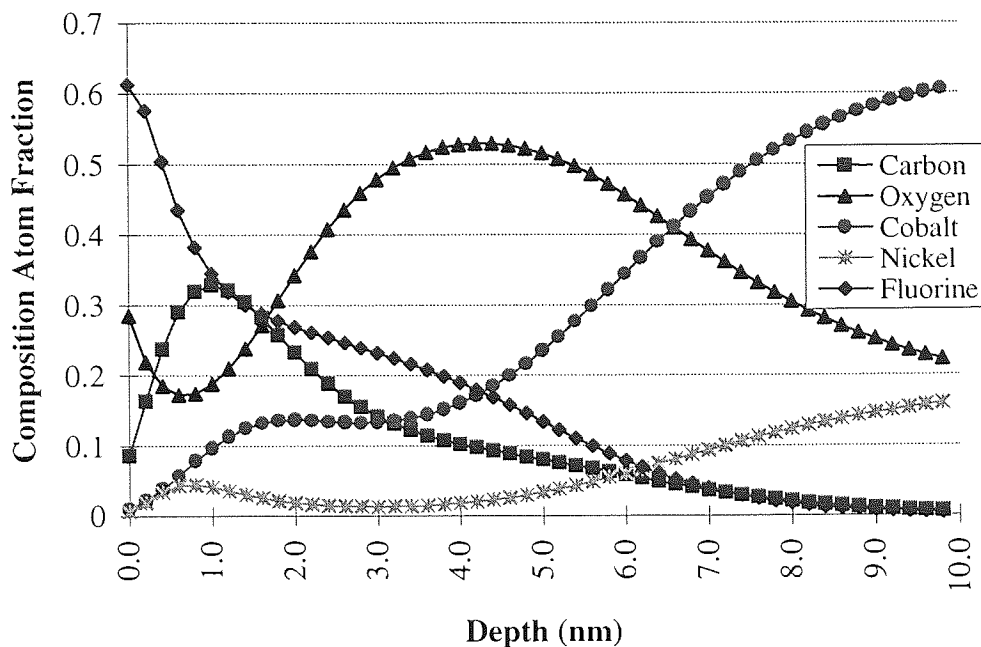
Figure 4.110 Determination of Lubricant Thickness on Tape ME#2 based on

Reconstruction of Depth Profile from ARXPS Data

4.6.3 Calculation of Layers Covering Magnetic Pigment in Tape MP#1

The total mean thickness of the layers covering the magnetic pigment were calculated from the electron attenuation of Fe 2p electrons in the overlayer and are shown in Table 4.2. The thickness values could be taken as absolute figures due to the assumptions that had to be made in order to simplify the complex matrices of the particulate sample surface. However, they could be regarded as being of the correct order and as a reliable indication of the relative overlayer thickness of the MP tape at each condition. The total mean thickness of the layers covering the magnetic pigment may have consisted of binder, lubricant and a carbonaceous contamination layer.

Assuming the characteristic photoelectrons obeyed a simple exponential attenuation law when they travelled through the overlayers, the relative thickness of the layers covering the magnetic pigment were calculated by assuming an attenuation length of 2.8 nm for Fe 2p3 photoelectrons and an initial concentration of 40 %. This value was not critical since the relative change in overlayer thickness was the same provided that 40 % was used in every calculation. Tape MP#1 had a microscopically rough surface and thus if the magic angle theory proposed by Gunter et al. [128] is shown to be correct, it would be appropriate to determine changes in the relative thickness of the overlayer by considering XPS data at 45° rather than by data taken at a normal to the tape surface. The Relative change in the thickness of overlayers covering the pigment for tape MP#1 are listed in Table 4.3 at various conditions, using data from both 0° and 45°.

Condition of Tape MP#1 Sample	Total Mean Thickness of Overlayers (nm) 0° TOA	Total Mean Thickness of Overlayers (nm) 45° TOA
Virgin	5.64	4.86
300 Cycles (Ambient)	5.59	4.43
5000 Cycles (Ambient)	5.38	4.20
5000 Cycles (High Humidity)	5.19	4.05

Table 4.3 *Total Mean Thickness of Layers Covering the Magnetic Pigment on Tape MP#1, Calculated from the Attenuation of Fe 2p3 Electrons in Overlayers at 0° and 45° TOA*

The same method that was used to calculate the relative thickness of overlayers covering

the magnetic pigment on tape MP#1 was also applied to the lubricant layer on tapes

ME#1, ME#2 and ME#3. In this case, the characteristic electrons had to be from the

magnetic thin film, such as Co 2p3. Data from a single angle could have been used but

as with tape MP#1, the relative thickness was calculated at $0°$ and at the magic angle of

$45°$ [128]. Table 4.4 lists the relative thickness of the lubricant on tapes ME#1, ME#2

and ME#3.

Tape Sample	Total Mean Thickness of Lubricant (nm) $0°$ TOA	Total Mean Thickness of Lubricant (nm) $45°$ TOA
ME#1	4.12	3.71
ME#2	2.30	1.98
ME#3 (Virgin)	6.56	4.60
ME#3 (450 Cycles)	5.18	3.24

Table 4.4 *Total Mean Thickness of Lubricant Covering the Magnetic thin Film on Tapes ME#1, ME#2*

and ME#3 Calculated from the Attenuation of Co 2p3 Electrons in Lubricant at $0°$ and $45°$ TOA

CHAPTER 5

DISCUSSION

5.1 Introduction

Lubrication in the case of metal evaporated thin film magnetic media is far more critical than for particulate media due to the internal structure of the two types of media. Particulate media consist of a binder system which is sufficiently porous to allow the binder to act as a reservoir, from which the surface lubricant can be constantly replenished, and which due to the nature of the low surface energy of the polymeric contact, will not suffer catastrophic failure if the lubricant film coverage is incomplete.

ME media rely totally on a thin boundary lubricant film for protection which must be extremely thin, in order to keep spacing losses to a minimum. Its areal coverage must be continuous and remain so for the expected lifetime of the media if severe wear and catastrophic failure are to be avoided. This is true for all ME tapes, irrespective of whether they have single or multilayer magnetic films. The lubricant layer on ME media must also protect the magnetic constituents of the media against corrosion since the tapes have to provide long term stability and be suitable for use in extreme environmental conditions.

The work described in this report has shown that for current commercial flexible magnetic media, particulate media possess better durability characteristics than ME media although this situation may change as the next generation of products are produced. The mechanisms of wear that were thought to be responsible for changes to the media surface and subsequent signal degradation during the durability tests are described for each type of media and comparisons made between the results.

5.2 Tape MP#1

5.2.1 Stop Motion Durability Tests : Tape MP#1

The durability of tape MP#1 was assessed using the same durability tests as those used for the three commercial ME tapes in order to determine comparative information. The stop motion tests for the MP tape revealed almost identical behaviour at low (10% RH, 25°C) and ambient (40%, 25°C) humidity conditions whereas at high humidity (85%, 25°C) conditions, the signal degradation was generally more severe. During stop motion tests, the signal tended to fluctuate within a greater band at high humidity conditions whereas during cycling tests, dropout growth tended to commence at an earlier number of cycles.

The coefficient of friction for particulate media remains small at relative humidities below 40% whereas at higher humidities, the coefficient of friction increases rapidly. The most probable explanation for the increase in frictional force is that at high humidity conditions, the forces present at the head-media interface change, possibly due the presence of meniscus forces and also from a change in the mechanical properties of the media bulk, though binder degradation. Miyoshi et al. [134] have shown that the adhesive force at the interface between ferrite and particulate tape remains low below 40% RH and increases substantially above 40%. It is likely that the water absorbed at the head media interface at humidities above 40% RH is the major reason for the increase in frictional force since the changes in the adhesive forces with increasing humidity are reversible and these forces can be accurately modelled in a high humidity environment by using meniscus theories.

The signal degradation profiles for tape MP#1 at high humidity conditions were worse in terms of signal variation than equivalent profiles at low and ambient conditions. The

greater variation in signal loss can be attributed to an increase in the adhesive force at the interface between the head and media. However, it appeared that whilst this led to a greater signal loss, the high humidity conditions also extended the projected time to failure for tape MP#1.

5.2.2 Cycling Durability Tests : Tape MP#1

The rate of dropout growth for tape MP#1 generally increased with the number of cycles for experiments at ambient and high humidity conditions. However, even after 5000 cycles, the dropout rate was still relatively small illustrating the excellent durability performance of particulate media. The greatest growth in dropout rate for tape MP#1 occurred in the 16 dB dropout class for widths of 20, 50 and 100 μs although there was also a small increase in the dropout rate for the 10 dB class. Binder depletion also occurred during cycling as shown in Figure 4.78. The detection of nitrogen following XPS analysis was due entirely to the existence of the binder system in the near surface region of the tape. The ratio of Fe:N steadily increased with cycling and was at a maximum when the tape was cycled for 5000 cycles at high humidity conditions. An increase in the percentage of magnetic pigment in the near surface region of the tape was unlikely through cycling alone and thus the most plausible explanation for the increase in Fe:N ratio was a decrease in the percentage of nitrogen through binder depletion.

One of the main differences between cycling and stop motion durability tests is that during a cycling test, the tape consistently moves within the tape guide system whereas in a stop motion test, the tape is always stationary. The tape will experience continuous tension and stress throughout a cycling test and hence the increase in dropout rate with increasing number of cycles for tape MP#1 was probably due to the cyclic stressing of the tape, ultimately resulting in partial wear of the surface through substrate fatigue.

5.3 Tapes ME#1, ME#2 and ME#3

A group of lubricants which satisfy the stringent criteria for use in ME media are perfluoropolyethers. The SIMS analyses performed on tapes ME#1 and ME#2 confirmed that lubricants of this type had indeed been used in each of these tapes. The backbone of the lubricant used in tape ME#1 was characteristic of the backbone of the perfluoropolyether lubricants, Z-deal and Z-dol, whereas for tape ME#2, the backbone of the lubricant was characteristic of the type used in Krytox. Thus, it was possible to identify the specific types of perfluoropolyethers on tapes ME#1 and ME#2 through SIMS analysis. However, further analysis would be needed before the relative performance of these two types of lubricant could be assessed. For instance, SIMS analysis on the surface of a cycled tape may produce a spectra with subtle changes to that of a spectra for virgin tape. There may be differences in the magnitude of peaks at certain masses, indicating changes had occurred to the lubricant on the media. However, the relative size of peaks cannot be taken as a definite guide to lubricant degradation since the size of the peaks are to some extent, also dependent on the experimental conditions at which the SIMS analysis was performed. Thus, conclusions from the SIMS spectra were limited to the identification of the lubricant type rather than to the relative performance of each lubricant. However, this in itself was an important finding since it enabled the lubricants to be characterised in terms of backbone and end-group. The lubricant thickness on each tape were subsequently determined from XPS measurements.

The XPS results indicated clear differences between the lubricants on tapes ME#1 and ME#2 that could be assigned to the relative mechanical and magnetic performance of the ME tape samples. The pseudo depth profiles for tapes ME#1 and ME#2 (Figures 4.63 and 4.64 respectively), revealed that exposure to the primary X-ray beam caused a decrease in the concentration of fluorine with time. However, for tape ME#1, the concentration of fluorine fell by 78% in 13 minutes after which the F signal remained

relatively constant whereas for tape ME#2, the decrease in F was by 40% in the same period. This indicated that there was a greater proportion of a semi-mobile, perhaps physisorbed, element in the lubricant of tape ME#1 than tape ME#2. This component of the lubricant would be available to repair localised film damage caused by tribological contact between the media and the heads of a recording system. Further evidence was provided by the results of Figure 4.98 which showed a higher relative proportion of F - C bonded material in the lubricant of tape ME#1 than in tape ME#2. Indeed the thickness measurements of the lubricant on the ME tapes showed that the thickness of the lubricant on tape ME#1 was greater than that on ME#2 (see Tables 4.2 and 4.4) and hence from these results alone, one might expect the tape to be afforded greater protection.

5.3.1 Stop Motion Durability Tests : Tapes ME#1, ME#2 and ME#3

The stop motion test results showed tape ME#1 had superior durability performance than tape ME#2 at ambient conditions. This was probably due to the thicker and more mobile lubricant layer since the stop motion test is particularly severe on the lubricant. In the case of tape ME#1, the lubricant layer was able to offer more protection against the continuous contact of the head and any partial surface damage could be repaired by the semi-mobile part of the lubricant. Tape ME#2 on the other hand did not have as much lubricant to protect the tape and thus the time to failure was much shorter. In addition, the mobile component of the lubricant on tape ME#2 was less which also contributed to the shorter times to failure.

The stop motion test results at high humidity conditions for tapes ME#1 and ME#2 revealed that the durability performance for each tape had improved from identical experiments performed in ambient conditions. The time to failure for each tape was

longer and the playback signal did not fluctuate or decrease by the same extent as at ambient conditions. Tape ME#2 benefited more than tape ME#1 from the humid environment since the time to failure for this tape at high humidity conditions was greater than that for ME#1 whereas at ambient conditions, the time to failure was longer for tape ME#1. Clearly, the tribological properties of both tapes were enhanced by the additional lubrication offered by the increased number of water molecules at high humidity conditions. The reduction in friction and adhesion at the contacting interface between the heads and the tapes may have occurred when the water molecules condensed and formed a film at the contacting surfaces, thus enhancing the lubrication at the interface. The absorbed water improved the overall durability of the contacting surfaces although the stiction component may have increased slightly due to the increased probability of menisci forming between the contacting head and media.

The same trend of improved performance at high humidity conditions was observed for tape ME#3 with both longer times to failure and less variation in the signal up to failure. Tape ME#3 also exhibited better performance than the other two ME tapes at ambient and high humidity conditions which suggested the protection afforded by the lubricant and DLC layer was more effective than either of the lubricants used on tapes ME#1 and ME#2. However, this enhanced protection was probably achieved at the expense of signal output since the thickness calculations from XPS analyses suggested the total thickness of the lubricant and DLC layers was greater than either of the lubricants on tapes ME#1 and ME#2.

5.3.1 Cycling Durability Tests : Tapes ME#1, ME#2 and ME#3

The results of the cycling tests for each of the ME tapes showed the number of dropouts was initially low but after a certain number of cycles, catastrophic dropout growth ensued, and this coincided with the tape surface becoming tacky. At this point, it was impossible to continue cycling the tape and the test was deemed to have been completed. For all three ME tapes, it was possible to achieve a greater number of cycles before the tape became tacky at high humidity conditions than was possible at ambient conditions.

For tape ME#1 at high humidity conditions, catastrophic dropout growth typically did not occur until between 600 and 700 cycles. This was far better than at ambient conditions when the number of cycles at which catastrophic dropout growth occurred was approximately 200 cycles. Similar improvements were observed for tapes ME#2 and ME#3. The improved performance of all three tapes at high humidity conditions was due to the additional lubrication afforded by the increased number of water molecules at the head-tape interface.

Tape ME#3 yielded the best cycling test durability results of all three ME tapes and this may have been due, in part, to the type of substrate used in its construction. The thickness was 6.7 µm compared to 10 µm for the substrates used in tapes ME#1 and ME#2. The thinner substrate gave the tape greater compliance since stiffness is related to overall tape thickness. A thinner tape would be able to follow the contours of the head and tape guide system more closely than a thicker tape and thus the tribological properties of the head-media interface would be different with smaller stresses experienced by the tape. The smaller stresses would ultimately reduce the rate of crack propagation within the tape and hence lead to improved durability.

5.4 Mechanisms of Wear

The mechanisms of wear for the MP and ME tapes were charted through the use of SEM micrographs at different stages of the durability tests. For instance, during the initial period of the stop motion tests, the output signal often increased temporarily before falling back to the original value. This was true for all the tapes, irrespective of whether they were MP or ME, and coincided with large asperities on the tape surface being deformed as a result of plastic flow after coming into contact with a recording head. In effect, the magnetic particles (or magnetic layer in the case of the ME tapes), would be closer to the head after the deformation of the asperities and thus the output signal would be greater due to the reduction in spacing loss.

5.4.1 Mechanism of Wear : Tape MP#1

The mechanisms of wear for tape MP#1 were isolated by examining the tape at different stages of the durability tests. In the case of tape MP#1, the wear processes that eventually lead to tape failure during a stop motion test were:-

(1) An initial period of plastic flow of large asperities on the tape surface on the area in contact with the head. This smoothing lead to a wear track but probably little or no material removal.

(2) Slender wear debris in the form of flakes were removed from the surface of the media, corresponding to delaminative removal of wear particles.

265

(3) A final catastrophic phase occurred at which large areas of the wear track were removed. At this stage, total signal failure occurred since the lubricant was unable to protect the tape any longer.

The same processes were responsible for wear at ambient and high humidity conditions. However, for an identical tape, the time to failure was generally extended for tests performed at high humidity conditions.

Mekala [135] calculated that in the case of head media interactions, temperatures as high as 600 °C could arise if a single asperity was in contact with a head. Such hostile localised environments could easily prolong plastic flow and lead to the creation of grooves on the media surface. The second stage of the wear process would arise from the continuous stressing of a single track, each time a head was in contact with the media. This would lead to the initiation of sub-surface fatigue cracks which would grow towards the surface upon further stressing of the media. When the cracks had extended to the surface, a delaminative wear particle (or flake) would be removed, leaving a wear scar similar to that shown in Figure 4.38.

In order for fatigue induced cracks to be initiated in the sub-surface region of the tape, a defect in the matrix must already exist since stress concentrations would only increase the possibility of crack propagation. Once delaminative removal of a wear particle had occurred, the final stage of catastrophic wear would follow very quickly and this was reflected in the stop motion test results which showed total signal failure occurred almost instantaneously. The debris produced from the delaminative wear process would become trapped between the head and the media, leading to three-body abrasive wear. The high frictional forces and acute stress concentrations associated with this type of wear would result in severe plastic deformation, leading to the production of further debris and an avalanche mechanism.

5.4.2 Mechanism of Wear : Tapes ME#1, ME#2 and ME#3

The mechanism of wear for the ME tapes was found to be similar to that for tape MP#1 although there were important differences. Firstly, each ME tape was topically lubricated and thus the lubricant acted as a classic boundary lubricant to provide a low surface energy film between the head and media. Also, the ME media had a distinct layered structure which naturally included discontinuities. Such discontinuities can be considered as defects and could well have been the starting place for fatigue induced crack initiation.

Examination of the scanning electron micrographs in Figures 4.46 - 4.49 clearly help to identify the wear mechanism for tape ME#1 when the tape was subjected to a stop motion test. Little wear was apparent on the surface of the tape for a running time of 2 hours but then after a few more hours, wear particles could be observed, as shown in Figure 4.46, and these corresponded to the start of surface delamination. As the running time increased further, a clear wear track became visible to the naked eye as shown in Figure 4.47. However, even at this stage of the stop motion test, the lubricant was still able to afford the tape sufficient protection in order to maintain a good signal output level.

The production of wafer particles through delaminative wear is clearly illustrated in Figure 4.48. The sub surface cracks would have extended to the surface of the tape giving rise to the wafer like particles. When these particles moved from the damaged area, the lubricant was no longer able to protect the tape from the excesses of the stop motion durability test. This process of surface delamination would proceed until catastrophic fatigue cracking and delaminative failure occurred, as shown in Figure 4.49. This is classic Suh [61] delaminative wear, where gradual breakdown of the lubricant film allowed head-metal contact to occur, leading to a work hardened film in the metal surface and the production of an immediate sub-surface discontinuity which then acted to

concentrate sub-surface fatigue cracks. Finally, the cracks would extend to the surface, leading to delaminative removal of material and ultimately to tape failure.

The cycling tests were far less demanding than the stop motion test in terms of the number of head passes per hour on a given track. However, the results of the cycling tests showed that large error growth occurred for all three ME tapes at ambient and high humidity conditions after relatively few passes. This may, however, also be explained in terms of delaminative wear since initially only small areas were affected, not great enough to influence total signal degradation, but the removed areas did result in errors or dropouts.

The cyclic stressing of the tapes during the cycling durability tests increased the stage at which subsurface cracks formed since the constant stressing of the tape would have lead to premature sub-surface crack formation. Furthermore, at the stage of catastrophic dropout growth, the surface of tape ME#1 was not as worn as that of ME#2 as illustrated in Figures 4.50 and 4.55 respectively. Accordingly, the dropout rate at a given number of cycles was higher for tape ME#2 than for tape ME#1.

One of the main reasons for the catastrophic dropout growth after such a short number of cycles for tape ME#2 was probably the use of a double magnetic layer in the construction of the tape. This provided an additional discontinuity within the tape which would have increased the possibility of sub-surface crack formation.

Tape ME#3 also had an additional layer compared to tape ME#1 due to the inclusion of a DLC layer. However, the results show that the DLC layer improved the durability of the tape, despite the additional discontinuity. This was probably due to the improved bonding that was possible between the magnetic film and the DLC layer compared to the bonding possible between the PFPE lubricant and the magnetic film.

5.5 Models for Determining Layer Thickness

The models used for determining the thickness of lubricant layer on the ME media had mixed success. Two uniform models were investigated but the Kimachi model was clearly not appropriate for analysis of thin film media since the calculated thickness of the lubricant varied as a function of analyser take-off angle. The Briggs and Seah uniform model produced better results and it was possible to determine actual values for the lubricant thickness. However, these values were too large since in the case of tape ME#1, the lubricant thickness was calculated to be 120 Å. This was too large since if the lubricant layer had been of such magnitude, it is extremely doubtful that the characteristic photoelectrons from the magnetic film (cobalt and nickel) would have been detected from XPS analysis.

The technique of reconstructing a depth profile from ARXPS data initially produced some encouraging results but after further analysis, it was clear that this method was extremely sensitive to the accuracy of the original XPS data and to the values of each attenuation length described in the prior model. The sensitivity of the model was such that the reconstruction could not be relied upon to produce an accurate depth profile.

The best model for determining the lubricant thickness was the method which assumed a simple exponential attenuation law of the photoelectrons to calculate the relative thickness of the lubricant overlayer. Whether it is best to use data at an analyser take-off angle of 0° or 45° needs to be investigated further and this could form the basis of further investigations.

CHAPTER 6

CONCLUSIONS

6.1 Conclusions

The results of this research have shown that thin film metal evaporated tapes exhibit significantly poorer durability than metal particle tapes and that single layer magnetic films with a DLC protective film and PFPE topical lubricant layer combine to form the best flexible magnetic thin film media available today.

Tapes ME#1 and ME#3 comprised of a single magnetic layer whereas tape ME#2 had a double magnetic layer. All the tapes were topically lubricated but tape ME#3 also had a DLC protective layer between the magnetic film and the PFPE lubricant. Tape ME#3 clearly possessed the best tribological characteristics of all three ME tapes investigated in this work and this was primarily due to the additional protection afforded by the DLC layer. The durability results for tape ME#2 indicated that a double layer magnetic structure was detrimental to the tribological performance of the media since the interface between the two layers acted as a focal plane for sub-surface cracks. This ultimately contributed to the poorer durability test results of tape ME#2 since the interface between the two magnetic layers was an additional discontinuity which made the tape more vulnerable to cyclic stressing.

The stop motion tests provided a severe examination of the durability of each tape and failure usually occurred as a result of delaminative wear. Wear particles were initially generated from surface delamination which eventually lead to catastrophic fatigue cracking and delaminative wear of the metal film. The cycling tests were a far less demanding test but delaminative wear was still evident, probably as a result of cyclic stressing. In the case of tape MP#1, the binder system produced both beneficial and detrimental effects to the durability of the tape. The binder system is a matrix which by its very nature did not incorporate any discontinuities. Thus, the effects of cyclic stressing were limited and far less important than for the three ME tapes. However,

binder depletion also occurred with increasing number of cycles and this could affect the long term mechanical stability of the media.

The environmental conditions under which the VCR and media were operated affected the tribological properties at the head-media interface. In order for the improved durability performance of the ME media at high humidity conditions to be realised, as reported in this research, the frictional and adhesive forces at the head-media interface must have been reduced - a reversal of the case for particulate media. This difference probably resulted from the significantly different structures of the two types of tape. In the case of the ME media, the water molecules acted to aid lubrication between the contacting surfaces at the head/media interface since the hydrophobic perfluoropolyether lubricant film provided a continuous layer which the water was unable to penetrate. However, for tape MP#1, the binder system absorbed the water molecules leading to media degradation.

The magnetic media industry will never produce storage devices that out perform solid state applications or optical devices in terms of access times or data retrieval rates. Thus, in the long term, the industry needs to maintain its competitiveness over such devices by increasing the areal recording density of magnetic media whilst maintaining the present very low cost of price per megabyte to the end user. In addition, the overall recording capacity of a single unit must continue to increase in order to offer another advantage over the competing technologies. However, the immediate challenge the industry faces is to further improve on the design of ME media by reducing the thickness of the DLC and PFPE layers in order to reduce the associated spacing losses without compromising the durability of the media. This will inherently yield superior magnetic recording characteristics.

6.2 Future Work

The latest commercial ME tapes primarily consist of the same basic structure of a single layer magnetic thin film in combination with a DLC protective coating and PFPE topical lubricant. The work described here has shown multilayer tapes exhibit an inferior durability and thus any future research should initially focus on single layer tapes. The availability of good quality experimental tapes would also be beneficial since this would enable tape durability to be correlated to changes in selected media variables such as the type and thickness of lubricant and DLC layer, evaporated thin film composition and oxygen flow rate during production of the thin film media.

The types of experiment to be performed on the tape samples would be similar to those described in this thesis but could be extended to obtain additional information. For instance, the durability of flexible magnetic media is clearly related to the environmental conditions at which the media is operated. Thus, further research could include an investigation into the effect that temperature has on the tribological performance of ME media and in particular to changes in the mechanical performance, magnetic performance and chemical state variations. It would also be useful to monitor topographical characteristics of the media such as surface roughness at various stages in the cycling and stop motion durability tests. These could subsequently be correlated to changes in error rate, output signal and friction.

Head-media interactions can significantly affect the performance of a system. Thus, further work could incorporate an analysis of the interactions at the head-media interface for different combinations of head and media. The performance of a complete range of materials such as glass, ceramics, metals and ferrites as a function of humidity and temperature for various media combinations could be investigated. Measurements could also be made for a complete range of head structures, similar to those used in production

systems but also for dummy heads produced from various single materials. The dummy heads would have to be geometrically identical to real head structures in order to exactly replicate the contact conditions of a working system. This will require the assistance of a specialised industrial collaborator since it is unlikely that many of the heads would be commercially available.
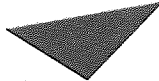
Appendix

Published Papers
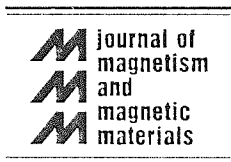
A study of the mechanical and magnetic performance of metal evaporated tape

M.S. Hempstock, J.L. Sullivan

Abstr

Th
medic
prese
helica
of sp
comm

1. Int

Th
produ
densit
nals w
ratio.
narrow
read/
losses
contac
these
(ME)
partici
metal
polym
(ME)
cial n
record
[2.3].
magne
dia du
layer
acteris
MI
contac
more
partici
polym

e magnetic
substrates
ape and in
entification
of the two

[6], is far
esent some
and failure
ured signal
analytical
ical failure

from lead-
e B) were
these tapes
ind cycling
recorders.
ions on the
m the tape
processing.
a tape to be
MHz (350
to the tape
absequently
he tester is
() classes of
e the initial
e tape was
ttern gener-
d field' test
cond blank
placed in
could com-
s (5 h) to

Cc

Aston University

Content has been removed for copyright reasons

The Durability and Signal Performance of Metal Evaporated and Metal Particle Tape

M. S. Hempstock and J. L. Sullivan
Aston University, Birmingham, B4 7ET, United Kingdom

Abstract —In this paper, we report on the durability performance of two commercial Hi-8 video tapes, a metal evaporated (ME) tape and a metal particle (MP) tape. Mechanical and physical changes in the surface of the tapes have been correlated to recording error measurements. Modified and adapted commercial Hi-8 recorders have been used for all the mechanical measurements and for sample generation whilst X-ray photo-electron spectroscopy (XPS) and scanning electron microscopy (SEM) have been

... through cycling tests and
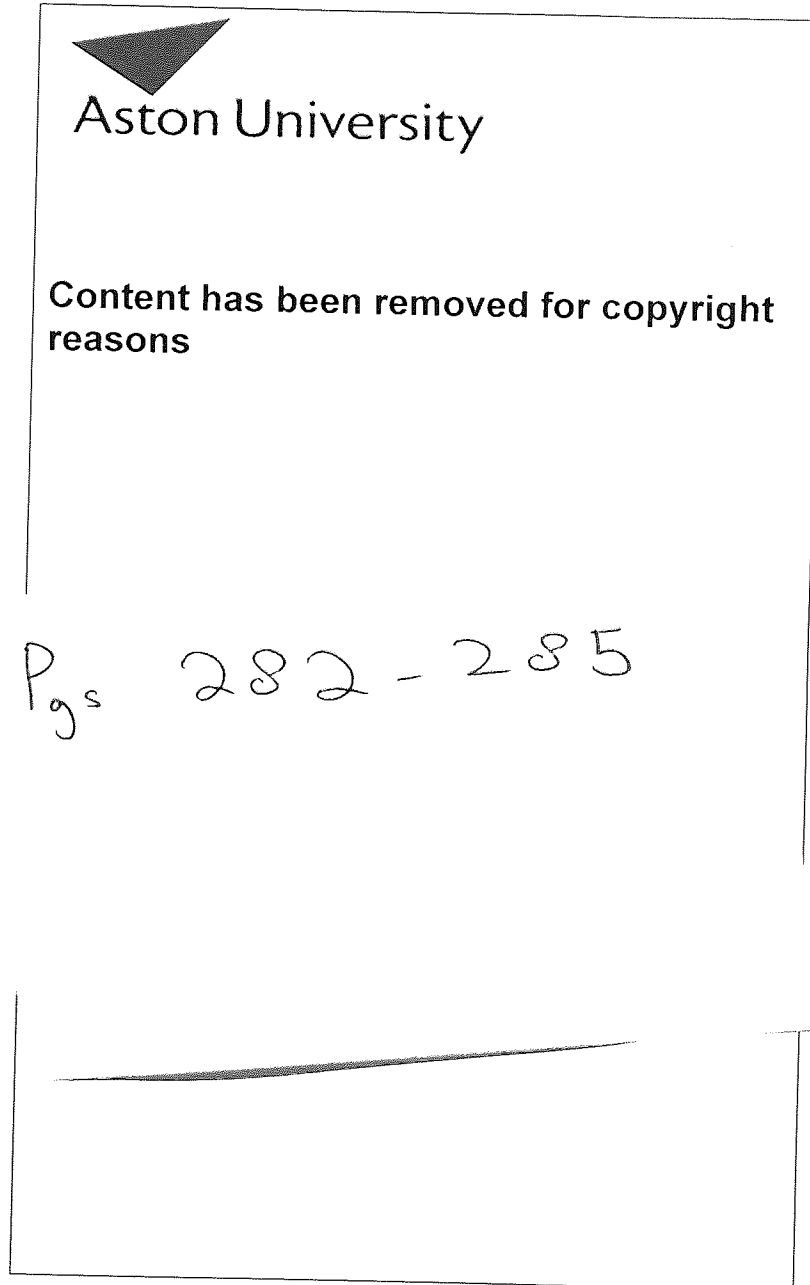
recorders were used

Pgs 282-285

changes in surface

m of wear.

The durability of commercially available ME and MP Hi-8 video tapes from a leading manufacturer was evaluated by cycling tests using modified Sony EVO-9500